12-2009

Production and Characterization of Novel Shaped Fibers for Fluid Sorption and Transport

Lisa Fuller

Clemson University, lisaf@clemson.edu

PRODUCTION AND CHARACTERIZATION OF NOVEL SHAPED FIBERS FOR FLUID SORPTION AND TRANSPORT

A Dissertation
Presented to
the Graduate School of
Clemson University

In Partial Fulfillment
of the Requirements for the Degree
Doctor of Philosophy
Materials Science and Engineering

---

by
Lisa Graham Fuller
December 2009

Accepted by:
Dr. Philip Brown, Committee Chair
Dr. Christine Cole
Dr. Douglas Hirt
Dr. Igor Luzinov

Abstract

This work investigated the production and characterization of novel shaped fibers for fluid adsorption and transport. Shaped fibers such as Y, H, and octolobal, as well as conventional round fibers, were extruded using a research melt extruder. The fibers were extruded from 18 melt flow index (MFI) polypropylene (PP) and blends of 18 MFI PP and 400 MFI PP. Hydrophilic spin finish Bozzetto Favorol SF2 was applied to the surface of extruded fibers and hydrophilic polyester additive LB-100 was included in the blend of some H fibers to increase the hydrophilicity of the fiber surface. The geometric shape retention of the extruded fibers was evaluated using scanning electron microscopy. The fluid adsorption and transport properties of the fibers were investigated using a low surface tension liquid and a high surface tension liquid. The shaped fibers were shown to have improved geometric shape retention with the addition of 400 MFI PP and were shown to have twice the fluid adsorption and transport capacities of the round fibers.

Micrographs of the fiber cross-sections obtained with a scanning electron microscope were used to visually determine the geometric shape retention of the fiber with respect to the spinneret hole design. While round, Y and octolobal fibers had excellent geometric shape retention regardless of polymer blend, H fibers showed improving geometric shape retention with increasing amounts of 400 MFI PP in the fiber blend. The perimeter and area of the fiber cross-section were measured from the micrograph and were used to calculate the shape factor for each shaped fiber.

The oil adsorption properties of the 18 MFI PP shaped and round fibers was evaluated using ASTM F-726. During the oil adsorption short test, the shaped fibers adsorbed

more than twice the oil that the round fibers adsorbed. The Y fibers were shown to be the most effective at oil adsorption and retention. The dynamic degradation test evaluated the ability of the fibers to adsorb oil in the presence of water. The shaped fibers again adsorbed twice the amount of oil that the round fibers adsorbed, with the Y and H fibers adsorbing the highest amounts of oil from the water. A comparison of the oil adsorption properties of Y and round fibers of increasing dpf showed that the Y fibers formed a cooperative structure that increased the oil adsorption beyond the adsorption of oil to the surface of the fibers.

Vertical wicking tests were used to investigate the wicking properties of the shaped and round fibers extruded with hydrophilic spin finish. When packed to have equal channel size, the shaped fibers wicked twice the amount of water the round fibers wicked. Second insult wicking tests on the H fibers showed that the improvement of geometric shape retention caused by adding 400 MFI PP to the fiber blend actually decreased the wicking properties of the fiber. The combination of the hydrophilic polyester additive LB-100 and the 400 MFI PP in the polymer blend, however, increased the wicking properties of the fiber as increasing amounts of 400 MFI PP were included.

Dedication

This work is dedicated to my family, friends and co-workers, without whom I would never have come this far.

To my parents, Richard and Barbara Fuller, for the support and encouragement you have provided through all the years. Without you, I would never have had the confidence necessary to achieve my goals.

To my siblings, Brandon Fuller and Laura McMillen, and my brother-in-law, Colin McMillen, for the ability to relax and laugh at my struggles and enjoy the perspective of those who have been where I am and those who have seen so much more.

To my friends and lab mates, for being there every day and sharing the incredible journey that is Graduate School. You made this process not only more livable, but also more enjoyable and exciting.

Acknowledgments

Table of Contents

List of Tables

ix

List of Figures

Chapter 1

Introduction

In 2000, Eastman Chemical Company (referred to hereafter as Eastman) and Procter & Gamble (referred to hereafter as P&G donated $38 million worth of equipment, patents, and intellectual property to Clemson University. These patents gave Clemson University the right to produce, research, and commercialize capillary surface materials (CSM) technology and capillary channel film (CCF) technology. The donation of these technologies allowed Clemson University to combine the knowledge and move the CSM and CCF research forward [1]. The investigation of polypropylene (PP) shaped fibers is one of the ways this technology is being utilized.

1.1 Shaped Fibers

Shaped fibers refer to fibers that have a cross-section other than round. Such fibers can be found in both natural fibers and synthetic fibers. Natural shaped fibers include cotton, silk, and wool. Cotton has a bean-shaped cross-section as a result of the collapse of the dehydrated lumen [2]. Silk has a generally triangular shape that accounts for its luster and wool, although mostly round, has scales along the fiber length [2].

Synthetic shaped fibers are used in industry to create aesthetic qualities that cannot be achieved using round fibers such as superior handle, softness, and openness as well as

special textures [3, 4]. Shaped fibers can be formed using a variety of methods including melt spinning, wet spinning, dry spinning [5] and conjugate spinning [4]. Shaped fibers can be melt spun from the same polymers used to extrude conventional round fibers including polyester, PP, polycarbonate, polytetrafluoroethylene (PTFE), and polyamides [6, 7, 8, 9, 10, 11, 12, 13, 14].

One of the first shaped fibers used in industry was a trilobal fiber designed to imitate the glossiness of silk fibers [4, 6]. Commonly spun fiber shapes now include hollow round, hollow triangle, hollow trilobal and hollow square fibers [5, 6, 7, 8, 9, 10, 11, 15, 16, 17, 18], rectangular, flat or arrow shaped fibers [4, 9, 12, 16, 17], modified trilobal fibers [4], fibers with channels (scalloped oval, hexachannel, cruciform [13] and CCP^{TM}(a.k.a. 4DG) [19]) and fibers shaped like letters (L, T, H, I, W, and Y [4, 20, 21]. These fiber shapes have been redrawn in Figure 1.1 for the reader's benefit.
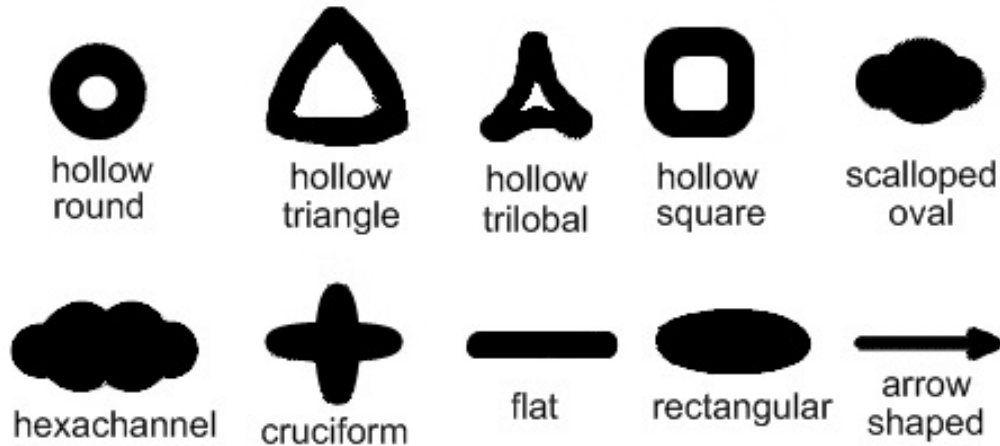
Figure 1.1: Examples of shaped fibers

After the advent of trilobal fibers as a synthetic silk, improvements to the trilobal shape (including a trilobal with grooves at the top of the lobes) improved the mimicry of the look and sound of silk fibers [4]. Bueno et. al. [13] further studied the effect of cross-sectional shape on the surface characteristics of knitted fabric. Bueno replaced conventional round fibers with fibers the authors described as scalloped oval fibers, hexachannel fibers and cruciform fibers (see Figure 1.1). They then measured the friction–roughness of the

fabric and correlated it to the moment of inertia of each fiber shape which was calculated according to

$$I_{fiber_{axial}} = \frac{\eta}{4 \times \pi} \times A^2 \tag{1.1}$$

where

$I_{fiber_{axial}}$ = moment of inertia relative to an axis

A = fiber cross-sectional area (m^2)

η = shape factor given by

$$\eta = \frac{P}{(4 \times \pi \times A)^{\frac{1}{2}}} \tag{1.2}$$

where

P = cross-sectional perimeter of the fiber (μm^2)

A = fiber cross-sectional area (μm^2) [13].

The analysis of these values and their relation to the friction–roughness of the fabric demonstrated that fibers with a cross-section closer to a flat tape were less rough[13]. Thus, softer knitted fabrics would likely be achieved by using tape-like fibers [13].

Melt spun hollow fibers are often used in insulation and wet spun hollow fibers have found a large market in filtering and various separations applications such as hemodialysis, microfiltration, ultrafiltration, reverse osmosis, and gas separation [5, 6, 7, 17, 18]. Trilobal fibers are still widely used in carpeting and apparel applications [4, 6]. The specialty fibers created by Eastman and P & G found applications in fluid sorption and capture. Some examples of the products developed from these fibers included diapers, sanitary napkins, and bandages [21, 22, 23, 24, 25, 26, 27, 28, 29, 30, 31, 32] as well as in other applications like doll hair [33], headbands [34], filters [35], insulation [36, 37] and liners for microwavable food containers [35].

Hollow fibers are by far the most popular 'shaped' fiber currently in use. The inclu-

3

sion of these fibers in filters has increased the attention on extruding consistently shaped hollow fibers. Lee et. al. [10] spun hollow fibers from polypropylene and used different drawing conditions to alter the final thickness of the wall and hollow areas. Research conducted by Oh et. al. [16] led to the conclusion that the temperature of the melt has the strongest effect on the size of the hollow portion in hollow polyethylene terephthalate fibers. Oh later reported the size of the hollow portion could be increased by increasing the mass throughput rate and decreasing the take-up speed [16]. Petrulis et. al. [11] extruded hollow round fibers from PP and polyamide chip and used the wall thickness and inner diameter to build a model that demonstrated the relationships between these values and similar values in conventional round fibers. One of the difficulties of extruding hollow shaped fibers is that the spinneret hole produces a fiber with gaps that must close as the fiber cools. Rwei [15] studied the effect of die swell on the hole formation of hollow fibers spun from PP and polybutylene terephthalate. In this work, Rwei demonstrated that extruding hollow fibers from PP or other vinyl-type polymers was extremely difficult as the elasticity of the polymer causes a large die swell and the resulting fiber has poor shape [15].

Although very little research has been conducted on the extrusion of the H and Octolobal fibers, the Y fiber is very similar to the common trilobal fiber. Indeed, the main difference between the Y fiber used in this work and trilobal fibers seen in carpets and other textile applications is the length of the fiber legs or lobes. Most trilobal fibers have shorter, thicker legs. In part, this is due to the difficulty of extruding a refined Y shape from a Y spinneret hole. In fact, Fortin et. al. [38] used a Y-shaped hole to spin round carbon fibers. The three rectangular slits that made up the Y spinneret hole forced the extruded material into higher alignment than that obtained with a round spinneret hole. This higher level of orientation improved the tensile and compressive strengths of the resulting fiber [38]. By comparison, Jung et. al. [9] used a similar Y shaped spinneret hole to extrude polyethylene terephthalate and PP trilobal fibers. By controlling the mass flow rate, spinning temperature and take-up speed, Jung was able to improve the shape of the trilobal fibers extruded from 15 MFI PP until they began to resemble slightly thick Y fibers

4

[9].

Takarada et. al. [17] found that the structural development of hollow fibers was very similar to that of conventional round fibers during extrusion. When extruding round fibers from these polymers, the surface tension forces of the polymer melt actually aid the fiber in retaining the round shape of the spinneret hole [3]. With shaped fibers, the surface tension and other forces cause the shape to be distorted from the original spinneret hole design. Ziabicki [39] stated that the cross-sectional shape of the fibers in the spinline would be somewhere between the shape of the spinneret hole and the shape of the final fiber. This means that to achieve a perfect or near-perfect shaped fiber (one that most resembles the spinneret hole design), a near-perfect shape must be achieved near the spinneret, before any drawing of the fiber occurs. Indeed, many researchers have found that drawing a shaped fiber does not drastically alter its shape, only its linear density and size [9, 12, 16]. This means that improving the geometric shape retention of a shaped fiber requires adjustments in the polymer melt after it is extruded but before it solidifies and is drawn.

Some researchers have theorized that the distortion of shape that occurs during shaped fiber extrusion is a result of stresses experienced by the polymer during its melt phase [40, 41]. The polymer melt experiences elongational stress and wall normal stress as it is forced through the spinneret holes [12, 15, 40]. Once the polymer exits the spinneret, the polymer undergoes stress relaxation in the form of die swell. The amount of die swell differs for every polymer and every spinneret design; however, Rwei showed that PP experienced more die swell than most condensation polymers due to its higher level of elasticity [15]. By controlling the factors that cause die swell, the shape of the extruded fiber can be improved. Improvements in shape have been seen when the surface energy of the polymer melt was reduced [20] as well as when the wall normal stress experienced by the polymer melt during extrusion was reduced [40].

1.2 Polypropylene

1.2.1 History and Synthesis

Polypropylene is a thermoplastic polymer from the polyolefin family [3, 42, 43]. Early attempts to synthesize a polymer from propylene (the monomer from which PP is made, Figure 1.2) resulted in non-crystalline oils that had little or no commercial use [3, 42]. The reason for this was a complete lack of stereoregularity within the materials. The question of stereoregularity within the PP chain was not raised until after the successful polymerization of other polymers from the polyolefin family. In 1953, Karl Ziegler discovered that using metal catalysts during synthesis could both inhibit and accelerate the reaction of monomers. With these catalysts, Ziegler successfully synthesized polyethylene at room temperature and atmospheric pressure, something never previously accomplished [43, 44]. He attempted to then synthesize a viable polymer from propylene but was unsuccessful. The following year, Guilio Natta used similar coordination catalysts to synthesize a version of PP [43, 44]. Natta's PP led to the discovery of the effects of stereoregularity on PP. Within his sample, he had isotactic, syndiotactic and atactic PP chains (Figure 1.3) [3, 42, 43, 44]. The atactic PP comprised the amorphous portion of the PP sample and the more crystalline portion was made of the isotactic and syndiotactic PP chains [43]. Isotactic PP is generally chosen for fiber extrusion over syndiotactic or atactic PP due to its increased crystallinity.

$$CH_2 = CH - CH_3$$
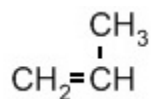
Figure 1.2: Propylene, also known as propene, the monomer from which PP is synthesized

The polymerization of isotactic PP by Natta was the first instance of stereospecific polymerization using $TiCl_4$, a coordination catalyst later dubbed a Ziegler-Natta catalyst [43]. Since that time, the production of PP has been modified to use more efficient and sophisticated catalysts [44]. The "First Generation" of Ziegler-Natta catalysts only resulted in approximately 90% of the product as isotactic PP [44]. Later generations of catalysts

a.

$$-\overset{\overset{\displaystyle CH_3}{|}}{\underset{\underset{\displaystyle H}{|}}{C}}-\overset{\overset{\displaystyle H}{|}}{\underset{\underset{\displaystyle H}{|}}{C}}-\overset{\overset{\displaystyle CH_3}{|}}{\underset{\underset{\displaystyle H}{|}}{C}}-\overset{\overset{\displaystyle H}{|}}{\underset{\underset{\displaystyle H}{|}}{C}}-\overset{\overset{\displaystyle CH_3}{|}}{\underset{\underset{\displaystyle H}{|}}{C}}-\overset{\overset{\displaystyle H}{|}}{\underset{\underset{\displaystyle H}{|}}{C}}-\overset{\overset{\displaystyle CH_3}{|}}{\underset{\underset{\displaystyle H}{|}}{C}}-\overset{\overset{\displaystyle H}{|}}{\underset{\underset{\displaystyle H}{|}}{C}}-$$

b.

$$-\overset{\overset{\displaystyle CH_3}{|}}{\underset{\underset{\displaystyle H}{|}}{C}}-\overset{\overset{\displaystyle H}{|}}{\underset{\underset{\displaystyle H}{|}}{C}}-\overset{\overset{\displaystyle H}{|}}{\underset{\underset{\displaystyle CH_3}{|}}{C}}-\overset{\overset{\displaystyle H}{|}}{\underset{\underset{\displaystyle H}{|}}{C}}-\overset{\overset{\displaystyle CH_3}{|}}{\underset{\underset{\displaystyle H}{|}}{C}}-\overset{\overset{\displaystyle H}{|}}{\underset{\underset{\displaystyle H}{|}}{C}}-\overset{\overset{\displaystyle H}{|}}{\underset{\underset{\displaystyle CH_3}{|}}{C}}-\overset{\overset{\displaystyle H}{|}}{\underset{\underset{\displaystyle H}{|}}{C}}-$$

c.

$$-\overset{\overset{\displaystyle CH_3}{|}}{\underset{\underset{\displaystyle H}{|}}{C}}-\overset{\overset{\displaystyle H}{|}}{\underset{\underset{\displaystyle H}{|}}{C}}-\overset{\overset{\displaystyle CH_3}{|}}{\underset{\underset{\displaystyle H}{|}}{C}}-\overset{\overset{\displaystyle H}{|}}{\underset{\underset{\displaystyle H}{|}}{C}}-\overset{\overset{\displaystyle CH_3}{|}}{\underset{\underset{\displaystyle H}{|}}{C}}-\overset{\overset{\displaystyle H}{|}}{\underset{\underset{\displaystyle H}{|}}{C}}-\overset{\overset{\displaystyle H}{|}}{\underset{\underset{\displaystyle CH_3}{|}}{C}}-\overset{\overset{\displaystyle H}{|}}{\underset{\underset{\displaystyle H}{|}}{C}}-$$
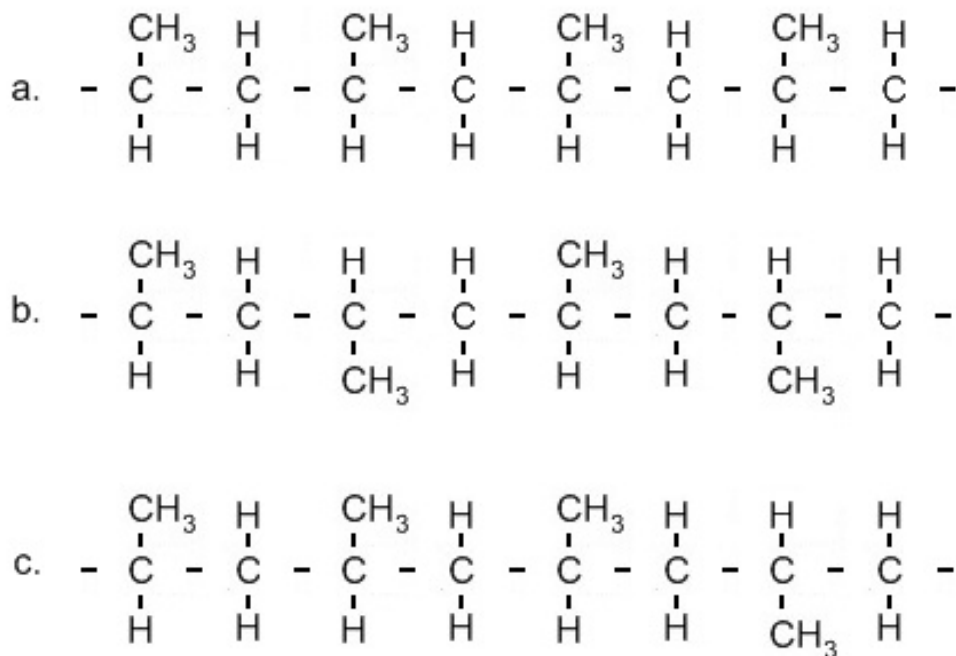
Figure 1.3: (a.) Isotactic PP, (b.) Syndiotactic PP, (c.) Atactic PP

within the Ziegler-Natta group, called metallocene initiators or catalysts, increase the iso-tactic portion of the polymer to 95–99% and allow a more tailorable molecular weight [44]. The mechanism for the polymerization of isotactic PP involves the stereoselective placement of monomers into a growing PP chain. The catalyst initiates the polymer chain and then also coordinates with the growing polymer chain and the monomer to force the monomer to orient appropriately for insertion [45]. The mechanism for this coordination and insertion is still under debate; however, the general theory is that the catalyst coordinates with both the polymer chain and the monomer to form a 'four-center cyclic transition state' that opens up the double bond within the monomer and begins the formation of a bond between the monomer and the growing chain [45]. Once the monomer bonds with the growing chain, the chain releases the catalyst and the catalyst again coordinates with the end of the polymer chain (the former monomer unit) [45].

For industrial production, the catalyst is formed into a slurry with purified heptane

and is sent to the reaction vessel along with propylene and a diluting agent (often cyclohexane) [3]. The mixture is placed under 2–4 atmospheres of pressure and is heated to a temperature between 50°C and 80°C. Under these conditions, isotactic PP forms and solidifies on the surface of the catalyst, causing the slurry to thicken [3]. Eventually, the now thick slurry is pumped to a flash tank where the unreacted monomer is removed from the system and recollected for later use [3]. Centrifuging the slurry removes the diluting agent and atactic polymer from the isotactic PP which is then separated from the catalyst with anhydrous isopropanol [3]. The resulting isotactic PP material can be turned into polymer chip and transported to other locations. An alternative method for the polymerization of PP is a gas-phase method wherein propylene monomer is converted into a gas phase prior to the addition of the catalyst [3].

1.2.2 Properties of Polypropylene

Isotactic PP was chosen as the main polymer for the extrusion of fibers in this work because of its robust chemical, biological and physical properties. PP is generally insoluble at low temperatures and can only be dissolved in a 'good' solvent such as xylene at temperatures above 80°C [43]. PP also shows excellent resistance to alkalies, detergents, and oil at room temperature [3]. PP also exhibits a resistance to water (hydrophobicity) and to the microorganisms found in water [3, 43]. Even when microorganisms do manage to attach themselves to a PP surface and begin to grow, they do not adversely affect the mechanical properties of the polymer [3].

The physical properties of PP vary with commercial grade. Regardless of commercial grade, PP has excellent mechanical properties such as toughness and resilience [42]. It retains good mechanical strength up to high temperatures [43] and resists abrasion [42]. The density of PP is lower than that of water at 0.90–0.91 g/cc [3, 43]. Most grades of isotactic PP exhibit a crystallinity around 60% [43] but this property can be highly dependent on the grade of commercial PP used. Commercial PP is generally categorized by Melt Flow Index (MFI). The MFI of a PP is determined by the weight of PP at 230°C that

flows through a standard die (normally 2.095 mm) under a standard load (usually 2.160 kg) in 10 minutes [46]. As a measurement of flow, the MFI of a PP indicates whether that material is of a high or low molecular weight. PP with a high MFI generally has a low molecular weight, while low MFI PP has a high molecular weight.

1.2.3 Applications of PP

The ability to synthesize PP in many MFIs and at a variety of molecular weights means that it can have very diverse applications. PP can be used in fiber extrusion, film extrusion, injection molding and blow molding [43, 44]. Injection molding allows the production of high-volume, three-dimensional PP parts such as automotive parts, battery cases, furniture, and toys [44, 47]. Blow molding is generally used for the production of bottles for condiments or toiletries [44, 47]. Extruded PP films can be used for things such as bags or candy covers [44]. PP films for packaging of food, clothing, and tobacco are also common [47]. PP can also be extruded on other materials as a coating in thicknesses down to 15 μm [44]. Fiber extrusion from PP can be used to create melt-blown or spunbonded fabrics as well as staple or continuous-filament yarns and tapes [44, 47]. This research focuses solely on the extrusion of continuous-filament yarns from PP.

1.2.4 Hydrophilic Polypropylene

Hydrophilic PP membranes have been used extensively in filtration. Membranes made from hydrophilic polymers are chemically and thermally less stable than PP membranes, which makes a modified PP membrane more resilient [48]. Hydrophilic PP fibers can also be used in fabrics that wick fluid away from the skin [49]. Although there are a number of ways to make PP hydrophilic, most methods can be placed into one of three categories: chemical modification of the PP, surface treatments, and blending of PP with other polymers or chemicals [50, 51, 52]. All three methods have been used with success, but have issues associated with the long-term applications of the resulting hydrophilic PP material.

9

The simplest method of making PP hydrophilic is to coat the film or fibers with a hydrophilic material. PP can be made hydrophilic with surface applications of spin finish, surfactants, alcohols, and amphiphilic polymers. Unfortunately, these applications are not a permanent solution and will wear off with time and use [48, 52].

Chemical modification of the surface generally results in a more permanent hydrophilic surface than a hydrophilic coating. Chemical modification includes the interfacial cross-linking of the PP with another polymer as well as the functionalization of PP with other side groups [48, 52, 53, 54, 55]. Korikov et. al. [55] prepared a hydrophilic ultrafiltration membrane by oxidizing PP with a chromic acid solution and then interfacially polymerizing the oxidized PP with poly(ethyleneimine). This method was used to hydrophilize the surface and the interior of hollow-fiber membranes [55]. Xu et. al. [48] grafted hollow fiber membranes with acrylic acid in a method that used benzoyl peroxide as an initiator for co-polymerization. By modifying the temperature and the amount of acrylic acid used in the procedure, the authors were able to control the amount of copolymerization that occurred at the surface of the PP fibers [48].

Another method of graft polymerization involves treating the PP membrane with plasma. Plasma treatment is generally followed by the grafting of a more hydrophilic polymer or compound onto the surface of the PP, thus rendering the material's surface more hydrophilic without changing the bulk material properties [56]. Experimental grafting of acrylonitrile, acrylic acid and various methacrylates have successfully rendered PP hydrophilic; however, a phenomena known as hydrophobic recovery (where the PP gradually recovers its hydrophobic nature) has limited the lifespan of these materials [48, 56, 57, 58]. A modified plasma treatment using organic monomers as well as gas was used by Garcia et. al. [56] and López et. al. [59]. This method, which used a methane-oxygen gas combination instead of the more conventional pure oxygen, nitrogen, or argon gas, has been shown to create a hydrophilic PP surface that is more robust [56, 59]. Although this method is more effective than plasma treatment using gas alone, both methods are limited in scale [52].

Blending is the most commonly used method for making PP hydrophilic [50]. The

advantage of using a blended PP fiber over a surface finish or treatment is that the hydrophilic material in a PP blend cannot be washed or abraded off. Although there are some issues with the structural compatibility of PP with other polymers, PP has been successfully blended to produce a more hydrophilic PP. Novák et. al. [51] successfully blended PP with up to 6% oxidized paraffin wax, increasing the hydrophilic nature of the polymer without any degradation of mechanical properties. Chung and Lee [53] blended the chemically modified PP-OH with unmodified PP to form a resulting membrane that showed excellent selectivity and antifouling. Mathiowitz et. al. [60] successfully prepared a PP dessicant by blending PP with poly(ethylene glycol) (PEG). The PEG formed hydrophilic channels within the hydrophobic PP structure [60]. Son et. al. [61] used a blend of PP and poly(ethylene-co-vinyl alcohol)create a blended PP fiber with an increased initial modulus and tenacity. In an alternate work, Son et. al. [62] used a blend of PP and phenolic resin to again make hydrophilic fibers without any reduction in physical properties. In industry, Ciba®developed hydrophilic additive Irgosurf^{TM}HL 560 specifically for the purpose of blending it with PP [63].

1.2.5   Extrusion of Polypropylene Fibers

PP fibers have been produced commercially by melt extrusion since the 1960s. The small size of the spinneret holes used in fiber extrusion generally requires the use of PP with a MFI from 10 to 30 [44]. It is possible to extrude PP with an MFI outside this range but it requires manipulation of the extruder conditions.

Extrusion begins with the placement of PP chip into the hopper (Figure 1.4). The hopper feeds the PP chip into the extruder screw. The extruder screw has three sections: the feed section, the compression section and the metering section [43]. The chip from the hopper is fed into the feed section of the screw. This section has the deepest flights of the entire screw. The PP chip is melted and compressed as it travels through the compression section of the screw where the depth of the flights has begun to decrease. The final section of the screw, the metering section, has the smallest depth flights and it has been recommended

that the length of this section should be somewhere between two to fourteen times the diameter of the screw [42, 43]. An extruder screw with a length to diameter ratio (L/D) of 24:1 or higher is recommended for extruding PP [42, 43]. In addition, the screw should have a compression ratio, the ratio of the volume of PP fed into the screw to the volume of PP discharged from the screw, of 3:1 or 4:1 [42, 43].

The metering section of the extruder screw feeds polymer directly into the spin head. The spin head contains a mesh screen that prevents solid contaminants present in the polymer chip from passing through to the spinneret and a metering pump that is used to regulate the flow of the polymer through the spinneret [42]. A secondary filter is sometimes placed immediately before the spinneret.

A spinneret can be described as a plate with holes (called capillaries) numbering anywhere from 10 to 2000 [3]. The spinneret is often the most important component of the spinning process as any irregularity in the shape of the capillaries or an incorrect l/d ratio (the length of the capillary to the diameter of the capillary) can result in failure of the extrusion process or extreme variations in the fibers produced [42]. The capillaries in spinnerets are specifically designed to reduce the stress present in the polymer upon exiting the spinneret [3].

The orientation of the molecules begins in the the spinneret where the flow of the polymer through the capillaries increases the orientation of the molecules along the axis of the fiber [3]. Although the polymer exits the spinneret in melt form, it quickly begins to cool and solidify. This rate of this solidification can be increased by using quench air or a quench bath [42]. Drawing the partially oriented polymer during the solidification process increases both the orientation and crystallinity of the fiber [3].

The extruded fiber is drawn at a temperature above its glass transition temperature on the godet rolls to further improve the crystallinity and orientation. The final product is collected on a package using a winder. Altering the extrusion variables such as the speed of the melt pump, the godet rolls and the winder will effect the final fiber produced during extrusion. The linear density of the resulting fiber can be raised or lowered by slowing

down and speeding up the draw roll or by changing the speed of the metering pump which effectively alters the spin-draw ratio [42]. A higher draw ratio, the ratio of the speed of the draw roll to the feed roll, increases the orientation of the fibers [44] and also improves the modulus of the fibers [42].
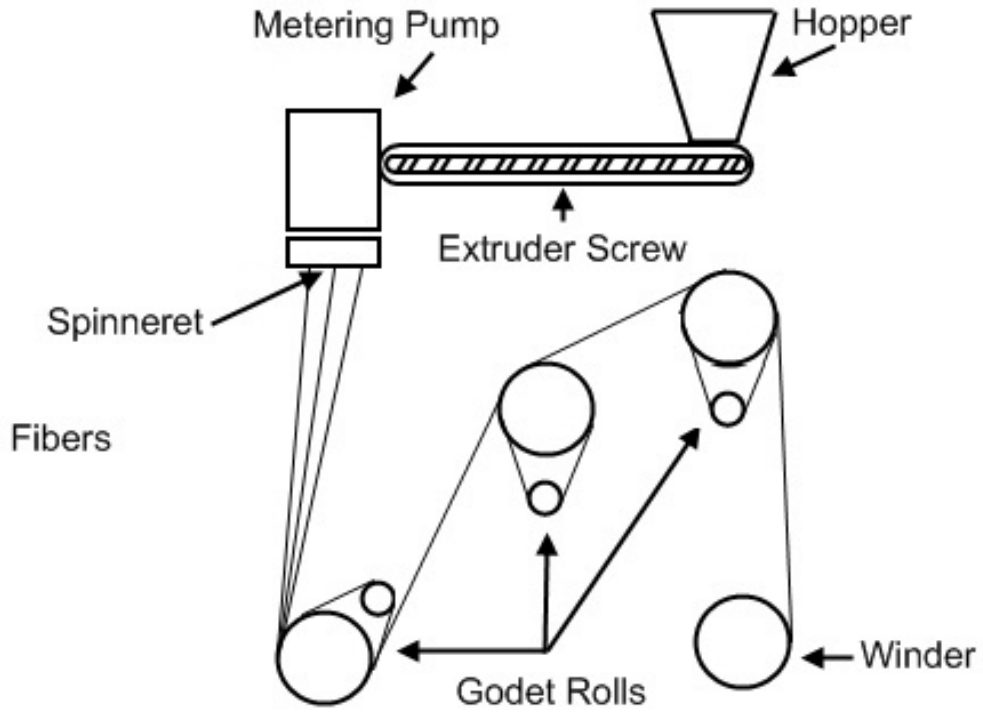
Figure 1.4: Diagram of an extruder used to extrude PP fibers

1.3 Adhesion of Fluids to a Solid Surface

For fluids to be adsorbed or transported by fibers, an attraction must exist between the surface of the fibers and the liquid. This attraction is referred to as 'wetting', which is defined as the displacement of one fluid by another (in this situation, the displacement of air by water or oil) in a three phase system (PP, air, and a liquid) [64]. Shaw distinguishes three types of wetting for liquids on solids in his book *Introduction to Colloid and Surface Chemistry*: adhesional, spreading and immersional wetting [64]. Adhesional wetting occurs when liquid contacts a solid for the first time and adheres to the surface. Spreading wetting occurs when a liquid already in contact with a surface spreads to cover more of the surface and immersional wetting occurs when the solid is immersed in a liquid [64].

1.3.1 Determination of Surface Tension or Energy

Whether wetting occurs or not is determined by the interactions of the three phases in the system. The boundary between a liquid or a solid and a gas is referred to as a surface and the energy of that surface is called surface tension or surface energy [64]. The boundary between a solid and a liquid is generally referred to as an interface [64]. The surface tension of liquids can be measured using methods such as the capillary rise method, the Wilhemy plate method, the ring method, the drop-weight method or the pendant (or sessile) drop profile method [64, 65]. The capillary rise method uses the distance a liquid climbs in a capillary tube of known diameter along with the density of the liquid and the liquid vapor to determine the surface tension[64]. The ring method and the Wilhemy plate method measure the force required to detach an implement (a ring or a plate, respectively) from the surface of a liquid[64]. The ring method is commonly used, but requires a correction factor for the non-vertical tension forces and ring-liquid interfacial shape[64, 65]. The Wilhelmy plate method is simpler and requires no corrections [65]. The drop-weight or drop-volume method involves measuring the drops that detach from a tube of liquid under the force of gravity [65]. This method is fairly accurate and simple as it allows one to count the

drops and measure either the weight or the volume of the collected drops [65]. The pendant drop method is a fairly simple test that captures the profile of a drop hanging from a tube or surface and uses the measurements of the drop as well as the density of the liquid to determine the surface tension [65].

Measuring the surface energy of a solid surface can be much more difficult than measuring the surface tension of a liquid. Some methods heat a solid near its melting temperature and use the flow of the solid under pressure to determine the surface energy [65]. A more common method for polymers is to use the contact angle of liquids on the solid surface to determine the surface energy. The Young-Dupre equation can also be used with a contact angle measured at equilibrium to calculate the surface energy of a solid [64]. Immersion of the solid in a liquid generates enough heat that the enthalpy of immersion can be related to the contact angle of the liquid on the solid [65]. It is also possible to measure the change in the surface energy of a solid using sorption isotherms, however, with this method it is often difficult to determine the surface energy of the solid as opposed to the surface energy of the solid in a vapor [65].

1.3.2 Energetic Determination of Wetting

Whether or not a liquid is likely to wet a solid can be determined theoretically using the surface energies and tensions of the materials involved. For adhesive wetting, when the liquid first comes into contact with the solid, the two main forces at work are the cohesion of the liquid (a measure of how difficult it is to separate the liquid) and the adhesion of the liquid to the surface of the material (a measure of how difficult it is to separate the two phases). The cohesion of the liquid (W_c) is equal to two times the liquid's surface tension (γ_{LG}) in the equation $W_c = 2\gamma_{LG}$. The work of adhesion in adhesional wetting is given by the Dupré equation

$$W_a = \gamma_{SG} + \gamma_{LG} - \gamma_{SL} \tag{1.3}$$

where

W_a = work of adhesion

γ_{SG} = interfacial energy between the solid and the gas

γ_{LG} = interfacial energy between the liquid and the gas

γ_{SL} = interfacial energy between the solid and the liquid [64].

This equation can also be rewritten to form the Young-Dupré equation

$$W_a = \gamma_{LG}(1 + cos\theta) \tag{1.4}$$

where

θ = contact angle of the liquid on the solid [64].

Using the Dupré equation (Equation 1.3) for cohesion of a liquid and the Young-Dupré equation (Equation 1.4), one can see that if the contact angle of the liquid on the solid is zero, the work of adhesion would equal the work of cohesion, or $2\gamma_{LG}$. This indicates that at a contact angle of zero, the liquid and solid are attracted to each other at least as much as the liquid is attracted to itself [64]. Conversely, if the liquid is attracted to itself more than to the solid, the contact angle will be greater than zero [64]. When true wetting occurs, i.e. the contact angle is zero, the liquid spreads across the surface of the solid in an action known as spreading wetting.

Spreading wetting occurs when the liquid is already in contact with the solid. This indicates that there is already an attraction between the liquid and the solid, but the tendency of the liquid to spread on the surface or to ball up in a drop on top of the surface is determined by the spreading coefficient (S). The spreading coefficient is given by

$$S = \gamma_{SG} - (\gamma_{SL} + \gamma_{LG}) \tag{1.5}$$

and if S is positive, spreading will occur spontaneously [64].

The final form of wetting, immersional wetting, involves immersing the entire surface of the solid into the liquid. As the solid is now within the liquid, the surface tension of the liquid is not affected and thus has no direct affect on the wetting of the liquid on the solid [64]. The equation for the immersion wetting of a solid is

$$-\Delta G_i = \gamma_{SG} - \gamma_{SL} = \gamma_{LG}cos\theta \tag{1.6}$$

where

ΔG_i = free energy change for immersion of a solid in liquid [64].

In this instance, the wetting of the liquid onto the solid is energetically favorable only if the surface energy of the solid is greater than the energy of the solid-liquid interface.

1.3.3 Capillary Rise

Capillary rise occurs when a liquid wets a surface completely. When a small tube (referred to as a capillary) is placed into a liquid, the wetting action of the liquid on the interior surface of the tube causes the liquid to rise. The height that the liquid reaches within the capillary can be related to the radius of the capillary and the surface tension of the liquid using a modification of the Young-Laplace pressure drop equation given by

$$h = \frac{2 \times \gamma \times cos\theta}{10 \times \rho \times g \times r} \tag{1.7}$$

where

h = rise of liquid in the capillary (cm)

γ = surface tension of the liquid (dynes/cm)

θ = contact angle of the liquid on the capillary surface (rad)

ρ = the density of the liquid (g/cc)

g = acceleration due to gravity (9.8 m/s^2)

r = radius of capillary (mm) [64, 65]

Given that all other variables in the equation remain the same (i.e., the same liquid is used, the same capillary material is used), decreasing the radius of the capillary will increase the height to which the liquid will rise [65].

Capillary action in fabrics is often referred to as wicking. The channels between fibers in a yarn and between the yarns in a fabric exert capillary forces on the liquid [49]. The capillaries in fabric are not perfectly round, but non-round capillaries can still exert a capillary force on liquids [66].

1.4 Oil Remediation by Sorbents

The high demands of modern society on petroleum and petroleum products cause a large amount of oil to be transported and handled worldwide. Oil spills have a negative impact on the environment. Oil spills on bodies of water result in a thick, greasy layer on the surface of the water and the dispersal of portions of the oil into the water and the air [67]. This dispersal leads to the ingestion of petroleum by marine animals and to the devastation of marine plant life [67]. For example, otters die from shock and hypothermia following an oil spill [67]. Marine animals are not the only ones affected – after the Exxon Valdez spill, 4,463 birds died almost immediately and others continued to die during the oil spill clean up [67]. Although oil spills are commonly associated with the catastrophic spills caused by transport tankers such as the Exxon Valdez, this is not the only way that oil spills occur. Other, more minor, accidents commonly occur during the transport and handling of oil. These accidents include, but are not limited to, spills during loading or offloading of tankers, pipeline ruptures, runoff from oil fields and refineries, accidents from drilling operations and even dumping of oily bilge water from ships [68, 69, 70, 71, 72]. Once the oil has been dumped into the body of water, it begins to undergo several processes including spreading, evaporation and emulsification that increase the oil density and viscosity and release toxic water-soluble chemicals [70, 71, 73]. The general approach to dealing with such

oil spills is to place restrictive oil booms around the oil spill in an attempt to contain or direct the oil and then to use either oil skimmers or sorbents to collect the oil [71, 72, 74, 75]. Sorbents are generally viewed as one of the most effective sorption methods and interact with the spilled oil to convert it from a liquid phase into a semi-solid phase that is more collectible [69, 71, 75, 76]. The best sorbents are materials that are very hydrophobic and oleophilic, inexpensive, readily available, and have a fast oil sorption rate [68, 74, 77].

There are three classes of sorbents: inorganic mineral products, organic natural products and organic synthetic products [68, 69, 70, 76]. Inorganic mineral products include minerals such as perlite, graphite, vermiculites and sorbent clays which are highly adsorbent but experience buoyancy problems when used for oil spills on water [69, 70, 76]. Perlite, an amorphous volcanic glass, was shown to adsorb 7.5 g of oil per gram of material by Bastani, et. al. [70].

Organic natural products such as cotton, milkweed, kapok, straw and wood fiber have been shown to have high oil sorption, but these materials are not naturally hydrophobic and often must be treated before use [71, 72, 73, 75, 76, 77, 78, 79]. Natural fibers that do not require treatment include fibers from Sugi trees, kapok trees, and silk floss trees. Fibers from the bark of a Sugi tree were used as an oil sorbent by Saito et. al. [78] and was shown to adsorb as much as 10 grams of oil per gram of sorbent. Kapok fiber is a hollow fiber harvested from the seedpods of kapok trees [80]. Lim and Huang [68] showed that this fiber can adsorb as much as 45 grams of oil per gram of fiber and that its natural coating made it ideal for adsorbing oil from water. However, kapok trees do not produce seedpods every year and harvesting the fiber requires extensive manual labor [81]. Another organic tree fiber, silk floss, was investigated by Annunciado et. al. [79] along with a number of other vegetable fibers. The sisal, sawdust, coir fiber, sponge gourd and leaves residues that Annunciado investigated never adsorbed more than 8 grams of oil per gram of sorbent; however, the silk-floss fibers adsorbed approximately 85 grams of oil per gram of fiber [79]. Silk floss collection requires the same seed pod harvesting technique as kapok fiber, limiting its ability to be produced in mass quantities. Using natural fibers as oil sorbents has been

proven to be effective, but sorbents cannot be mass produced from these materials.

Organic synthetic products, which include such things as PP, polyurethane, and other synthetic polymers, have been shown to have low water sorption [73, 79, 82]. Indeed, PP and polyurethane sorbent materials are the most common sorbent for oil spill remediation, with PP in particular being used because of its ability to float on water [68, 72, 73, 74, 78]. Kondo [74] found that PP sorbents required rigidity and the ability to maintain their shape in order to adsorb the highest amount of oil. Teas et. al. [69] compared a non-woven PP sorbent to various organic natural products and reported that PP out-adsorbed all the other materials by adsorbing approximately 4.5 grams of oil per gram of sorbent material. A comparison of stitch-bonded, needle-punched, and melt-blown PP fabrics was completed by Wei and his associates [73] in order to determine the most effective construction for sorption by a PP fabric. The fabric with the highest porosity showed the highest sorption initially but did not retain the oil after a period of drainage [73]. Fabrics with similar porosities but finer fibers had similar sorption and higher oil retention, indicating that the most effective PP sorbent would have small fibers in a highly porous structure [73]. All the tests conducted on PP fibers used the conventional round fiber shape.

1.5   Current Work

This research explored the advantages of using the shaped polymer fibers developed by Eastman and P&G over conventional round fibers. Three shaped fibers were evaluated: an H shaped fiber developed by P&G, a Y shaped fiber and an Octolobal fiber developed by Eastman (Figure 1.5). These shaped fibers, often referred to as capillary channeled polymer fibers, have channels within the fiber and a higher surface area than conventional round fibers. The channels within the H fiber are square-bottomed with parallel legs, while the Octolobal fiber has parallel-legged channels that are somewhat rounded at the base. These open channels can act independently to wick fluid which allows a single filament of

H or Octolobal fibers to transport fluid. This wicking action is the reason the H fibers were dubbed "spontaneously wicking" in the patents [22, 83, 19]. The channels in the Y fibers are much larger and there is approximately a 120° angle between the legs. These channels do not wick independently; however, it was hypothesized that the larger channels and longer legs of the Y fibers would allow adjacent fibers to work cooperatively and wick more fluid than the fibers with independently wicking channels.

Figure 1.5: Y, Octolobal and H fibers used in this research. (Fibers are to scale.)

The increased surface area of the shaped fibers indicated to Eastman and P&G that these fibers would have improved fluid sorption and transport properties over round fibers. The two companies began to develop these products, focusing mainly on polyester fiber, but were unable to continue their work because of conflicting patents. Using the donations of the collective works, Clemson has avoided the patent conflicts and carried the research further than the individual companies were able. In this work, shaped fibers from both companies were extruded from polypropylene, an inexpensive but robust material, and were evaluated to determine their transport and sorption capabilities. The three shaped fibers were characterized to determine if the "spontaneously wicking" H and Octolobal fiber shapes were more effective at adsorbing and transporting liquid than the "cooperative" Y fibers. These three shaped fibers were also compared to conventional round fibers to determine their effectiveness against materials already in use.

The work of numerous authors has shown that blending PP with hydrophilic polymers can indeed increase the hydrophilicity of the resulting fibers or films. To this end,

three additives, LB-100, R-3000 NAJ and Velvetol, were investigated in this work for use in a PP polyblend fiber. The additives were supplied by Hexion Specialty Chemicals and were polyester derivatives that were reported to have hydrophilic properties superior to that of PP. The focus of a portion of this work was to determine if blending these additives with PP would result in the polyblend PP fiber gaining some of the hydrophilic properties of the additives.

Chapter 2

Experimental

2.1 Materials

Table 2.1: Materials Utilized

Chemical/Material	Supplier	Description
18 MFI PP	Atofina	small white pellets Molecular Formula $(C_3H_6)_n$
400 MFI PP		small white pellets Molecular Formula $(C_3H_6)_n$
LB-100	Hexion Specialty Chemicals	polyester additive
R-3000 NAJ	Hexion Specialty Chemicals	polyester additive
Velvetol	Hexion Specialty Chemicals	polyester additive
Liquid Nitrogen	Airgas National Welders	
Favorol SF2	Bozzetto GMBH	hydrophilic spin finish
Low Viscosity Embedding Media	Electron Microscopy Sciences	embedding resin
Acid Red 1	Sigma–Aldrich	CAS 3734-67-6
Southern Home Canola Oil	Local grocery store	
Havoline 10W-40 Motor Oil	Ace Hardware	

Table 2.1: Materials Utilized

Chemical/Material	Supplier	Description
n-Tetradecane	MP Biomedicals, LLC	MW198.4, 500ml, 99% pure, CAT#156775
Hexadecane	TCI America	MW226.44, 500ml, 98% pure, CAT#C61220C
Heptadecane	MP Biomedicals, LLC	MW240.5, 100ml, 99% pure, CAT#157307
n-Pentadecane	ACROS Organics	MW212.4, 250ml, 99% pure, CAT#129822500

2.2 Characterization of Polymers and Fibers

2.2.1 Determination of Thermal Characteristics

2.2.1.1 Thermogravimetric Analysis

Thermogravimetric analysis (TGA) is a technique used to analyze the effect of thermal changes on a sample's mass. When this technique is used with polymer samples, it is possible to determine the amount of water or solvent in the polymer sample, the mass loss of the sample over a specific temperature range, and the final decomposition temperature of the polymer. In order to do this, a TGA instrument records the initial mass of a sample and then tracks the sample mass very closely over a previously determined heating scheme. Results are often plotted as a comparison of the mass of the sample as a percentage of the initial mass versus the temperature of the system. When the sample is held at a constant temperature, the thermogram can also show the mass percentage versus time. Any mass loss, whether it is due to solvent or water evaporation or polymer degradation, is seen as a downward step of the curve in both representations [84].

A Hi-Res TGA 2950 Thermogravimetric Analyzer was used to obtain the mass loss characteristics of the polymers used in these experiments. The polymers examined were 18

melt flow index (MFI) PP from Atofina, 400 MFI PP, and three polyester additives from Hexion Specialty Chemicals: LB-100, R-3000 NAJ, and Velvetol. Each polymer was evaluated using two temperature schemes: one designed to determine the ultimate degradation temperature of the polymer and a second scheme designed to analyze the mass loss of the polymer across temperatures normally experienced in a melt extruder.

For both temperature schemes, samples between 5 and 10 mg of the polymer were cut and placed into a clean platinum pan. The pan was loaded into the TGA and a the instrument was purged with nitrogen. Thermal Analysis software from TA Instruments, Inc. was used to control the temperature scheme of each experiment. Initially, the samples were heated from 30°C to 600°C at a rate of 20°C per minute and a nitrogen flow rate of 40 ml/min. The thermograms that resulted from these experiments showed the final degradation temperature of the polymer samples as well as any other large degradation or evaporation steps. Further experiments were conducted on new samples. These samples were heated from 30°C to 240°C at a rate of 20°C per minute and a nitrogen flow rate of 40 ml/min. This heating cycle was followed by an isothermal step which held the samples at 240°C for 45 minutes. The thermograms from these experiments detailed the mass loss of the samples when held at a constant temperature.

2.2.1.2 Differential Scanning Calorimetry

Differential scanning calorimetry (DSC) is often used to evaluate the thermal characteristics of polymer samples. When using DSC, it is possible to monitor chemicals reactions and physical changes if they are caused by changes in temperature. For this analysis, a sample is heated along with a reference under a nitrogen (or another similar inert gas) purge. The heat flows to the sample and the reference are monitored and used to calculate the heat capacity and temperature of the sample. The heat flow to the sample is plotted versus the temperature to give a differential thermogram that identifies phase transitions. In semi-crystalline polymers, it is often possible to see exothermic peaks for crystallization and endothermic peaks for melting. In cases where the polymer sample is not highly crys-

talline, a baseline shift that corresponds to the glass transition temperature (T_g) of the sample can be observed, indicating a change in the heat capacity of the sample [84].

A DSC 2920 Differential Scanning Calorimeter made by TA Instruments was used to analyze the polyester additives, the 18 MFI PP, the 400 MFI PP and any fibers extruded from these polymers. For the polymer chips, a small piece of the chip, between 5 and 10 mg, was placed into a DSC pan. For the fiber samples, the fibers were cut into small pieces and laid in parallel within the pan. The fiber samples averaged around 3 to 5 mg. Once the samples were sealed within the DSC pan, they were placed into the DSC chamber and the programmed temperature scheme was initiated. The samples were heated from -50°C to 220°C at a rate of 20°C per minute under a nitrogen flow rate of 40 ml/min. The samples were held at 220°C for one minute in an isothermal step while the DSC chamber was opened. The samples were removed from the chamber and quenched immediately on a bar previously cooled in liquid nitrogen. The thermograms resulting from these experiments gave information on the polymers in their as received state and on the fibers in their as spun state. Once the DSC sample chamber had cooled to room temperature, the quenched samples were reloaded and the same experiment was run a second time using the above heating regime. The second thermogram detailed the changes after erasing the thermal history of the samples.

A second analysis of the samples was conducted using a similar method to the one described above. The samples for this analysis were prepared in the same way and were heated from 0°C to 220°C at a rate of 20°C per minute under a nitrogen flow rate of 40 ml/min. At this point, instead of quenching the sample, the sample was left in the instrument and was cooled at a rate of 10°C per minute back to 0°C. The samples were reheated from 0°C to 220°C at a rate of 20°C per minute again. The thermogram resulting from this experiment revealed the crystallization peak of the sample upon cooling. The melting endotherms from the first and second heating cycles detailed the crystallinity of the sample prior to the cooling cycle and after.

2.2.2 Attenuated Total Reflection Infrared Spectroscopy

Fourier transform infrared (FTIR) spectroscopy uses radiation from the mid-infrared (IR) spectral region (from 4000 to 200 cm^{-1}) to excite the bonds within molecules. In order to absorb IR radiation, a molecule has to form a dipole moment as it vibrates or rotates. The molecule can then absorb the IR radiation if it is equal to either the vibrational or the rotational frequency of the molecule. The FTIR uses a Michelson Interferometer to analyze the energy beam after it passes through the sample. The interferometer produces an interferogram that is converted by a fourier transform to an IR spectrum for the sample. Attenuated total reflection infrared spectroscopy uses the same components as transmission FTIR, however instead of passing energy through the sample, the ATR attachment allows energy to be reflected off the surface of a material. The makes the ATR approach more effective for polymer samples as the material is difficult for FTIR absorption analysis. The resulting interferogram collected by reflecting the IR radiation off the polymer sample is converted by fourier transform to an IR spectrum. These spectra are used to analyze and sometimes identify the polymer [84].

The polyester additives used in this research were analyzed using a Thermo-Nicolet Magna 550 FTIR with an ATR accessory and Omnic software. A small chip of each sample was cut using a razor blade and placed onto the clean diamond window of the FTIR. The tower of the ATR accessory was lowered and tightened down on the sample and the sample spectrum was collected. A background spectrum was also collected and the final results for the scan were displayed. After the analysis was completed, ATR corrections were performed on the spectra to make them comparable to transmission FTIR spectra. Corrections were made to the baselines of the spectra to counteract the baseline shift caused by the ATR. The sample spectra were analyzed to determine the major peaks and were compared to other spectra in the software library in order to identify the sample based on its chemical make-up.

2.2.3 Contact Angle Measurements

2.2.3.1 Sample Preparation for Contact Angle Measurements

The three polyester additives from Hexion Specialty Chemicals were evaluated to determine their water contact angle. The polyesters were made into films using a Carver 60 Ton Economy Motorized Press and a rectangular mold that was used to shape the films. The rectangular areas of the mold were filled with approximately 1.5 g of polyester additive and the mold was placed between two metal plates. This plate-mold-plate setup was inserted into the Carver press and the instrument was set to 3000 PSI and a temperature of $140°C$. Although the pressure on the polymer samples was unknown, the conditions were sufficient to produce flat films (1cm x 4 cm x 0.2 cm) suitable for use in contact angle measurements. After five minutes, the temperature was reduced and the samples were removed and separated from the mold.

2.2.3.2 Measuring the Water Contact Angle

The contact angle (Θ) at which water and a polymer meet in air is determined by the triple interface of the liquid droplet, the solid polymer, and the gaseous air. The contact angle is determined by the angle measured between the tangent to the liquid's surface from the line of contact with the solid and the solid's surface [85]. If Θ is less than $90°$, the liquid is considered to wet the solid, whereas if Θ is greater than $90°$, the liquid does not wet the solid [85]. Contact angle is normally measured using a sessile drop, or a drop which sits on a flat surface. A photograph is taken of the triple interface of the droplet, solid, and air and later analyzed using software made for this purpose [85].

The contact angle of the prepared films was determined using a Krüss GmbH camera and Drop Shape Analysis software using the sessile drop method. A microsyringe was used to suspend a small droplet of water above the polyester film. The droplet was slowly lower until it came into contact with the film. The microsyringe was then retracted until it was no longer connected to the droplet. The droplet was allowed to rest for 30 seconds on the

surface of the film and then the angle of the droplet on the surface of the film was measured utilizing the camera and software.

2.3 Fiber Extrusion and Characterization

2.3.1 Extrusion of Polypropylene Fibers

All of the fibers used in this research were prepared using a Research Melt Extrusion Machine, Model REM-3P-24 constructed by Hills R & D, Inc. This extruder was equipped with a 1.0" screw with four heating zones. The melt pump capacities utilized during the course of this research were: 0.297 cc/rev, 0.584 cc/rev and 1.168 cc/rev. The capacity of the melt pump was taken into account when spinning and the drawing and winding speeds were adjusted accordingly.

2.3.1.1 Fiber Coding

The fibers produced and characterized in this research involved a large number of production variables. Although the major variable in the fibers was the shape, the blend of PP used to extrude the fibers also changed. The variables were shape, polymer blend, PP MFI, fiber size (DPF), hydrophilic additives in the polymer blend, and spin finishes placed onto the fiber. The large collection of variables involved in these experiments required that a coding system be developed to help the reader easily identify which fiber is being discussed.

The fibers were labeled to facilitate easy identification and recognition as shown in Figure 2.1. The first letter for each fiber designation represents the shape of the fiber, where H and Y are the corresponding cross-sections and R refers to round (conventional) fibers. The number following the first letter states the goal DPF for the fiber extrusion. Thus, all fibers designed to be 30 dpf are labeled with a 30, and 60, 90, 120, etc. correspond to 60 dpf, 90 dpf, 120 dpf and so on. The number following the hyphen designates the polymer mixture used as the base of the fiber. #1 represents a fiber spun from 100% 18 MFI PP, #2 represents a mixture of 90% 18 MFI PP and 10% 400 MFI PP, #3 represents a mixture

of 75% 18 MFI PP and 25% 400 MFI PP, and #5 represents a mixture of 50% 18 MFI PP and 50% 400 MFI PP. The final letter designates what additive or spin finish was added to the fiber. Fibers without a final letter represent the extruded fiber in its neat form - with no additives or spin finishes. An "S" shows that the fiber had the Bozetto Spin Finish Favorsol SF2 added to the surface of the fibers during extrusion and an "A" shows that 5% of polyester additive LB-100 was added w/w to the PP blend before extrusion. Tables 3.4, 3.5 and 3.6 list the label, shape, polymer blend, and spin finish or additive for each fiber.

Figure 2.1: An example of a fiber label
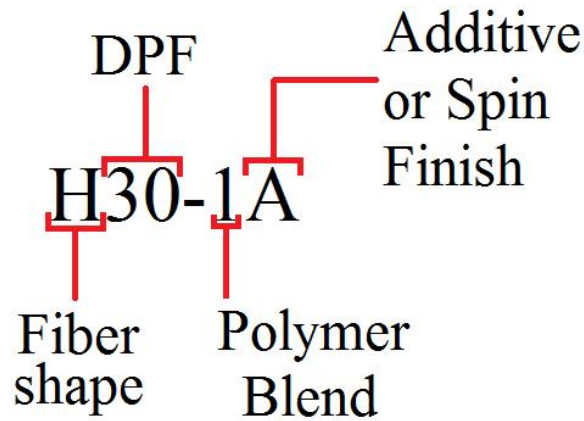
Table 2.2: Compositions of Round fibers

Label	Shape	Polymer Blend	Spin Finish
R30-1	Round	100% 18 MFI PP	none
R30-1S	Round	100% 18 MFI PP	SF2
R30-2	Round	90% 18 MFI PP, 10% 400 MFI PP	none
R30-2S	Round	90% 18 MFI PP, 10% 400 MFI PP	SF2
R30-3	Round	75% 18 MFI PP, 25% 400 MFI PP	none
R30-3S	Round	75% 18 MFI PP, 25% 400 MFI PP	SF2
R30-4	Round	50% 18 MFI PP, 50% 400 MFI PP	none
R30-4S	Round	50% 18 MFI PP, 50% 400 MFI PP	SF2
R60-1	Round	100% 18 MFI PP	none
R90-1	Round	100% 18 MFI PP	none
R120-1	Round	100% 18 MFI PP	none
R150-1	Round	100% 18 MFI PP	none
R180-1	Round	100% 18 MFI PP	none

Table 2.3: Compositions of Y fibers

Label	Shape	Polymer Blend	Spin Finish
Y30-1	Y	100% 18 MFI PP	none
Y30-1S	Y	100% 18 MFI PP	SF2
Y30-2	Y	90% 18 MFI PP, 10% 400 MFI PP	none
Y30-2S	Y	90% 18 MFI PP, 10% 400 MFI PP	SF2
Y30-3	Y	75% 18 MFI PP, 25% 400 MFI PP	none
Y30-3S	Y	75% 18 MFI PP, 25% 400 MFI PP	SF2
Y30-4	Y	50% 18 MFI PP, 50% 400 MFI PP	none
Y30-4S	Y	50% 18 MFI PP, 50% 400 MFI PP	SF2
Y60-1	Y	100% 18 MFI PP	none
Y90-1	Y	100% 18 MFI PP	none
Y120-1	Y	100% 18 MFI PP	none
Y150-1	Y	100% 18 MFI PP	none
Y180-1	Y	100% 18 MFI PP	none

Table 2.4: Compositions of H fibers

Label	Shape	Polymer Blend	Spin Finish
H30-1	H	100% 18 MFI PP	none
H30-1S	H	100% 18 MFI PP	SF2
H30-2	H	90% 18 MFI PP, 10% 400 MFI PP	none
H30-2S	H	90% 18 MFI PP, 10% 400 MFI PP	SF2
H30-3	H	75% 18 MFI PP, 25% 400 MFI PP	none
H30-3S	H	75% 18 MFI PP, 25% 400 MFI PP	SF2
H30-4	H	50% 18 MFI PP, 50% 400 MFI PP	none
H30-4S	H	50% 18 MFI PP, 50% 400 MFI PP	SF2
H30-1A	H	100% 18 MFI PP with 5% LB-100 w/w	none
H30-2A	H	90% 18 MFI PP, 10% 400 MFI PP with 5% LB-100 w/w	none
H30-3A	H	75% 18 MFI PP, 25% 400 MFI PP with 5% LB-100 w/w	none
H30-4A	H	50% 18 MFI PP, 50% 400 MFI PP with 5% LB-100 w/w	none

Table 2.5: Composition of the Octolobal fiber

Label	Shape	Polymer Blend	Spin Finish
O30-1	Octolobal	100% 18 MFI PP	none

31

2.3.1.2 18 MFI PP Fibers

PP fibers were extruded from Atofina chip with a MFI of 18. The chip was heated across the four extruder zones until it reached 240°C at the final zone. This temperature was maintained in the extruder spin head. The PP melt was extruded into three shapes from spinnerets: round fiber, fiber with an H cross-section, and fiber with a Y cross-section. Holes from each of these spinnerets are shown in Figure 2.2.

(a) Round spinneret hole

(b) Y spinneret hole

(c) H spinneret hole

(d) Octalobal spinneret hole
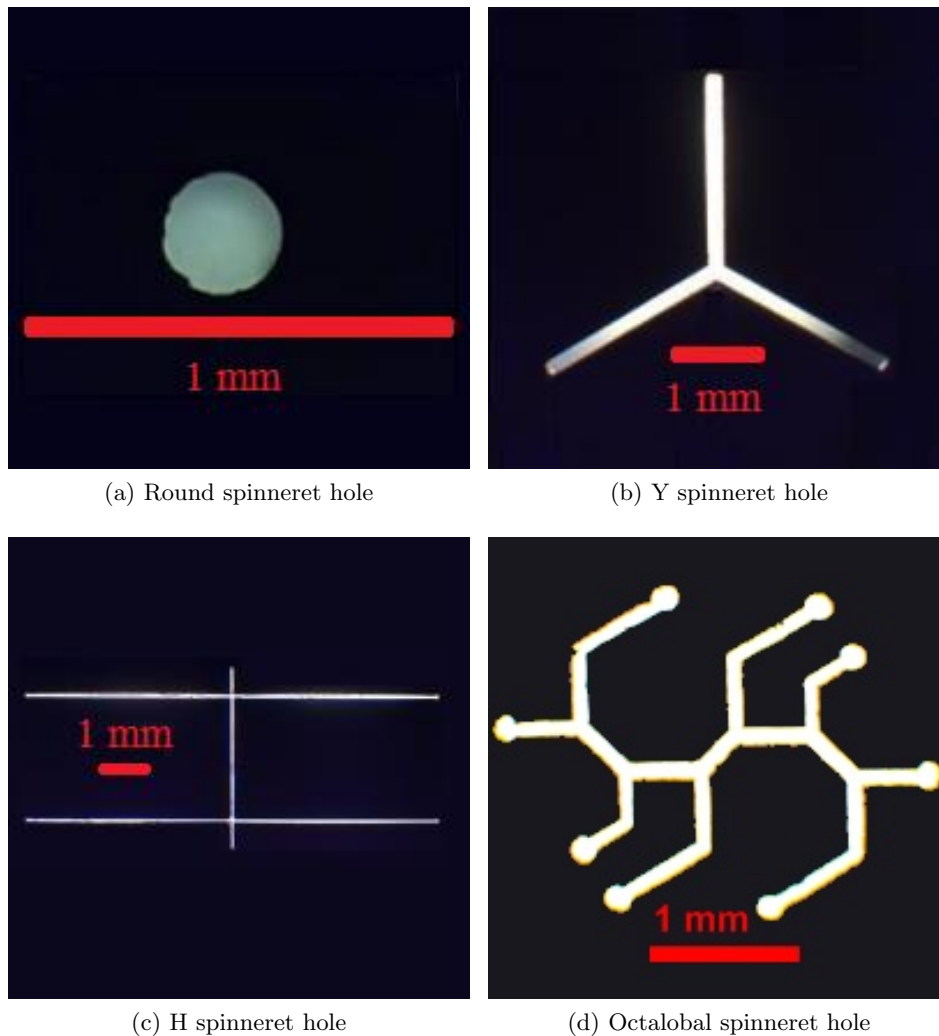
Figure 2.2: Round and shaped spinneret holes used in the production of fibers

Two spinnerets were utilized to produce the round fibers at the linear densities

required. The first spinneret had 27 holes and the second spinneret had 3 holes. The spinneret with 3 holes was used to produce fibers with larger filaments than was possible with the original 27 hole spinneret. The extrusion conditions for these fibers are located in Table 2.6. The spinneret for H fibers had 16 holes and the one for Y shaped fibers had 5 holes. The extrusion conditions for the Y fibers are located in Table 2.7 and the conditions for the H fibers are located in Table 2.8. The extruded fibers were collected onto a package using a Leesona Tension Winder. During extrusion, the initial fibers were collected without any spin finishes, but for some fibers, a second package was collected after a hydrophilic spin finish, Favorol SF2, was applied. The finish pump was a two stream Slack & Parr metering pump with 0.146 cc/rev/stream. The finish was applied at .584 cc/min for all fibers.

Table 2.6: Extruder profiles for round fibers with 100% 18 MFI PP

| Yarn | Polymer | No. of Filaments | Extruder (°C) | | | | Melt Pump | | Spin Line | | | | |
			Zone 1	Zone 2	Zone 3	Zone 4	Speed (rpm)	Capacity (cc/rev)	Spin Finish	Feed Roll (rpm)	Draw Roll (rpm)	Relax Roll (rpm)	Goal DPF
R30-1S	18 MFI PP	27	180	200	215	230	35.8	0.297	SF2	50	90	90	30
R30-1	18 MFI PP	27	180	200	215	230	35.8	0.297	N/A	50	90	90	30
R60-1	18 MFI PP	3	180	200	220	240	19.0	0.584	N/A	250	400	425	60
R90-1	18 MFI PP	3	180	200	220	240	19.0	0.584	N/A	200	250	295	90
R120-1	18 MFI PP	3	180	200	220	240	19.0	0.584	N/A	100	220	230	120
R150-1	18 MFI PP	3	180	200	220	240	19.0	0.584	N/A	100	165	170	150
R180-1	18 MFI PP	3	180	200	220	240	19.0	0.584	N/A	100	135	145	180

34

Table 2.7: Extruder profiles for Y fibers with 100% 18 MFI PP

| Yarn | Polymer | No. of Filaments | Extruder (°C) | | | | Melt Pump | | Spin Finish | Spin Line | | | |
			Zone 1	Zone 2	Zone 3	Zone 4	Speed (rpm)	Capacity (cc/rev)		Feed Roll (rpm)	Draw Roll (rpm)	Relax Roll (rpm)	Goal DPF
Y30-1S	18 MFI PP	5	180	200	215	230	35.8	0.297	SF2	275	450	500	30
Y30-1	18 MFI PP	5	180	200	215	230	35.8	0.297	N/A	275	450	500	30
Y30-1	18 MFI PP	5	180	200	215	230	9.0	1.168	N/A	275	480	530	30
Y60-1	18 MFI PP	5	180	220	230	240	9.1	1.168	N/A	150	240	245	60
Y90-1	18 MFI PP	5	180	220	230	240	9.1	1.168	N/A	100	150	162	90
Y120-1	18 MFI PP	5	180	220	230	240	9.1	1.168	N/A	70	120	123	120
Y150-1	18 MFI PP	5	180	220	230	240	9.1	1.168	N/A	50	90	100	150
Y180-1	18 MFI PP	5	180	220	230	240	9.1	1.168	N/A	50	90	95	180

Table 2.8: Extruder profiles for H shaped fibers with 100% 18 MFI PP

Yarn	Polymer	No. of Filaments	Extruder (°C)				Melt Pump		Spin Finish	Spin Line			Goal DPF
			Zone 1	Zone 2	Zone 3	Zone 4	Speed (rpm)	Capacity (cc/rev)		Feed Roll (rpm)	Draw Roll (rpm)	Relax Roll (rpm)	
H30-1S	18 MFI PP	16	180	205	230	250	35.8	0.297	SF2	70	110	150	30
H30-1S	18 MFI PP	16	180	205	230	250	8.9	1.168	SF2	70	110	150	30
H30-1	18 MFI PP	16	180	205	230	250	35.8	0.297	N/A	70	110	150	30

2.3.1.3 400 Melt Flow Index Polypropylene

Three different blends of the 18 MFI and 400 MFI PP were prepared for comparison with the fibers extruded from only 18 MFI PP. Blends were prepared on a weight by weight basis where the percentages of each polymer were determined based on the total combined weight of the polymers. The first blend was prepared from 90% of the 18 MFI PP and 10% of the 400 MFI PP by weight. The second blend was 75% of the 18 MFI PP and 25% of the 400 MFI PP by weight and the third blend was 50% of the 18 MFI and 50% of the 400 MFI by weight.

In order to make the fiber blends, each type of polymer was weighed out into a plastic bag. The bag was shaken until an even mixture was observed by eye and the polymer was placed into the extruder hopper. The extrusion conditions for the round fibers can be found in Table 2.9. The extrusion conditions for the Y shaped fibers and H shaped fibers can be found in Tables 2.10 and 2.11.

2.3.1.4 Hydrophilic Polyester Additives

Hydrophilic polyester additive LB-100 was incorporated into the PP fibers at a 5% weight by weight loading. The extrusion process was conducted as previously discussed. The extrusion profiles for these fibers are shown in Table 2.12.

Table 2.9: Extruder profiles for Round fibers with 18 and 400 MFI PP

Yarn	Polymer	No. of Filaments	Extruder (°C)				Melt Pump		Spin Finish	Spin Line			Goal DPF
			Zone 1	Zone 2	Zone 3	Zone 4	Speed (rpm)	Capacity (cc/rev)		Feed Roll (rpm)	Draw Roll (rpm)	Relax Roll (rpm)	
R30-2S	18 MFI PP, 400 MFI PP	27	180	200	215	225	35.8	0.297	SF2	60	90	90	30
R30-2	18 MFI PP, 400 MFI PP	27	180	200	215	225	35.8	0.297	N/A	60	90	90	30
R30-3S	18 MFI PP, 400 MFI PP	27	180	200	215	225	35.8	0.297	SF2	60	90	90	30
R30-3	18 MFI PP, 400 MFI PP	27	180	200	215	225	35.8	0.297	N/A	60	90	90	30
R30-4S	18 MFI PP, 400 MFI PP	27	180	200	215	225	35.8	0.297	SF2	60	90	90	30
R30-4	18 MFI PP, 400 MFI PP	27	180	200	215	225	35.8	0.297	N/A	60	90	90	30

Table 2.10: Extruder profiles for Y shaped fibers with 18 and 400 MFI PP

Yarn	Polymer	No. of Filaments	Extruder (°C)				Melt Pump		Spin Finish	Spin Line			
			Zone 1	Zone 2	Zone 3	Zone 4	Speed (rpm)	Capacity (cc/rev)		Feed Roll (rpm)	Draw Roll (rpm)	Relax Roll (rpm)	Goal DPF
Y30-2S	18 MFI PP, 400 MFI PP	5	180	200	215	225	35.8	0.297	SF2	275	460	510	30
Y30-2	18 MFI PP, 400 MFI PP	5	180	200	215	225	35.8	0.297	N/A	275	460	510	30
Y30-3S	18 MFI PP, 400 MFI PP	5	180	200	215	225	35.8	0.297	SF2	275	460	500	30
Y30-3	18 MFI PP, 400 MFI PP	5	180	200	215	225	35.8	0.297	N/A	275	460	500	30
Y30-4S	18 MFI PP, 400 MFI PP	5	180	200	215	225	35.8	0.297	SF2	275	460	500	30
Y30-4	18 MFI PP, 400 MFI PP	5	180	200	215	225	35.8	0.297	N/A	275	460	500	30

Table 2.11: Extruder profiles for H shaped fibers with 18 and 400 MFI PP

Yarn	Polymer	No. of Filaments	Extruder (°C)				Melt Pump		Spin Finish	Spin Line			Goal DPF
			Zone 1	Zone 2	Zone 3	Zone 4	Speed (rpm)	Capacity (cc/rev)		Feed Roll (rpm)	Draw Roll (rpm)	Relax Roll (rpm)	
H30-2S	18 MFI PP, 400 MFI PP	16	180	200	220	240	35.8	0.297	SF2	75	150	150	30
H30-2	18 MFI PP, 400 MFI PP	16	180	200	220	240	35.8	0.297	N/A	75	150	150	30
H30-3S	18 MFI PP, 400 MFI PP	16	180	200	220	230	35.8	0.297	SF2	77.5	155	155	30
H30-3	18 MFI PP, 400 MFI PP	16	180	200	220	230	35.8	0.297	N/A	77.5	155	155	30
H30-4S	18 MFI PP, 400 MFI PP	16	180	200	215	220	35.8	0.297	SF2	77.5	155	155	30
H30-4	18 MFI PP, 400 MFI PP	16	180	200	215	220	35.8	0.297	N/A	77.5	155	155	30

Table 2.12: Extruder profiles for H shaped fibers with hydrophilic polyester additives

Yarn	Polymer	No. of Filaments	Extruder (°C)				Melt Pump		Spin Finish	Spin Line			Goal DPF
			Zone 1	Zone 2	Zone 3	Zone 4	Speed (rpm)	Capacity (cc/rev)		Feed Roll (rpm)	Draw Roll (rpm)	Relax Roll (rpm)	
H30-1A	18 MFI PP, LB-100	16	180	205	230	245	35.8	0.297	N/A	75	130	150	30
H30-2A	18 MFI PP, 400 MFI PP, LB-100	16	180	200	220	240	35.8	0.297	N/A	70	100	140	30
H30-3A	18 MFI PP, 400 MFI PP, LB-100	16	180	200	220	235	35.8	0.297	N/A	77.5	135	155	30
H30-4A	18 MFI PP, 400 MFI PP, LB-100	16	180	200	215	220	35.8	0.297	N/A	77.5	135	155	30

2.4 Determination of the Linear Density of the Yarns

Each extruded fiber sample was weighed to determine its linear density. Three 100 meter skeins were prepared using a Yarn Reel from Industrial Laboratory Equipment Co. Inc. (model #ILE-5-SKRH-1M and serial #1192909). Each skein was weighed on a Sartorius BP221S balance to determine the mass. The mass was used to calculate the denier per filament (dpf) of each fiber sample according to Equation 2.1, where X is the weight in grams of an individual skein and Y is the number of filaments in the fiber sample. The average of the three measurements was used as the dpf of the fiber samples for all future calculations.

$$\text{dpf} = \frac{X \,\text{grams}}{9000\text{m} \times Y \,\text{filaments}} \tag{2.1}$$

2.5 Microscopic Examination of Fibers

2.5.1 Preparation of the Fiber Samples

Samples of each fiber were prepared for microscopic examination using a Beem Embedding Capsule as shown in Figure 2.3. LocTite Gel Control super glue was used to fill the hole at the bottom of the Beem capsule. The capsule was then filled with Low Viscosity Embedding Media. The embedding resin was prepared ahead of time for use with the samples by using the standard "firm" recipe as described in the instructions included with the resin kit.

A 10ml syringe with 20 gauge needle was used to completely fill the capsule containing the fiber sample with resin. The sample was then placed into a Sheldon Manufacturing, Inc. oven at 70°C for 8 hours to cure. Once cured, the sample was removed from the oven, the fiber secured to the stand was clipped with scissors, and the capsule was separated from the stand.

2.5.2   Microtoming of the Fiber Samples

Samples were microtomed using a Reichert-Jung Ultracut E Microtome. Once the resin sample was separated from the Beem capsule, it was placed into the holder of the microtome and the tip was sliced away by a glass blade in sections approximately 100 - 200 nanometers thick until a smooth surface was achieved.

2.5.3   Microscopy

Micrographs of the fiber cross-sections contained within the microtomed resin samples were taken using a Hitachi Scanning Electron Microscope (SEM) 3400. The resin sample was placed on an aluminum stand and a piece of copper tape was applied around the tip to reduce the charging of the sample by making it more conductive. The microscope was utilized in the variable pressure setting with a pressure of 30 Pa, a beam current of 20 kV, and a working distance of approximately 20 mm. These pressure and current settings were chosen to reduce the charging of the sample during viewing.

Figure 2.3: The stand and Beem capsule setup used to prepare microscope samples
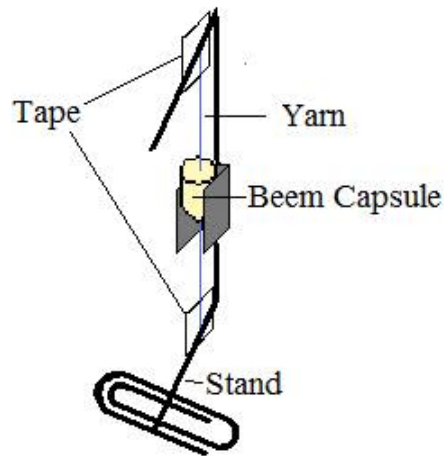
2.6   Analysis of Micrographs

The micrographs obtained from the SEM were analyzed using the Universal Desktop Ruler v3.0.1211 from AVPSoft.com. This program enabled the user to trace the outline of the fiber with connected short line segments and was first calibrated using the scale bar from the micrograph. The program used this scale to measure the perimeter and area of the enclosed section (in this case the fiber cross-section). The cross-sections of at least fifteen filaments were measured for each extruded fiber using the method described. The values for perimeter and area of the cross-section were recorded and an average value was reported for each fiber.

2.7   Oil Sorption Testing

2.7.1   Oil Analysis

Three oils were evaluated for possible use in research determining the oil sorption properties of the extruded fibers. The three oils were Canola Oil, Havoline 10W-40 Motor Oil and a 1:1:1:1 mixture of n-Tetradecane, Hexadecane, Heptadecane and n-Pentadecane. The canola oil was chosen because it is recommended by ASTM F-726 for a 'medium' oil type. Havoline 10W-40 was used because it was more viscous than the canola oil, and the 1:1:1:1 mixture of the four oils was used because it is listed as a Crude Oil standard by ASTM D5307 [86] and could be replicated exactly by other researchers. The 1:1:1:1 mixture of the four oils was prepared by combining equal weights of each oil.

2.7.1.1   Density of Oils

The density of the oils was determined using a 100 ml KIMAX USA volumetric flask. The flask was filled to the 100 ml mark and weighed. The mass of the flask was subtracted from the mass and the resulting mass of oil was used to determine the density. At least three measurements were made for each oil and the average was taken.

2.7.1.2   Viscosity of Oils

The viscosity of the oils was measured using a TA Instruments AR 2000 Advanced Rheometer. The "Steady State Flow" method was used with a cone geometry of 0.5° and a diameter of 60 mm. The gap size for the experiments was 14 µm as specified by the cone geometry. The viscosity was measured over a range of shear rates from 1 1/s to 100 1/s for the higher viscosity oils and from 1 1/s to 1000 1/s for the extremely low viscosity oil. The viscosity was measured on a log scale with four measurements made per decade. Measurements were accepted only if equilibrium had been reached. Equilibrium was defined as four consecutive readings where the percent change was less than 5%.

2.7.1.3   Surface Tension of Oils

The surface tension of a liquid is defined as the 'force per unit length acting on an imaginary line drawn in the surface' [85]. Surface tension is generally measured in N/m or mN/m. It can be measured using a pendant drop, or a drop that hangs from a surface. When measuring surface tension, the surface the drop hangs from is normally a syringe tip of known diameter. The force that adheres the drop to the surface of the syringe tip is the surface tension. When the drop becomes large enough, the force of gravity on the drop overcomes the surface tension and the drop will fall off the tip. While the drop is suspended from the tip, an image of the drop can be captured and analyzed using software designed for this purpose [85]. The surface tension of the oils was measured using a Drop Shape Analysis instrument with the pendant drop method. The instrument used a Krüss GmbH Camera, Model DSA10, and DSA for Windows 9x/NT4.0 Software which analyzed the pictures taken by the camera.

A microsyringe with a needle of 0.5 mm diameter was filled with the sample fluid. A small drop was carefully produced at the end of the needle, an image was captured, and an analysis was performed using the DSA software. The results reported for each drop included the volume of the drop in microliters, the area of the drop in the picture in micrometers squared, and the surface tension of the liquid in mN/m. At least 10 measurements were

made for each type of oil tested and the average was reported.

2.7.2 Sample Preparation for Oil Sorption

Packages of fiber prepared as described in Section 2.3.1 were wound off using a Fidelity Machine Company, Inc. yarn reel. The skeins of fiber were cut into 2 inch segments and separated by hand to limit mechanical binding at the tips. The cut fiber was conditioned for 24 hours at 23°C and 50% relative humidity. After conditioning, the fibers were placed in cages approximately 5 cm x 5 cm x 10 cm to allow for testing. Two types of cages were used, a Polypropylene Netting XN2950 cage and a Phifer Brite Aluminum Screening cage. The mass of each cage was determined using a balance. Each cage was filled with approximately 1 ± 0.01 g of fiber.

2.7.3 Oil Sorption - Short Test

The Oil Sorption - Short Test was performed as directed in ASTM F 726 section 9.3 with the exception that the sample sizes used were 1 g of material instead of 4 g and a 1L jar was used instead of a 4L jar. 1 gram of the caged pre-conditioned fiber was placed in a 1 L jar filled with the test oil. After 15 minutes, the fiber sample was removed from the jar and was drained for 30 seconds. The sample was weighed to determine the amount of oil adsorbed by the fiber. At least three samples were run on each fiber.

2.7.4 Dynamic Degradation Test

The Dynamic Degradation Test was performed as directed in ASTM F 726 section 9.2 with the exception that the sample sizes used were 1 g of material instead of 4 g and a 1L jar was used instead of a 4L jar. 1 gram of the caged pre-conditioned fiber was sealed in a 1 L jar with 500 grams of water inside. The jar was placed on its side in a Lab-Line Multi Wrist Shaker (model 3589 and serial #1002-1696). The jar was shaken at 150 rpms for 15 minutes. The contents of the jar were allowed to settle for 2 minutes and then the fiber was removed and drained for 30 seconds. The caged fiber sample was weighed to determine the

amount of water picked up by the fiber.

The same sample was then placed into a 1 L jar containing water and a designated amount of oil. Three different levels of oil were used for this test: 10 g, 20 g, and 30 g of oil in 500 g of water. At least three samples of each fiber type were tested for each oil amount. Once the caged fiber was sealed in the jar with the water and oil, the jar was placed on its side in the Lab Line Multi Wrist Shaker and shaken at 150 rpm for 15 minutes. The jar was then removed and the contents were allowed to settle for 2 minutes. The caged fiber sample was then removed from the jar and allowed to drain for 30 seconds. The sample was placed in a pre-weighed pan and the amount of water and oil adsorbed by the fiber was determined.

In order to remove the water from the sample and get an accurate measure of how much oil was adsorbed, the samples were placed in a Sheldon Manufacturing, Inc. oven for 48 hours at 75°C. As the fiber had been conditioned prior to the test, the samples were then returned to a conditioned room for 24 hours before a final mass was taken from the samples. This mass was used with the known mass of the fiber and cage to determine the amount of oil adsorbed by the fibers. The average of the samples tested for each fiber was reported.

2.8   Water Sorption Testing

2.8.1   Sample Preparation

Two sorption methods were used to compare the round fibers to the fibers with H cross-section and Y cross-section. Although the fibers were all approximately the same linear density, the differences in cross-sectional shape made comparison more complex. The first method employed involved the creation of samples with the same number of filaments. Due to the similar dpf, these samples also were approximately the same mass. The second method employed the inter-fiber capillary distance (D) created by Tennessee Eastman [30]. This factor is given by Equation 2.2 where SV is the specific volume of the sample in

cc/g, ρ_P is the density of the polymer, and P is the perimeter of the fiber cross-section as measured in Section 2.6. Three levels of D were used to compared the fibers: 50, 75, and 100 microns.

$$D = \frac{4\left(SV - \frac{1}{\rho_P}\right) \times dpf \times 10^3}{9P} \qquad (2.2)$$

Equation 2.2 was used to calculate the amount of fiber necessary for each sample by solving for the specific volume needed for the 50, 75 and 100 micron inter-fiber capillary distances. The volume of the sample tube used to contain the fiber was calculated using the diameter of the tube and the length of the tube plus one centimeter. The additional centimeter of length was used to allow the fiber inside the sample tube to contact the testing fluid without any interference from the tube. The amount of fiber needed to meet the desired specific volume was calculated and a skein of the appropriate amount of fiber was wound off on a skein winder.

Once the skein of fiber was prepared, a piece of metal wire approximately twice the length of the sample tubes was threaded through the center of the skein and folded in two. This metal wire was then used to pull the doubled skein through the pre-weighed sample tube. The metal wire was removed and the fiber was cut to within one centimeter of the desired sample length. The sample was then weighed and trimmed until the sample was within ±0.0100 g of the desired sample mass. The mass of the sample was recorded and the sample was labeled according to its inter-fiber capillary distance and its fiber shape.

2.8.2 First Insult Wicking

2.8.2.1 Short Samples

Samples were prepared as described in section 2.8.1 with sample tubes of 5 cm length and fiber of 6 cm lengths. A beaker of water with 0.25% dye was placed on the balance and a computer was connected to the balance. WinWedge$^{\text{TM}}$v3.4.0 Standard Edition software from TAL Technologies was used to record the mass of fluid on the balance every 500

milliseconds. The fiber sample was suspended vertically above the solution of fluid on the balance and the WinWedge^TMsoftware was initiated. The software was initiated and then the sample was lowered into the fluid so that approximately half a centimeter of fiber was below the surface of the fluid. The software recorded the reduction in the mass of fluid over the course of the test. This data was used to calculate the mass of fluid picked up by the fibers over the course of the test. The samples were normalized so that time = 0 seconds was the moment the fibers contacted the surface of the liquid.

2.8.2.2   Long Samples

Samples were prepared as described in section 2.8.1 with sample tubes of 20 cm length and fiber of 21 cm lengths. The samples were suspended vertically above a balance with the one centimeter of fiber that was not encased within the sample tube at the bottom of the sample. A beaker of water with 0.25% dye was placed on the balance and a computer was connected to the balance. WinWedge^TMv3.4.0 Standard Edition software from TAL Technologies was used to record the mass of fluid on the balance every 500 milliseconds. The recording software was started and then the sample suspended above the balance was slowly lowered until the fiber was approximately half a centimeter into the liquid. The sample was allowed to remain suspended in the liquid for 30 minutes. The fibers wicked fluid vertically from the balance, resulting in a decreasing mass of fluid. This decrease in the fluid mass was recorded by the software and was used to calculate the amount of fluid wicked upward. All of the fiber samples were normalized so that time = 0 seconds was the moment the fibers touched the liquid and began to draw fluid away from the balance. This point was determined as the initial decrease in the mass of the fluid.

2.8.3   Second Insult Wicking

A 40 cm long tube with an inner diameter of 3/8" was used for the second insult wicking tests. The samples for this experiment were prepared with a D of 50 microns. These samples were prepared by winding off the appropriate amount of yarn for each fiber sample

on the yarn reel. Each skein of fiber collected was in the form of a circle and was secured at one point with a piece of wire so that it would not unravel during preparation. After this, each skein was weighed on the Sartorius balance and cut to a length of 43 centimeters, which left it at a mass of approximately 3.5 grams. The skeins were rinsed in warm water until wet and then placed in a VWR Sonicator, Model 150HT, for 30 minutes at 60°C. The skeins were removed and drawn through the 40 cm lengths of clear vinyl tubing with a piece of metal wire. The end of the skein was then sliced open and the resulting sample was reweighed.

The samples prepared for wicking were placed in a stand which held them in a curved position with the ends a height of 13 cm apart. This stand was placed so that the lower end of the sample was over the balance. The higher end of the sample was then placed in a dish containing 300 ml of water with 0.025 ppm dye added for visibility. The timer for the test was begun once the upper end of the sample was placed in the dish of water. The test was run for 30 minutes and the amount of water dripped into the pan on the balance was recorded every 30 seconds.

2.8.4   Determination of Fluid Capacity of Fiber Bundles

Fiber samples were prepared in 5 cm long sample tubes. One end of the prepared fiber sample was placed into a beaker of water. The sample was held upright until water wicked to the top of the sample. The entire sample was then held underwater at an angle until no more air bubbles formed at the end of the sample. This method was used to try to minimize the amount of air trapped in the sample by the water wicking from both ends of the fiber. The sample was soaked in the water for two minutes before it was removed and allowed to drain so that excess water not trapped by the fibers could leave. The outside of the sample tube was dried with a cloth and the sample was weighed. The pre-determined mass of the tube and fibers was subtracted from the final mass of the sample to determine the amount of water retained by the sample.

Chapter 3

Results and Discussion: Polymer, Additive and Fiber Characterization

3.1 Rationale

The purpose of this research was to investigate the use of shaped fibers for fluid transport and sorption. Previous research on H fibers spun from 18 MFI PP and 35 MFI PP confirmed that the extrusion of shaped fibers was not as simple as the extrusion of conventional round fibers [87]. During the extrusion process three observations were made: the individual fibers did not maintain the shape of the spinneret holes, the fibers extruded from the lower MFI PP maintained better geometric shape retention relative to the spinneret design, and the temperature of the polymer melt affected the shape of the fibers. The extrusion of the shaped fibers for this research was conducted with the 18 MFI PP as it produced shapes that were more resemblant of the shaped spinneret holes. The temperature of the polymer melt could not be varied greatly without negatively influencing the spinnability of the PP, so an alternative method was required to lower the melt temperature of the polymer before it exited the spinneret. Independently controlled heating bands with

thermocouples near the spinneret face were implemented. The heating bands were set at a slightly lower temperature than that of the polymer melt, allowing the melt to cool by a few degrees immediately before exiting the spinneret. These two adjustments to the extrusion process improved the shape of the H fibers but still did not result in fibers with a higher level of geometric shape retention. Shape distortion of the fiber was still occurring as a result of unequal stresses across the fiber. The exterior surfaces of the H fiber cooled faster than the inner surfaces, increasing the stress across the fiber and distorting the shape as it cooled. This problem was addressed by Eastman in US Patent 5753166 by using additives to reduce the surface energy of the melt [20]. Eastman determined that the distortion of the shape was related to the melt viscosity–to–surface tension ratio and stated that adding silicone, silicone copolymer or fluoro-aliphatic polymeric ester would reduce the surface tension and thus improve the shape of the fiber. Although using these additives was effective, silicone has a detrimental effect on the burning behavior of polyester [88]. Also, reducing the surface energy of the fibers would cause increased hydrophobicity and thus would make water transport and sorption (one of the goals of this work) more difficult.

A personal communication from Dr. Brown and Dr. Stevens discussed the observation of a differential stress across a C shaped fiber during extrusion [89]. The researchers extruded a C shaped fiber from a low MFI PP. As the fiber cooled, the two tips of the C fiber would separate and the fiber would resemble a flat, twisted film instead of a C. To address this problem, Drs. Brown and Stevens added 400 MFI PP to the melt. They believed that because the higher MFI PP had a lower molecular weight, it would not experience the same stress as the original polymer. The higher MFI PP would be able to move to the surface of the fiber and alleviate the stress at the surface induced by the unequal cooling. The removal of the cooling stress would result in a higher geometric shape retention of the fiber as compared to the spinneret. Although this diffusion phenomenon could not be measured or observed in PP, it has been observed in polyester fibers [90]. Cyclic oligomers in poly(ethylene terephthalate) (PET) fibers were observed to diffuse to the surface of the fibers during heat treatment. The migration of the oligomers occurred rapidly and the

oligomers formed crystals on the surface of the fiber. The observed diffusion phenomenon in PET encouraged Drs. Brown and Stevens to use the higher MFI PP in their PP fibers. When the 400 MFI PP was added to the melt for the C fibers, a large improvement was seen in the geometric shape retention. By directing quench air at the center of the C shape, so that the inner surface of the C cooled first, a nearly perfect C shape was achieved near the spinneret and was maintained through the winding process. The results of their research prompted the use of 400 MFI PP in this project to improve the geometric shape retention of the H fibers.

The thermal characterization of the polymers and fibers used in this research was done to measure the effect of the 400 MFI PP on the fiber. Visual observation of the extruded H fibers confirmed that the 400 MFI PP improved the geometric shape retention. However, the effect of the 400 MFI PP on the fiber thermal properties was unknown. Analyzing the as received polymers and the as spun fibers made from blends of these polymers would reveal if the addition of the 400 MFI PP induced higher or lower crystallinity within the fibers or if it caused a shift in the melting temperature. A shift in the degree of crystallinity of the fiber may explain how the addition of 400 MFI PP improved the overall shape of the fibers. A thermal analysis of the extruded fibers would also reveal what effect the shape of the fiber had on its thermal properties, i.e. whether an H shape fiber was more crystalline than a round fiber or vice versa.

The final group of polymers analyzed during this research was the hydrophilic polyester additives from Hexion Specialty Chemicals. These polymers were investigated to determine if blending them with PP would result in hydrophilic PP fibers. The three polyesters were analyzed to determine if they were indeed spinnable with the 18 and 400 MFI PP blends or if they were going to degrade during extrusion. Analysis of the additives themselves helped to determine some of the functional groups within the polymers and to identify which was the most hydrophilic. Further thermal analysis of the fibers extruded with these additives would determine whether the additive was acting to suppress the crystallization of the PP or whether it had any effect on the thermal properties.

3.2 Thermal Examination of Polymers and Additives

3.2.1 Thermogravimetric Analysis (TGA)

3.2.1.1 18 and 400 MFI PP

The thermal properties of all of the polymers used in extruding fibers were examined to determine their resilience to the extrusion process. Although the 18 MFI PP is commonly used in extrusion, the 400 MFI PP had been used in a limited number of trials. Thermal analysis of both polymers would reveal whether the 400 MFI PP was as stable as the 18 MFI PP during extrusion, whether or not it could be extruded at the same temperatures, and whether it could be extruded in air or if it required a nitrogen purge. To determine the degradation temperature, each polymer was heated from 30°C to 600°C at a rate of 20°C per minute. This degradation was initially conducted under an air purge with a flow rate of 40 ml/min and then was repeated using a new sample under a nitrogen purge with a flow rate of 40 ml/min. While the polymers were not extruded under a nitrogen purge, the amount of contact the polymer melt had with air was minimized by the design of the extruder screw.

Although the degradation of the samples would determine whether or not the 400 MFI PP would be stable at the normal extrusion temperature for 18 MFI PP, it would not determine its stability when held at that temperature for a long period of time. Any polymer used in extrusion would be rapidly heated to a temperature above the melting temperature of the polymer and would then dwell in the extruder screw until it was forced through the spinneret. The thermal stability of the polymers when held at the final extrusion temperature for an extended dwell time was determined with TGA. These polymer samples were heated from 30°C to 240°C at a rate of 20°C per minute and then were maintained at 240°C for 40 minutes. These samples were initially evaluated under an air purge and a new sample was evaluated using a nitrogen purge. The stability of the 400 MFI PP under this scheme determined if it could be extruded with the 18 MFI PP or if it would degrade in the screw during extrusion.
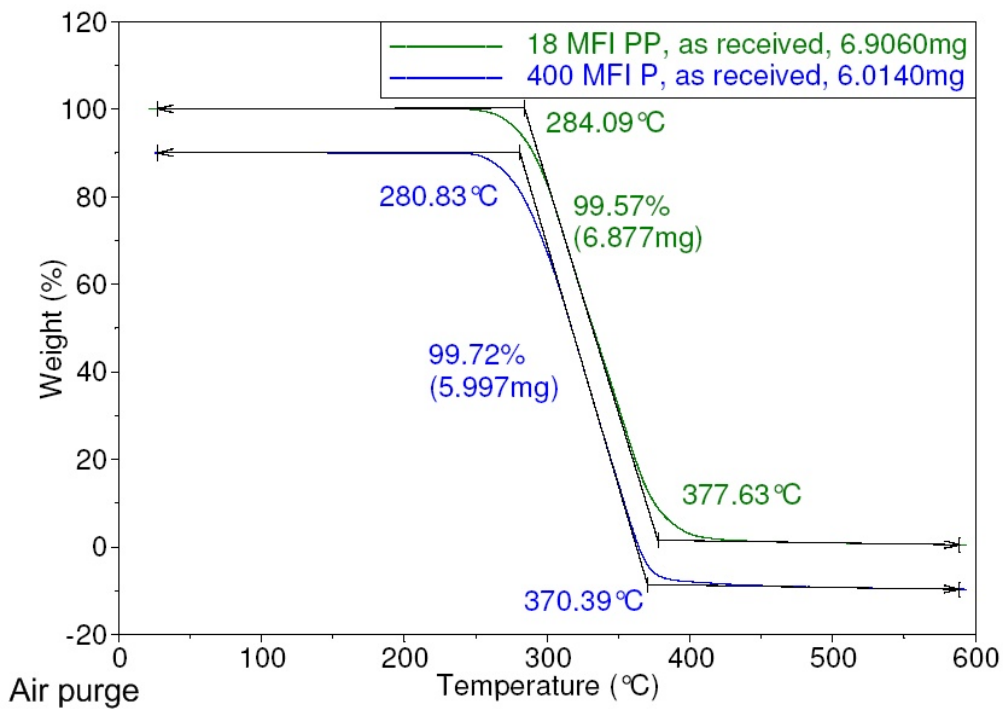
Figure 3.1: Degradation of 18 MFI and 400 MFI PP under air purge
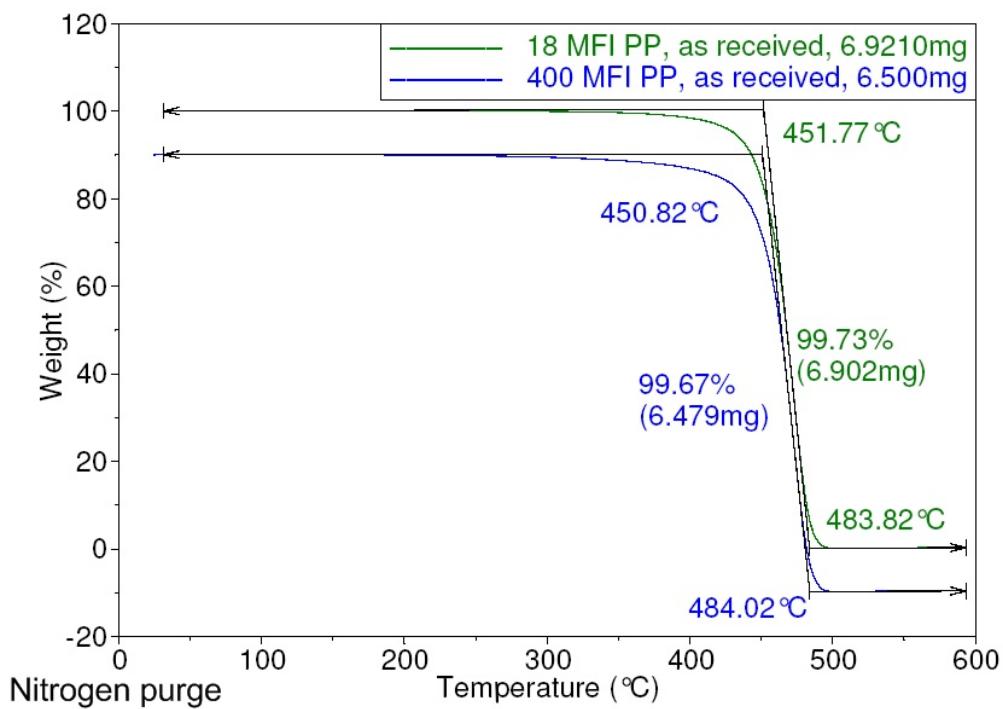
Figure 3.2: Degradation of 18 MFI and 400 MFI PP under nitrogen purge

Figure 3.1 shows the degradation of 18 MFI PP and 400 MFI PP under an air purge. The line representing the degradation of 400 MFI PP was offset to facilitate reading of the thermogram. The degradation of the polymers was analyzed using TA Universal Analysis software. Under an air purge, the major degradation step of the 18 MFI PP occurred with an extrapolated onset temperature of 284°C and an extrapolated offset temperature of 378°C. This degradation step accounted for the loss of 99.6% of the polymer sample. The 400 MFI PP degraded at a slightly lower extrapolated onset temperature of 281°C and extrapolated offset temperature of 370°C. The sample lost 99.7% of its sample mass in this degradation step. The slightly lower extrapolated onset and offset temperatures for the 400 MFI PP were likely related to the shorter chain length of the PP chains within the sample compared to that of the 18 MFI PP sample. The thermogram showed that the two PPs began degrading approximately 40°C above the typical extrusion temperature of PP in air. This indicated that the polymers were suitable for extrusion under an atmosphere of air.

Figure 3.2 shows the same two polymers, 18 MFI PP and 400 MFI PP, degrading under a nitrogen purge. In this environment, the 18 MFI PP had an extrapolated degradation onset temperature of 452°C, an extrapolated degradation offset temperature of 484°C and a mass loss of 99.7% of the original sample weight. The 400 MFI PP experienced an extrapolated degradation onset temperature of 451°C, an extrapolated degradation offset temperature of 484°C and a mass loss of 99.7%. For both polymers, a nitrogen purge raised the degradation temperature of the sample by approximately 170°C. The mass loss of the original sample weight was essentially the same for both polymers under nitrogen and air purges; however, the degradation occurred at a much higher temperature under a nitrogen purge than under an air purge. If the degradation temperature of the two polymers had been too low under an air purge, running the polymers in the extruder under a nitrogen purge would have raised the degradation temperature of the polymers to a sufficient level for extrusion.

The second temperature scheme was designed to emulate the dwell time and temperature that the polymer would experience during extrusion. This emulation did not re-

produce the rapid heating of the polymer in the extruder, however the polymer was held at the extrusion temperature for a reasonable residence time. For the purpose of this research, the PP chip was extruded at 240°C and passed through the extruder after approximately 30 minutes. The TGA scheme heated the polymer from 30°C to 240°C and maintained this temperature for 45 minutes in emulation of the extrusion process. The degradation of the polymer samples over this time period was recorded and analyzed. The amount of degradation and percent mass loss of the samples were used to determine if the 400 MFI PP was suitable for spinning with the 18 MFI PP at these temperatures.

In Figure 3.3, the degradation of the polymers under an air purge was plotted against the time. The temperature of the instrument, represented by the red line on the thermogram, reached 240°C in approximately 10 minutes and then stayed at that temperature for the remainder of the run. The line representative of the 400 MFI PP sample was offset within the figure to increase the readability of the thermogram. Under an air purge, the 18 MFI PP sample experienced a weight loss of 67.2% during the time it was held at 240°C. The 400 MFI PP experienced a weight loss of 75.9% of its original sample weight. This indicated that in an open air system, the polymer would not be spinnable at all. Although there is air within an extruder screw, the screw barrel is only open to air at the hopper where the chip is loaded. Beyond the hopper, the extruder screw does not have any areas open to the air until the polymer exits the spinneret. The polymer is open to the air at the throat of the extruder, but the temperature of the first extruder heating zone was only 180°C. The extrusion temperature was reached at the final extruder heating zone, where very little air was present. The ability of the polymers to be spun indicates that there is minimal air in the screw and the polymers do not degrade in the screw as much as was indicated by the thermal analysis under air.

To determine if the polymers degraded to the same extent in an atmosphere with less air, the same heating regime was conducted under a nitrogen purge. Figure 3.4 shows the stability of the 18 MFI PP and 400 MFI PP under a nitrogen purge. As in Figure 3.3, the red line indicates the temperature of the instrument and the results for the 400 MFI

57
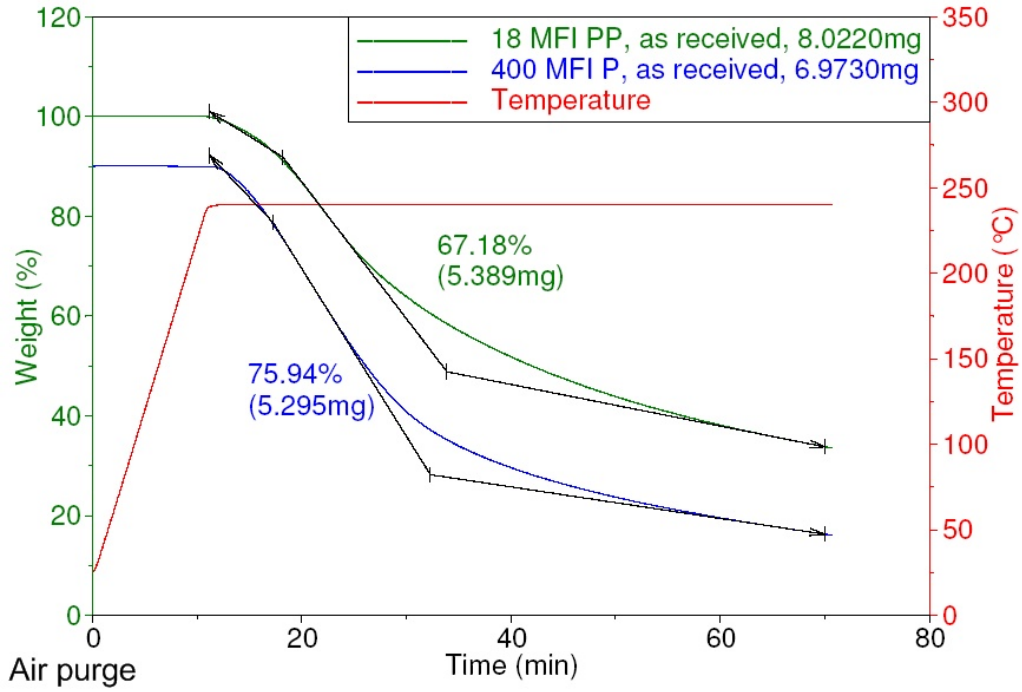
Figure 3.3: Degradation of 18 MFI and 400 MFI PP during an isothermal evaluation at 240°C under air purge
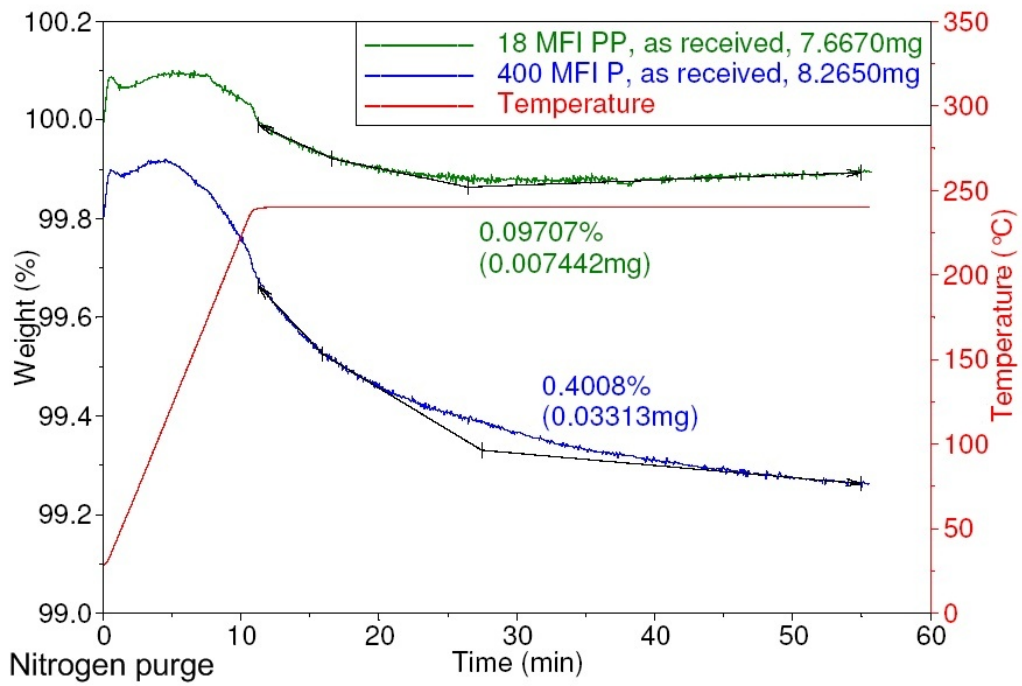
Figure 3.4: Degradation of 18 MFI and 400 MFI PP during an isothermal evaluation at 240°C under nitrogen purge

PP sample have been offset to improve readability. Under a nitrogen purge, the 18 MFI PP had a mass loss of 0.0971%, much less than the previous degradation of 67.2% under an air purge. Similarly, the 400 MFI PP had a mass loss of 0.401% under a nitrogen purge, which was much lower than its loss of 75.9% under an air purge. The lack of degradation in a nitrogen atmosphere showed that when the polymers were not exposed to air, they did not degrade as readily.

3.2.1.2 Polyester Additives

The same two heating regimens were used to analyze the spinnability of the three hydrophilic polyester additives from Hexion Chemicals: LB-100, R-3000 NAJ and Velvetol. These regimens were conducted under an air purge and a second time under a nitrogen purge. Very little information was available about the structure and properties of the polyester additives. The degradation temperature for these polyester additives was important in determining their spinnability with PP. Also, the weight loss during an extended dwell at 240°C would determine whether or not the polymers would survive the extrusion process. A large amount of weight loss during the extrusion process would result in a build up of degraded polymer, oligomer or other components within the extruder screw. Any build up could cause the extrusion process to fail. Also, if the polyester additives degraded within the screw, they would not be found in the final fiber product.

Figure 3.5 shows the degradation of the three polyester additives under an air purge. The degradation occurring from room temperature to 240°C is enlarged and shown in Figure 3.6. Under air, the LB-100 sample degraded 92.6% with an extrapolated onset degradation temperature of 369.1°C. The R-3000 NAJ sample degraded 88.8% with an extrapolated onset of degradation of 398.9°C. The Velvetol sample degraded 97.3% with an extrapolated onset temperature of 289.5°C. From room temperature to 240°C, the LB-100, R-3000 NAJ and Velvetol lost 1.42%, 0.500% and 2.01% of the initial sample weight respectively.

Figure 3.7 depicts the degradation of the three polyester additives under nitrogen.

59

Figure 3.5: Degradation of polyester additives LB-100, R-3000 NAJ and Velvetol at a heating rate of 20°C/min under an air purge of 40 ml/min

Figure 3.6: Enhanced region from Figure 3.5: Degradation of polyester additives LB-100, R-3000 NAJ and Velvetol, weight loss analyzed at 240°C

The degradation occurring from room temperature to 240°C is shown in Figure 3.8. Under nitrogen, the LB-100 sample degraded 84.8% with an extrapolated onset degradation temperature of 412.1°C. The R-3000 NAJ sample degraded 81.9% with an extrapolated onset of degradation of 415.0°C. The Velvetol sample degraded 96.9% with an extrapolated onset temperature of 395.8°C. From room temperature to 240°C, the LB-100, R-3000 NAJ and Velvetol lost 1.12%, 0.546% and 0.435% of the initial sample weight respectively.

The three polyester additives were also subjected to the second TGA scheme emulating the dwell time of a normal extrusion process. This procedure heated the samples from 30°C to 240°C and then held the samples at 240°C for 45 minutes. The procedure was conducted both under an atmosphere of air and and later an atmosphere of nitrogen. The degradation occurring under air is shown in Figure 3.9 and the degradation occurring under nitrogen in Figure 3.10. In Figures 3.9 and 3.10 the curves representing the R-3000 NAJ and Velvetol samples were offset from the LB-100 sample by approximately 10% and 20% in Figure 3.9 and and by 1% and 2% in Figure 3.10 to enhance the readability of the thermogram. During the isothermal step at 240°C, the LB-100 sample experienced a loss of 2.77% of its original weight under air and a loss of 0.346% under nitrogen. The R-3000 NAJ sample lost 4.94% of its weight under air and 0.163% under nitrogen. The Velvetol sample experienced a loss of 44.0% of its original mass under air and a loss of 0.336% under nitrogen. The significant weight loss of Velvetol under air but not under nitrogen indicates that for this additive it may be preferable to perform extrusion under a nitrogen purge.

As expected, all the three polyester additives degraded less under a nitrogen atmosphere. Two polymer samples, LB-100 and R-3000 NAJ, did not degrade extensively in air which indicated it may be possible to extrude these additives under air. Typically, the addition of the additive to a fiber extrusion process occurs at only a few percent. At this loading, the slight degradation of the LB-100 and R-3000 NAJ samples as seen by Figure 3.9 suggests that the spinnability of the PP would not be affected.
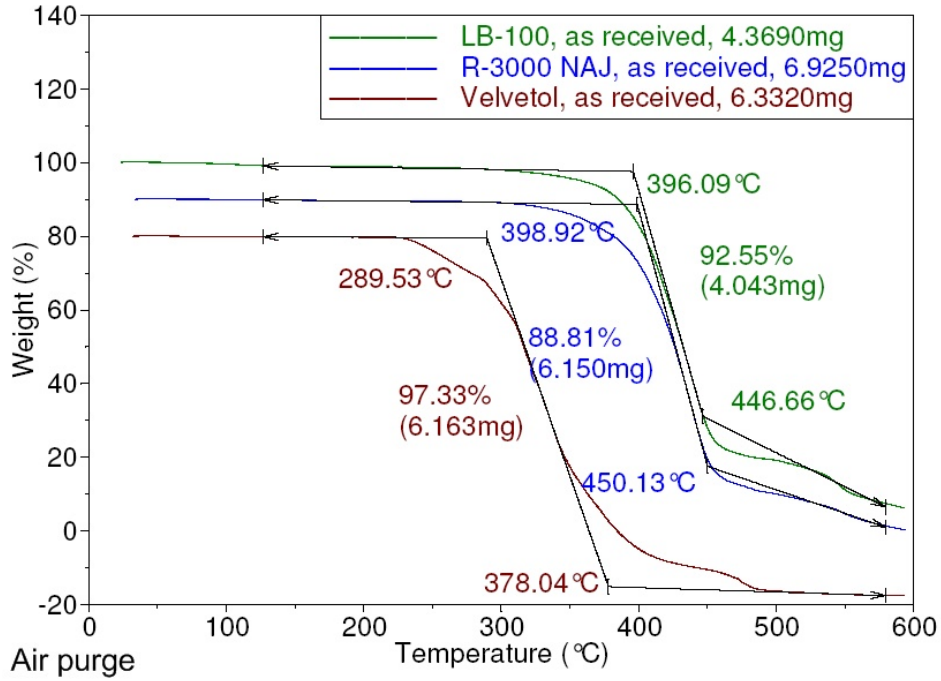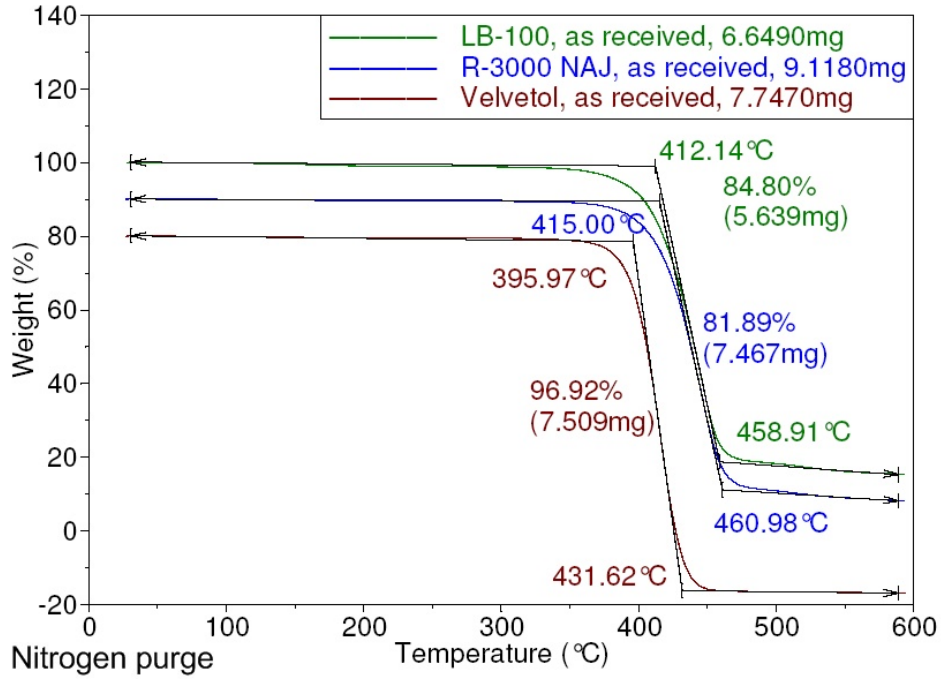
Figure 3.7: Degradation of polyester additives LB-100, R-3000 NAJ and Velvetol at a heating rate of 20°C/min under an nitrogen purge of 40 ml/min
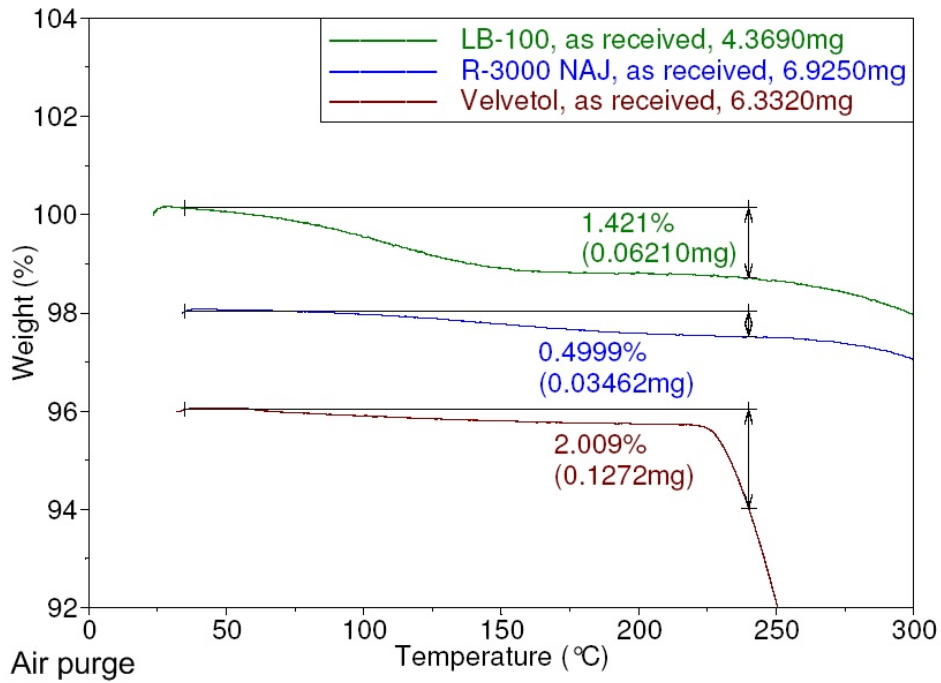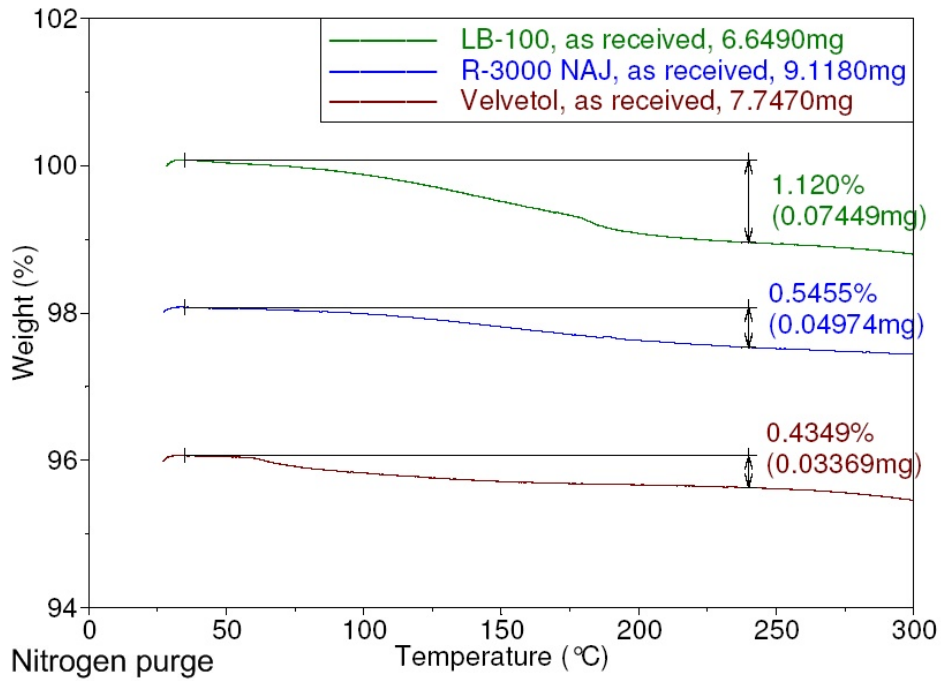

Figure 3.8: Enhanced region from Figure 3.7: Degradation of polyester additives LB-100, R-3000 NAJ and Velvetol, weight loss analyzed at 240°C
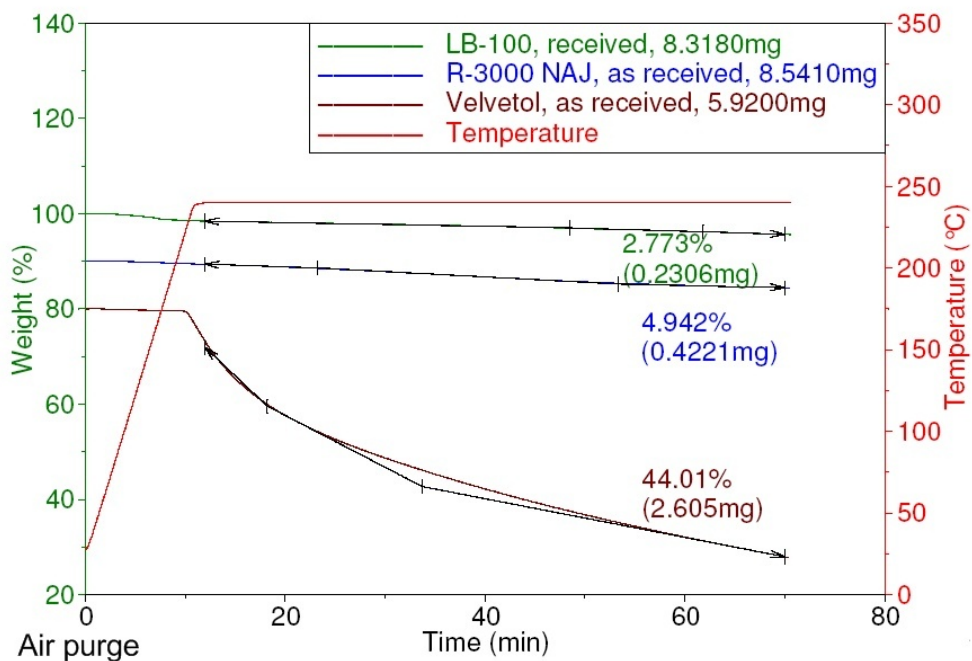
Figure 3.9: Degradation of Polyester Additives LB-100, R-3000 NAJ and Velvetol at 240°C with an air purge of 40 ml/min
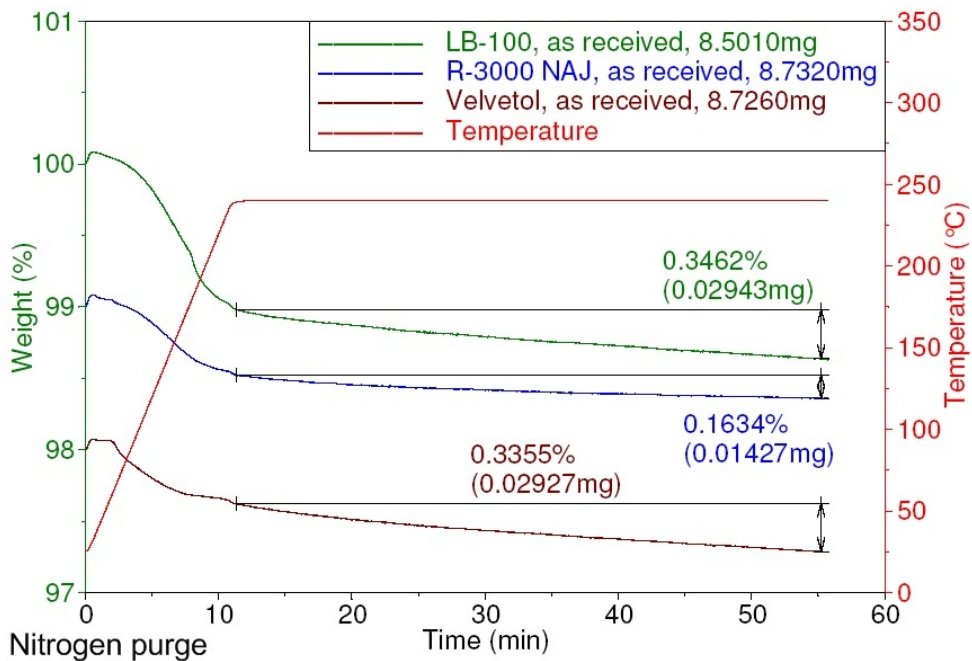
Figure 3.10: Degradation of Polyester Additives LB-100, R-3000 NAJ and Velvetol at 240°C with a nitrogen purge of 40 ml/min

3.2.2 Differential Scanning Calorimetry (DSC)

A small chip of each of the polymers and additives used in extrusion was evaluated using the TA Instruments DSC 2920 Differential Scanning Calorimeter and the procedure described in Chapter 2. The polymers were analyzed to determine their thermal properties such as melting and glass transition temperatures and the percent crystallinity of the polymers in their as received form. This information was compared to the thermal properties of the spun fibers to determine if the extrusion process or polymer blending changed any of the thermal properties.

The first run of the DSC on a polymer sample characterized the physical aging the polymer experienced. The goal of quenching and rerunning samples was to remove the thermal history of the polymers and additives. However, PP can crystallize between the time the sample is removed from the DSC and the time it is placed on the liquid nitrogen cooled iron bar. This resulted in both the as received samples and the post quench samples having a similar level of crystallinity. The crystallinity of a sample was determined using the equation given by Nielsen, et. al [91]

$$\chi^c = \frac{H}{H_0} \frac{\rho^a}{\rho^c} \left[1 - \left(1 - \frac{\rho^a}{\rho^c} \right) \right] \tag{3.1}$$

where χ^c is the crystallinity of the polymer, H is the measured heat of fusion, H_0 is the theoretical heat of fusion for a 100% crystalline polymer, ρ^a is the density of the amorphous sections of the polymer (0.85 g/cm^3) and ρ^c is the density of the crystalline sections (0.936 g/cm^3). The theoretical heat of fusion for PP was taken to be 165 J/g for this work [92].

3.2.2.1 18 and 400 MFI PP

DSC analysis of as received and post quench 18 MFI PP and 400 MFI PP samples are shown in Figures 3.11 and 3.12. The samples were heated at a rate of 20°C per minute under a nitrogen purge from -50°C to 240°C at which point they were quenched and the

heating sequence was repeated. The thermograms representing the quenched samples were offset so the two curves could be easily distinguished. Interpretation of the thermograms is shown in Table 3.1.

Table 3.1: Peak melting temperatures, enthalpies of melting, and calculated percent crystallinities for the as received and post quench samples of 18 MFI PP and 400 MFI PP

Sample	T_m (°C)	H_m (J/g)	χ_c
18 MFI PP, as received	167.7	84.8	42%
18 MFI PP, post quench	163.7	79.8	40%
400 MFI PP, as received	165.0	74.9	37%
400 MFI PP, post quench	165.6	82.7	41%

Although the melting peaks of both the 18 MFI and 400 MFI pp were visible during DSC evaluation, the glass transition temperature (T_g) of the polymers was not. The Polymer Handbook [93] lists the T_g of PP as occurring around -17°C. The DSC, however, was not sensitive enough to detect this transition in PP. The DSC measures the change in the heat capacity of a material and the change in the heat capacity of the PP at the T_g is not significant enough for the DSC to detect.

As presented in Figure 3.11, Figure 3.12 and Table 3.1 the peak melting temperatures and melting enthalpies for the 18 MFI PP and 400 MFI PP were very similar at 167.6°C and 84.8 J/g and 165.0°C and 74.9 J/g respectively. The percent crystallinity was calculated using Equation 3.1 and is shown in Table 3.1. After the samples were quenched, there appeared to be a slight change in peak melting temperature and crystallinity, but these differences were not significant. As previously mentioned, PP cannot be quenched to an amorphous state as exhibited by both the 18 MFI PP which is conventionally used in fiber extrusion and by the 400 MFI PP which is more novel.

Although crystallization occurred between the time the 400 MFI PP sample was removed from the instrument and when it was quenched, a small exothermic peak was also visible on the post quench curve of Figure 3.12. This exothermic peak was thought to be due to a small amount of crystallization of the sample; however, due to the peak broadness,
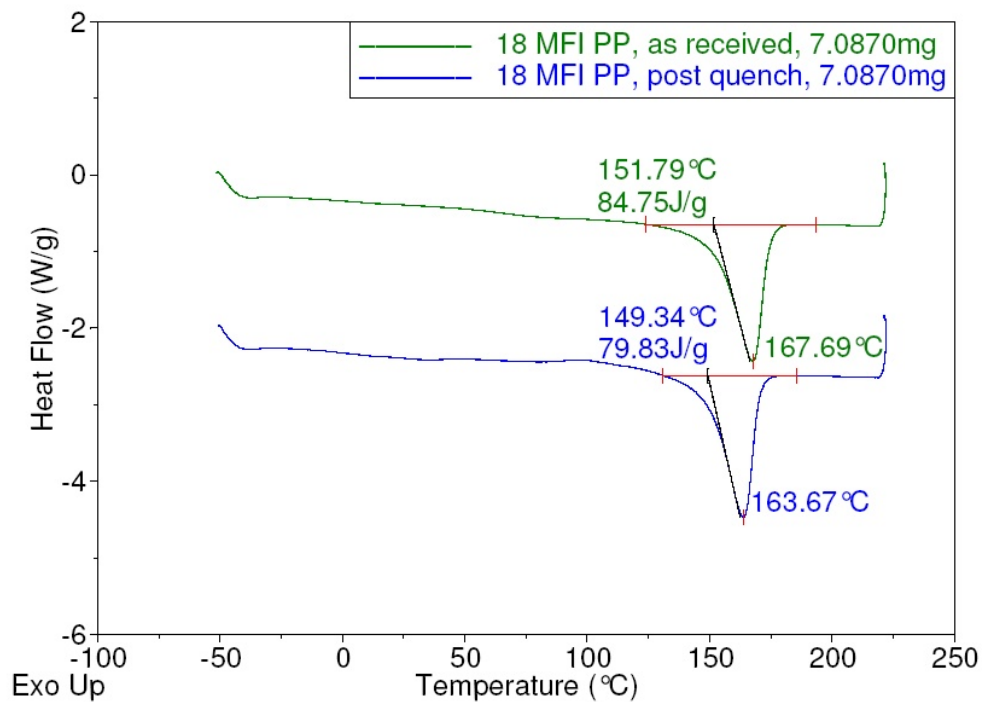
Figure 3.11: Thermal analysis of 18 MFI PP before and after quenching
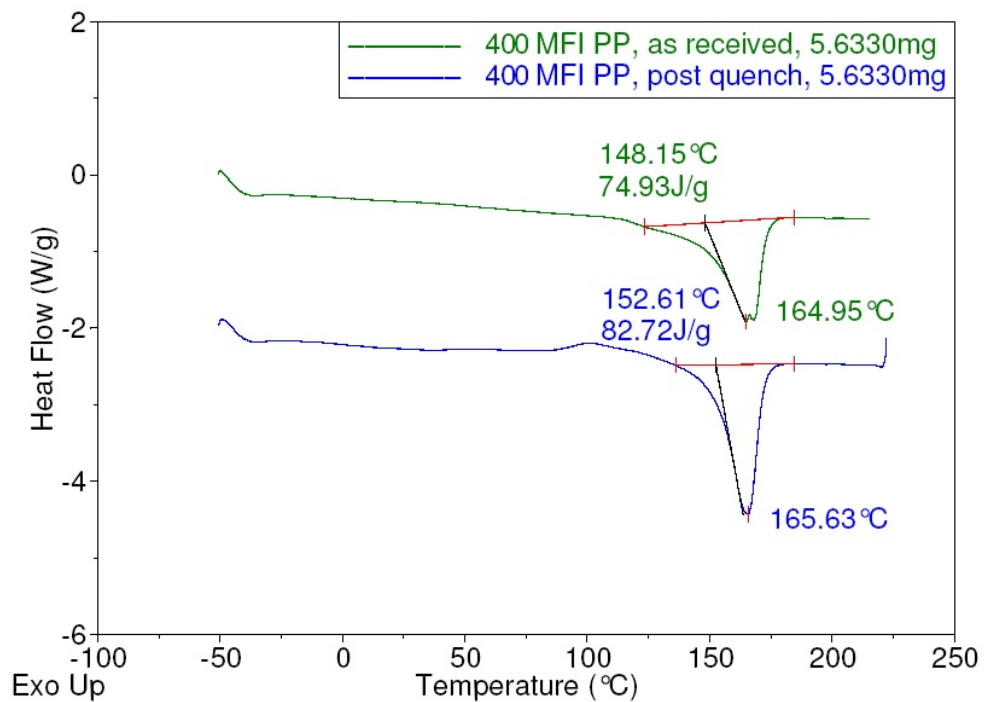
Figure 3.12: Thermal analysis of 400 MFI pp before and after quenching

this peak was difficult to resolve.

3.2.2.2 Polyester Additives

The three polyester additives were also tested using the TA Instruments DSC. The thermal analysis of the as received polyester additive LB-100 revealed a T_g with a considerable physical aging peak in Figure 3.13. A small melting endotherm was observed at a peak temperature of 158.4°C and an enthalpy of melting of 0.778 J/g. This small peak did not show up on the post quench of the sample, indicating that the quenching step had successfully frozen the polymer in an amorphous state and the heating regime used was not sufficient to recrystallize the material. On the quench rerun, the T_g had an inflection point of 37.86°C. The pre-quenched polymer sample showed a large physical aging peak immediately after the T_g that was not visible during the second run. Although the mobility of polymer chains below T_g is small, it is not zero [94]. Thus, given sufficient time, the chains within the polymer relax, even below T_g. When the polymer is heated above T_g, thermodynamic equilibrium is reached and the history or relaxation of the polymer is erased [94].

Unlike the LB-100 polyester additive, the as received R-3000 NAJ sample did not experience a melting peak during thermal testing. The thermogram for the as received and post quench samples is shown in Figure 3.14. The lack of a melting peak showed that the polymer was largely amorphous in its chip form. A distinctive T_g did appear on both the first run of the R-3000 NAJ sample and on the second, post-quenched run. The as received polymer sample also showed a large physical aging peak immediately following the T_g. The presence of this peak indicated that the polymer chains changed configuration over time even though they were above their T_g. The extrapolated midpoint of the T_g for the as received sample was 60.24°C. For the post quench sample, the T_g was extrapolated at 54.23°C. The shift in the T_g was explainable by the effect of the aging peak on the analysis of the T_g of the as received sample. The inflection points of the T_g portion of the curve were measured in the aging peak instead of on the curve baseline. This increased the
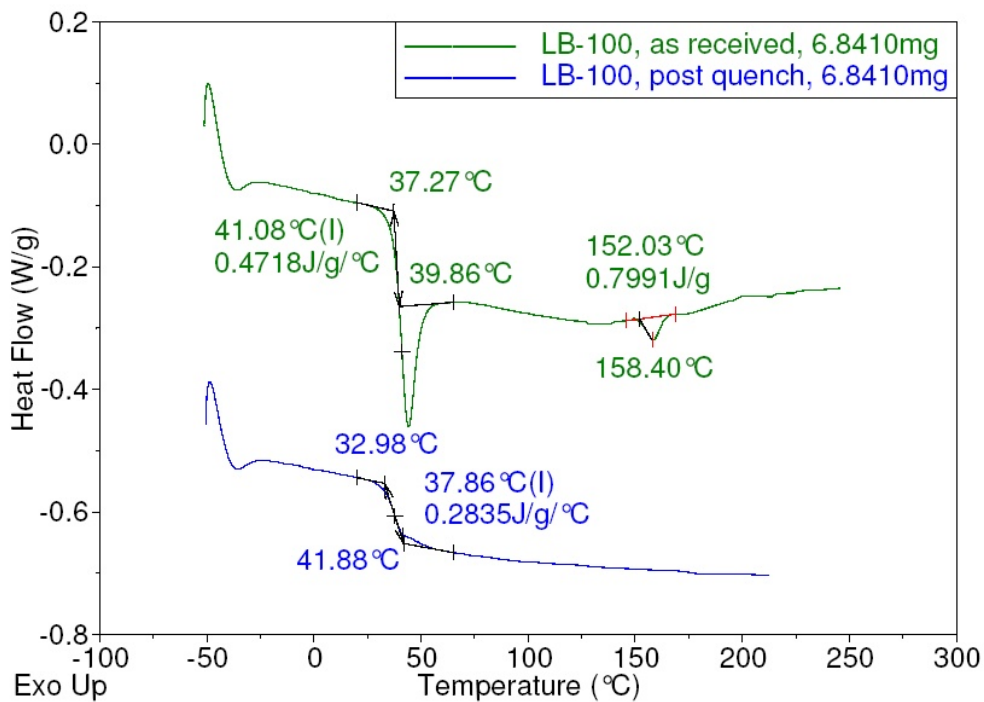
Figure 3.13: Thermal analysis of polyester additive LB-100 before and after quenching
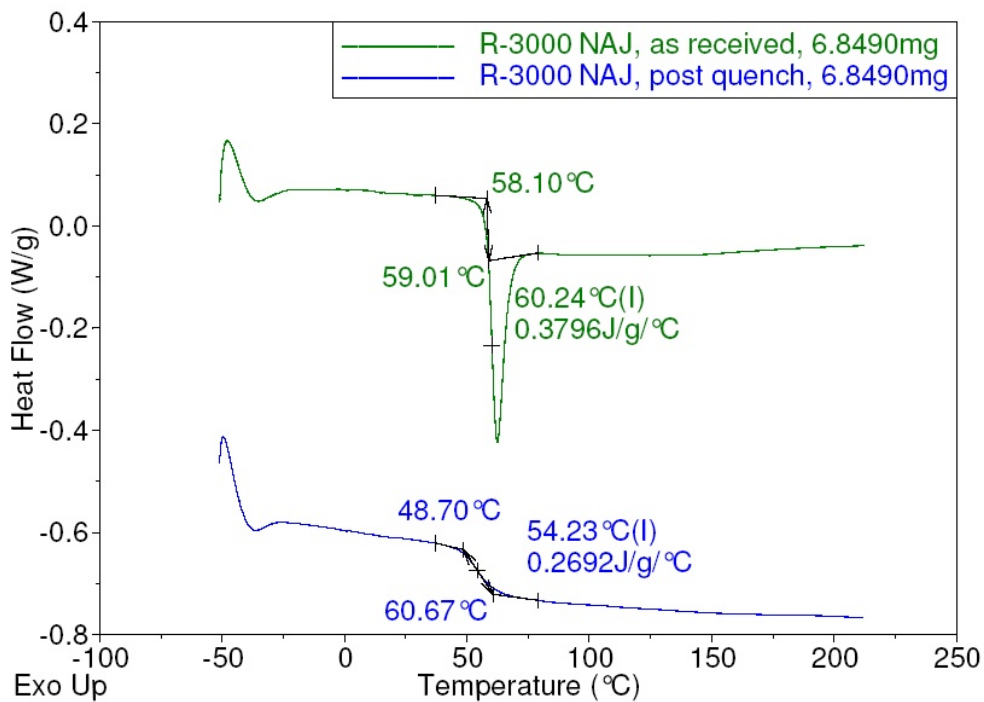
Figure 3.14: Thermal analysis of polyester additive R-3000 NAJ before and after quenching

extrapolated midpoint of the T_g.

The thermal characterization of the final hydrophilic polyester additive, Velvetol, is shown in Figure 3.15. Of the previous polyester additives, LB-100 experienced both a T_g and a melting peak while the R-3000 NAJ sample only showed a T_g. Velvetol was unlike either of these samples as it did not undergo any T_g during the DSC experiments. Instead, the only major thermal change in the sample was a melting peak that occurred for both the as received sample and the post quench sample. The as received sample had a peak melting temperature of 54.57°C and an enthalpy of melting of 111 J/g. The post quench sample had a peak melting temperature of 48.01°C and an enthalpy of melting of 82.3 J/g. As the sample was quenched and no crystallization peak was observed on the post quench thermogram, the sample must have undergone some crystallization between the time it was removed from the instrument and when it was placed on the bar cooled with liquid nitrogen. The decreased melting temperature and enthalpy of melting indicated that the crystals that formed within the post quench sample were different in size and perfection from the as received sample. Since the polyester additive was of unknown structure, the theoretical H_m of the Velvetol could not be determined and thus no percent crystallinity could be calculated for the sample.

The thermal data for the three polyester additives is shown in Table 3.2. In summary, the LB-100 sample was largely amorphous with small amounts of crystallinity, the R-3000 NAJ was amorphous and the Velvetol sample was crystalline.
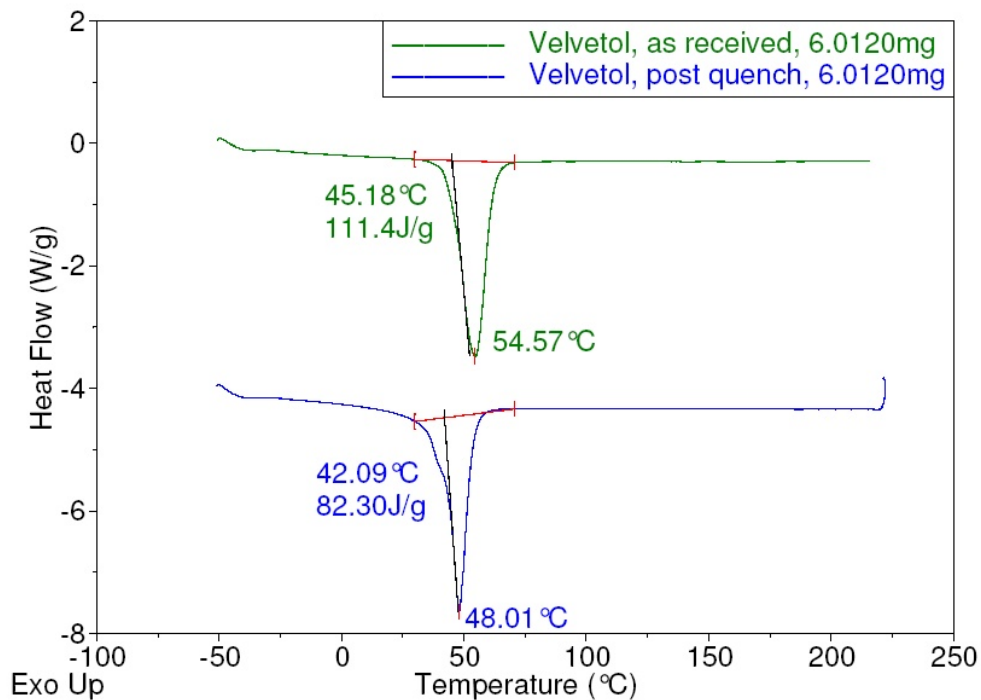
Figure 3.15: Thermal analysis of polyester additive Velvetol before and after quenching

Table 3.2: Peak melting temperatures, enthalpies of melting, and calculated percent crystallinities for the as received and post quench samples of polyester additives LB-100, R-3000 NAJ, and Velvetol

Sample	T_g (°C)	T_m (°C)	H_m (J/g)
LB-100, as received	41.1	158	0.799
LB-100, post quench	37.9	N/A	N/A
R-3000 NAJ, as received	60.2	N/A	N/A
R-3000 NAJ, post quench	54.2	N/A	N/A
Velvetol, as received	N/A	54.6	111
Velvetol, post quench	N/A	48.0	82.3

3.2.3 ATR–IR

The three polyester additives LB-100, R-3000 NAJ and Velvetol, were analyzed using the Thermo-Nicolet Magna 550 FTIR with ATR accessory. The additives had been described as polyester derivatives by Hexion, the company that supplied them. However, nothing else was known about the structure of these polyester additives. FTIR was used to gather more information about the structure of each additive. Polyester samples display a number of peaks in an ATR spectrum. The characteristic peaks for polyester would be the peaks for the ester group within the polymer structure. The ester group causes two strong peaks: the first peak is from the C=O stretching and the second peak is from the C–O stretching. The C=O absorption band occurs around 1730-1715 cm^{-1} for benzoate esters or unsaturated esters [95]. The C–O peak for stretching occurs between 1300-1000 cm^{-1}, depending on the type of ester and whether or not it is unsaturated [95]. These two peaks represent the characteristic ester found in most polyester polymers. A peak around 3500 cm^{-1} indicates the sorption of energy by stretching O–H groups that were intermolecularly hydrogen bonded[95]. The presence of this peak generally indicates that the polymer will be slightly hydrophilic.

The ATR spectrum for the LB-100 polyester additive is shown in Figure 3.16. The most prominent peak of the spectrum for the polyester additive occurred at 1715 cm^{-1}. This peak fell within the range for the absorption band of benzoate esters (1730–1715 cm^{-1}). The next significant peak occurred at 1223 cm^{-1}, which was within the range for the stretching of the C–O bond of unsaturated esters (1300–1160 cm^{-1}). A second absorbance peak at 1300 cm^{-1} falls within the same range. Another prominent feature in the spectrum for LB-100 was the broad peak occurring at 3423 cm^{-1}. This peak resulted from the absorption of energy by stretching O–H groups that were intermolecularly hydrogen bonded [95].

Some peaks from the LB-100 ATR spectrum were discernible and could be identified. The structure of this additive was compared to other polymers already in the ATR library. Figure 3.17 shows the best match for LB-100 determined by the library software of the Thermo-Nicolet Magna. The closest match for the LB-100 was a water dispersible polyester
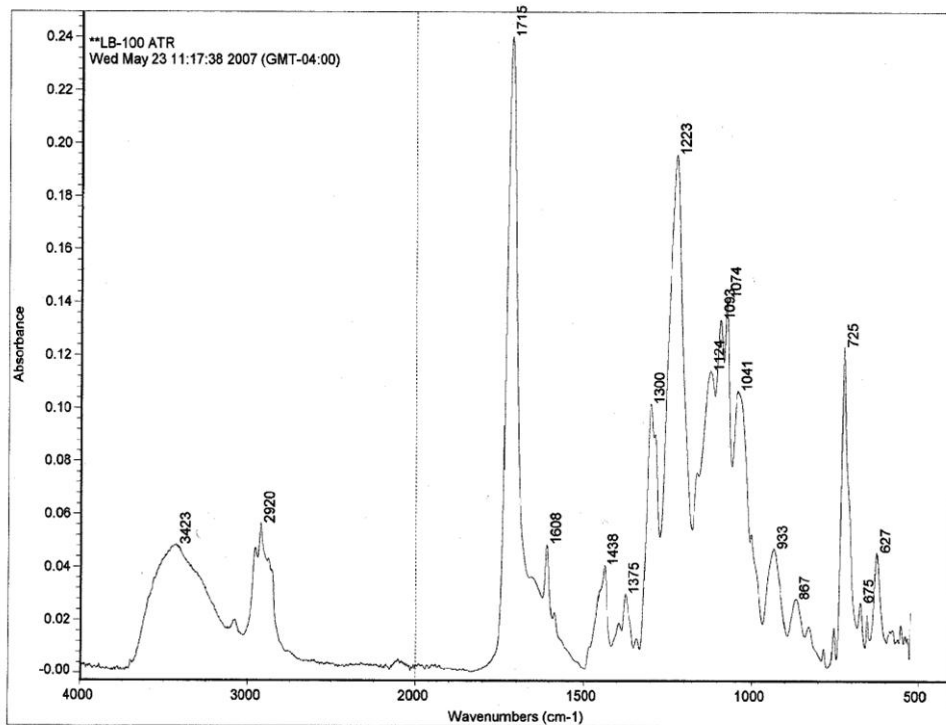
Figure 3.16: ATR spectrum for LB-100 polyester additive
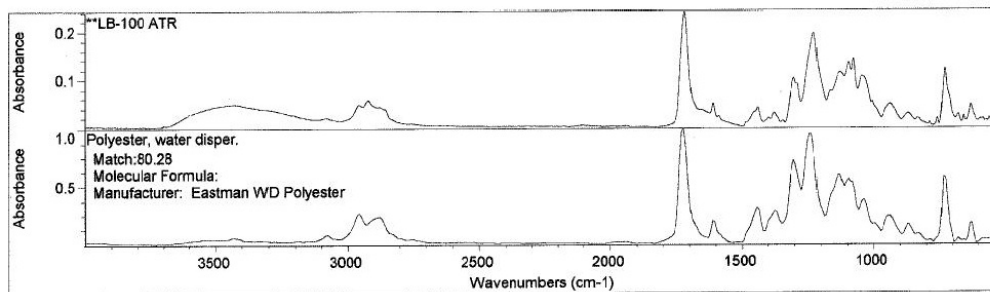
Figure 3.17: Matching spectra for LB-100 polyester additive

manufactured by Eastman. The two spectra had similar absorbance peaks below 3000 cm^{-1}, but the water dispersible polyester was missing the very broad peak around 3500 cm^{-1} that the LB-100 had. They also had similar peaks around 1715 cm^{-1} (the absorbance peak for the C=O bond). Although the match was only 80%, the similarity of the two polymers encouraged further exploration into the origin of the LB-100 polymer sample. A search of Eastman's website showed that Eastman also had a product identified as LB-100. Although the LB-100 used in this project was obtained from Hexion Specialty Chemicals, it is possible that Hexion obtained this product from Eastman originally. Eastman's LB-100 polymer is a sulfopolyester used for sizing[96]. Although the product was intended for use as a size on warp yarns, the hydrophilic nature of the sulfonated polyester made it ideal for the water sorption purposes of this project.

The ATR spectrum for the R-3000 NAJ polyester additive is shown in Figure 3.18. This polyester additive was similar to the LB-100 additive in that the most prominent peak of the spectrum for the polyester additive occurred at 1713 cm^{-1}, very close to where the peak occurred for the LB-100. This peak fell within the range for the absorption band of benzoate esters (1730–1715 cm^{-1}). The next significant peak occurred at 1242 cm^{-1}, which was within the range for the C–O bond of unsaturated esters (1300–1160 cm^{-1}). R-3000 NAJ also had a broad peak occurring at 3424 cm^{-1} as a result of the absorption of energy by stretching O–H groups that were intermolecularly hydrogen bonded [95].

The library for the Thermo-Nicolet Magna 550 FTIR-ATR reported that the closest identifiable polymer that matched the R-3000 NAJ spectrum was a poly(butylene tereph-thalate) (PBT) chip. The spectrum for the PBT chip was a 86% match for the spectrum of the R-3000 NAJ. The two spectra for these polymers are shown in Figure 3.19.

The final polyester additive evaluated using ATR was the Velvetol sample. The Velvetol spectra in Figure 3.20 showed the characteristic peak at 1715 cm^{-1} that represented the absorbance of the C=O bond in the ester. The peak at 1262 cm^{-1} correlated to the C–O bond with the ester. Another very strong peak was observed at 1097 cm^{-1}. This peak did not occur as strongly as in the other two polyester additives, although it did appear in the
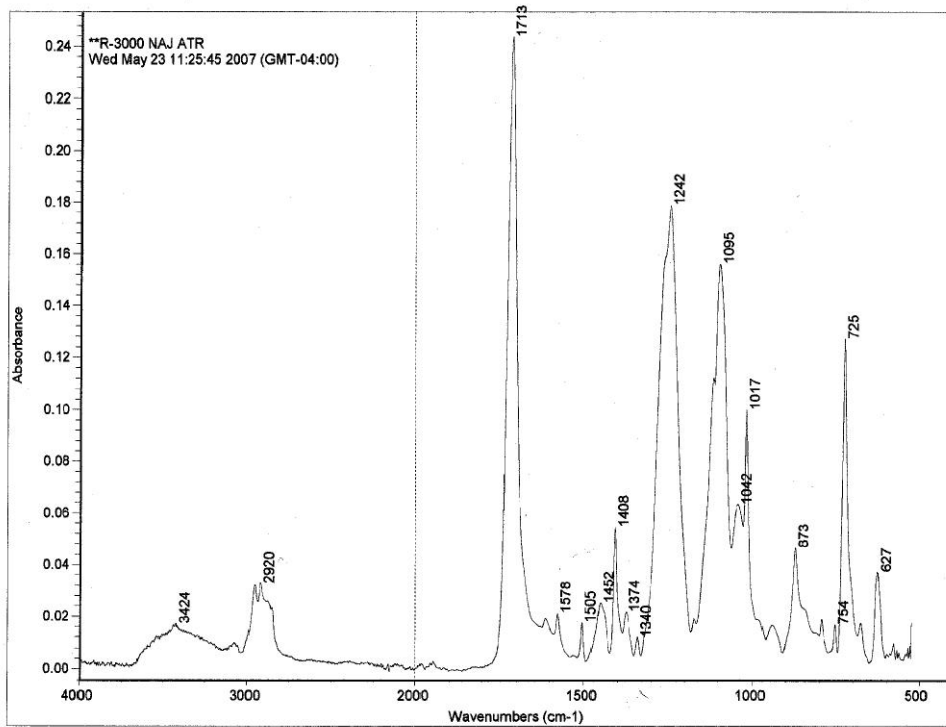
Figure 3.18: ATR spectrum for R-3000 NAJ polyester additive
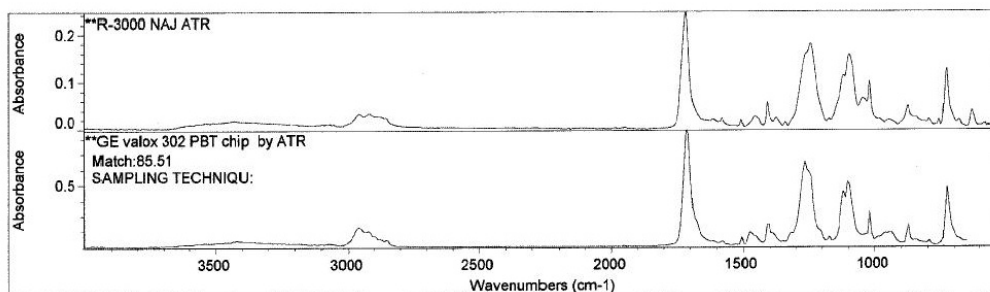
Figure 3.19: Matching spectra for R-3000 NAJ polyester additive

R-3000 NAJ sample spectrum. This peak was possibly representative of an additional ether linkage within the polymer structure. Ether linkages absorb energy around the 1150–1085 cm^{-1} due to the asymmetrical stretching of the C–O–C bond[95].
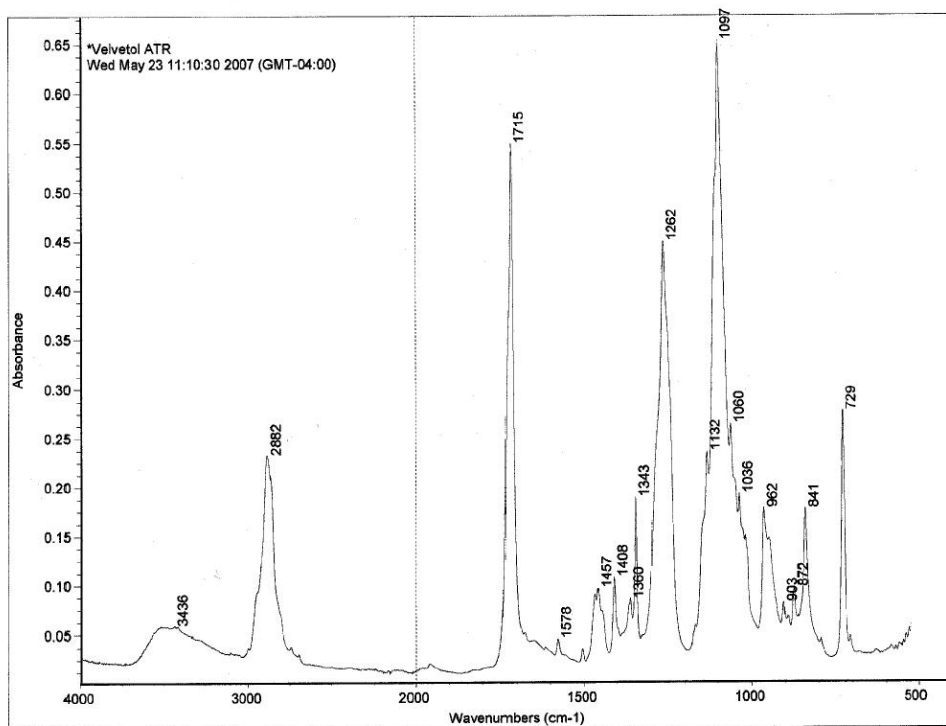
Figure 3.20: ATR spectrum for Velvetol polyester additive
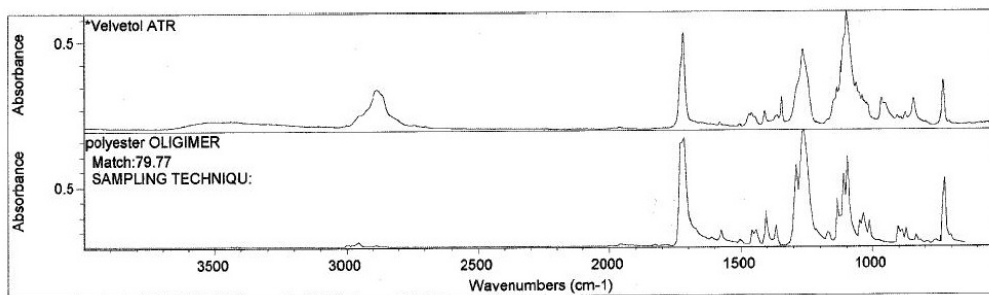
Figure 3.21: Matching spectra for Velvetol polyester additive

The closest match to the Velvetol spectrum occurred at 80% and was a polyester oligomer sample. This match is shown in Figure 3.21. The spectra appeared to match

below the 2000 cm^{-1} region and but it did not match above this region. This comparison did not account for the peak occuring at 1079 cm^{-1}. Using a subtraction algorithm, the spectra for poly(ethylene terephthalate) was subtracted from the spectrum of Velvetol and the resulting spectrum was compared to the spectra stored in the library. The result of this search is shown in Figure 3.22. This search showed that the closest match to the spectrum that included the major features in both the upper and lower regions of the spectrum was poly(ethylene oxide) (PEO). PEO is identical to the polymer poly(ethylene glycol) (PEG), a common comonomer for polyesters. The difference between PEO and PEG is the molecular weight of the material and the methods by which the polymers are synthesized. PEG generally has a molecular weight below 100,000 g/mol and anything above 100,000 g/mol is considered PEO[97]. Thus there are two possibilities: that the material is a comonomer of a polyester and PEG or that it is a blend of a polyester and PEO.

As expected, the examination of the three polyester additives did not conclusively identify the structures. None of the additives could be matched 100% with the library database and this was expected as these were new polymer formulations developed by Hexion Specialty Chemicals.
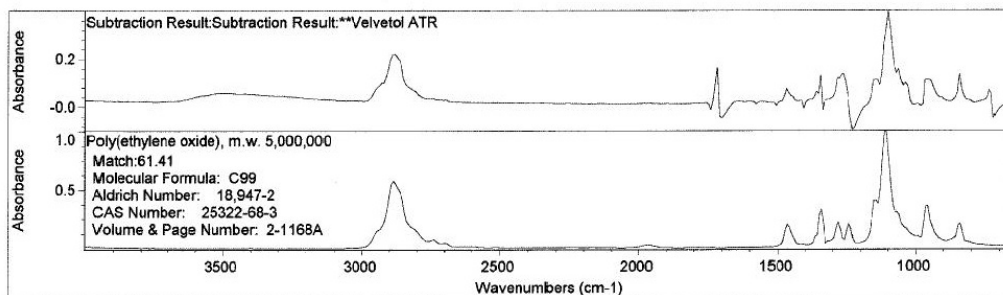
Figure 3.22: Matching spectra for Velvetol polyester additive

3.2.4   Contact Angle

The contact angle of the three polyester additives was determined using Drop Shape Analysis software and a Krüss camera. The contact angle was tested on polymer films prepared using the Carver 60 Ton Economy Motorized Press. The three polyester additives, LB-100, R-3000 NAJ and Velvetol, were tested to determine the extent of their hydrophilicity or hydrophobicity. At least five measurements were made on each flat film. The average of the measurements was used to determine the polyester additive that was the most hydrophilic. The average contact angle for each polymer is shown in Table 3.3.

Table 3.3: Water Contact Angle of Hydrophilic Polyester Additives

Additive	LB-100	R-3000 NAJ	Velvetol[a]
Contact angle (°)	71.8	87.8	66.5

[a]Contact angle as measured immediately upon placing drop

The polyester additive Velvetol had the lowest contact angle of 66.5° (and thus was the most hydrophilic additive). However, the contact angle of the Velvetol film had to be determined immediately upon placing the droplet of water on the film instead of allowing it to sit on the film for 30 seconds as procedure dictated. If the droplet of water sat on the Velvetol film for any length of time, the polymer film would begin to swell noticeably. This swelling caused peaks to form within the droplet of water. As time progressed, the peaks would swell to a height taller than the droplet being absorbed. The swelling nature of the polymer, although beneficial for possible uses of capturing and holding fluid within a fiber, would not be effective for transporting water within the fiber channels, which was the main goal of using these additives. This swelling upon contact with water along with the previously noted thermal instability during a long dwell under air at extrusion temperatures made Velvetol the least likely choice for extrusion with PP.

With Velvetol excluded, the lowest water contact angle was the polyester additive LB-100 at 71.8°. R-3000 NAJ had a contact angle of 87.75° and thus was no longer considered hydrophilic. The lower contact angle of LB-100 made it the most desirable for extrusion

with PP to make a hydrophilic PP fiber. The thermal characteristics of the polymer, described in Section 3.2.1 determined that LB-100 was not the most thermally stable of the three polyester additives; however, the amount of polymer lost during extrusion would be an insignificant amount and would not affect the spinnability of the resulting fiber. For these reasons, the polyester additive LB-100 was the additive chosen to be used in extrusion.

3.3 Fiber Characterization

3.3.1 Coding System for Fibers

The fibers were coded to identify them according to their fiber shape, dpf, polymer blend and whether or not a spin finish or additive was used to extrude the fiber. The coding process was described in Chapter 2, but Figure 3.23 and Tables 2.2, 2.3, 2.4 and 2.5 have been repeated to remind the reader how the labels were defined. The first field of the label was the fiber shape, designated using one of four letters: H for the H shaped fibers, Y for the Y shaped fibers, O for the Octolobal fibers (aka 4DG) and R for the round shaped fibers. The second field describes the dpf of each fiber as a two or three digit number representing the desired dpf of the yarn upon extrusion. The value following the hyphen represented the blend of polymers used to extrude the polymers (1 for 100% 18 MFI PP, 2 for a 90/10 blend of 18 MFI PP and 400 MFI PP, 3 for a 75/25 blend of the two polymers and 4 for a 50/50 blend). The final field of the label was blank or was an S or an A. The S represented the application of the spin finish Favorol SF2 while the A represented the polyester additive LB-100. If no letter followed the final number, no additive or spin finish was used during the extrusion of the fibers.
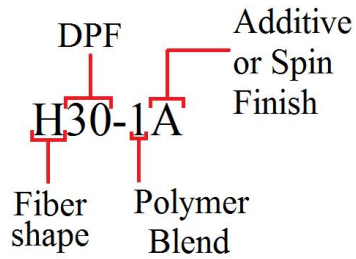
Figure 3.23: An example of a fiber label

Table 3.4: Compositions of Round fibers

Label	Shape	Polymer Blend	Spin Finish	DPF
R30-1	Round	100% 18 MFI PP	none	30.6
R30-1S	Round	100% 18 MFI PP	SF2	30.5
R30-2	Round	90% 18 MFI PP, 10% 400 MFI PP	none	30.3
R30-2S	Round	90% 18 MFI PP, 10% 400 MFI PP	SF2	30.7
R30-3	Round	75% 18 MFI PP, 25% 400 MFI PP	none	30.7
R30-3S	Round	75% 18 MFI PP, 25% 400 MFI PP	SF2	30.6
R30-4	Round	50% 18 MFI PP, 50% 400 MFI PP	none	30.2
R30-4S	Round	50% 18 MFI PP, 50% 400 MFI PP	SF2	30.5
R60-1	Round	100% 18 MFI PP	none	61.0
R90-1	Round	100% 18 MFI PP	none	87.3
R120-1	Round	100% 18 MFI PP	none	119.9
R150-1	Round	100% 18 MFI PP	none	151.8
R180-1	Round	100% 18 MFI PP	none	179.8

Table 3.5: Compositions and Linear Densities of Y fibers

Label	Shape	Polymer Blend	Spin Finish	DPF
Y30-1	Y	100% 18 MFI PP	SF2	29.8
Y30-1S	Y	100% 18 MFI PP	SF2	30.1
Y30-2	Y	90% 18 MFI PP, 10% 400 MFI PP	none	31.3
Y30-2S	Y	90% 18 MFI PP, 10% 400 MFI PP	SF2	29.3
Y30-3	Y	75% 18 MFI PP, 25% 400 MFI PP	none	30.7
Y30-3S	Y	75% 18 MFI PP, 25% 400 MFI PP	SF2	30.0
Y30-4	Y	50% 18 MFI PP, 50% 400 MFI PP	none	29.8
Y30-4S	Y	50% 18 MFI PP, 50% 400 MFI PP	SF2	29.8
Y60-1	Y	100% 18 MFI PP	none	61.2
Y90-1	Y	100% 18 MFI PP	none	92.3
Y120-1	Y	100% 18 MFI PP	none	123.7
Y150-1	Y	100% 18 MFI PP	none	148.7
Y180-1	Y	100% 18 MFI PP	none	181.3

Table 3.6: Compositions and Linear Densities of H fibers

Label	Shape	Polymer Blend	Spin Finish	DPF
H30-1	H	100% 18 MFI PP	none	30.3
H30-1S	H	100% 18 MFI PP	SF2	30.8
H30-1A	H	100% 18 MFI PP with 5% LB-100 w/w	none	31.2
H30-2	H	90% 18 MFI PP, 10% 400 MFI PP	none	31.4
H30-2S	H	90% 18 MFI PP, 10% 400 MFI PP	SF2	30.9
H30-2A	H	90% 18 MFI PP, 10% 400 MFI PP with 5% LB-100 w/w	none	33.9
H30-3	H	75% 18 MFI PP, 25% 400 MFI PP	none	30.8
H30-3S	H	75% 18 MFI PP, 25% 400 MFI PP	SF2	30.5
H30-3A	H	75% 18 MFI PP, 25% 400 MFI PP with 5% LB-100 w/w	none	29.5
H30-4	H	50% 18 MFI PP, 50% 400 MFI PP	none	29.8
H30-4S	H	50% 18 MFI PP, 50% 400 MFI PP	SF2	29.8
H30-4A	H	50% 18 MFI PP, 50% 400 MFI PP with 5% LB-100 w/w	none	30.4

3.3.2 Linear Density of Extruded Fibers

The linear density of the fibers was determined as described in Section 2.4. The initial conditions for extruding the fibers at the desired linear density were calculated using a simple mass balance equation. After an initial batch of fibers was measured, the conditions were altered to pinpoint the desired dpf. The linear density of each fiber is listed in Table 3.7. The fibers were extruded to meet a goal dpf, regardless of cross-sectional shape. The original fibers were spun to be 30 dpf; however, further research required that larger fibers be produced for testing.

Table 3.7: Linear Densities of Fibers

Fiber	DPF	Fiber	DPF	Fiber	DPF
R30-1	30.6	Y30-1	29.8	H30-1	30.3
R30-1S	30.5	Y30-1S	30.1	H30-1S	30.8
R30-2	30.3	Y30-2	31.3	H30-2	31.4
R30-2S	30.7	Y30-2S	29.3	H30-2S	30.9
R30-3	30.7	Y30-3	30.7	H30-3	30.8
R30-3S	30.6	Y30-3S	30.0	H30-3S	30.5
R30-4	30.2	Y30-4	29.8	H30-4	29.8
R30-4S	30.5	Y30-4S	29.8	H30-4S	29.8
R60-1	61.0	Y60-1	61.2	H30-1A	31.2
R90-1	87.3	Y90-1	92.3	H30-2A	33.9
R120-1	119.9	Y120-1	123.7	H30-3A	29.5
R150-1	151.8	Y150-1	148.7	H30-4A	30.4
R180-1	179.8	Y180-1	181.3	O30-1	30.7

3.3.3 Thermal Characterization of Fibers

3.3.3.1 DSC

Heating Curves The thermal properties of the spun fibers were tested using the DSC instrument and the method described in Chapter 2. This was the same method used on the PPs and polyester additives. The individual thermograms for the fibers are included in Appendix A, but the important thermal data for the twelve fibers spun from blends of 18 and 400 MFI PP is shown in Table 3.8. All of the fibers had a similar melting temperature which was comparable to the melting temperature of the post-quenched 18 MFI PP and 400 MFI PP samples. The enthalpies of melting were also comparable to those of the original polymer samples [79.8 J/g for 18 MFI PP and 82.7 J/g for 400 MFI PP (post quench)]. There was no trend in the percent crystallinities of the fibers based on the fiber shape or the fiber composition. Specifically, the shape of the fiber did not affect the crystallinity of the samples by a significant amount.

Table 3.8: Thermal data obtained from a DSC for fibers spun from 18 MFI PP and 400 MFI PP

Fiber	As Spun			Post Quench		
	T_m (°C)	H_m (J/g)	χ_c	T_m (°C)	H_m (J/g)	χ_c
R30-1	164.2	83.8	42%	163.3	83.4	42%
R30-2	163.3	90.1	45%	161.5	81.6	41%
R30-3	162.8	93.0	46%	162.6	88.9	44%
R30-4	162.6	87.5	44%	162.2	84.7	42%
Y30-1	163.2	87.1	44%	161.9	84.2	42%
Y30-2	163.1	86.9	43%	161.8	83.9	42%
Y30-3	163.3	90.3	45%	161.5	88.5	44%
Y30-4	163.0	90.0	45%	161.8	89.0	44%
H30-1	162.4	84.2	42%	161.3	83.2	42%
H30-2	162.2	89.1	45%	163.5	84.7	42%
H30-3	162.2	88.0	44%	161.1	85.3	43%
H30-4	162.2	92.9	46%	163.0	88.4	44%

Table 3.9 compares the thermal data of the four H fibers spun with polyester additive LB-100 to the four H fibers spun without any polyester additive. The thermograms for these fibers are located in Appendix A. As previously shown in Section 3.2.2, the LB-100 polyester

additive had a T_g around 37°C. However, no change in heat capacity attributable to the LB-100 at its T_g was observed in the polyblend fibers.

Table 3.9: Thermal data obtained form a DSC for H fibers spun from 18 MFI PP and 400 MFI PP and H fibers spun from the same blend with an additional 5% of LB-100 polyester additive

Fiber	As Spun			Post Quench		
	T_m (°C)	H_m (J/g)	χ_c	T_m (°C)	H_m (J/g)	χ_c
H30-1	162.4	84.2	42%	161.3	83.2	42%
H30-2	162.2	89.1	45%	163.5	84.7	42%
H30-3	162.2	88.0	44%	161.1	85.3	43%
H30-4	162.2	92.9	46%	163.0	88.4	44%
H30-1A	162.0	83.3	42%	162.5	80.0	40%
H30-2A	162.6	79.4	40%	162.8	79.4	40%
H30-3A	162.2	85.2	43%	162.0	83.2	42%
H30-4A	162.1	85.3	43%	162.7	81.0	40%

Cooling Curves   It is well established that PP crystallizes too quickly to quench the polymer melt to an amorphous state. Thus, cooling curves were run on the 18 MFI and 400 MFI PP samples to establish a baseline crystallization for each polymer and on the polyblend fibers. Only round fibers were used in this study. Each of the cooling curves showed a crystallization peak and the data is shown in Table 3.10. The samples were heated to 220°C and the samples were cooled to 0°C at a cooling rate of 10°C/min. This cooling cycle resulted in the observance of a crystallization peak on the thermogram for each of the samples.

Table 3.10: Crystallization Temperatures, Enthalpies and Percent Crystallinity for 18 MFI PP, 400 MFI PP, and polyblend fibers after a cooling cycle

Polymer or Fiber	T_c (°C)	H_c (J/g)	χ_c
18 MFI PP	111.1	96.7	48%
400 MFI PP	110.6	100.	50%
R30-1	116.0	95.3	48%
R30-2	117.2	94.5	47%
R30-3	117.1	102.	51%
R30-4	116.4	94.8	47%

The cooling curves for these polymers and fibers are shown in Appendix A. One of the goals of this analysis was to determine if blending the two PPs had an effect on the crystallization temperature or percent crystallinity of the polymer melt. There was no significant difference in the crystallization temperatures of the 18 MFI PP and the 400 MFI PP. Although the fibers display a higher crystallization temperature than the polymers, the temperature is not affected by the polymer blend.

3.3.3.2   TGA

TGA was run on selected H fibers. While this analysis could also have been performed on the round and Y fibers of the same constitution, the shape of the fiber should have no effect on the degradation of the polymer. The H fibers with and without additives were evaluated using the TGA instrument with a nitrogen purge with a flow rate of 40

ml/min. Previous testing showed that 18 MFI PP and 400 MFI PP had an extrapolated onset of degradation around 451°C and the LB-100 polyester additive had an extrapolated onset of degradation at 412°C. Although it was impossible to discern between the two PP samples using this technique, the temperature gap between the degradation onset temperatures of the PP and the polyester additive was expected to cause an effect on the fiber degradation. The fibers were heated from room temperature to 500°C and the resulting curves were overlaid for each type of fiber blend.

Figure 3.24 shows the result of testing on fibers H30-1 and H30-1A. The inset shows an analysis of the two curves and provides extrapolated onset temperatures of degradation that are slightly lower than the temperatures observed for the original PP samples. However, when the curve for the H30-1 fiber was compared to the curve for the H30-1A fiber, a marked difference was visible just before the large degradation step. The H30-1A fiber began degrading at an extrapolated onset temperature of 439°C, prior to the H30-1 sample at 444°C, thus a small gap was visible between the two samples starting around 375°C. This gap indicated that the LB-100 portion of fiber H30-1A had already begun to degrade by the time the degradation temperature for PP was reached. Similar comparisons made between the H30-2 and H30-2A fibers, the H30-3 and H30-3A fibers, and the H30-4 and H30-4A fibers in Figures 3.25, 3.26 and 3.27 show that this occurs in every case where LB-100 was added to the blend. This observed degradation coupled with the previous DSC data indicated that the LB-100 was indeed present in the extruded fiber but its loading was too low to directly influence the thermal properties of the PP in the fiber.
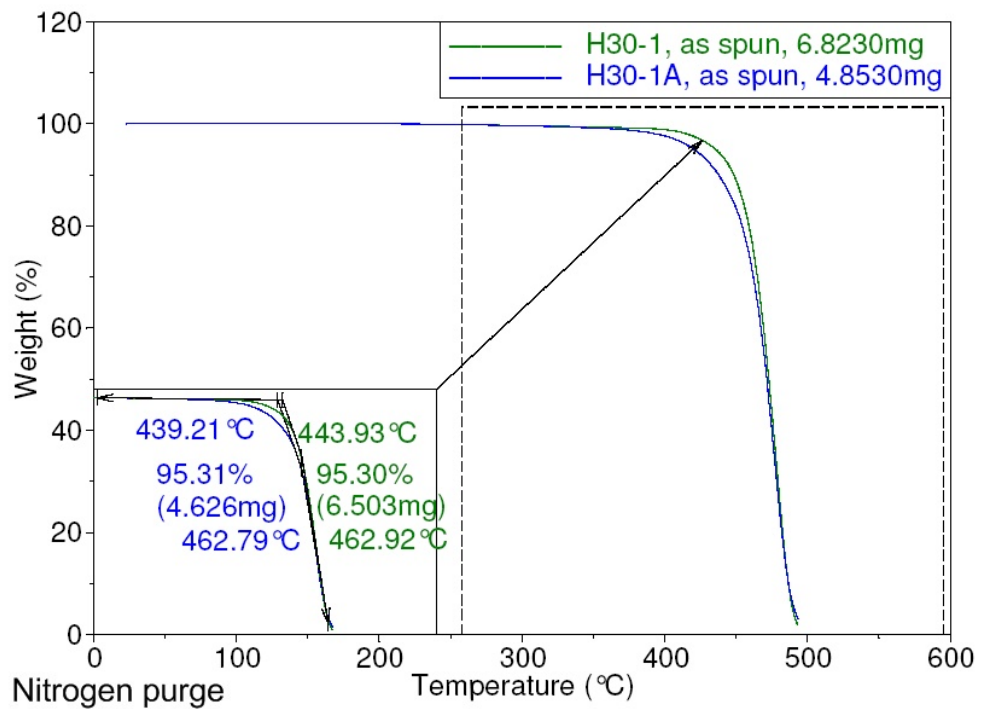
Figure 3.24: Degradation of Fibers H30-1 and H30-1A under nitrogen purge
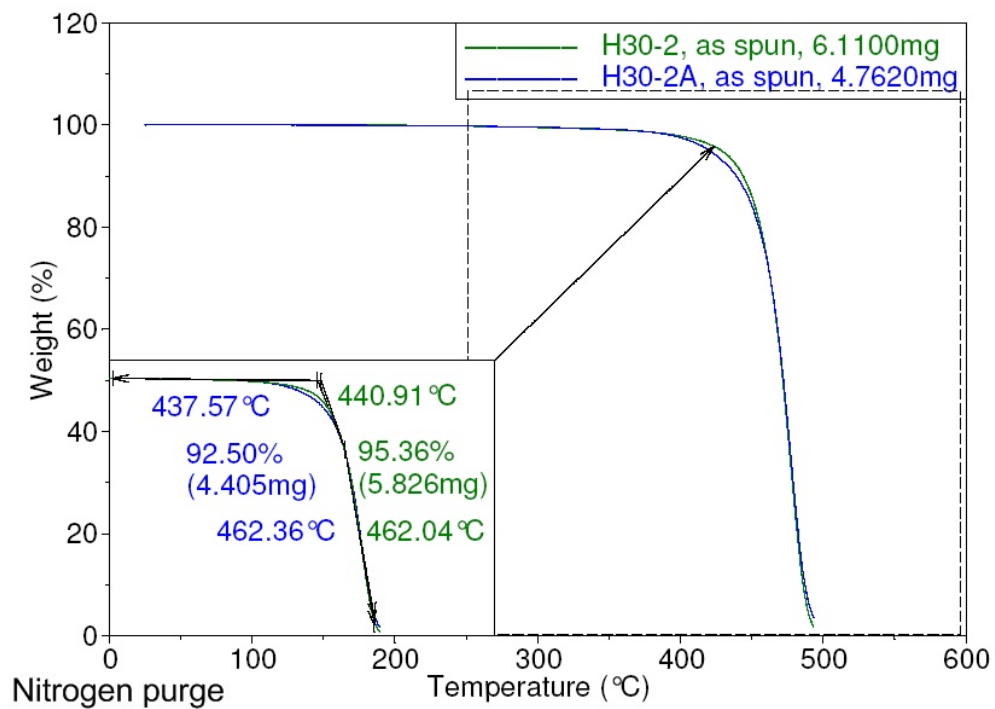
Figure 3.25: Degradation of Fibers H30-2 and H30-2A under nitrogen purge

87
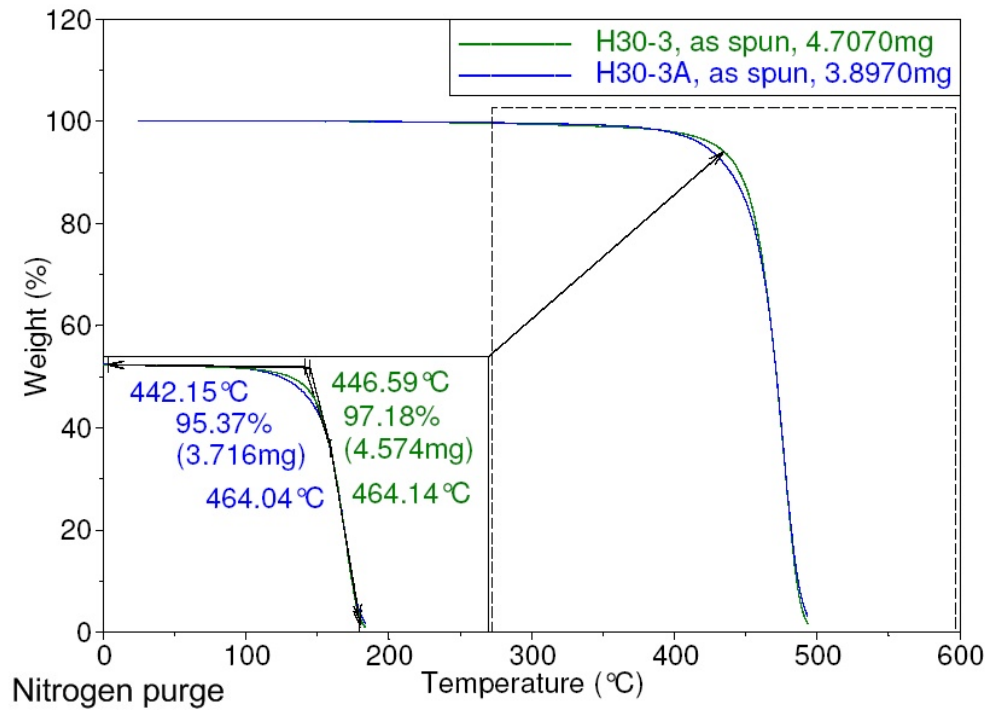
Figure 3.26: Degradation of Fibers H30-3 and H30-3A under nitrogen purge
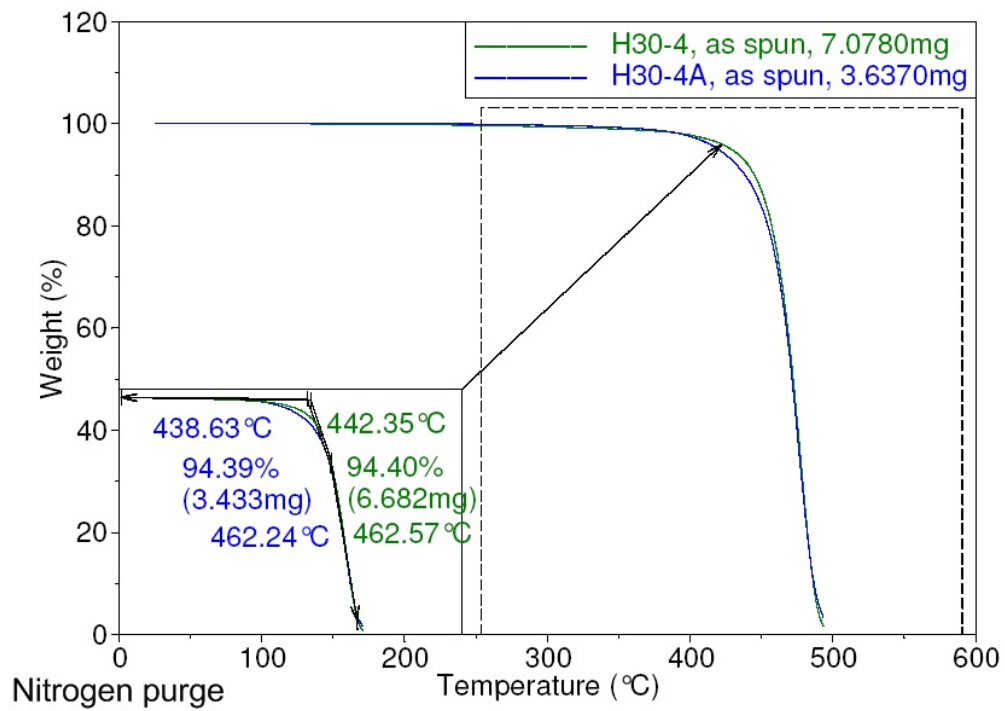
Figure 3.27: Degradation of Fibers H30-4 and H30-1A under nitrogen purge

Chapter 4

Results and Discussion: Fiber Geometry and Geometric Shape Retention

4.1 Retention of Spinneret Shape by Shaped Fibers

One of the most difficult aspects of extruding shaped fibers is maintaining the shape of the spinneret in the cross-section of the resulting fibers. Some researchers have theorized that shape distortion in melt extruded fibers is due to the stresses within the polymer as it exits the spinneret [40, 41]. These stresses undergo relaxation immediately upon exiting the spinneret, which results in a phenomenon known as die swell. Polypropylene seems to experience more die swell than other polymers due to its high level of elasticity [15]. To reduce the die swell, lower molecular weight polymers can be blended with the base polymer. The smaller molecules of the 400 MFI PP have a shorter relaxation time than the 18 MFI PP. By this reasoning, the die swell of extruded 400 MFI PP would be smaller than the die swell of 18 MFI PP [98]. However, Koopmans [98] suggests that a maximum level of die swell exists for polymers beyond a certain molecular weight as the longer polymer chains become entangled. If the 18 MFI PP experiences entangling of the polymer chains

and thus reduced die swell, an addition of 400 MFI PP may reduce the entanglement and actually result in increased die swell.

In this work, 400 MFI PP was blended with the original 18 MFI PP to reduce the shape distortion of the H fibers. When extruded with solely 18 MFI PP, the round and Y fibers did not experience much if any shape distortion although they did experience a large die swell. However, polyblend round and Y fibers (fibers extruded from 18 MFI PP and 400 MFI PP) were extruded as well as polyblend H fibers to determine the effect the low molecular weight PP had on the fiber shape.

4.2   Characterization of Fiber Geometries

The extruded fibers were set in epoxy resin and the resulting resin samples were microtomed so that the cross-section of the fiber was visible. These resin samples were viewed under variable pressure on a Hitachi 3400 SEM. The cross-section of each extruded fiber was photographed and analyzed using Universal Desktop software. The H, Y, and Octolobal fibers were compared to conventional round fibers to demonstrate the difference in surface area relative to fiber shape.

4.2.1   Characterization of round fibers extruded from 18 MFI PP and 400 MFI PP

Fibers produced from 18 MFI PP and 400 MFI PP were produced using the process described in Chapter 2. The four blends of polymer used were extruded in an as spun condition and then again with a spin finish added to the fiber. The round fibers extruded from 18 MFI PP and the three blends of 18 MFI PP and 400 MFI PP are shown in Figure 4.1. The fiber extruded with 100% 18 MFI PP is shown in Figure 4.1a with the 90/10, 75/25 and 50/50 blends of 18 MFI PP and 400 MFI PP shown in Figures 4.1b, 4.1c and 4.1d respectively.

The shape of the individual fibers in each bundle was consistent with the conven-
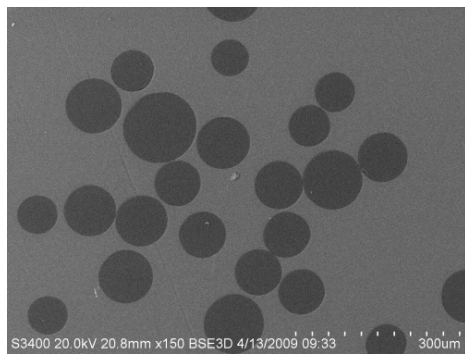
(a) R30-1
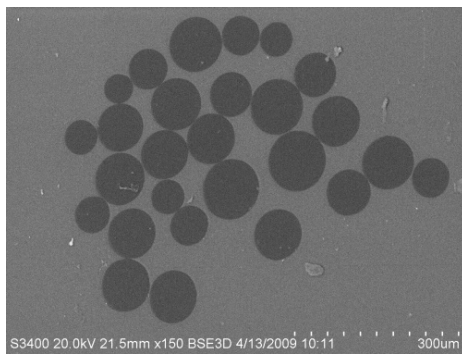
(b) R30-2
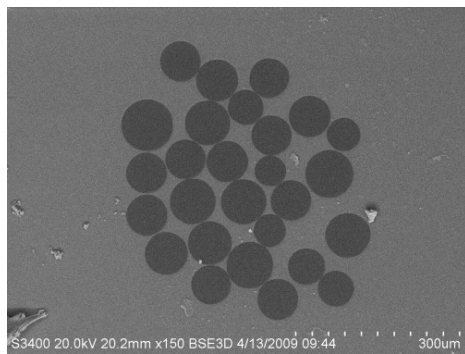
(c) R30-3
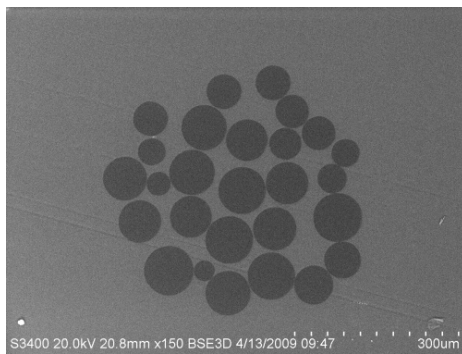
(d) R30-4

Figure 4.1: 30 dpf round fibers extruded from 18 MFI PP and 400 MFI PP

tional round spinneret used. The addition of 400 MFI PP did not appear to change the shape of the round fibers. The variation in size of the fibers was likely caused by variations in the the distribution of the polymer across the spinneret during extrusion. This was not unusual for a small scale research extruder. Although the size discrepancy exists, it was taken into account when the dpf of each fiber was calculated. The linear density of each fiber is an average value and thus allows for variation in the size of the fibers. As shown in Table 4.1, the dpf of the fibers was very similar even though the composition of the fibers changed. The average perimeter and average area of the cross-section of each fiber were calculated using measurements of at least 20 individual fibers.

Table 4.1: DPF, Cross-sectional Perimeter and Cross-sectional Area of round fibers extruded from 18 MFI PP and 400 MFI PP

Fiber	dpf (g/9000m)	Perimeter [SD] (μm)	Area [SD] (μm^2)
R30-1	30.6	259 [37]	5643 [1575]
R30-1S	30.5	270 [38]	6136 [1715]
R30-2	30.3	257 [46]	5640 [1872]
R30-2S	30.7	204 [21]	3555 [720]
R30-3	30.7	279 [32]	6606 [1544]
R30-3S	30.6	238 [17]	4712 [688]
R30-4	30.2	230 [32]	4540 [1223]
R30-4S	30.5	230 [36]	4532 [1315]

4.2.2 Characterization of Y fibers extruded from 18 MFI PP and 400 MFI PP

The Y fibers were extruded using methods similar to those of the round fibers. Again, the four polymer blends of 18 and 400 MFI PP were used and the resulting fibers are shown in Figures 4.2a, 4.2b, 4.2c and 4.2d. The overall shape of the Y fibers had no discernible change with the addition of the 400 MFI PP. Due to the open channeled, three-sided shape of the Y fiber, the stress induced by cooling would have been equivalent at every face of the fiber surface. This would mean that very little shape distortion would occur during the extrusion of the Y fibers. As there was no stress differential, the addition of the 400 MFI PP did not change the cross-sectional shape of the fibers in any discernable way. The final Y fiber, Y30-4, shown in Figure 4.2d, had slightly thicker legs than the other Y fibers. This may indicate that the large amount (50%) of 400 MFI PP in the polymer blend resulted in extensive die swell that exceeded that of the other fibers. The amount of variation in the size of the Y fibers was les than the variation in the size of the round fibers. Table 4.2 lists the dpf, cross-sectional perimeter and cross-sectional area of each of the Y fibers extruded with varying levels of 18 MFI and 400 MFI PP.

Table 4.2: DPF, Cross-sectional Perimeter and Cross-sectional Area of Y fibers extruded from 18 MFI PP and 400 MFI PP

Fiber	dpf (g/9000m)	Perimeter [SD] (μm)	Area [SD] (μm^2)
Y30-1	29.8	467 [71]	3143 [891]
Y30-1S	30.1	518 [58]	3921 [933]
Y30-2	31.3	502 [58]	3853 [749]
Y30-2S	29.3	550 [81]	4687 [1289]
Y30-3	30.7	473 [92]	3977 [1491]
Y30-3S	30.0	558 [105]	5749 [1902]
Y30-4	29.8	480 [70]	5047 [1539]
Y30-4S	29.8	434 [84]	4535 [1715]

(a) Y30-1

(b) Y30-2

(c) Y30-3

(d) Y30-4
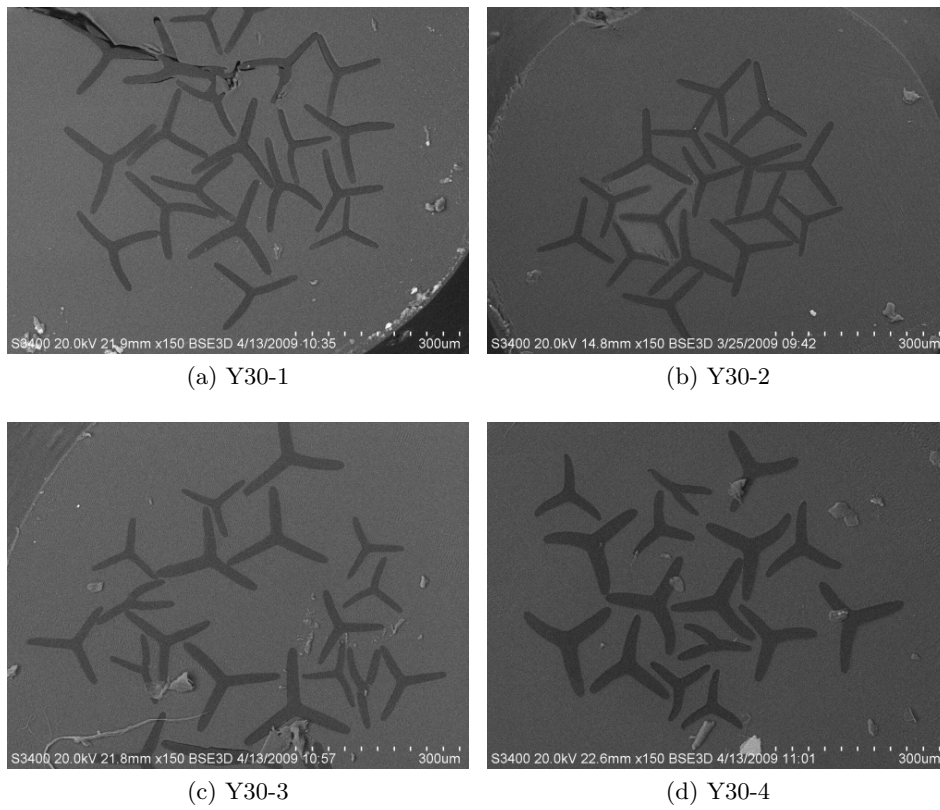
Figure 4.2: 30 dpf Y fibers extruded from of 18 MFI and 400 MFI PP

4.2.3 Characterization of H fibers extruded from 18 MFI PP and 400 MFI PP

The 30 dpf H fibers with different levels of 18 MFI PP and 400 MFI PP are shown in Figure 4.3. Figure 4.3a shows the 100% 18 MFI PP H fiber, H30-1. The cross-sections of these fibers show that the overall H shape from the spinneret was maintained during extrusion, however the legs of the H fibers did not connect with the cross-bars at a 90° angle. The H fibers had thick cross-bars and long, thin legs extending out from the cross-bar. In some cases, the legs were thicker and showed signs of having curled at the end during extrusion. The micrograph of the H30-1 fiber cross-section also showed a large disparity in the size of the fibers. Although this was seen in the extrusion of the round and the Y fibers, the inconsistency in size became more pronounced with the extrusion of the H fibers. Regardless of size, the cross-sections of the H30-1 filaments all maintained a distinctive, if distorted, H shape. This shape is as good as if not better than any H fibers seen in the Eastman patent portfolio [23, 24].

The fibers shown in Figures 4.3b, 4.3c and 4.3d all contained 400 MFI PP in the melt. The 400 MFI PP was added to increase the geometric shape retention of the fibers with respect to the spinneret holes. The initial thought was that the 400 MFI PP would have shorter chains than the 18 MFI PP and thus would be more mobile within the extruded polymer fiber. The more mobile 400 MFI PP chains would then be able to relieve some of the stress on the fiber surface caused by cooling and therefore a better geometric shape retention would result. Due to the lower viscosity of the 400 MFI PP, the temperatures of the polymer melt had to be lowered slightly. Figure 4.3b shows the fiber that was extruded with 10% of the melt composed of 400 MFI PP. The linear density of these fibers was similar to that of the H30-1 fiber, however, the shape appeared to improve slightly. The H fibers still did not have straight legs and 90° angles at their connecting points, but the legs of the fibers had begun to slim and elongate. The cross-bar of the fiber was also thinner for most of the fibers than in the H30-1 sample.

The H30-3 fiber had 25% of the polymer melt composed of 400 MFI PP. Figure 4.3c shows that the fiber shape had changed slightly in that the legs of the H were even thinner

(a) H30-1

(b) H30-2

(c) H30-3

(d) H30-4
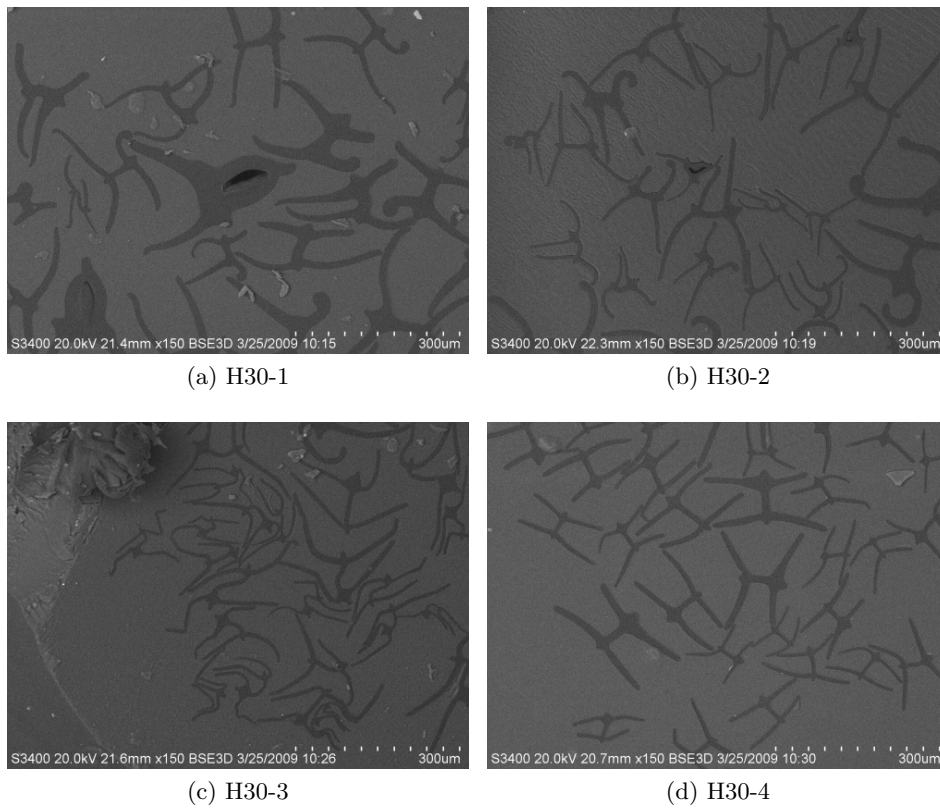
Figure 4.3: 30 dpf H fibers extruded from 18 MFI PP and 400 MFI PP

than previously observed and there were very few thick places within the fibers. However, the geometric shape retention of the fibers did not improve drastically. The legs of the fibers were still bent and curled in every direction.

The H30-4 fiber was extruded from 50% 400 MFI PP and 50% 18 MFI PP and is shown in Figure 4.3d. These fibers showed an improved geometric shape retention compared to the three previous fibers. The legs and cross-bars of these H fibers were thin and straight and did not bend or curl outwards. The cross-bar met the legs at an angle much closer to 90° than in any of the other H fiber cross-sections. Although these fibers still did not constitute a "perfect" H shape, the cross-sectional retention of the spinneret shape was much greater than the previous three fibers.

The dpf, cross-sectional perimeter and cross-sectional area for each of the H fibers discussed in this section are shown in Table 4.3. The values reported for perimeter and cross-section are the averages of a minimum of 20 fiber measurements. The H fibers were spun to be the same linear density. However, as previously noted, the H shaped fibers experienced a more drastic size distribution within the fiber bundle than the round or the Y fibers. This range of fiber sizes was reflected in the standard deviation of each measurement that is included in brackets beside the average values for the cross-sectional perimeter and cross-sectional area.

Table 4.3: DPF, Cross-sectional Perimeter and Cross-sectional Area of H fibers extruded from 18 MFI PP and 400 MFI PP

Fiber	dpf (g/9000m)	Perimeter [SD] (μm)	Area [SD] (μm^2)
H30-1	30.3	941 [206]	4257 [1129]
H30-1S	30.8	702 [138]	3731 [1230]
H30-2	31.4	968 [288]	5806 [2854]
H30-2S	30.9	705 [197]	3163 [1455]
H30-3	30.8	959 [249]	4641 [1959]
H30-3S	30.5	778 [225]	3666 [1963]
H30-4	29.8	769 [251]	5015 [2873]
H30-4S	29.8	722 [144]	4233 [1733]

4.2.4 Characterization of Octolobal fibers extruded from 18 MFI PP

The Octolobal fiber used in this work was fiber O30-1, shown in Figure 4.4. This fiber was extruded from 100% 18 MFI PP using methods similar to that of the other fibers. The shape of the fibers resembled the shape of the spinneret hole from which it was extruded. Very little thickening or distortion was observed with this fiber. The dpf, cross-sectional perimeter and cross-sectional area of the Octolobal fiber are shown in Table 4.4.
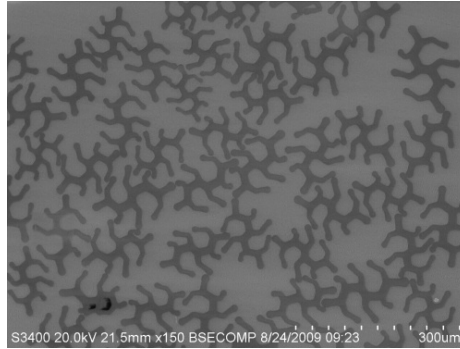
Figure 4.4: 30 dpf Octolobal fibers extruded from 18 MFI PP

Table 4.4: DPF, Cross-sectional Perimeter and Cross-sectional Area of the Octolobal fiber extruded from 100% 18 MFI PP

Fiber	dpf (g/9000m)	Perimeter [SD] (μm)	Area [SD] (μm^2)
O30-1	30.7	752 [55]	4441 [578]

4.2.5 Comparison of round fibers and shaped fibers of the same dpf and polymer blend

The original goal of this research was to compare the properties of shaped fibers with conventional round fibers of the same dpf. The four fibers, R30-1, Y30-1, H30-1, and O30-1 are shown in Figure 4.5. These four fibers were prepared from 100% 18 MFI PP and were extruded to be 30 dpf. Although the weight of all the fibers was the same, the surface area of the shaped fibers was drastically different from that of the round. Table 4.5 shows the dpf, cross-sectional perimeter and cross-sectional area for the three fibers. Fiber R30-1 had a cross-sectional perimeter of 259 μm. Fibers Y30-1, H30-1 and O30-1 had

cross-sectional perimeters of 467 μm, 941 μm and 752 μm, respectively. These values are the average calculated from measurements of at least 15 individual filaments for each fiber.

(a) R30-1

(b) Y30-1

(c) H30-1

(d) O30-1
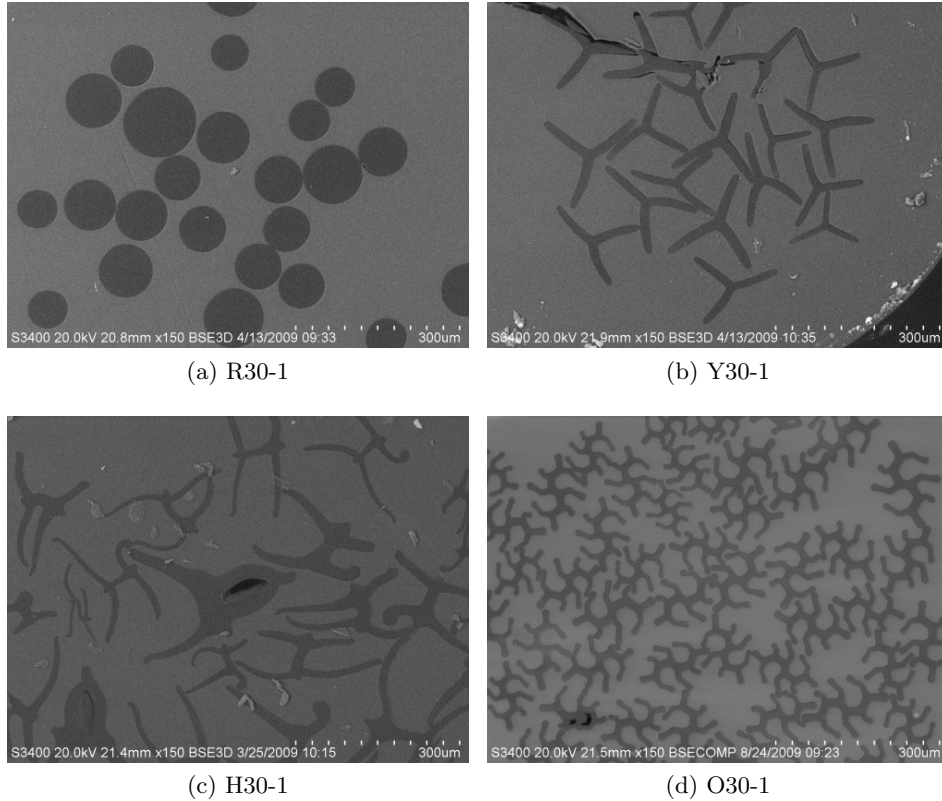
Figure 4.5: H, Y, Octolobal and Round fibers of comparable dpf extruded from 18 MFI PP

The surface area of the shaped fibers was 2-3 times the original surface area of the round fibers of the same dpf. This increased surface area provided additional area for fluids or particles to adsorb to the fiber surface. The long, thin legs of the shaped fibers caused the formation of capillary channels between fibers to be more likely. Round fibers form channels between the fibers at points where they touch, or come close to touching, another fiber. The wide, long-legged Y fibers theoretically build large, open channels between fibers. The H fibers have by nature channels built into the shape, but may also be able to build channels between fibers. Even if the legs of the H deviate from the desired 90° angle, the bent legs can still form channels with other bent legs on the same fiber. The legs, when bent, can also in theory form the same inter-fiber capillaries that the Y were designed to

form. The Octolobal fibers have numerous channels built into the shape; however, the legs that form the fiber channels are bent and less interaction with the legs of other Octalobal fibers is possible as compared to the Y or H fibers.

Table 4.5: DPF, Cross-sectional Perimeter and Cross-sectional Area of the round fiber and three shaped fibers extruded from 18 MFI PP

Fiber	dpf (g/9000m)	Perimeter [SD] (μm)	Area [SD] (μm^2)
R30-1	30.6	259 [37]	5643 [1575]
Y30-1	29.8	467 [71]	3143 [891]
H30-1	30.3	941 [206]	4257 [1129]
O30-1	30.7	752 [55]	4441 [578]

4.2.6   H Fibers extruded with LB-100 Polyester Additive

The H fibers extruded with additive LB-100 were extruded to have the same linear density as the previous fibers: approximately 30 dpf. The fibers were extruded with the same four blends of 18 and 400 MFI PP, but an additional 5% w/w of LB-100 was added to each polymer blend before extruding. The extrusion temperatures remained relatively the same as for the fibers without the LB-100. The cross-section for fibers H30-1A, H30-2A, H30-3A and H30-4A are shown in Figure 4.6. The addition of the LB-100 did not deteriorate the shape of the H fibers in the H30-1A fiber, shown in Figure 4.6a. In fact, observations made from the SEM micrographs of the fibers in Figures 4.6a, 4.6b and 4.6c gives the appearance that the shape has improved compared to fibers H30-1, H30-2, H30-3 and H30-4 as shown in Figure 4.3. All of these fibers showed a slightly improved shape in terms of thick spots around the cross-bar and evenness of the fiber legs when compared to the fibers without any LB-100 additive. The only fiber to show a decrease in the retention of the rigid H shape was fiber H30-4A. Fiber H30-4 (shown in Figure 4.3d) shows H fibers with thin, even legs that attach to the cross-bar at angles approaching 90°. Fiber H30-4A did not seem to exhibit the same rigidness of legs and the high degree of geometric shape retention seen in fiber H30-4, although this may have been due to the winding process. The fibers with additive LB-100 could be wound but not without significant effort on the part

of the operator.

(a) H30-1A

(b) H30-2A

(c) H30-3A

(d) H30-4A
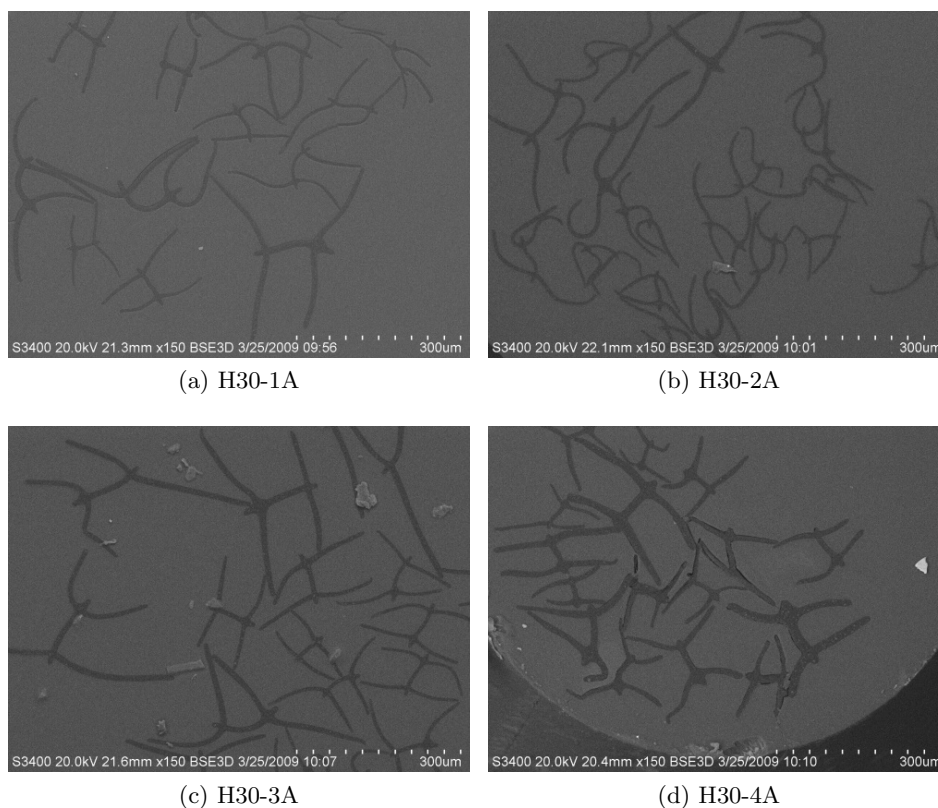
Figure 4.6: 30 dpf H fibers extruded from 18 MFI and 400 MFI PP with 5% LB-100 w/w

The cross-sectional perimeter and cross-sectional area of the fibers were similar for fibers H30-1A, H30-2A and H30-3A. The actual measurements are shown in Table 4.6. The thickening of the legs and cross-bar of H30-4A caused the perimeter to be slightly lower than the other fibers in this series. However, the cross-sectional area of H30-4A was essentially the same as the other fibers.

Table 4.6: DPF, Cross-sectional Perimeter and Cross-sectional Area of H fibers extruded from 18 and 400 MFI PP with 5% LB-100 w/w

Fiber	dpf (g/9000m)	Perimeter [SD] (μm)	Area [SD] (μm^2)
H30-1A	31.2	1045 [334]	4580 [2326]
H30-2A	33.9	1053 [195]	4597 [1395]
H30-3A	29.5	1138 [312]	5982 [2495]
H30-4A	30.4	813 [197]	5057 [2416]

4.2.7 Round and Y Fibers with Increasing Linear Density

Fibers with increasing linear density were extruded to facilitate the comparison of round and Y fibers based on surface area and dpf. The original fibers were extruded with a goal dpf of 30. For further comparison, fibers were extruded to meet goal dpfs of 60, 90, 120, 150, and 180. All of these fibers were extruded using 100% 18 MFI PP only. Only the round spinneret and the Y spinneret were used because the H shape was harder to maintain using only 18 MFI PP. The extreme variation of the H shape and the thicknesses of the legs and cross-bars made any comparison based on the dpf or surface area of the H fiber very complex. The repeatable shape of the Y and round fibers made comparison more feasible.

The cross-sections of the six round fibers used for comparison are shown in Figure 4.7. The cross-sections were all photographed at 65 magnification. The size of the round fiber cross-sections obviously increased from Figure 4.7a which shows the 30 dpf fiber to Figure 4.7f where the 180 dpf fiber is pictured. The diameter of fiber Y30-1 was approximately 82 μm and the diameter of the Y180-1 was approximately 182 μm. The average area of the cross-sections of the 30 dpf and 180 dpf round fibers increased from 5643 μm^2 to 29028 μm^2, an increase of approximately five times. Size variation occurred within each fiber, resulting in large and small round fibers in each cross-section. The values reported for each fiber were the averages calculated from measuring all the fibers pictured.

Although the size of the round fibers changed drastically as the dpf went from 30 to 180, the shape of the round fibers remained consistent. The same is true for the Y fibers pictured in Figure 4.8. Fiber Y30-1, pictured in Figure 4.8a, had long, thin legs. The same held true for all of the Y fibers as the dpf increased. The only observed change in the Y fibers as the size increased was that the legs thickened and lengthened. The original shape held regardless of linear density. The length of the legs for the Y30-1 fiber was approximately 82 μm and for the Y180-1 fiber was approximately 218 μm, an increase of two and a half times the length of the legs on the Y30-1 fiber. The area of the Y30-1 fiber was approximately 3143 μm^2 and the area of the Y180-1 fiber had an average cross-sectional area of 27029 μm^2. The measurements for the round and Y fibers from 30 to 180 dpf are listed in Table 4.7.

(a) R30-1

(b) R60-1

(c) R90-1

(d) R120-1

(e) R150-1

(f) R180-1
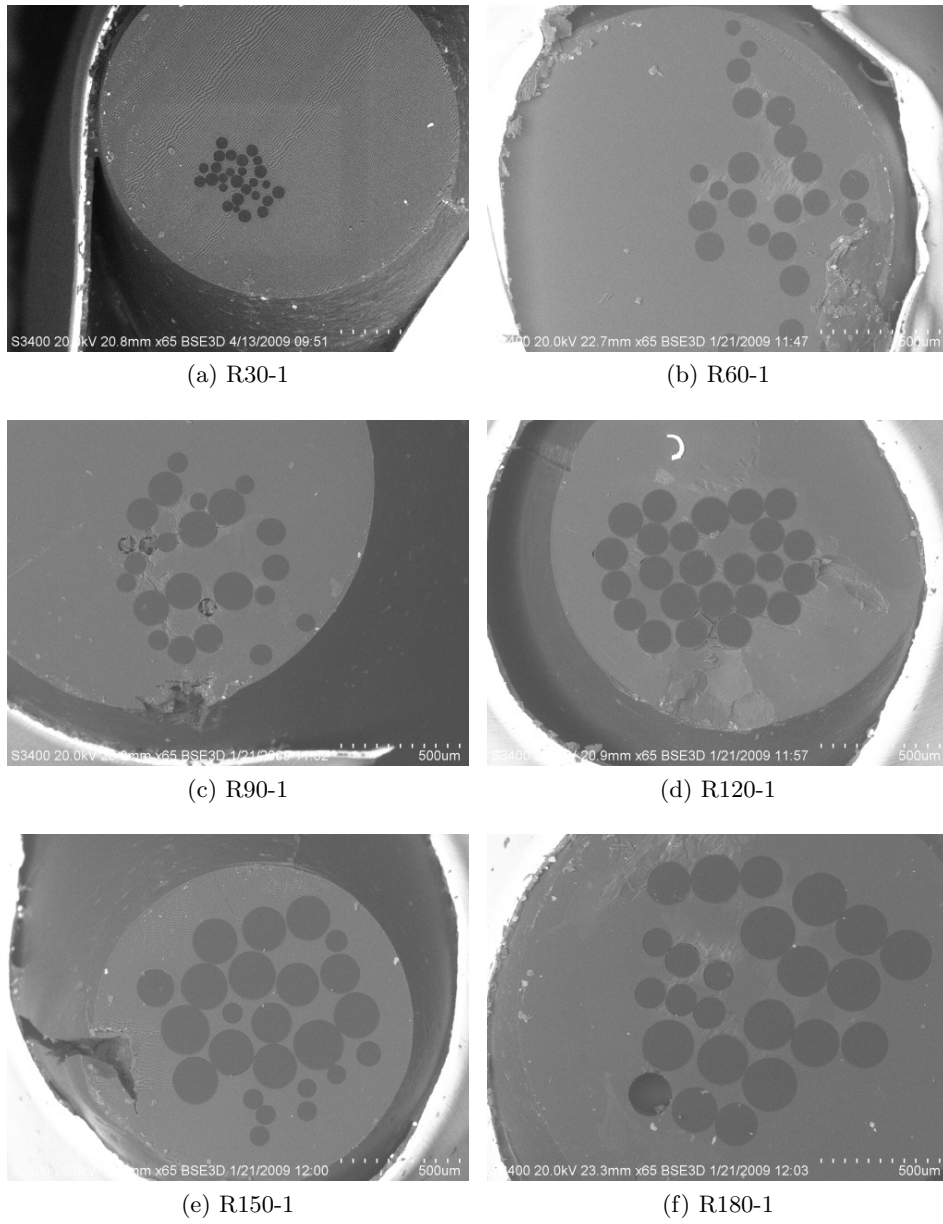
Figure 4.7: 100% 18 MFI PP Round fibers from 30 dpf to 180 dpf

103
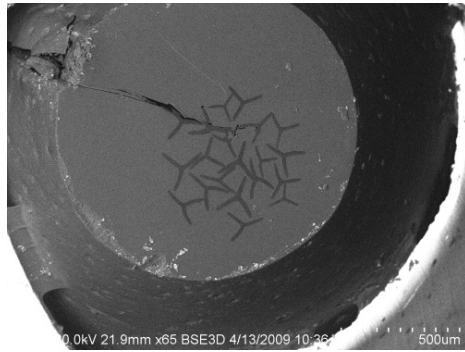
(a) Y30-1
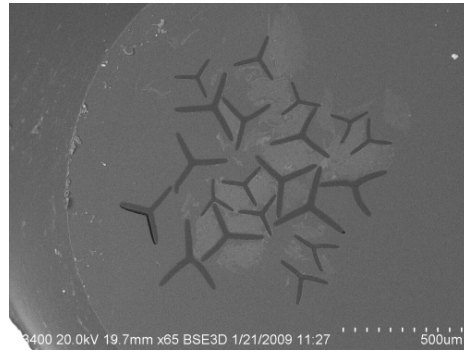
(b) Y60-1
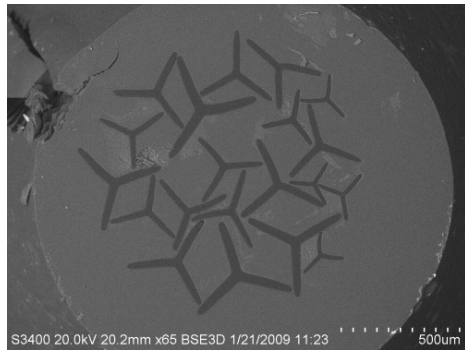
(c) Y90-1
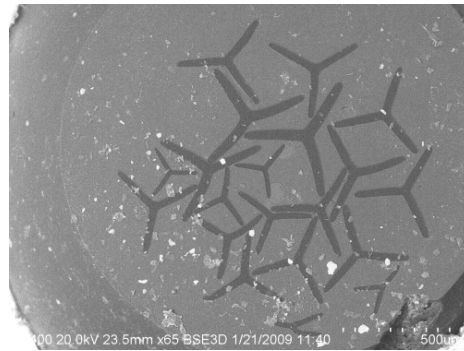
(d) Y120-1
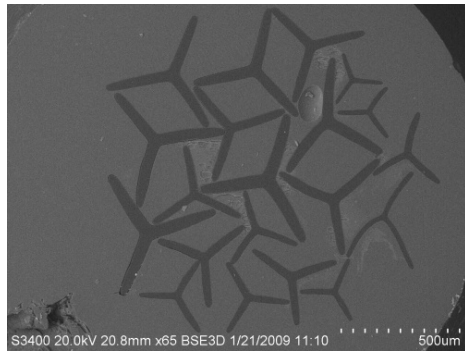
(e) Y150-1
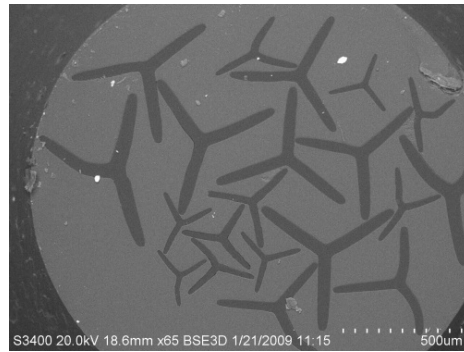
(f) Y180-1

Figure 4.8: 100% 18 MFI PP Y fibers from 30 dpf to 180 dpf

Table 4.7: DPF, Cross-sectional Perimeter and Cross-sectional Area of Round and Y Fibers with Increasing Linear Density

Fiber	dpf (g/9000m)	Perimeter [SD] (μm)	Area [SD] (μm^2)
R30-1	30.6	259 [37]	5643 [1575]
R60-1	61.0	339 [65]	10546 [3210]
R90-1	87.3	356 [102]	11424 [6057]
R120-1	119.9	434 [21]	16027 [1511]
R150-1	151.8	467 [163]	20327 [11543]
R180-1	179.8	571 [114]	29028 [10223]
Y30-1	29.8	467 [71]	3143 [891]
Y60-1	61.2	746 [168]	8498 [3489]
Y90-1	92.3	1012 [249]	15045 [6953]
Y120-1	123.7	1138 [254]	18226 [7715]
Y150-1	148.7	1272 [308]	23504 [11039]
Y180-1	181.3	1339 [444]	27029 [16120]

4.3 Fiber Shape Factor

One of the main focuses of this work was the extrusion of shaped fibers having a high geometric shape retention with respect to the spinneret holes.

The Shape Factor (η) of a fiber was given in U.S. Patent 5753166 as

$$\eta = \frac{P}{(4 \times \pi \times A)^{\frac{1}{2}}} \tag{4.1}$$

where

P = cross-sectional perimeter of the fiber (μm^2)

A = fiber cross-sectional area (μm^2) [20].

This same shape factor equation was used by Bueno, et. al. [13] in their work to correlate fiber shape and fabric properties. This equation relates the perimeter and area of the fiber cross-section in such a way that fibers with long, thin legs (and thus a larger perimeter) will have high shape factors. The shape factor equation is designed so that a perfectly round fiber will have a shape factor of 1.

4.3.1 Round Fibers

The shape factors for the round fibers extruded in this research are shown in Table 4.8. Although the shape factor for a theoretical round fiber is equal to 1, real round fibers have a slight distortion of shape that results in numbers that are slightly less than one. The 30 dpf round fibers all had a shape factor of approximately 0.97, but the larger dpf fibers had slightly lower shape factor values.

Table 4.8: Shape factor for round fibers

Fiber	Shape Factor (η)
R30-1	0.97
R30-1S	0.97
R30-2	0.97
R30-2S	0.97
R30-3	0.97
R30-3S	0.98
R30-4	0.96
R30-4S	0.96
R60-1	0.93
R90-1	0.94
R120-1	0.97
R150-1	0.92
R180-1	0.95

4.3.2 Y Fibers

The shape factors for the Y fibers are shown in Table 4.9. The average shape factor for the 30 dpf Y fibers was 2.14. This shape factor is approximately twice that of the round fibers, which seems logical considering that the Y fibers have twice the cross-sectional perimeter of the round fibers for an approximately equal cross-sectional area. The shape factor of the Y fibers did not change significantly with relation to the size of the fiber, however a slight change was observed with the inclusion of 25% and 50% 400 MFI PP in the fiber blend (the Y30-3 and Y30-4 fibers, respectively). The micrographs in Section 4.2.2 show a slight thickening of the fiber legs for the Y30-4 fiber compared to the Y30-1 fiber. This would indicate that the thicker legs of the fiber resulted in a lower shape factor, which agrees with the initial assessment that fibers with the longest, thinnest legs would have the highest shape factor.

Table 4.9: Shape factor for Y fibers

Fiber	Shape Factor (η)
Y30-1	2.35
Y30-1S	2.33
Y30-2	2.28
Y30-2S	2.27
Y30-3	2.12
Y30-3S	2.08
Y30-4	1.91
Y30-4S	1.82
Y60-1	2.28
Y90-1	2.33
Y120-1	2.38
Y150-1	2.34
Y180-1	2.30

4.3.3 H Fibers

Table 4.10 lists the shape factors for all of the H fibers, including those fibers with hydrophilic polyester additive. The average shape factor for the 30 dpf H fibers was 3.69. The shape factor of the H fibers varied drastically from fiber to fiber as the cross-sections of these fibers displayed a large range of fiber sizes and the fibers themselves had a dramatic change in leg thickness.

Table 4.10: Shape factor for H fibers

Fiber	Shape Factor (η)
H30-1	4.07
H30-1S	3.24
H30-2	3.58
H30-2S	3.54
H30-3	3.97
H30-3S	3.62
H30-4	3.06
H30-4S	3.13
H30-1A	4.36
H30-2A	4.38
H30-3A	4.15
H30-4A	3.23

4.3.4 Octolobal Fibers

Only one Octolobal fiber was extruded for this work, O30-1. This fiber had a shape factor of 3.18. This shape factor fell between the Y fibers at 2.14 and the H fibers at 3.69. Interestingly, although the Octolobal fibers have more channels than the H, the H fiber has a higher shape factor as it has a higher cross-sectional perimeter.

4.3.5 Improvement of Shape Factor

In the same patent where the shape factor equation was defined [20], Eastman stated that an improvement in shape due to additives could be calculated by

$$\%\text{improvement} = \frac{\eta_a \times 100}{\eta} - 100 \qquad (4.2)$$

where

$\%$ improvement = the improvement in the shape factor

η_a = shape factor of fiber with additives

η = shape factor of original fiber [20].

A positive $\%$ improvement would indicate that the shape of the fiber had improved, while a negative $\%$ improvement would indicate the deterioration of the shape. Unfortunately, using this method to compare the shape of the fibers places an increased emphasis on the length and thinness of the fiber legs. In other words, the shape of the fiber would only show an improvement if the legs were longer and thinner. This means that there is no actual correlation between the $\%$ improvement based on shape factor and the improved geometric shape retention of the fiber in comparison to the original spinneret hole.

Chapter 5

Results and Discussion: Oil Sorption Using Shaped Fibers

5.1 Oil Remediation and Shaped Fibers

Polypropylene fibers are commonly used as an oil remediation sorbent [68, 74, 78, 79, 82]. In general, the hydrophobic nature of PP makes it an excellent candidate for oil sorption. When PP is used for oil spills on water, very little water is adsorbed by the PP due to its hydrophobic nature. The increased surface area of shaped fibers such as H, Y, and Octolobal fibers could potentially lead to a higher oil sorption compared to round fibers of the same denier. ASTM F726, the Standard Test Method for Sorbent Performance of Adsorbents, was used to determine the capacity these shaped fibers had for oil in comparison to conventional round fibers. The initial step of testing the fibers for oil sorption was to determine the optimal oil for the test purposes. The ASTM standard provided guidelines to identify appropriate testing oils using properties such as viscosity and density. Three oils were selected for possible use in the oil sorption testing. The three oils used were Canola Oil, Havoline 10W-40, and a 1:1:1:1 mixture of n-Tetradecane, Hexadecane, Heptadecane and n-Pentadecane which is listed as a "Crude Oil Internal Standard" for gas chromatography analysis by Sigma-Aldrich [86]. ASTM F726 included a table describing testing oils based on

density and viscosity. The three oils, canola oil, Havoline 10W-40 and the internal standard, were evaluated to determine their density, viscosity, and surface tension. The surface tension of the oils was measured to determine if one oil would have a higher preference for PP than the other oils. Only four fibers were tested for oil sorption capabilities: R30-1, Y30-1, H30-1 and O30-1. These fibers (made from only 18 MFI PP) were used because the author desired to compare the sorption of these fibers to reported sorption levels in literature [69]. Since the fibers tested in literature were generally neat PP fibers, in this work, only the neat PP fibers without any additives or spin finishes were evaluated.

In oil sorption, the fibers encounter oil in an immersion setting. In other words, the fibers are submerged in oil (or in a oil/water mixture) that completely covers the fibers. For PP fibers in oil, the immersional wetting is energetically favorable because the contact angle of oil on PP is less than 90° and as stated in Chapter 1, $-\Delta G_i = \gamma_{LG} cos\theta$. Therefore, the ability of the fibers to adsorb oil on their surface is not being measured in these procedures - the oil surrounds the fibers during testing and thus is already in contact with the surface. Instead, the ability of the fibers to *retain* the oil is being investigated. The channels within the fibers were expected to play a large role in the retention of the oil. The H and Octolobal fibers have channels with parallel sides. These channels would likely be able to exert some capillary force on the oil that would help trap the oil in the channels once the fibers were removed from the oil bath. The Y fibers do not have the same type of channels. The channels in the Y fibers are most likely too large and too wide to exert capillary forces on the oil held by a single fiber. However, the channels within the Y fibers were designed to interact with other channels to form a structure that could retain fluid, although the exact interaction of the fibers to form such a system is not known and was not investigated in this work.

5.2 Characterization of Oils

5.2.1 Determination of Oil Density

The density of each oil was determined using the method described in Section 2.7.1.1. The average densities of the three oils are shown in Table 5.1 along with the values from literature and MSDS sheets.

Table 5.1: Density of Canola Oil, Havoline 10W-40 and 1:1:1:1 Standard Oil Mixture as measured and from literature

Oil	Canola Oil	Havoline 10W-40	Standard Mixture
Measured Density (g/cc)	0.9153	0.8663	0.7666
Reported Density (g/cc)	0.905-0.912 [99]	0.8713 [100]	0.763 [86]

The standard for oil testing that was used for this research, ASTM F 726, divided oils into four categories: Light, Medium, Heavy and Weathered. The distinguishing factor for each group is the viscosity range as the density ranges overlap. The table from ASTM F 726 is shown in Figure 5.2. According to the density ranges given, the measured and cited value of density for Canola oil was firmly within the 'Medium' oil type category. The Havoline 10W-40 motor oil had a density that fell into both the 'Light' and 'Medium' categories based on the measured value but was at the lower end of the 'Medium' oil type only based on the cited density value. The standard oil mixture, with a density of 0.7666 g/cc, fell below the lowest of the density ranges; however, this oil mixture was evaluated further because it was recommended by the advisory committee because of its well defined composition.

Table 5.2: Oil Types and Properties, taken from ASTM F 726 [101]

Oil Type	Viscosity Range	Density Range	Example
Light	1 to 10 cP	0.820 to 0.870 g/cm^3	Diesel fuel
Medium	200 to 400 cP	0.860 to 0.970 g/cm^3	Crude oil, canola oil
Heavy	1500 to 2500 cP	0.930 to 1.000 g/cm^3	Bunker C or residual fuel
Weathered	8000 to 10000 cP	0.930 to 1.000 g/cm^3	Emulsified crude oil

5.2.2 Determination of Oil Viscosity

The viscosity of each of the three oils was determined using the TA Instruments AR 2000 Advanced Rheometer. The Havoline 10W-40 and the Canola oil were evaluated at shear rates from 1 1/s to 100 1/s; however, the internal standard mixture was of such a low viscosity that higher shear rates were used (up to 1000 1/s) to gather more data where the instrument was able to reach equilibrium. Any point where the instrument failed to reach equilibrium was considered invalid and was not reported. Figure 5.1 shows the viscosity measurements of the three oils on a log/log scale.

Although all three oils experienced slight thinning with increased shear rate, the difference in the viscosities of the oils was distinct. The internal standard had a viscosity from 3–6 cP, the canola oil ranged from 57–64 cP and the Havoline 10W-40 motor oil had a viscosity range of 144–171 cP. Based on these viscosities, the internal standard oil would fall into the "Light" oil type specified in ASTM F 726 and the 10W-40 and canola oil would fall somewhere between the "Light" and "Medium" oil types (see Table 5.2).

5.2.3 Determination of Oil Surface Tension

The surface tension of the three oils was measured using the method described in Section 2.7.1.3. Ten droplets were measured for each oil and the average surface tension was calculated from those measurements. The calculated average surface tension for each oil is displayed in Table 5.3.

Table 5.3: Surface Energies of oils and PP

Oil	Surface Tension (mN/m)
Canola	28.20 ± 0.44
Havoline 10W-40	35.35 ± 0.32
Internal Standard	32.33 ± 0.88
PP	30.5 [102]

The surface energy of PP has been measured as 30.5 mN/m [102]. For fluid to spread across a solid surface, the work of adhesion between the fluid and solid must be
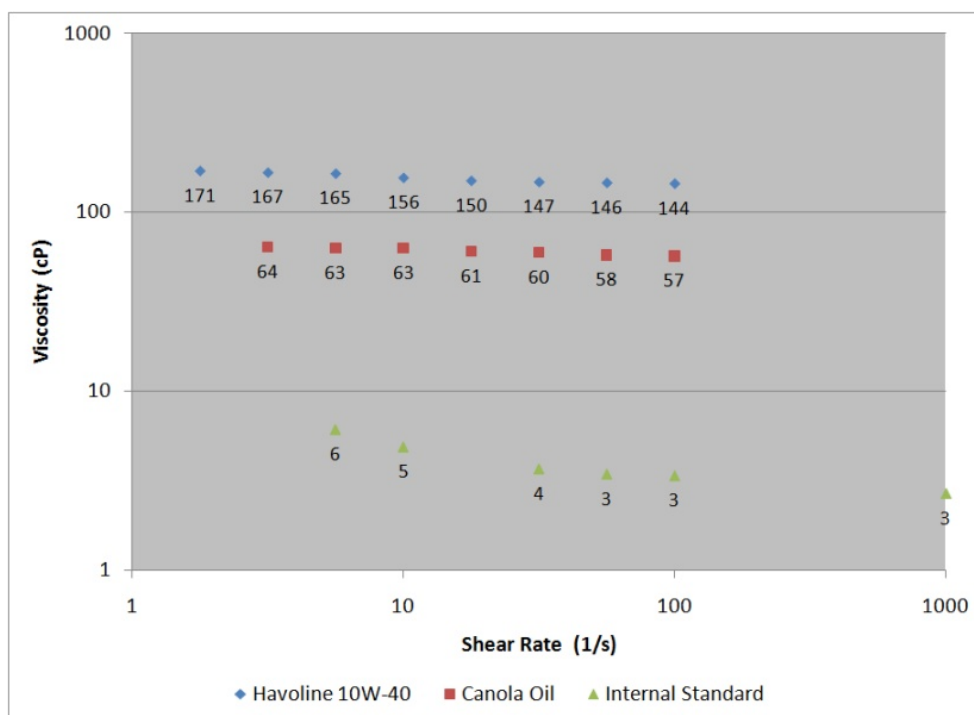
Figure 5.1: Viscosity measurements of the three oils using the AR 2000 Advanced Rheometer
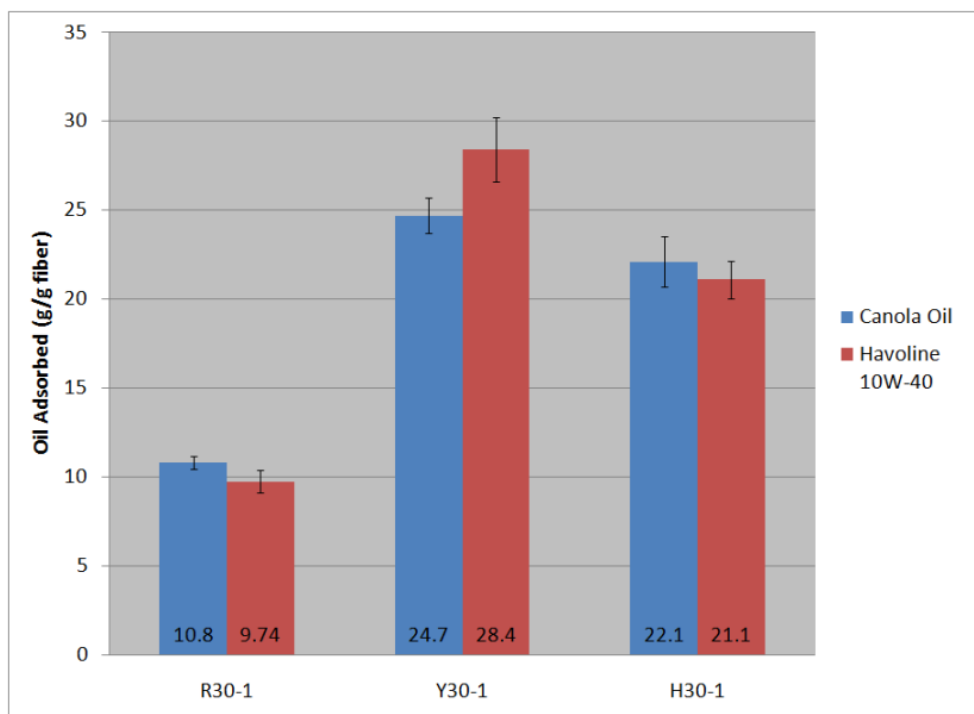

Figure 5.2: Oil sorptions of loose R30-1, Y30-1, and H30-1 fibers after 15 minutes of submersion in Canola and Havoline 10W-40

greater than the work of cohesion within the fluid. In addition, fluids will spread more easily on surfaces of similar surface energy. The similarity of the surface energies of the PP and the oils indicated that the three oils would spread on the surface.

5.3   Preliminary Oil Testing

The results from the characterization of the three oils showed that the Internal Standard mixture had an extremely low viscosity, making it a poor choice for simulating a fuel oil spill. This internal standard was originally designed as a gas chromatography internal standard, not as a simulant for oil spills, which further justified its exclusion from oil sorption testing. The canola oil and the Havoline 10W-40 had essentially the same density and surface energy and similar viscosities, so further testing was required to determine which oil would be more appropriate for testing. Preliminary oil tests were used to determine the sorption level of the oils for the R30-1, Y30-1 and H30-1 fibers. One gram of loose fiber was placed into a 1 L jar full of the specified oil for 15 minutes. After this time, the oil and fibers were poured through a strainer and were allowed to drain for 30 seconds before being transferred to a weigh pan. The act of pouring the fibers into the strainer caused more oil to collect on top of the fiber mass and could not drain through in 30 seconds. This increased the amount of oil some samples adsorbed. Additionally, some of the fibers were found to stick to the side of the testing cell and were virtually impossible to collect.

The results from the preliminary test are shown in Figure 5.2. The R30-1 and H30-1 fiber samples adsorbed more canola oil than 10W-40 oil. The Y30-1 fiber samples adsorbed more 10W-40 oil. This increased sorption of the 10W-40 oil by the Y30-1 fiber samples may show that the large channels created by the long-legged, open structure of the Y fibers can adsorb the viscous oil more quickly than the more square channels of the H30-1 fibers. Regardless, the comparison of the two oils revealed that the sorption levels were very similar for each type of fibers. The internal standard mixture was rejected because its low viscosity made it unsuitable for simulating crude oil sorption, even though the repeatability

116

of its components was desirable. Based on the results from the oil density, viscosity, surface tension tests and the preliminary testing, the canola oil and the motor oil were equally qualified to serve as an oil for these tests. The inclusion of canola oil in the ASTM standard made it more desirable as a testing material. This choice was legitimized by the inclusion of Canola oil as a representation of a fuel oil spill. In addition, the 10W-40 motor oil had a strong odor that was offensive to other laboratory workers and it also required special disposal procedures, thus the canola oil was the preferred oil for further testing.

5.4 Oil Sorption Tests ASTM F-726 Modified

The Standard Test Method for Sorbent Performance of Adsorbents, ASTM F-726, was the standard consulted for the oil sorption testing. The standard defined four types of sorbents. Type I sorbent is a roll, film or sheet of material, Type II sorbent is loose or particulate material that has to be removed from liquids using scoops or similar equipment, Type III sorbent is enclosed in a fabric or netting, like pillow or booms and Type IV sorbent was an agglomeration unit (an open mesh) designed for high viscosity oils. The fibers used in these experiments were classified as a Type II adsorbent based on these definitions. The standard recommends a 4 L jar for the Dynamic Degradation testing, however, the equipment available to simulate the wave-like nature of a body of water could only accommodate a 1 L jar. Since the testing cell had to be modified to be $\frac{1}{4}$ of its original size, the fiber samples were also scaled down from the recommended 4g of material to 1g of material. Additionally, when using shaped PP fibers, 4g of material inherently occupies a larger volume than 4g of round fiber. The tests were designed to determine the sorption capacity of the fibers without any significant spacial constraints, thus the increased volume of the fiber samples required a large testing cell. As previously discussed, a 1 L jar was necessary for equipment compatibility, and 4g of shaped fiber would not fit comfortably within this jar, so the smaller fiber sample of 1 g was required.

In order to maintain the fiber mass and reduce the loss of fibers throughout the test,

117

an open cage system of PP mesh with holes 4 mm by 5 mm was constructed to hold the fiber samples. This insured that the fibers did not disperse within the testing cell or stick to the side of the testing cell walls, inhibiting collection, as discussed in Section 5.3. The standard actually recommends a basket for testing and collection of type II sorbent during the oil sorption short test, however a basket would also retain some of the fibers and affect the results of the test.

5.4.1   Oil Sorption Short Test

The Oil Sorption Short Test determined the maximum capacity of the fibers for canola. To this end, no water was added to the testing cell, only oil. The testing cell was filled with oil to a height that was greater than the size of the sample. The fibers to be evaluated were the R30-1, Y30-1, H30-1 and O30-1 fibers. The standard recommends that three samples be tested for each adsorbent and an average value of oil sorption calculated. If the individual samples deviated from the average by more than 15% of the mean, the samples were discarded and new samples were tested as directed by the standard. The resulting average oil sorptions for the R30-1, Y30-1, H30-1 and O30-1 fibers are shown in Figure 5.3. Although the data was reported in grams of oil adsorbed per gram of fiber, the reader should note that the samples were all approximately 1 gram, so the total sorption of oil was very similar for each sample.

Table 5.4: Surface area (SA) and oil sorption for 30 dpf yarns

Yarn	Avg. No. of Filaments	Sorption per Filament (g/fil)	SA of 1 Filament (μm)	Avg. SA of 1g Sample (m^2)	Sorption by SA (g/m^2)
R30-1	5878	2.06×10^{-3}	1.32×10^7	0.077	156
Y30-1	5967	3.71×10^{-3}	2.37×10^7	0.142	157
H30-1	5817	3.57×10^{-3}	4.78×10^7	0.281	74.7
O30-1	5798	2.70×10^{-3}	3.82×10^7	0.222	70.6

Figure 5.3 clearly shows that the round fibers were unable to adsorb as much oil as any of the shaped fibers. The data from Figure 5.3 was further analyzed to determine the
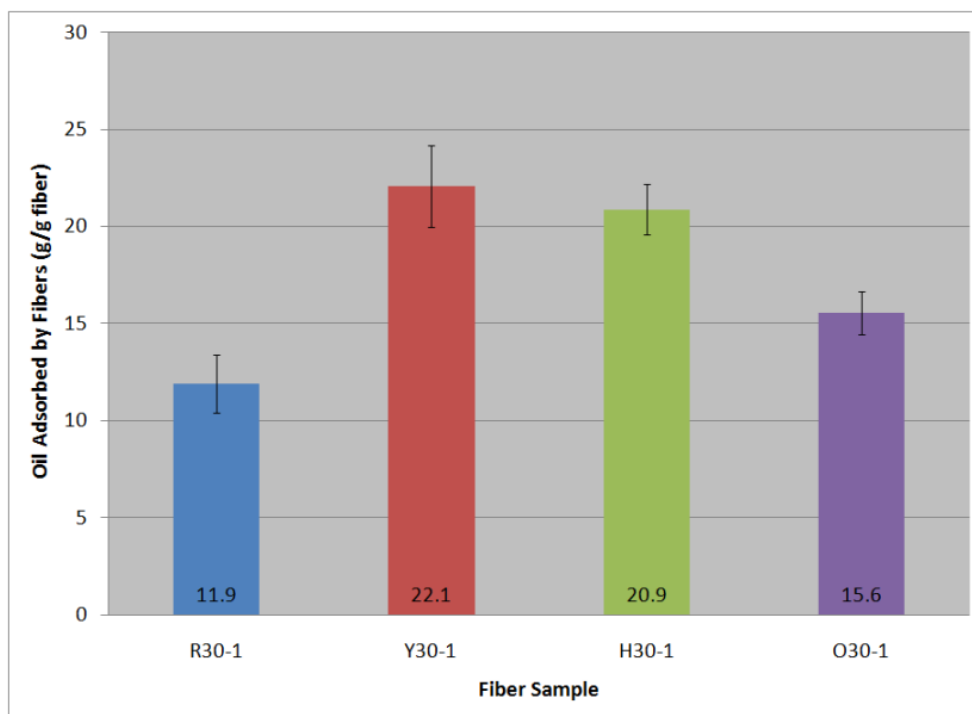
Figure 5.3: Oil sorptions of R30-1, Y30-1, H30-1 and O30-1 fibers after 15 minutes of submersion

amount of oil adsorbed per filament and per square meter of surface area. The relevant data and results for these calculations can be found in Table 5.4. The average number of filaments was approximately the same for all four fiber samples as the fibers were all approximately 30 dpf and the fiber samples all weighed 1 gram. Due to this, the adsorbance of oil in grams per filament follows the same trend as the samples in Figure 5.3. When compared on a basis of sorption by surface area of the samples, the R30-1 fiber samples adsorbed 156 g/m^2. The Y30-1 fiber samples adsorbed a similar amount at 157 g/m^2.

The data in Figure 5.3 shows that the round fibers sorbed 11.9 grams of oil per gram of fiber. The Y30-1 fiber bundles sorbed 22.1 g of oil/g of fiber, the H30-1 fiber bundles sorbed 20.9 g/g of fiber and the O30-1 fiber sorbed 15.6 g/g of fiber. The Y30-1 fiber sample sorbed almost twice the amount of oil of the round fiber sample. This ratio of sorption was very similar to the ratio of surface area for the fibers. The round fibers had on average a perimeter of 254 μm and the Y fibers were almost twice that at 467 μm. This

119

could indicate that oil sorption is based solely on surface area for fibers. However, if this were the case, then one might expect to see an even higher oil sorption from the O30-1 and H30-1 fiber samples, as the average perimeters of the Octolobal and H fibers were higher than the Y at 752 μm and 941 μm, respectively. Instead, as can be seen, the Octolobal and H fiber samples sorbed less oil than the Y30-1 fiber samples but more than the round fiber samples. Thus, the oil sorption capacity of the fiber bundles does not appear to be based solely on the sorption of oil to the surface of the fibers.

The failure of the Octolobal and H fibers to adsorb as much oil as was expected based on the Y fiber results could indicate one of two things: that some factor in the design or shape of the Octolobal and H fibers inhibited the oil sorption, or that the Y fibers actually sorbed more oil than should have been expected. If the problem lies with the H and Octolobal fibers, one must conclude that there is something about the designed shape of these fibers that limits the interaction of oil with the surface of the fibers in some areas. The main difference between the shape of the Y fibers and the shapes of the Octolobal and H fibers is the type of channel within the fiber. The Octolobal and H fibers have round or square bottomed channels with legs extending parallel to each other from the bottom of the channel. The Y fibers do not have a flat bottom channel and instead have legs extending at 120 degrees from each other. The parallel leg structure of the channels within the H and Octolobal fibers may indeed be limiting the amount of oil that can gain access to and thus adhere to the surfaces inside those channels. The channels within the fibers were designed to act as individual capillaries. When liquid enters a capillary from both ends, air can often be trapped in the center of the capillary. Although the channels within the H and Octolobal fibers are also open to liquid at the side, any air in the channels of the fibers immediately before immersion into the oil could become trapped as air bubbles. These air bubbles would take up space that oil could occupy and thus reduce the sorption of oil. Another possibility is that the channels within these fibers are actually too small to hold the amount of oil that would otherwise adhere to the surface area available within the channel. If the PP surface can adhere an oil layer that is thicker than $\frac{1}{2}$ the width of the channel, the existence of

the channel would actually decrease the amount of oil sorbed. The legs of each individual H and Octolobal fiber may also be interacting with the legs of other fibers in a negative manner. Any overlapping of the legs would decrease the size of the available channels and cause them to have a lower capacity.

The second possibility is that the H and Octolobal fibers were adsorbing to their full capacity, but that the Y fibers actually sorbed more than was expected based on their structure. In this case, the long-legged, open channels of the Y fibers may actually be able to hold more oil than the channels of the H and Octolobal fibers. In addition, the inter-fiber structure formed by the Y fibers may also have a much higher capacity than the inter-fiber structures formed from the H and Octolobal fibers. Although the legs of the H fibers could possibly interact with fibers nearby, they were not designed to extend from the main body of the fiber at an angle that would increase the likelihood of this interaction. This statement is also true for the O30-1 fibers and the Octolobal fibers have even shorter legs than the H fibers. This open, inter-connected structure of the Y fibers may have further enhanced the sorption properties of the fibers and increased the amount of oil sorbed. The existence of such a structure is supported by the openness of the Y fiber samples prior to testing. The Y fibers had the highest openness of any of the shaped fiber samples. The round fibers, even when physically seperated to provide more openness to the fiber sample, settled on the bottom of the sample cage. Although the H and Octolobal fibers had a higher level of openness than the round fibers, they were still more compact than the Y fibers. As no force was used to pack the fibers together, the degree of openness of each fiber sample was based solely on the fiber shape. The natural tendency of the Y fibers to form an open structure when dry provided larger voids for fluid to fill and the same shape resulted in a more open structure once the sample had sorbed fluid.

In order to understand how the fibers were packing once they had sorbed oil, a visual representation of the oil laden fibers was prepared. This representation was based on the amount of oil sorbed per filament for each of the round and shaped fibers as calculated from the total oil sorbed by the sample and the number of filaments in each sample. The

121

following assumptions were made:

- Every fiber in the sample collected to its maximum capacity (there were no air bubbles in the fiber/oil sample).

- Every fiber in the sample on average collected the same amount of oil.

- The oil on an individual fiber coated the entire fiber length, thus the length of the fiber and the length portion of the oil volume were equal.

Using the calculated volume of oil sorbed by each fiber, the oil density as measured in Section 5.2.1 and an average fiber length of 2 in (5.08 cm), it was possible to determine the cross-sectional area the oil would occupy. Table 5.5 shows the calculated values for each of the round and shaped fibers. By adding the calculated cross-sectional area of the oil and the measured cross-sectional areas of the fibers, it was possible to determine the radius of a circle of oil surrounding a fiber. Figure 5.4 shows the circles representative of oil sorption for each of the round and shaped fibers to scale. However, this cannot be used to represent a system that contains thousands of fibers. The fibers on the outside of the sample may have an sorbed oil layer that approaches a circular configuration at some points, but the interior fibers must all be surrounded by a continuous sea of oil. A more effective approach for mapping oil-fiber interactions is to designate a shape around the fiber that contains the same calculated area of oil but is also repeatable in a tiled format. An example of plausible shapes is also shown in Figure 5.5. These fibers and the areas outlined by the shape around them are to scale. These figures can also be used to show the relative distances of the fibers within the oil "sea". Figure 5.6 is a two-dimensional representation of a complex three-dimensional reality imagined in the imagination of the imaginer. This fairly simple, yet remarkable representation clearly shows that although the Octolobal and H fibers have a higher surface area than the Y fibers, the Y fibers assemble to enhance the overall oil sorption capacity. There is no expectation that real systems will orient along the lines of Figure 5.6. Each fiber assembly will orient differently based on the fiber interactions

and shape. This representation is just that, a representation meant to assist the reader in visualizing the different levels of oil sorption.

Table 5.5: Oil sorption per filament and calculated areas for sorbed oil for 30 dpf yarns

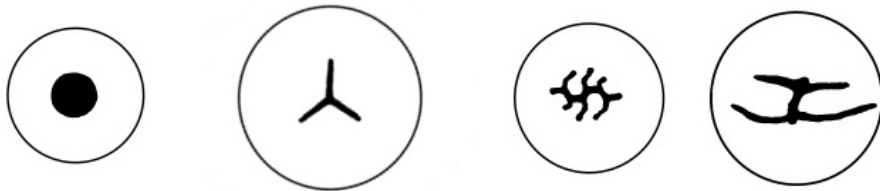| Fiber	Oil vol. / filament (cc/fil)	Cross-sectional area of oil (μm^2)	Radius of circle with area of oil + fiber area (μm)
R30-1	0.00224	44071	126
Y30-1	0.00404	79546	162
O30-1	0.00294	57865	141
H30-1	0.00388	76360	160

Figure 5.4: To scale comparison of fibers and their calculated oil sorption per filament as represented by a circle
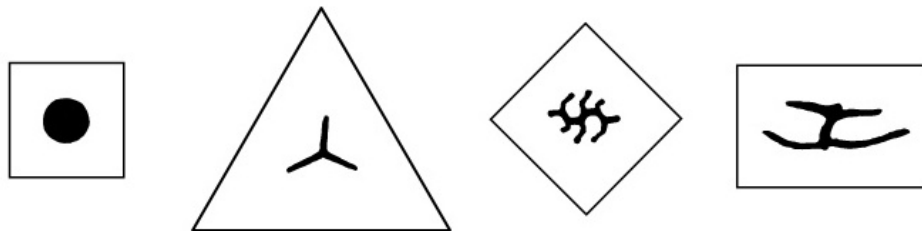

Figure 5.5: To scale comparison of fibers and their calculated oil sorption per filament as represented by tileable shapes
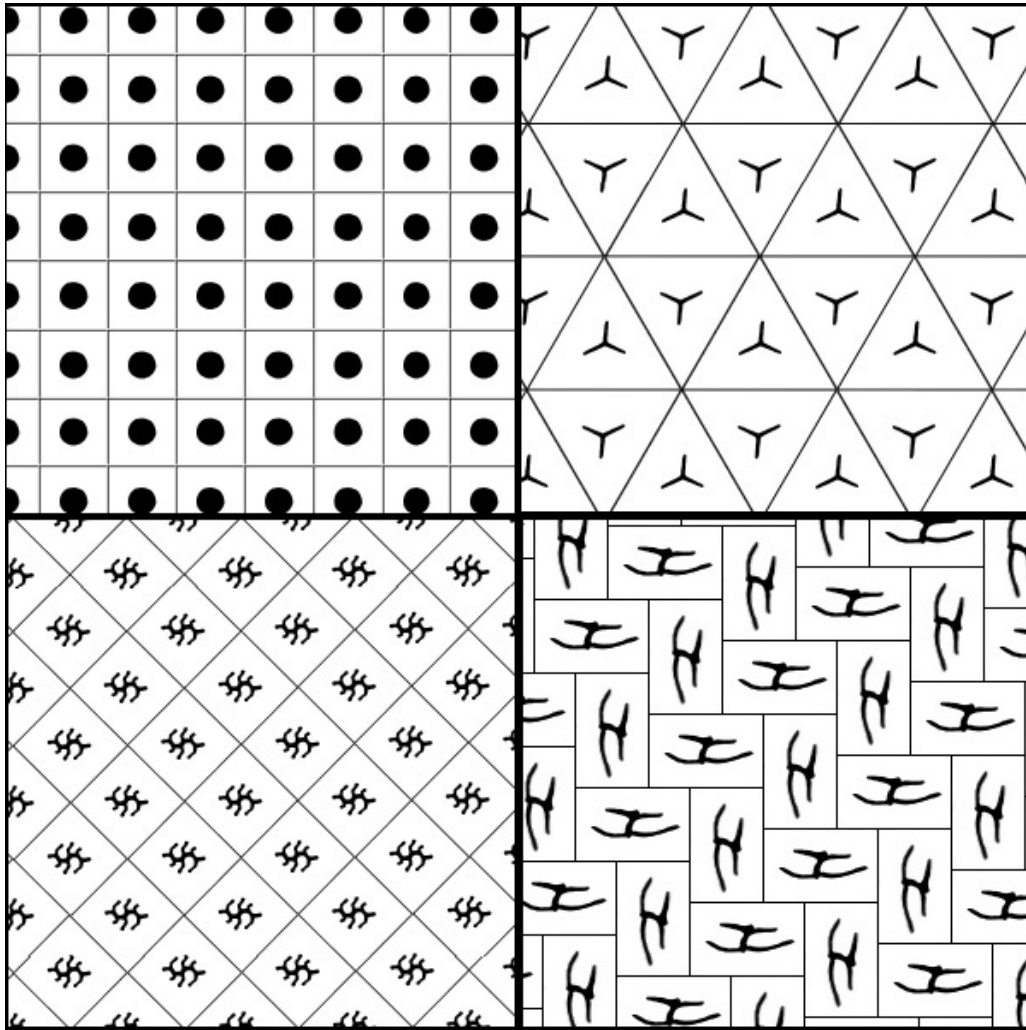
123

Figure 5.6: To scale comparison of fibers and their calculated oil sorption per filament in a tiled format

5.4.2 Dynamic Degradation Testing

Although the oil sorption properties of the shaped fibers in pure oil were shown to be much greater than those of the round fibers, a second procedure was used to determine whether these same four fibers were as effective in removing oil from water. The dynamic degradation test from ASTM F726 allows the materials being examined to be tested for water sorbency as well as oil sorbency in the presence of water. To achieve this, the samples are first exposed to water and then exposed to a water/oil mixture of 2 L of water and 3 mL of oil. As with the previous method, this method was modified to use a smaller, 1 L jar. This method was also modified to include more oil as the previous tests had already indicated an sorption capacity much higher than 3 mL (2.75 g) of oil. For the purpose of this work, three different amounts of oil were used: 10 g, 20 g, and 30 g of oil, each in 500 g of water. These amounts of oil were also used in the work of Teas, et. al. wherein the authors tested various sorbent materials at a loading of 10 g, 20 g, 30 g, 40 g, and 50 g of oil in water [69]. Three samples of caged fiber were tested for each amount of oil. The average amount of oil sorbed by the caged fiber sample is shown in Figure 5.7. The values presented here represent the the total mass of oil sorbed by both the cage and the fibers. For the experiments conducted with 10 g of oil, all three fibers were able to sorb almost the full amount of oil. The caged fiber samples of H30-1 sorbed an average of 9.67 g of oil out of 10 g of oil or 97% of the oil present, the caged fiber samples of Y30-1 sample sorbed an average of 9.89 g of oil (99%) and the O30-1 caged fiber samples sorbed an average of 8.79 g of oil at 88%. By comparison, the caged R30-1 fiber sorbed 7.94 g of oil, or 79% of the oil in the system. With only 10 g of oil in the system, all four fibers sorbed a similar amount. However, the capacity of the fiber samples (as determined in only oil and shown in Figure 5.3) was more than 10 g for all four fibers. This indicated that a larger amount of oil was necessary in the system to distinguish between the sorption properties of the fibers, hence the test method was modified again to include an increased volume of oil.

The maximum sorption capacity for the fibers (as determined by the Oil Sorption Short Test [Section 5.4.1]) was 11.9 g, 22.1 g, 20.9 g, and 15.6 g for the R30-1, Y30-1, H30-1
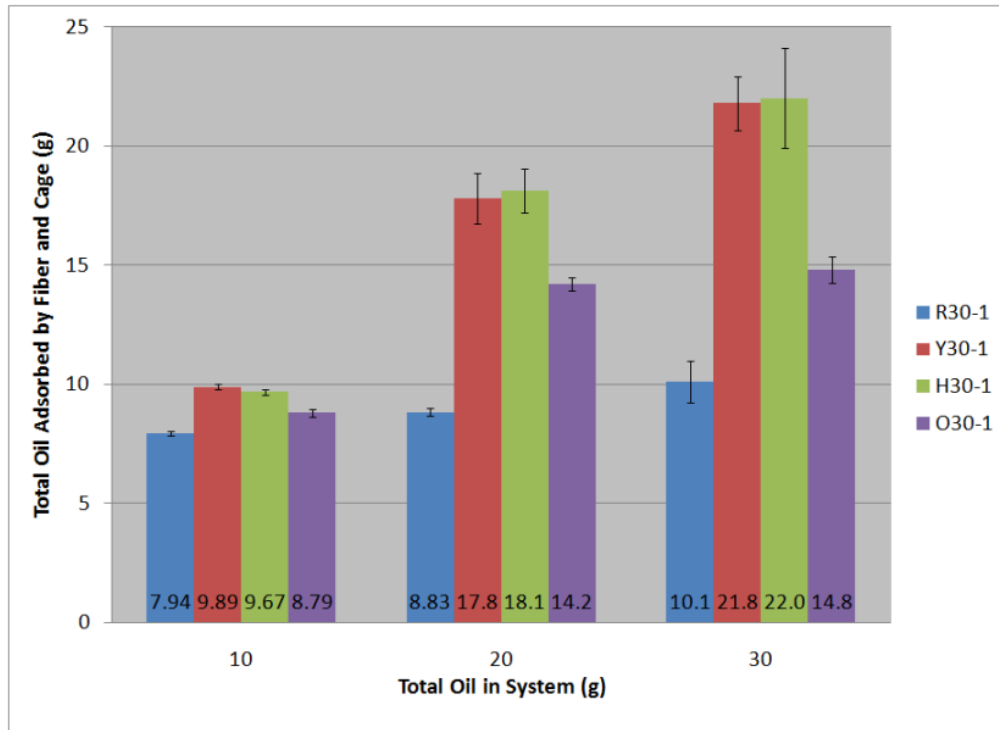
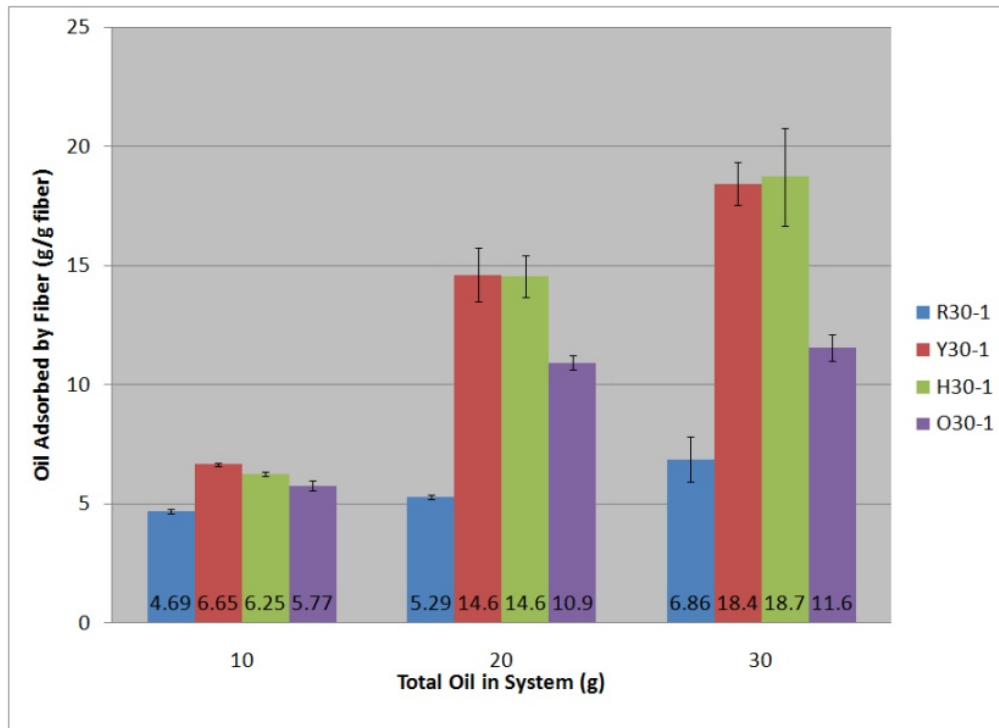Figure 5.7: Total oil sorption during Degradation Oil Testing

Figure 5.8: Oil sorbed by fibers alone during Degradation Oil Testing

126

and O30-1 fiber samples respectively. At these sorption capacities, a difference between the round and shaped fibers could be expected to be seen at a level of 20 g in the oil/water system. Indeed, the values for the four fibers in Figure 5.7 show this to be the case. Even with 20 g of oil in the system, the R30-1 caged fiber sample could only sorb a total of 8.83 g of oil, only 44% of the oil. The Y30-1 and H30-1 fiber samples sorbed more than twice this amount at 17.8 and 18.1 g of oil respectively. These values correlate to 89% and 91% of the oil. Even at this level of sorption, these values are less than the maximum capacities of these fibers. The O30-1 fiber samples sorbed 14.2 g of oil (71% of the available). This sorption of oil from water was the closest to the maximum capacity for all the fibers tested. This implies that the numerous small channels in the Octolobal fibers increase the attractive force on the oil. The H fiber has channels, but it does not have as many as the Octolobal. The Y fiber's channels are too large to contribute a strong capillary force to attraction. However, the limited capacity of the Octolobal fiber's channels makes them less desirable than the H and Y fibers, even if they are more likely to sorb their full capacity.

When 30 g of canola oil was placed into water, the amount of oil in the system exceeded the capacity of all three fibers. This was done on purpose to try to force the fiber samples to sorb to their maximum capacity. At 30 g of oil in water, the R30-1 caged fiber sorbed 10.10 g of oil, the Y30-1 caged fiber sorbed 21.78 g, the H30-1 caged fiber sorbed an average of 22.05 g of oil and the O30-1 caged fiber sorbed 14.8 g of oil. At these levels, the fibers had sorbed almost to their maximum capacities. Indeed, the H30-1 fiber samples sorbed slightly more oil than the maximum capacity indicated in the previous Oil Sorption - Short Test. As these values of sorption include not only the fibers but also the fiber cage, this indicates that a portion of the sorbed oil was sorbed by the cage.

Figure 5.8 shows the amount of oil sorbed by the fibers after being normalized for the amount of oil sorbed by the cages. The cages used for these experiments were made from PP so that they would float on water and to minimize any change in the attraction of the oil to the fibers. Empty cages were subjected to the same experimental conditions as the fibers at the same three levels of oil in water and a value of how much oil the cages

127

would sorb was calculated in terms of grams of oil per gram of cage material. The empty PP cage sorbed 0.367 g, 0.430 g and 0.442 g of oil per gram of cage material for 10 g, 20 g, and 30 g of oil in the system, respectively. These values were used as the maximum amount of oil each cage could have sorbed, although adding fiber to the testing cell may have actually reduced how much oil was sorbed by the cage. The total amount of oil sorbed was adjusted based on the oil theoretically sorbed by the cage and then the adjusted oil amount was divided by the weight of the fiber samples. The results are presented in Figure 5.8.

When the sorption amounts were adjusted for the possible sorption of oil by the cages, the figure clearly showed that the Y30-1, H30-1 and O30-1 fiber samples did not sorb their full capacity of oil, even at the 30 dpf level. Although the increased presence of oil gave results closer to full capacity (as determined by the oil sorption short test), at no point was the maximum capacity reached. The implication of this is that the oil-water exchange is not complete after the 15 minute test cycle. The results of the adjusted oil sorption during dynamic degradation (Figure 5.8) showed that the shaped fibers were able to sorb two to three times the amount of oil that the round fiber did for the 20 g and 30 g oil samples. The Y30-1 and H30-1 fiber samples sorbed more oil in all three experimental set-ups than did the O30-1 fiber samples, again indicating that the longer, thinner legs of the Y and H shapes created a more effective sorption matrix than the more compact and shorter legs of the Octolobal fibers. Although the work of Teas, et. al. tested sorbents with 40 and 50 g of oil in the water as well, these levels were not used as the fibers were approaching a maximum capacity at 30 g of oil in the water. Additionally, regardless of how much oil was included in the procedure, the sorbents evaluated by Teas, et. al. never sorbed more than 5 g of oil [69].

5.5 Oil Sorption Tests in Aluminum Cages

Another cage was constructed from a material with a higher density and a smaller mesh structure with holes 2 mm by 2 mm. This new cage material was used to see if these factors influenced the sorption properties of the fibers. The higher density cage material caused the PP fibers to sink within the testing cell. In an instance where a vessel carrying oil sank, like the *Prestige* that sank in the Galicia Bank Region [103], a cage that was denser than water could be used to place the sorbents around the oil leaks. In such a case, a small mesh would be desirable to limit the ability of the local marine life to get caught in the cages.

The same experiments previously conducted with the PP cages were conducted on the H30-1, Y30-1, and R30-1 fibers in aluminum cages using the Oil Sorption - Short Test and the Dynamic Degradation Testing. The Octolobal fibers were not tested as these tests were conducted prior to their inclusion in this research. These experiments were conducted to determine whether the cage material affected the results of the experiments. Figure 5.12 shows the results of the oil sorption short test. These results agree with the previous tests with the PP cages in that the shaped fiber samples sorbed three times as much oil as the round fiber samples; however, the Y fiber samples sorbed less oil than the H fiber samples. Previously, the Y fiber samples sorbed more oil than any of the other fibers, but the change in cage material affected their sorption capacity. This was thought to be due to one of two factors: the aluminum cages had a slightly smaller volume than the previously used PP cages and the aluminum cages had a smaller mesh size than the PP cages.

The dynamic degradation test was conducted in the same manner for the aluminum cages as it was for the PP cages. Figure 5.10 shows the total sorption amounts for the three fibers and their cages and Figure 5.11 shows the sorption of oil attributed to the fibers alone after adjusting for the cage sorption of approximately 1.2 grams of oil per gram of cage. The H and Y fiber samples sorbed more oil than the round fiber samples, with each type of fiber absorbing increasing amounts as the total amount of oil in the system increased.

A distinction between the experiments with PP cages and the experiments with aluminum cages was that the Y30-1 fibers did not exhibit a higher sorption of oil than the H30-1 fibers. However, the level of sorption was similar for the two fibers, which is remarkable as the Y fibers have a much lower surface area than that of the H fibers. As was observed previously with the PP cages, the fiber samples approached their maximum capacity during the fiber degradation testing, but never fully reached it.
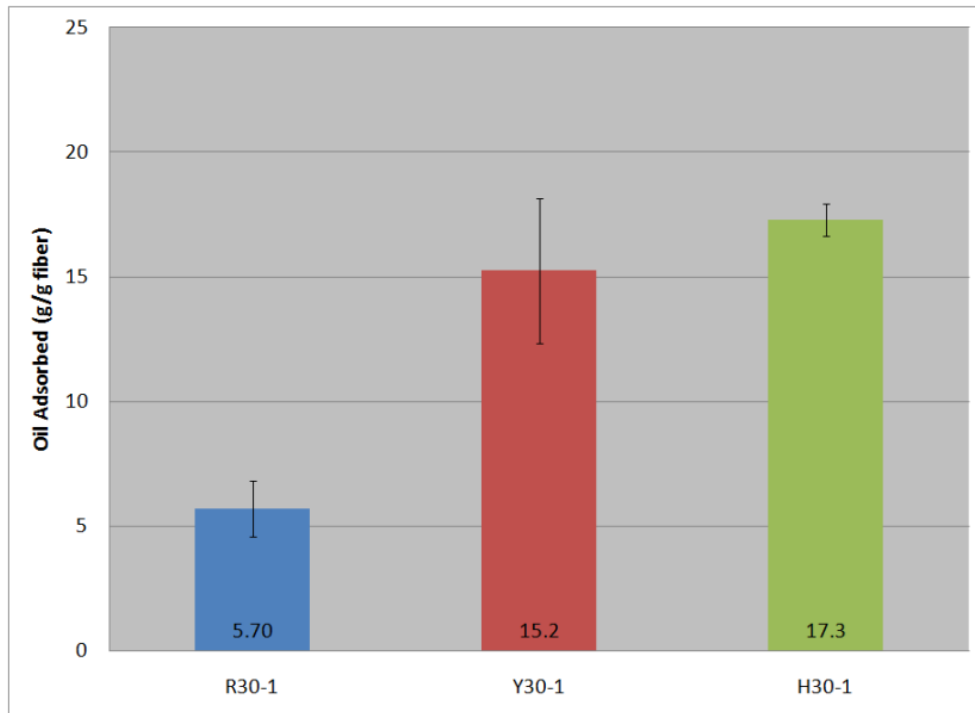
Figure 5.9: Oil sorption of R30-1, Y30-1 and H30-1 fibers in Aluminum Cages during a Short Oil Sorption Test
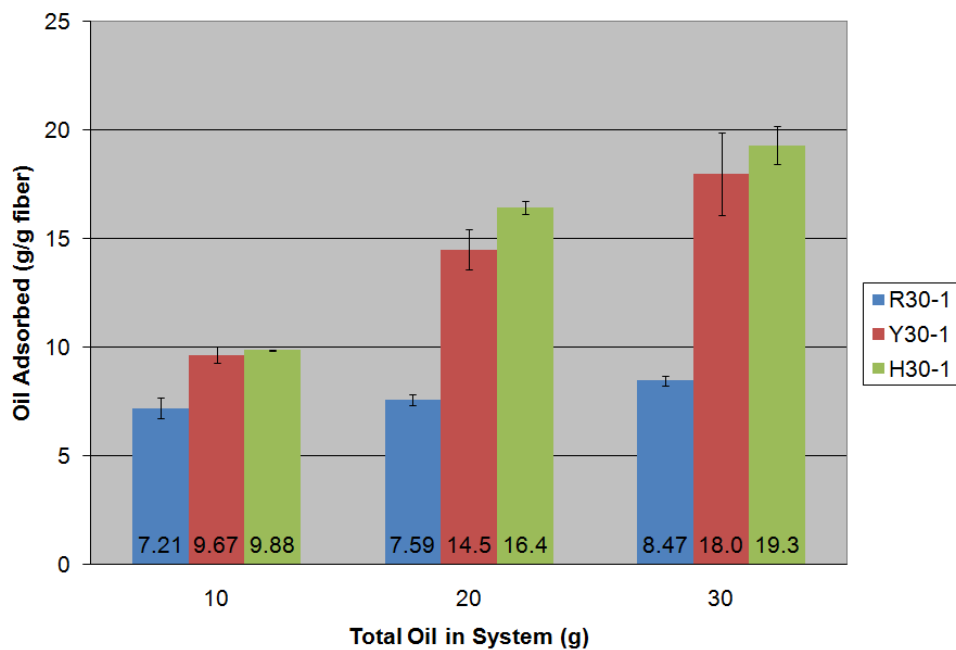

Figure 5.10: Total oil sorbed by cage and fibers during Dynamic Degradation testing with aluminum cages
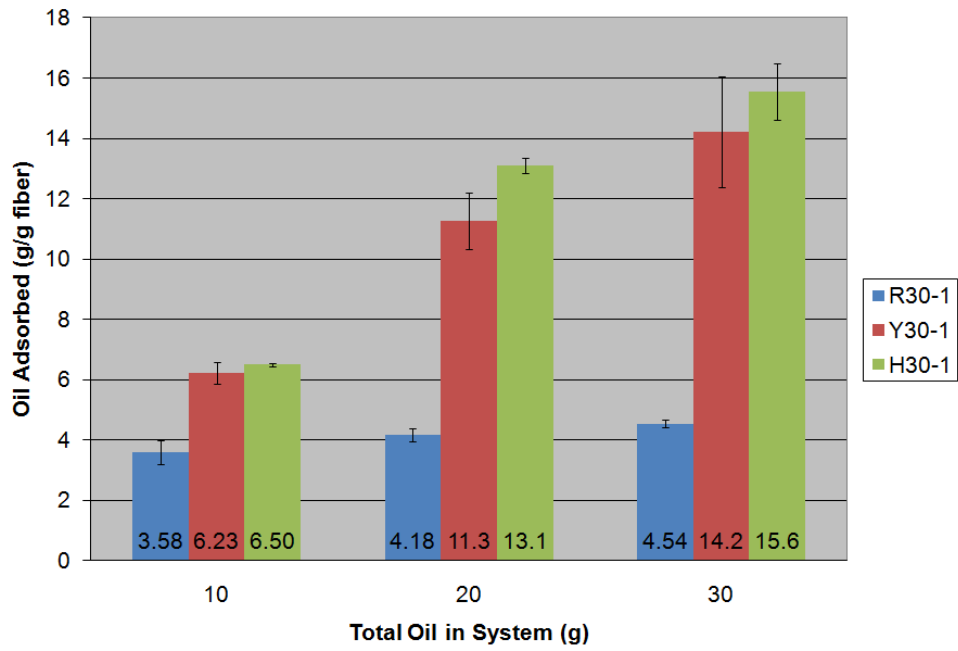
131

Figure 5.11: Oil sorbed by fibers only during Dynamic Degradation testing with aluminum cages
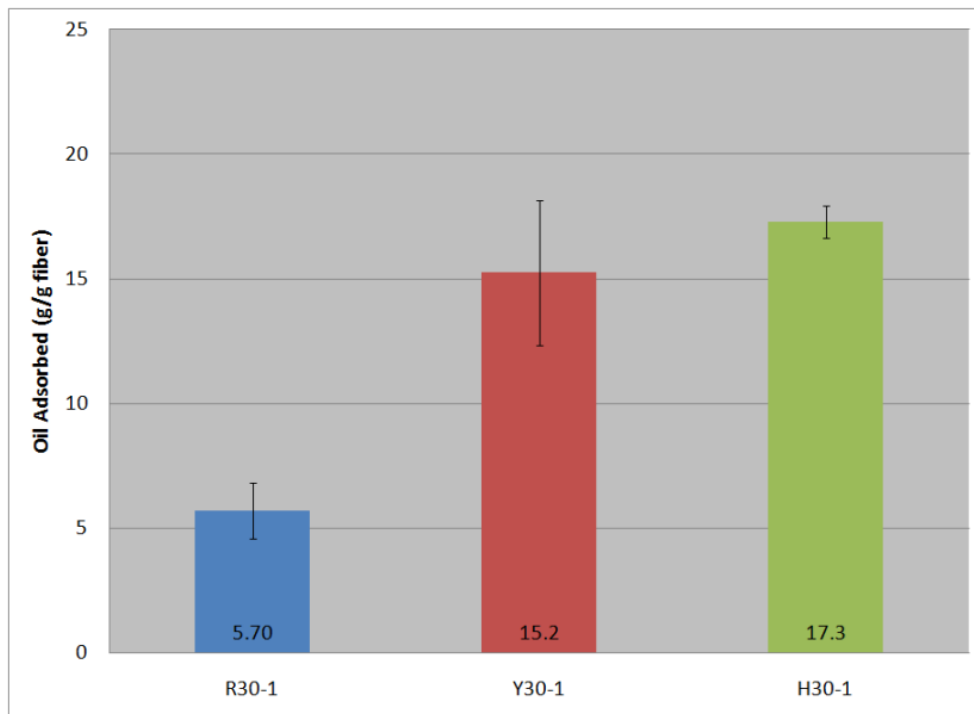

Figure 5.12: Oil sorption of R30-1, Y30-1 and H30-1 fibers in Aluminum Cages during a Short Oil Sorption Test

5.6 Oil Sorption of Round and Y Fibers of Increasing DPF

5.6.1 Comparison Based on Constant Mass

Round and Y fibers were extruded from 18 MFI PP at linear densities of 60, 90, 120, 150 and 180 dpf. These fibers were prepared and tested in the same manner as the fibers in Section 5.4: 1 g of fiber was tested for each sample.

The results for the oil sorption of round and Y fibers from 30 to 180 dpf for samples with the same mass of 1 g of fiber are shown in Figure 5.13. The average mass, number of filaments, and surface area of each fiber sample are shown in Table 5.6. Figure 5.13 shows the amount of oil sorbed by the fibers after adjusting for the oil sorption of the cage used to contain the fibers. The smaller dpf fibers were able to sorb more oil than the larger dpf fibers, regardless of cross-sectional shape. This decrease in oil sorption was due to the smaller number of filaments within the larger dpf samples. As the dpf increased from 30 to 180, the number of filaments in the sample decreased from around 6000 filaments to just under 1000 filaments. Also, with increasing dpf, the surface area to volume ratio of the samples decreases. These factors contributed to the decreasing total surface area of the samples as the dpf increased, reducing the volume of oil that could be sorbed to the surface. In any case, the sorption of the fiber samples will be limited simply by decreasing the number of filaments in the sample. Compared on a weight basis, smaller dpf fibers had a higher sorption than the larger dpf fibers. When looking at practical uses in industry or environmental cleanup, the highest sorption ratio of oil to fiber mass would be the most desirable. The results would indicate that Y fibers even smaller than 30 dpf would sorb more oil; however, the extrusion of these fibers is limited by the thickness of the legs of the Y fibers. As the legs of the 30 dpf Y fibers were on average 15 μm, extruding Y fibers with thinner legs would be nearly impossible on the extruder used. Instead, a bicomponent extruder could be used to form Y fibers with extremely thin leg (in the range of 1-10 μm) by using an islands in the sea approach. Unfortunately, this technology was not available at the time of this work and thus was not evaluated.
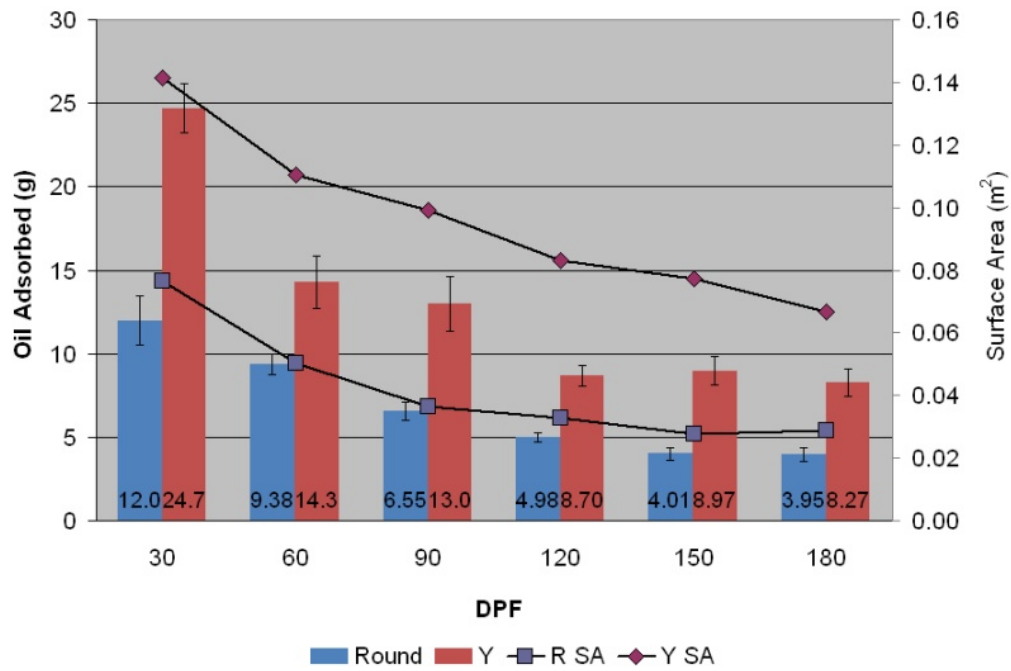
Figure 5.13: Oil sorption of Y and Round fibers from 30 to 180 dpf for samples with the same mass

Table 5.6: Number of Filaments and Total Surface Area for 1 g Fiber Samples

Yarn	Sample mass (g)	Number of Filaments	Total Surface Area (m^2)
R30-1	1.00	5818	0.0766
R60-1	1.00	2915	0.0503
R90-1	0.994	2016	0.0365
R120-1	1.00	1484	0.0328
R150-1	1.00	1176	0.0262
R180-1	1.00	988	0.0287
Y30-1	1.00	5968	0.142
Y60-1	1.01	2910	0.110
Y90-1	1.00	1927	0.0991
Y120-1	1.00	1438	0.0832
Y150-1	1.00	1195	0.0772
Y180-1	1.00	981	0.0668

134

5.6.2 Comparison Based on Constant Number of Filaments

In Section 5.4.1, the Y fibers were shown to sorb more oil than either the H or the Octolobal fibers, even though the surface area of the Y fibers was much less than that of the other shaped fibers. Two factors were discussed as possible reasons for this phenomenon. The shape of the parallel-legged channels within the H and Octolobal fibers may have decreased their oil capacity and the legs of the fibers may have interacted with other fibers to negatively affect the sorption of oil. Alternatively, the Y fibers may have worked cooperatively to form a structure that sorbed more oil than could normally be attributed to the measured surface area of the Y fibers. As this was an immersion test where the oil flooded the fibers, the capillaries within the fibers were not used to draw oil in, but instead acted to hold on to the oil already in the channels during draining. Thus, the Y fibers did not only have larger channels that sorbed more oil, the fiber channels also held on to more oil during the 30 s drainage period. In Section 5.6.1, round and Y fibers of increasing dpf were evaluated at an equivalent sample mass and it was shown that the smaller dpf fibers sorbed more oil. However, by maintaining a mass of 1 g for all of the fiber samples, smallest dpf fibers also had the largest surface area.

By changing the procedure of the test to maintain a constant number of filaments instead of a constant mass, the total surface area of the fiber samples increased with increasing dpf. In addition, the surface area of the R150-1 and R180-1 fiber samples would be within the same range as the surface areas of the Y30-1 and Y60-1 fiber samples. This would allow a comparison of two fiber samples with similar surface areas but different cross-sectional shapes. This comparison would answer the question as to whether the Y fibers are forming a structure that increases the oil sorption over that expected for the surface area. If the round and Y fiber samples with similar surface area sorb a similar amount of oil, that would show there is no increased sorption due to the Y fiber interactions. If instead the Y fiber samples still sorb more oil than the round fiber samples, this would indicate a cooperative fiber matrix exists within the Y fiber sample.

For this comparison of the fibers, the procedure from Section 5.6.1 was repeated

with one significant change: instead of using a constant mass of fiber, a constant number of filaments was used. The number of filaments per sample was based on the original 30 dpf round and Y fiber samples and was fixed at 5900 filaments. Maintaining an equal number of filaments per sample obviously meant that the mass of the fiber samples increased as the dpf increased. Essentially, the mass of the samples increased by one gram for every 30 dpf increase so that the 30 dpf fiber samples were 1 gram, the 60 dpf fiber samples were 2 grams and the 180 dpf fiber samples were approximately 6 grams. The average mass, number of filaments, and surface area of the fiber samples are shown in Table 5.7.

Table 5.7: Number of Filaments and Total Surface Area for Equivalent Filament Number Fiber Samples

Yarn	Sample mass (g)	Number of Filaments	Total Surface Area (m^2)
R30-1	1.01	5818	0.066
R60-1	2.04	5926	0.102
R90-1	2.91	5910	0.107
R120-1	4.00	5903	0.130
R150-1	5.06	5904	0.141
R180-1	5.99	5904	0.172
Y30-1	1.00	5968	0.142
Y60-1	2.04	5909	0.224
Y90-1	3.08	5908	0.304
Y120-1	4.13	5909	0.342
Y150-1	4.96	5904	0.382
Y180-1	6.04	5904	0.402

The amount of oil sorbed by the fiber samples (adjusted from the total sorption for the cage sorption) is shown in Figure 5.14. When the number of filaments remained constant from sample to sample, there was a slight increase in the oil sorption as the dpf of the fibers increased. It was suggested that one of the reasons the H and Octolobal fibers did not sorb more than the Y fibers in previous testing was because their shape restricted their sorption. However, the large dpf Y fibers had no more shape restriction than the small Y fibers, so one might expect them to show a large increase in sorption due to increased surface area. The surface area of the Y30-1 fiber samples was 0.142 m^2 and the surface area

of the Y180-1 fiber samples was 0.402 m^2, almost three times larger than the Y30-1 fiber samples. This increase of surface area would lead one to expect an increase of oil sorption of the same factor. Instead, the Y180-1 fiber samples sorbed only 30.9 g of oil while the Y30-1 fiber samples sorbed 24.7. The failure of the Y180-1 fiber samples to sorb almost three times the weight of oil as the Y30-1 fibers indicates that the surface area of the samples was not the only contributing factor to sorbing more oil. It also indicates that the larger Y fibers cannot form the same cooperative structure the 30 dpf Y fibers build that increases the oil sorption.

Figure 5.15 shows the results of the same procedure when presented as oil sorbed in grams per gram of fiber. This figure looks very similar to Figure 5.13, the same procedure conducted with samples of the same mass. This similarity in results indicates that the fiber samples do indeed have an average sorption in grams of oil per gram of fiber that is consistent for each dpf fiber regardless of the fiber bundle size.

Unlike the previous procedure using 1 g samples where the larger DPF fiber samples had a smaller overall surface area, the samples in this experiment showed an increased surface area as the DPF of the fiber increased. The shape of the Y fibers, with its larger surface area per filament than the round fibers, meant that the Y30-1 fiber had a surface area that fell in between those of the R150-1 fiber and the R180-1 fiber. If the surface area was the only factor that determined the oil sorption for these fibers, this would have meant that the Y30-1 fiber would have an oil sorption within the range of the R150-1 and R180-1 fibers. However, Figure 5.14 showed that the Y30-1 fiber sorbed 22.2 g of oil while the R150-1 fiber sorbed only 14.7 g and the R180-1 fiber sorbed 16.8 g of oil. This indicated that although the surface area was similar, the cooperative structure created by the Y fiber was able to sorb more oil than the interactions of the round fibers. This structure is also likely to be the reason that the Y fibers sorb more oil than the H fibers during the oil sorption short test. The results in Figure 5.14 also show a trend wherein fibers of increasingly smaller dpf sorb increasing amounts of oil. Thus, fiber bundle samples prepared from the smaller dpf Y fibers (the fibers with the highest surface area to volume ratio) have better sorption
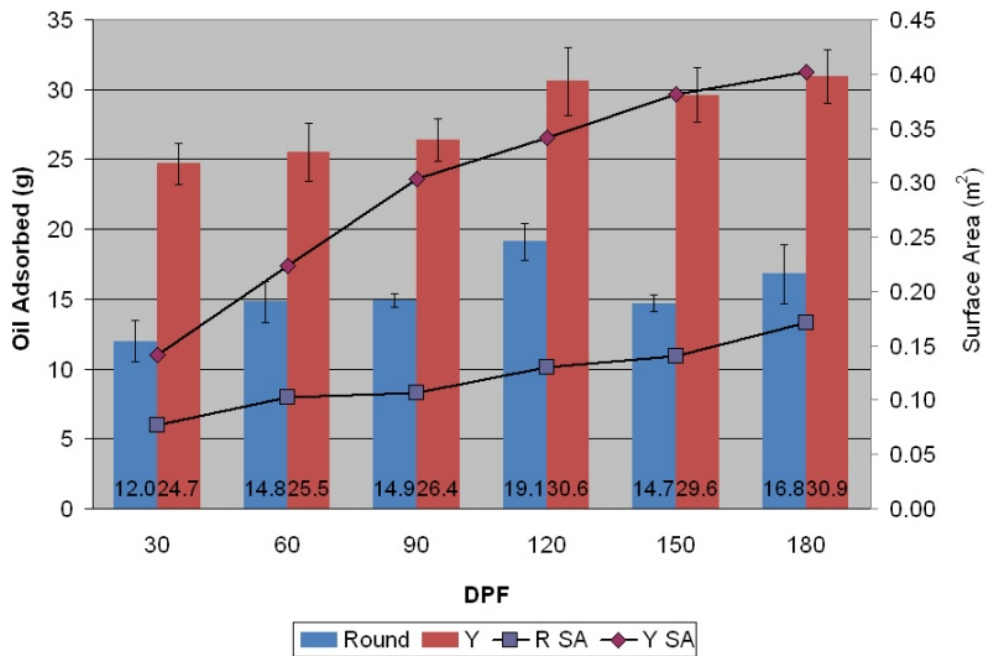
137

Figure 5.14: Total oil sorption of Y and Round fibers from 30 to 180 dpf for samples with the same number of filaments
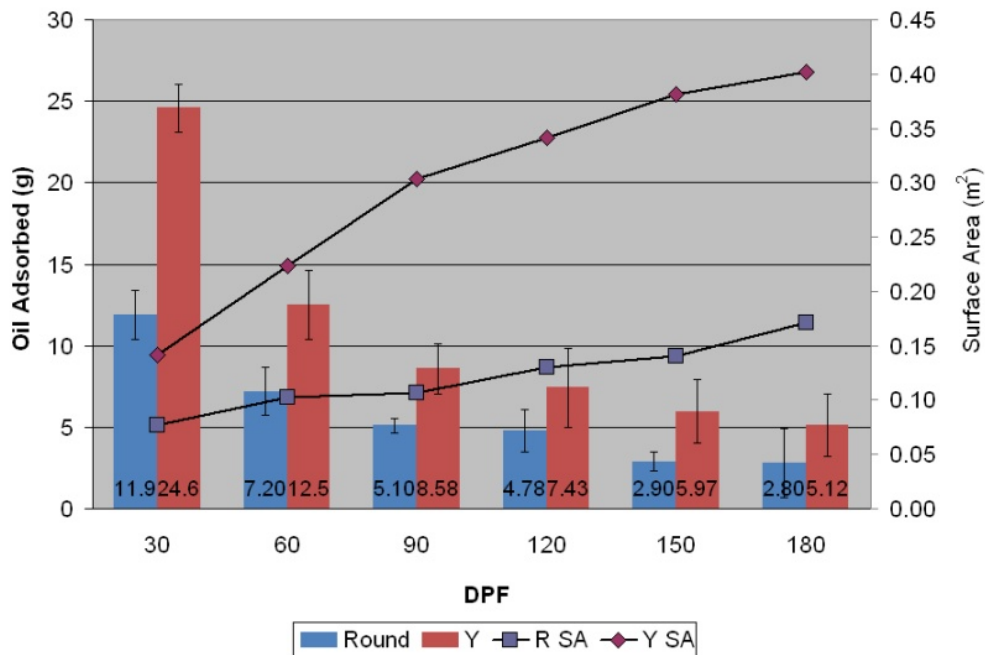

Figure 5.15: Oil sorption per gram of fiber for Y and Round fibers from 30 to 180 dpf for samples with the same number of filaments

properties. This would lead one to expect that using even smaller dpf Y fibers would lead to even higher oil sorption; however, the lowest dpf Y fiber that could be extruded by direct melt spinning was a 30 dpf fiber. In order to reduce the dpf further, alternative extrusion technologies like bicomponent extrusion would need to be used.

Chapter 6

Results and Discussion: Water Sorption and Transport Using Shaped Fibers

6.1 Shaped fibers for water transport: is there a best shape?

Eastman, the producer of both the H, Y and Octolobal fibers, designed the fibers to transport fluid in products such as diapers and feminine napkins [30]. Additionally, US Patent 6342299 claimed that fiber bundles of at least two fibers could transport fluid even if an individual fiber could not [30]. What seems to be important in the patent literature is the shape of the fiber, the geometric shape retention with respect to the spinneret, and the size of the fiber channels. Chapter 4 focused on making fibers of different shapes and sizes and fibers with hydrophilic additives or conventional hydrophilic spin finish. This chapter compares the water wicking and transport properties of the round fibers with the H and Y fibers. Water sorption and transport was measured using the fibers that were extruded with the spin finish Bozzetto Favorol SF2 and the fibers extruded with the hydrophilic polyester additive LB-100. PP by itself is a hydrophobic material and thus would not transport water unless it was modified to be hydrophilic. The effectiveness of the hydrophilic

polyester additive was measured by comparing the fibers extruded with the spin finish to those extruded with LB-100.

6.1.1 Bundle Structure and the Inter-fiber Capillary Width (D)

The patents defined bundle structure using Equation 6.1 developed by Eastman: the average inter-fiber capillary width (D, measured in µm)

$$D = \frac{4 \left(SV - \frac{1}{\rho_P} \right) \times dpf \times 10^3}{9P} \tag{6.1}$$

where

SV = specific volume of the bundle (cc/g)

ρ_P = density of the polymer used to make the fiber (0.91 g/cc for PP)

dpf = linear density of the fiber in g/9000 m and

P = perimeter of the cross-section of the fiber (µm).

In patents regarding the shaped fibers, Eastman stated that bundles would have a D of "about 25 to 400 microns, preferably 60 to 300 microns and more preferably 100 to 300 microns" [30]. Eastman described the bundle structure as being comprised of "two or more synthetic fibers, preferably 8 to 50,000 fibers" [30]. The number of fibers (8) was not justified in the patents but they did suggest the concept of a minimum number of fibers required to establish a fluid adsorbing bundle. In terms of evaluating the bundle technology, Eastman used only 8 fibers per bundle [104]. The Eastman patents focus heavily on the utilization of PET fibers. This technology was designated '4-bundle' by Eastman as the fibers were used in bundles and '4' was the internal company code for PET.

This work investigated aspects of the bundle technology, including Equation 6.1, as it was the only structural description of the bundles besides the number of filaments. Three D values (50, 75, and 100 microns) were chosen within the range established by Eastman in the patents and the amount of fiber necessary for each D was calculated using the known

volume of a polymer tube. In this way, the overall volume of the tube remained the same for each sample and the calculated D was based solely on the mass of fibers. In fact, the practical range of D was limited by the strength and packing limitations of the fibers. The Y fibers could not be packed into or pulled through a tube to achieve a D below 50 microns. Additionally, round fibers, due to their nature, are unable to fill the space of a sample tube at a D above 100 microns because they will simply fall out.

6.2   First Insult Wicking

First insult wicking occurs when dry samples come into contact with fluid, in this case, water. In order for first insult wicking to occur, the fibers must have an attraction to the water. This attraction is normally determined by the surface energy of the polymer fibers. PP is a hydrophobic polymer; however, adding spin finish to the fibers raises the surface energy so that it is compatible with water. The ATR spectrum for the Bozzetto Favorol SF2 spin finish that was applied to the PP fibers is shown in Figure 6.1. This spectrum shows a strong peak at 1100 cm^{-1} which correlates to the presence of alcohol end or side groups within the spin finish [95]. The broad peak at 3464 cm^{-1} shows there is an sorption of energy by stretching O–H groups that were intermolecularly hydrogen bonded [95]. Two other strong peaks occur at 2922 and 2855 cm^{-1}, a strong indication of methylene groups within the molecular structure of the spin finish [95]. Figure 6.2 shows the comparison of the ATR spectrum for Bozzetto Favorol SF2 to the spectrum of a fatty acid polyglycol ester. These two compounds had a 94% match based on their spectra. The peaks within the ATR spectrum for Bozetto SF2 and its match to the polyglycol ester indicate that the spin finish was likely a form of a polyglycol ester that had a large number of O-H groups along the chain. A coating of this spin finish on the PP fibers would increase the hydrophilic nature of the fibers until the coating wore off or was washed off.

During initial testing, it was determined that the fibers with spin finish were able to wick water from a dry state; however, the as spun fibers and the fibers with the LB-100
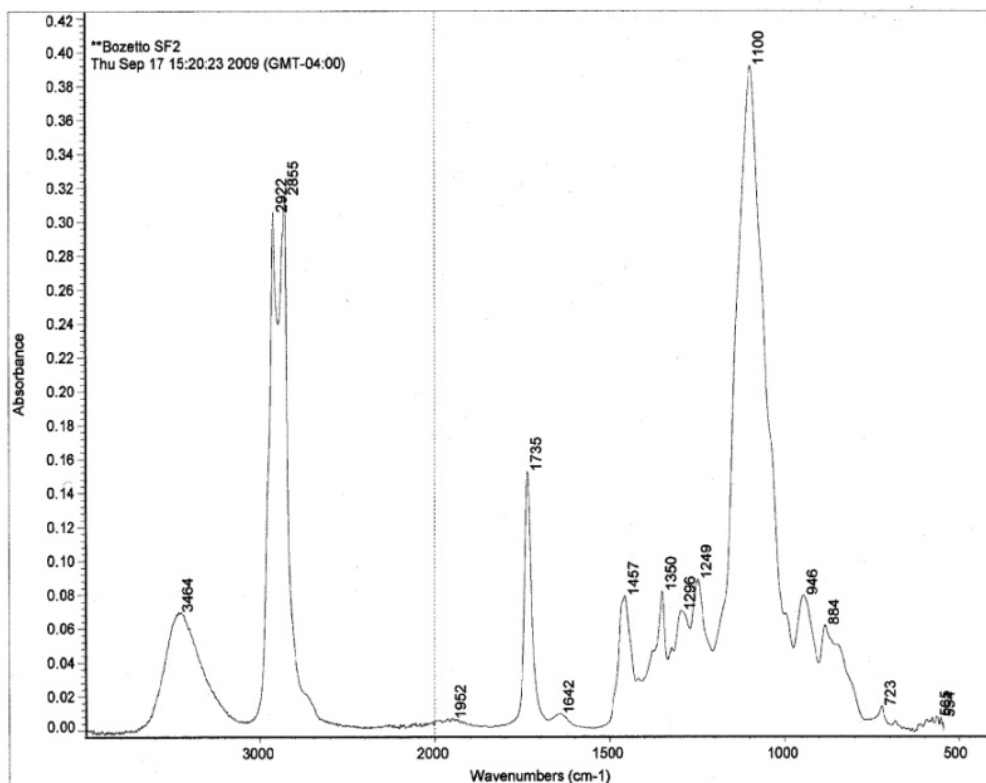
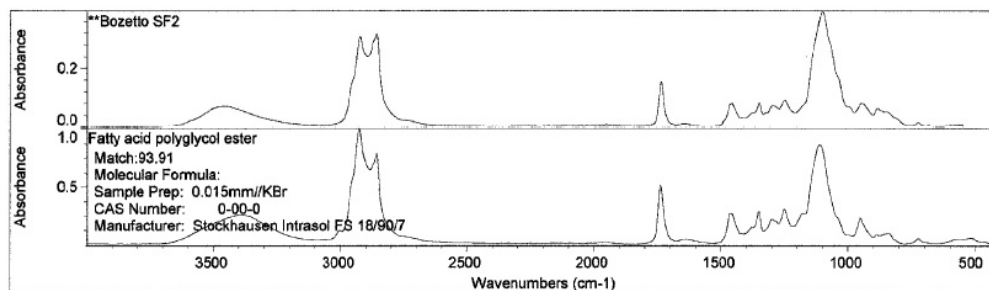Figure 6.1: ATR spectrum for Bozzetto Favorol SF2 hydrophilic spin finish

Figure 6.2: Comparison of the ATR spectrum for Bozzetto Favorol SF2 hydrophilic spin finish with the spectrum of polyglycol ester

additive did not transport water when dry. Thus, the only fibers tested for the first insult wicking were those with spin finish.

6.2.1 Short Samples

6.2.1.1 Comparison of fiber bundle samples prepared from 18 MFI PP fiber only

Fiber bundles were prepared as described in Section 2.8.1 from the fibers listed in Table 6.1. These fibers were extruded with the spin finish Bozzetto Favorol SF2 and were used for this evaluation of water transport properties. Vertical wicking tests were conducted using the method detailed in Section 2.8.2.1. The length of the fiber bundles was chosen to be shorter than the maximum vertical wicking height of the shaped fibers. Figure 6.3 shows the result of a vertical wicking experiment on fiber samples prepared from H30-1S, Y30-1S and R30-1S at D's of 50, 75, and 100 microns. The H30-1S and Y30-1S bundles approached the maximum wicking capacity (which was similar to the maximum volumetric capacity for these samples specifically) within 3 or 4 minutes and the water sorption tailed off after that point. The R30-1S fiber bundles approached maximum capacity more quickly than the shaped fibers, reaching equilibrium after approximately 1 minute. The capacity of the shaped fibers was higher than that of the round - the H30-1S and Y30-1S samples, regardless of the D, adsorbed approximately twice the water of the R30-1S fiber samples. This showed that the shaped fibers with channels built into the fibers were more effective at transporting water in a vertical wicking environment. However, it should be noted that the maximum volumetric capacity for the round fiber samples was slightly lower than for the shaped fiber samples due to the amount of fiber in the testing tube.

The sorption in grams of water per gram of fiber of the fiber bundles from the vertical wicking experiment was calculated and the results of these calculations are shown in Figure 6.4. The amount of water per gram of fiber the bundles sorbed increased as the D of the fiber bundle increased. The reason for this was twofold. First, the amount of fiber in each bundle affected the maximum amount of water each sample could adsorb,
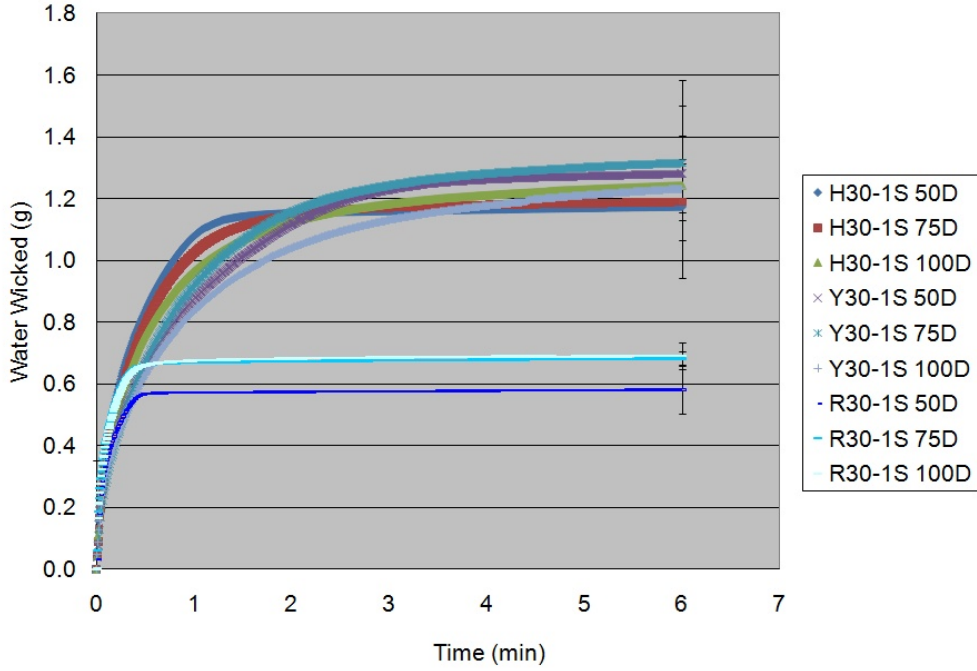
Figure 6.3: Vertical wicking for short samples prepared from R30-1S, Y30-1S and H30-1S at D's of 50, 75 and 100 microns
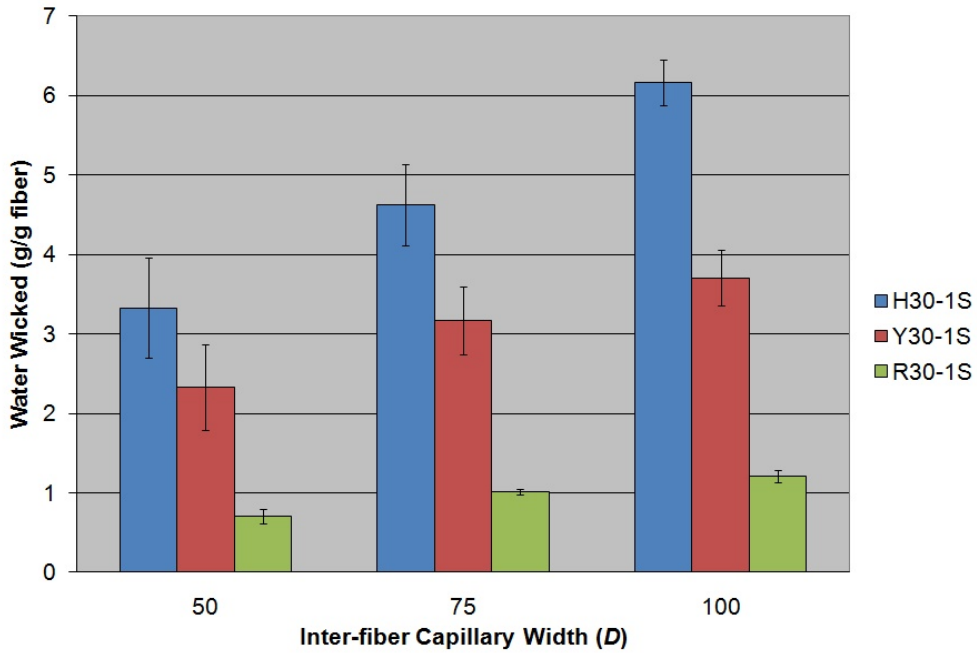

Figure 6.4: Water adsorbed during vertical wicking for short samples in grams of water per gram of fiber

145

Table 6.1: Fibers used in Fluid Wicking and Transport Testing

Fiber	Shape	Polymer Blend	Spin Finish
R30-1S	Round	100% 18 MFI PP	SF2
R30-2S	Round	90% 18 MFI PP, 10% 400 MFI PP	SF2
R30-3S	Round	75% 18 MFI PP, 25% 400 MFI PP	SF2
R30-4S	Round	50% 18 MFI PP, 50% 400 MFI PP	SF2
Y30-1S	Y	100% 18 MFI PP	SF2
Y30-2S	Y	90% 18 MFI PP, 10% 400 MFI PP	SF2
Y30-3S	Y	75% 18 MFI PP, 25% 400 MFI PP	SF2
Y30-4S	Y	50% 18 MFI PP, 50% 400 MFI PP	SF2
H30-1S	H	100% 18 MFI PP	SF2
H30-2S	H	90% 18 MFI PP, 10% 400 MFI PP	SF2
H30-3S	H	75% 18 MFI PP, 25% 400 MFI PP	SF2
H30-4S	H	50% 18 MFI PP, 50% 400 MFI PP	SF2

as the fiber took up space that the water might have been able to fill otherwise. As the D increased, the amount of fiber in each bundle decreased. For example, there was more space for the water to fill in the bundles with a D of 75 microns than in the bundles with a D of 50 microns. The bundles with a D of 100 microns had the most empty space for water to fill. However, the total amount of water adsorbed by the fiber samples was the same for each fiber shape regardless of the D. This meant that the mass of water was fairly constant, but the mass of fiber being used in the calculation of grams of water per gram of fiber decreased. Thus, results based on a g/g metric favor decreasing amounts of fiber and consequently fiber samples with a high D. The samples with a D of 100 microns also adsorb a higher mass of water per filament than the samples with a D of 50 and 75 microns, indicating that increasing the distance between the filaments actually improves their water wicking capabilities. No effort was made to determine the distance between filaments that results in the maximum increased water wicking as increasing the D beyond a certain point results in the fibers falling out of the tube.

6.2.1.2 Comparison of round, Y and H polyblend fiber bundle samples with a D of 75 microns

The same wicking procedure was carried out on fiber bundles prepared to have a D of 75 microns from the polyblend fibers (fibers with varying levels of 18 MFI PP and 400 MFI PP) with spin finish. The average water sorption of these fiber bundles was compared to the sorption of the R30-1S, Y30-1S and H30-1S fiber bundles with a D of 75 microns in Figures 6.5, 6.6, and 6.7. As the fibers were all of the same dpf, all fibers of the same shape had approximately the same weight of fiber in each fiber bundle.

The 400 MFI PP was added to the fiber blend to improve the shape of the fibers, as was discussed in Chapter 3. For the round fibers, the shape was fairly constant regardless of which polymer the fibers were extruded from. When the Y fibers were extruded from only 18 MFI PP, the shape was already quite reflective of the spinneret hole. Adding 400 MFI PP to the fiber blend did not greatly affect the shape of the fibers. However, the effect of the 400 MFI PP on the geometric shape retention of the H fibers was significant, as increasing levels of 400 MFI PP resulted in increasingly improved shape. Primarily, the effect of the geometric shape retention on wicking was investigated for the H shaped fibers. As the round and Y fibers had no change in shape, these samples acted effectively as a control for the experiment. In addition, this investigation allowed a further comparison of the capacities of the H and Y shaped fibers using a new experimental procedure and water in the place of the oil used in Chapter 4.

Figure 6.5 shows the wicking of water by the R30-1S, R30-2S, R30-3S and R30-4S fiber bundle samples. As the fiber bundles were prepared to a D of 75 microns from round fibers of the same shape and DPF, no variation in wicking was expected due to the increasing levels of 400 MFI PP in the fibers. As shown in Figure 6.5, no correlation was evident between the wicking ability of the fiber bundle samples and the composition of the fiber.

Figure 6.6 shows the results of the same procedure on the Y30-1S, Y30-2S, Y30-3S, and Y30-4S fibers. As with the round fibers, there was no significant difference in the shapes

147

of the fibers with the addition of 400 MFI PP. No clear correlation between water wicking and 400 MFI PP was expected, nor was a correlation observed.

The sorption of the H fiber bundle samples are shown in Figure 6.7. For these fibers, a correlation between the inclusion of 400 MFI PP in the polymer blend and the wicking properties was expected. Initially, it was assumed that improved shape would increase the wicking abilities of the fibers and indeed, the perfection of the H shape resulted in an increased rate of initial wicking. This increased rate was likely due to the improvement in the shape of the channels with the H fibers. The legs forming the channels with the poorly shaped H fibers were splayed outward, increasing the size of the channel. When the legs of the H fibers straightened, the channels within the fiber became smaller, resulting in a higher capillary force within the channel. However, even though the initial rate of wicking increased, the data in Figure 6.7 shows that the improved fiber shape resulted in a decrease in maximum wicking capacity. The improved shape of the H fiber may have resulted in fewer interactions between the legs of adjacent fibers, leading to fewer inter-fiber capillaries. In addition, the distorted H shape commonly seen in the H30-1S fiber cross-section appear to have larger channels because the legs of the channels are angled away from each other, creating a larger area that can adsorb and hold water. The smaller, more perfect channels achieved with the improvement of the fiber shape had a lower capacity. Additionally, when the legs were distorted and splayed outward, the fiber almost formed four channels instead of two. Perfecting the channel shape eliminated any channels created by the splayed legs. This improved wicking due to poor geometric shape retention was not seen with the Y and round fibers as there was no alteration of shape with the addition of 400 MFI PP.
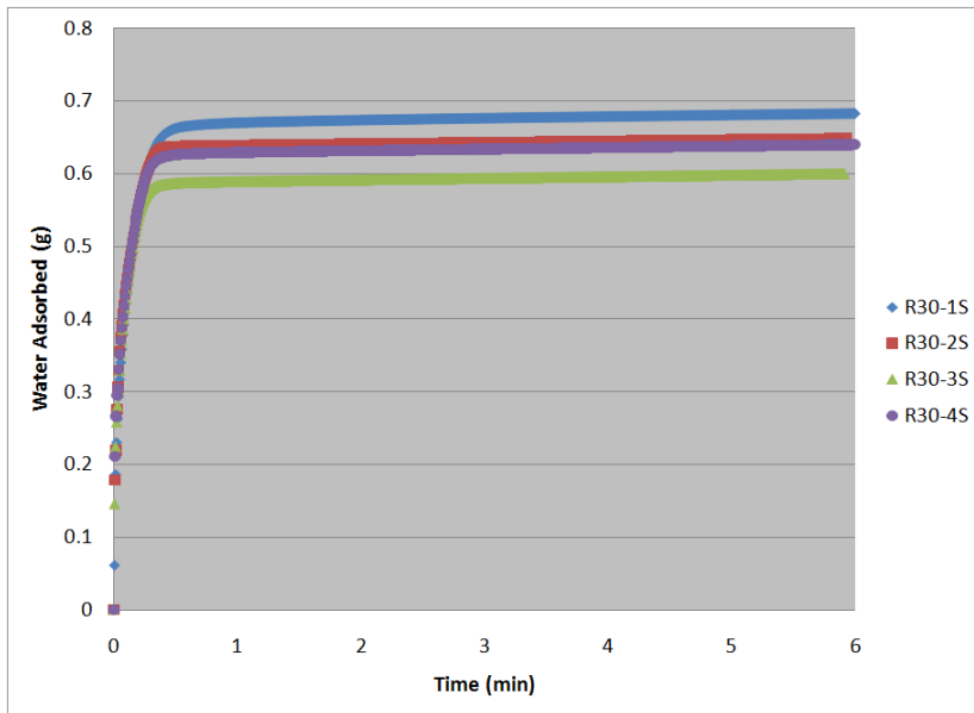
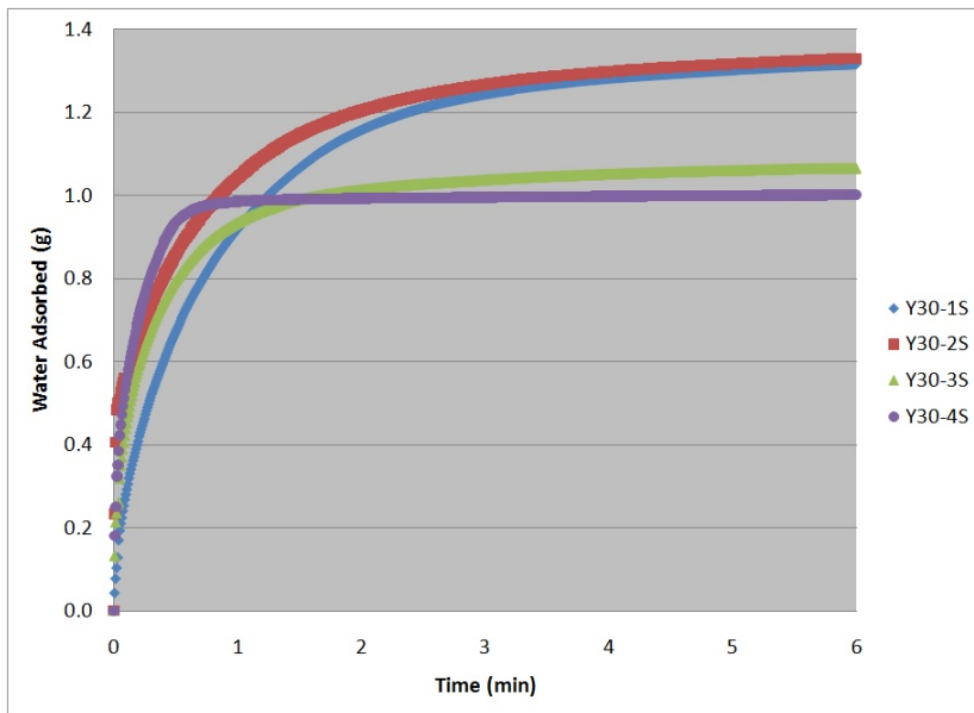Figure 6.5: Vertical wicking for round fiber samples with a D of 75 microns.

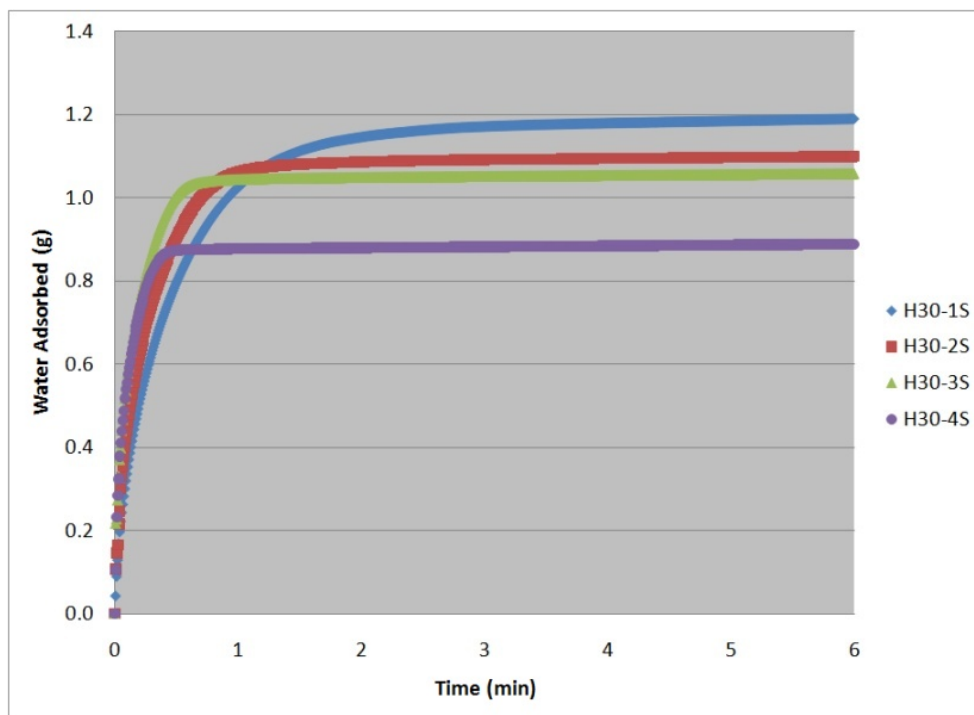Figure 6.6: Vertical wicking for Y fiber samples with a D of 75 microns.

Figure 6.7: Vertical wicking for H fiber samples with a D of 75 microns.

6.2.2 Long Samples

The fiber bundles for the second wicking test were designed to be much longer than the maximum wicking height of the shaped fibers. The maximum height of wicking was determined only cursorily in initial tests. A definitive calculation of maximum wicking height in the fiber bundles was not possible as the exact shape and size of the channels within and between fibers was unknown. It was determined that bundles created from the H, Y and round fibers could not wick fluid to a height of 20 cm during the testing period, so this distance was chosen. As the height to which the water climbed within the bundles could not be reliably measured, the weight of water wicked by the fiber bundle samples was used as a basis for comparison.

For this evaluation of wicking properties, only the H30-1S, Y30-1S, and R30-1S fibers were used. The smallest inter-fiber capillary width (D) of 50 microns from the work with the short fiber bundle samples was chosen. Figure 6.8 shows that the Y30-1S fiber bundles adsorbed an amount of water similar to the amount the H30-1S fiber bundles adsorbed. The sorption of water by both the H30-1S and Y30-1S fiber bundles was much higher than the sorption of the R30-1S fiber bundles. Although no distinction could be made between the H fiber bundles and the Y fiber bundles in sorption, the presence of channels within the fibers improved the sorption of the fibers. The lack of distinction between the H fiber bundles and the Y fiber bundles indicated that the shape of the channel within the fiber, whether it was square-bottomed or not, did not determine the wicking capabilities of the fiber. Instead, the presence of the channels and the number of channels had more effect than the shape of those channels.

The same experiment was conducted on a set of samples with equal filament number (2060 filaments). The mass used as the standard for comparison was set as the mass of the H fiber samples with a D of 50 microns. Figure 6.9 shows the results from this experiment. When the samples were of equal mass, the H fiber samples were able to adsorb slightly more water than the Y fiber samples. The round fiber samples were unable to retain the same volume of fluid as the shaped fibers.
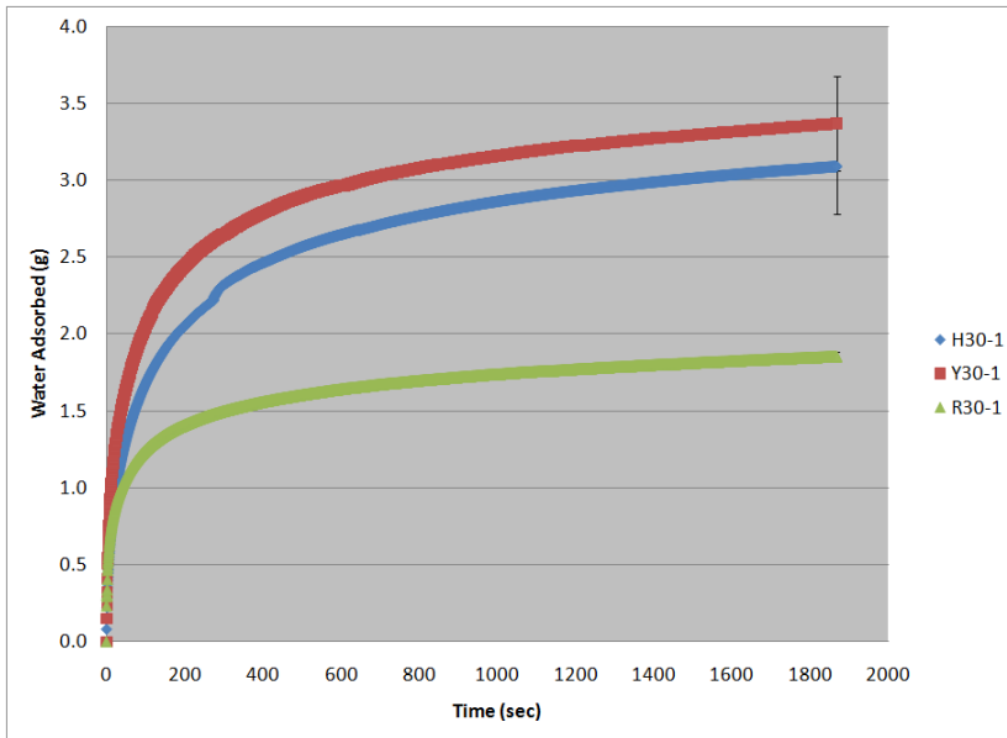
151

Figure 6.8: Vertical wicking for long samples with a D of 50 microns
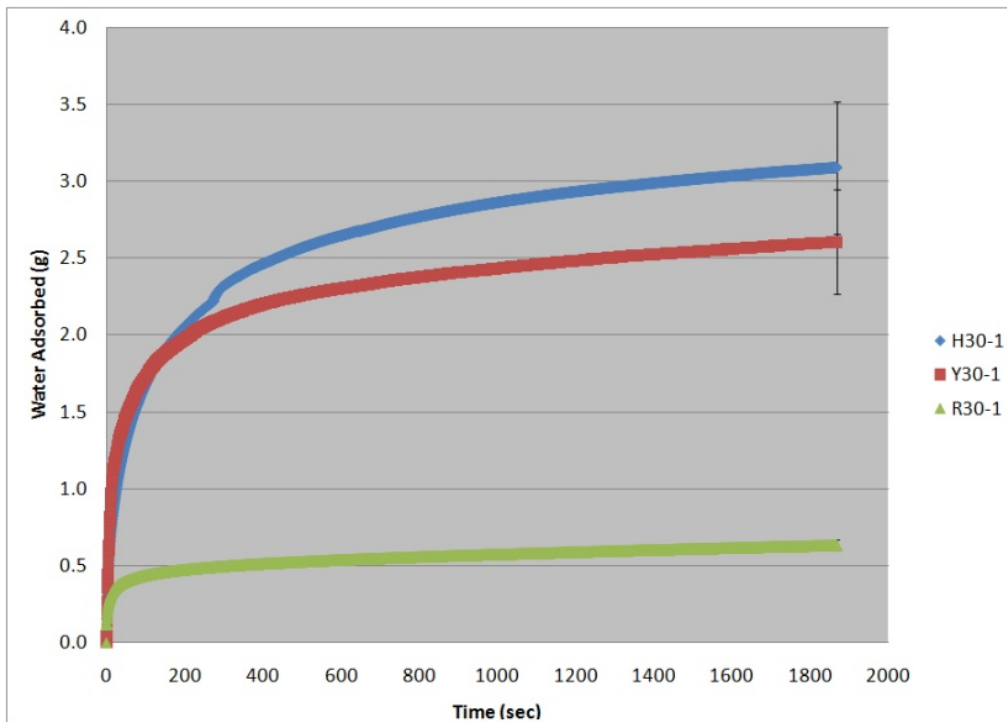

Figure 6.9: Vertical wicking for long samples with 2060 filaments

The amount of water that the fibers wicked vertically (in grams) was used to determine the height the water reached. The results are provided in Table 6.2. The calculated height (h_w) is a purely theoretical value as the fiber samples wicked fluid to various heights within a single sample. The calculated height based on the mass of water wicked by the fiber samples is given by

$$h_w = \frac{V_w \times l_t}{V_t - V_f} \tag{6.2}$$

where

   h_w = theoretical height of water based on wicked water volume (cm)

   l_t = length of testing tube (cm)

   V_w = volume of water wicked by fiber sample (cc)

   V_t = volume of empty testing tube (cc)

   V_f = volume of fiber in testing tube (cc).

The height calculated from the mass of water wicked by the fiber samples was compared to the theoretical rise in a capillary of similar size (i.e., a capillary of radius = D). This comparison could be made because all of the capillaries within the fiber sample were assumed to be the same size and it was assumed that all capillaries had the same vertical rise. Using the Young-Laplace capillary rise equation [64, 65]

$$h_D = \frac{2 \times \gamma \times cos\theta}{10 \times \rho \times g \times r} \tag{6.3}$$

where

   h_D = theoretical height of water based on D (cm)

   γ = surface tension of the liquid (dynes/cm)

   θ = contact angle of the liquid on the capillary surface (rad)

   ρ = the density of the liquid (g/cc)

   g = acceleration due to gravity (9.8 m/s^2)

r = radius of capillary (mm) [in this instance, equivalent to a D of 50 microns]

the theoretical height of water in a capillary of a similar size was determined for each fiber sample. For the fiber samples with equivalent filament number, the D was calculated for each fiber shape individually and the capillary rise was determined using that specific D. These values can be found in Table 6.2. For the fiber samples prepared with a D of 50 microns, the capillary rise (h_D) was very close to the theoretical height of the water in the sample tubes (h_w). The Y30-1 fibers had a slightly higher h_w than the capillary rise for a 50 micron capillary, indicating that those fibers may actually have been packed slightly closer together than the calculated D. The fibers compared on an equivalent number of filaments showed that the change in D had a very strong effect on the vertical wicking capabilities of the fiber samples. The increased D (and thus increased effective capillary size) caused the wicking capabilities to decrease significantly. The round fibers with a calculated D of 190 microns did not wick the amount of water necessary to reach the same capillary rise as a 190 micron capillary, indicating that the round fiber samples did not actually form channels of this size. The Y fiber samples again wicked slightly more fluid than was expected which again indicates that the actual channels within the fiber sample were slightly smaller than 90 microns.

There was a strong similarity between the calculated height of water in the fiber samples and the capillary rise in capillaries with a radius of the D for the samples. This indicates that the D calculation is an effective representation of the size of the channels in the fiber sample. Using the D calculation with a shaped fiber allows the preparation of channeled fiber bundles with a much smaller mass of fiber than that needed for round fibers.

154

Table 6.2: Calculated theoretical height of water from water mass (h_w) and capillary size (based on D) (h_D) in fiber wicking samples

Fiber	Test Procedure	h_w (cm)	h_D (cm)
R30-1S	$D = 50$	13.2	14.8
Y30-1S	$D = 50$	17.0	14.8
H30-1S	$D = 50$	12.8	14.8
R30-1S	2060 Fil. ($D = 190$)	2.64	6.12
Y30-1S	2060 Fil. ($D = 90$)	10.8	8.16
H30-1S	2060 Fil. ($D = 50$)	13.2	14.8

6.3 Second Insult Wicking

Initially, the H fibers with polyester additive (H30-1A, H30-2A, H30-3A and H30-4A) were tested with the fibers extruded with spin finish in a first-insult wicking setup. Although the polyester additive was designed to increase the hydrophilic nature of the surface of the PP fiber, its effect on the PP surface was not strong enough to allow first-insult wicking to occur. This meant that fibers with polyester additive were not as hydrophilic as the fibers coated with hydrophilic spin finish. However, in order to characterize the fibers with hydrophilic additive, a different experimental method was required.

A second insult wicking test takes fibers that have been pre-wet and places them in a down-hill transport situation. For this work, the fiber samples were soaked in water and then placed into tubes. The tube was attached to a stand and the upper end of the tube was inserted into a water bath. The lower end of the tube was suspended over a balance and the mass of water transported by the tube was recorded over twenty minutes. This down-hill set-up could potentially act as a siphon; however, if these fiber bundles were acting solely as siphons, there would be no change in transport based on the fiber chemistry. To determine if this were the case, the four H fibers without spin finish or hydrophilic additives were subjected to the same procedure as the H fibers coated with spin finish and the H fibers with hydrophilic additive.

6.3.1 H fibers without Spin Finish or Hydrophilic Polyester Additives

Figure 6.10 shows the results of the second insult wicking experiment for the as spun H30-1 to H30-4 fibers. These fibers had no spin finish and no hydrophilic polyester additive and were extruded solely from 18 MFI PP or blends of 18 MFI PP and 400 MFI PP. With no spin finish coating or additive designed to make the fibers hydrophilic, these fibers were expected to show poor transport capabilities. As expected, the fibers were not able to transport a large amount of water as the hydrophobic nature of the PP decreased the amount of water being adsorbed from the water bath. As the fibers were pre-wet before

being placed into the testing tube, it is entirely possible that no actual transportation occurred and the water being collected was simply the water from the pre-wetting step dripping out of the sample. The maximum amount of water transported by these fibers was 2.73 grams by the H30-1 fiber. In Section 6.2.1.2, the improved geometric shape retention of the H fibers resulted in decreased wicking capability. Even without any hydrophilic component, the H fibers with the worst geometric shape retention were again shown to have the best transport properties.

6.3.2   H fibers with Spin Finish

Figure 6.11 shows the transport capabilities of H fibers coated with spin finish Bozzetto Favorol SF2 during extrusion. The same relationship observed with neat fibers between fiber shape and fluid transportation was observed here. The H30-1S fiber was the most effective at water transport with a maximum of 11.9 grams of water transported in 20 minutes. The three other polyblend fibers did not transport as much fluid as the H30-1S fibers and showed decreasing transport capabilities as the level of 400 MFI PP in the polymer blend increased and the shape improved. The amount of fluid transported by the H30-1S fibers was much larger than the amount of water trapped inside the fibers during pre-wetting. This indicated that the fibers did indeed transport water and that the hydrophilic spin finish placed on the fibers allowed the previously ineffective fibers to work as fluid transporters. The large increase in water transportation with the addition of spin finish to the fibers also indicates that these fibers were not acting solely as siphons. If the fibers within their testing tubes were acting as siphons, the transported amount of water would have remained constant, regardless of the surface chemistry (hydrophobic or hydrophilic) of the PP fibers.

6.3.3   H fibers with Hydrophilic Polyester Additive LB-100

The goal of adding the polyester additive to the polymer blend was to create fibers with properties similar to a hydrophilic spin finish. The use of an additive instead of a spin
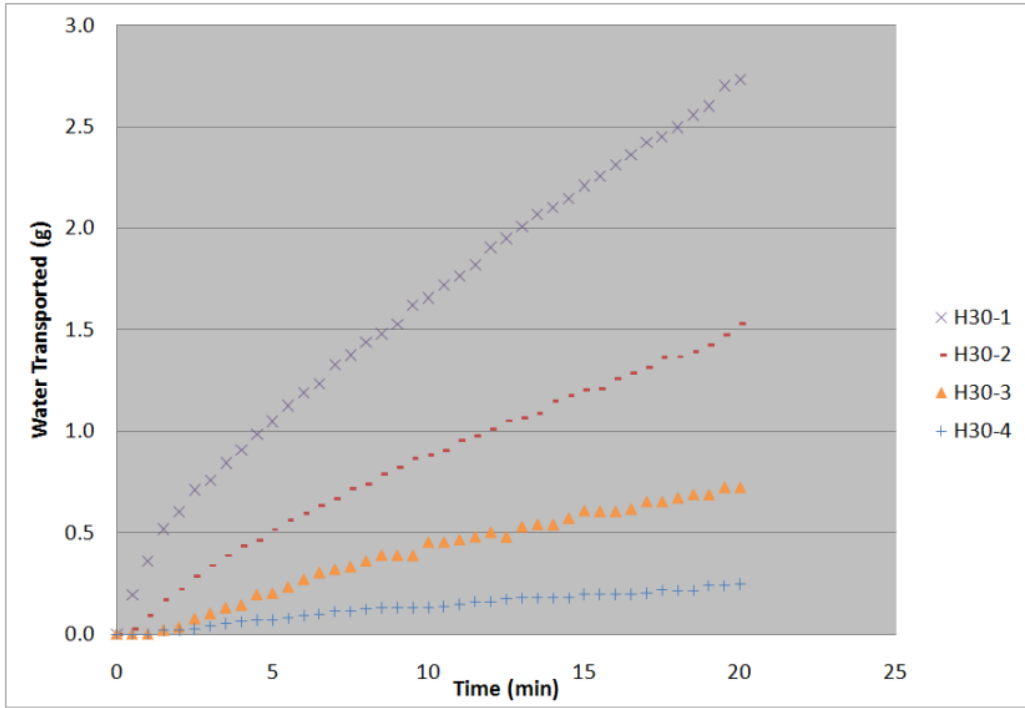
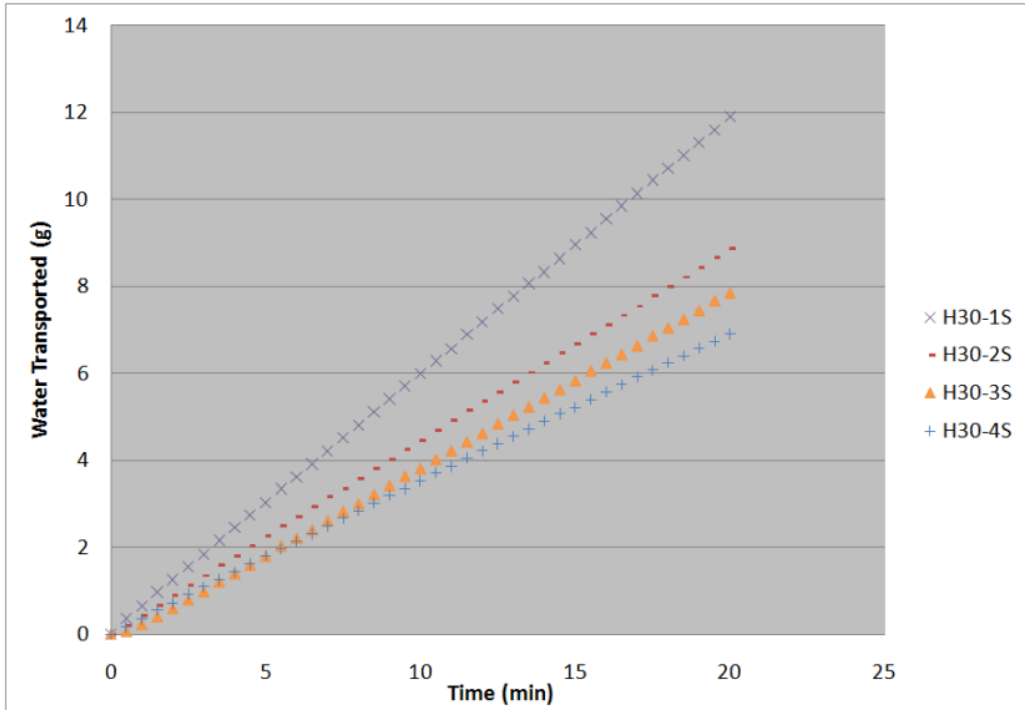Figure 6.10: Second insult wicking for as spun fibers

Figure 6.11: Second insult wicking for samples with spin finish Favorol SF2

finish meant that these properties could not be removed by washing or abrasion, unlike the hydrophilic spin finish. Obviously, the fibers with LB-100 in the polymer blend were not as hydrophilic as the fibers with spin finish as they were unable to wick water when dry. However, the hydrophilicity of the fibers was affected by the addition of the additive. Figure 6.12 shows the results of the second insult wicking experiment on the H fibers with additive. The highest amount of water transported by the H fibers without any hydrophilic spin finish or additive was 2.7 g. All of the H fibers with hydrophilic polyester additive LB-100 transported more fluid than this, indicating that the hydrophilicity of the fibers was increased with the addition of the LB-100.

6.3.3.1   Contradictory Phenomena

As expected, the fibers with the additive were not as effective as the fibers with spin finish as none could match the transport properties of the H30-1S fiber samples. However, an interesting trend was revealed within Figure 6.12. Previously, the fibers showed decreased transport with increasing levels of 400 MFI PP because the improvement in shape hindered the water transportation. For the H fibers with additive, this trend was not observed. Rather, the exact opposite was true. The H30-4A fibers, which had 50% 400 MFI PP in the blend, and the H30-3A fibers with 25% 400 MFI PP were shown to transport the greatest amount of water. The H30-1A fibers, with no 400 MFI PP in the fiber blend, transported the least amount of water. With the addition of the hydrophilic polyester additive to these fibers, increasing amounts of 400 MFI PP in the blend resulted in increased water transport.

As the improved shape was already shown to have a negative effect on transport properties, the presence of both 400 MFI PP and the hydrophilic polyester additive LB-100 must have caused the increased transport abilities. It is possible that the 400 MFI PP, having a shorter chain length than the 18 MFI PP, was able to move toward the surface of the fibers during the extrusion process. With the addition of the LB-100 to the melt, it is also possible that the 400 MFI PP simultaneously moved the LB-100 closer to the surface. With increasing amounts of 400 MFI PP, the LB-100 was forced toward the surface more strongly

or perhaps spread out on the surface more evenly, resulting in improved hydrophilicity and thus higher transport.

This interaction of the 400 MFI PP and the polyester additive is the only explanation that makes sense at this time. This possible phenomenon is supported by the fact that the H30-2A fibers, with only 10% of the 400 MFI PP in the polymer blend, experienced a slightly increased transport capability when compared to the H30-1A fibers (made from 100% 18 MFI PP). A much larger increase was seen with the addition of 25% 400 MFI PP to the fiber blend, however. The transport properties of the fibers appear to reach a plateau in the H30-3A fibers (a blend of 75% 18 and 25% 400 MFI PP) because the H30-4A fibers with a 50/50 blend of the two PPs did not exhibit improved transport properties. This indicates that using more 400 MFI PP in the fiber blend would not further increase the hydrophilic properties. Using an additive that was even more hydrophilic than the LB-100 polyester additive might cause an increased hydrophilicity, but such an additive would also need to meet the thermal stability requirements for extrusion.
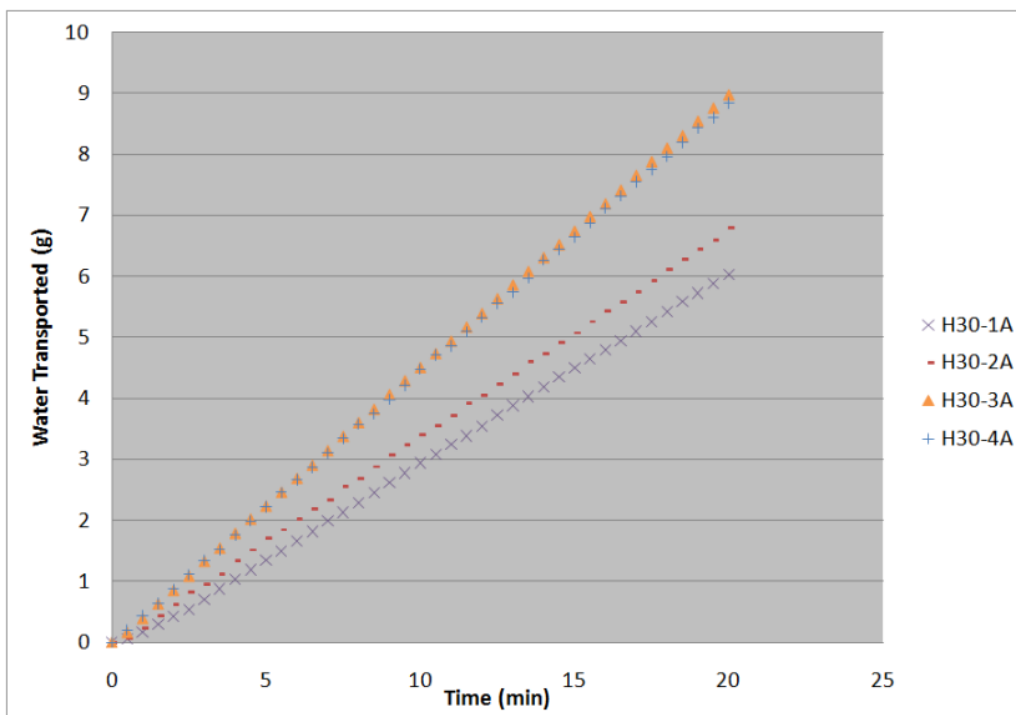
Figure 6.12: Second insult wicking for samples with polyester additive LB-100

6.4   Bundle Structure and Equivalent Filament Numbers

After comparing the properties of the shaped and round fibers based on the inter-fiber capillary width (D), a second comparison was also made using the same number of filaments. As the fibers were all spun to be the same dpf, comparing the same number of filaments meant that the samples were all approximately the same weight as well. For industrial applications, this corresponds to using the least amount of material to obtain the strongest desired effect. The D calculation used by Eastman requires more material for particular shapes than others; thus, in the author's opinion, this is not an effective evaluation tool for industry. By defining a set number of filaments in each sample to be tested, the mass of PP in each sample could be standardized. Additionally, with this new metric, the cost would remain the same, regardless of fiber shape.

Maintaining a constant number of filaments would also show how the changing number of channels within each fiber shape affects the sorption properties of the fiber bundle. The round fibers have no channels in the shape, but could form channels between fibers. The Y fibers have three channels and the H fibers have two channels if the H shape is strictly retained and potentially three or four if it is slightly distorted. A comparison based on the same number of filaments could determine the increased fluid retention capacity of the fiber bundle with different shaped fibers.

6.5   Maximum Fluid Capacity of Fiber Bundles

Fiber bundles were prepared as described in Section 2.8.2.1. One set of bundle samples was prepared with a D of 75 microns and another with 1600 filaments per bundle sample. The average void volume was calculated for the fiber samples using the known volume of the sample tube and the mass and polymer density of the fiber samples. The average void volumes for the samples with a D of 75 microns are shown in Figure 6.13 and for the samples with 1600 filaments in Figure 6.14.

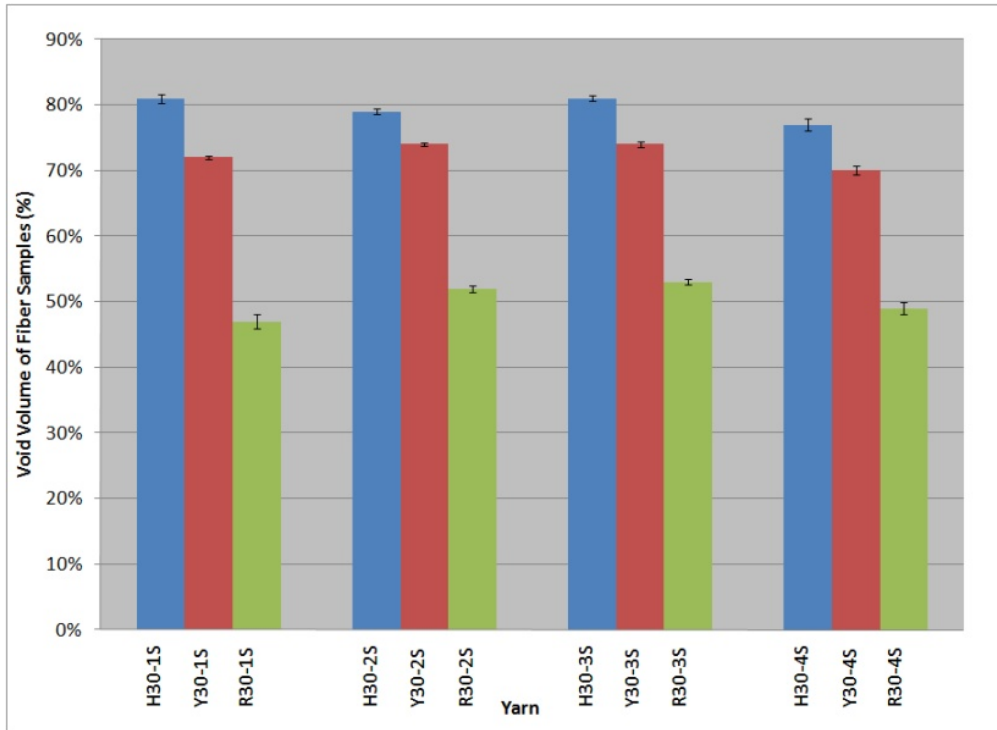The void volumes depicted in Figure 6.13 varied for H, Y and round samples with a

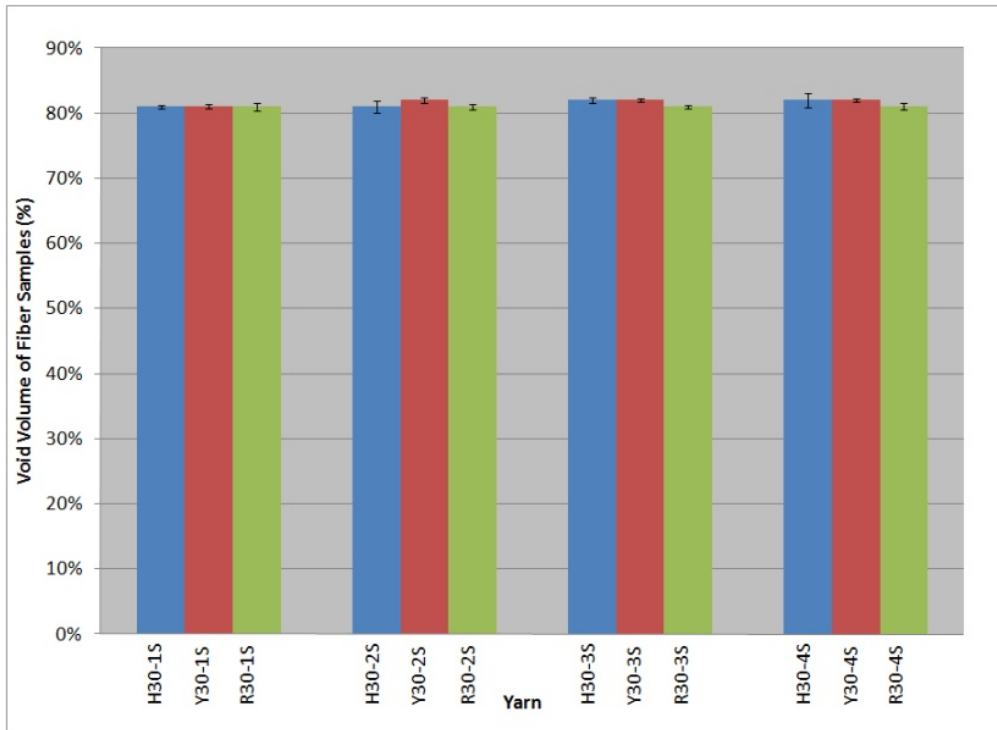Figure 6.13: Calculated void volume of fiber samples with a D of 75 microns

Figure 6.14: Calculated void volume of fiber samples with 1600 filaments

163

D of 75 microns. The differences in void volume were due to the calculation of the inter-fiber capillary width (D) and its influence upon the number of fibers in each bundle. Thus, fiber bundles can have equivalent D values with lower masses if there is an increase in individual fiber perimeter. As the round fibers had the smallest perimeter, those bundle samples had the highest mass of fiber in them and thus the lowest void volume. Conversely, the H fibers had the largest perimeter, resulting in a bundle with a low mass and the largest void volume. The Y fiber bundles fell between the H and round fiber bundles in void volume. For the 1600 filament bundles, the void volume was essentially the same for every sample (see Figure 6.14), regardless of shape, because all the fibers were extruded to have equivalent dpfs.

The fiber bundles were tested as described in Section 2.8.4. The weight of water that each bundle retained allowed the calculation of the maximum fluid capacity of the bundle to be a percentage of the sample tube volume. Figures 6.15 and 6.16 show the maximum fluid retention capacity for the fiber samples with a D of 75 microns and the samples with 1600 filaments, respectively. For the samples with a D of 75 microns, the H fiber samples had the highest fluid capacity and the round fiber samples had the lowest capacity. This trend was also observed for the void volumes of these samples. The Y fiber samples tended to have the maximum capacities of the samples with 1600 filaments and the round fiber samples had the lowest capacities when all samples had similar void volumes.

Although the disparity between the H fiber samples and the Y and round fiber samples seems very high in Figure 6.15, one must remember that the void volumes of these samples were also quite disparate. The void volume of the samples with a D of 75 microns is compared to the maximum fluid capacity of the same samples in Table 6.3. Almost all of the fiber samples filled the void space with fluid to within 1% or 2% of its maximum. This indicated that the samples prepared with a D of 75 microns were filled almost completely with water and very little air was left in the fiber samples.

The same data for the samples with 1600 filaments in shown in Table 6.4. Although the weight of the H fiber samples for this setup was the same as for the previous setup,
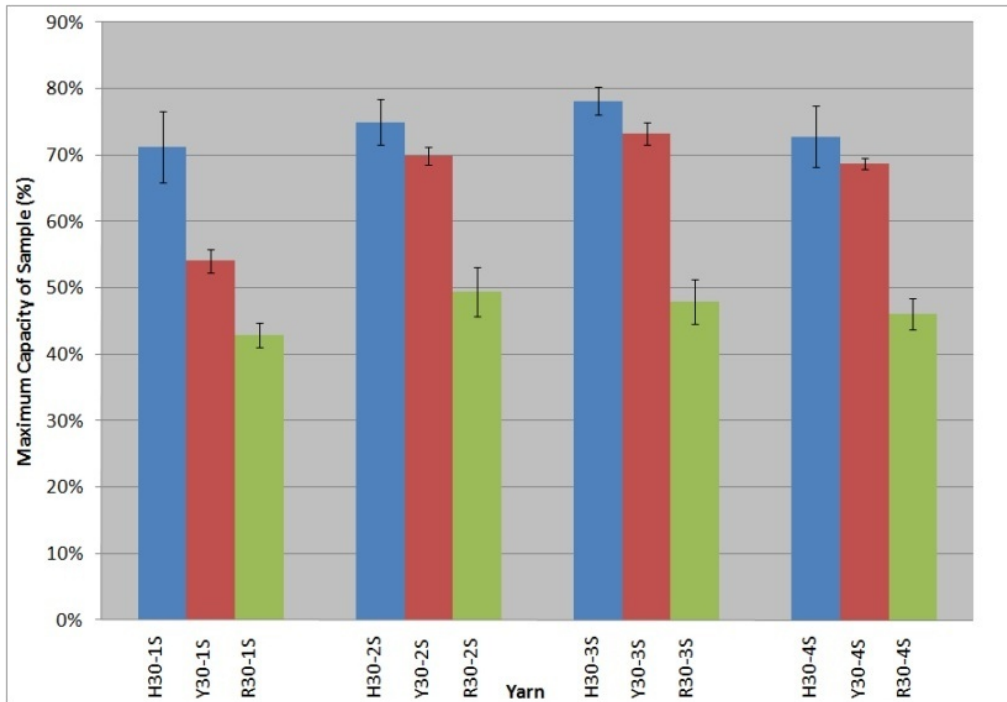
Figure 6.15: The measured maximum capacity of fluid retention for fiber samples with a D of 75 microns
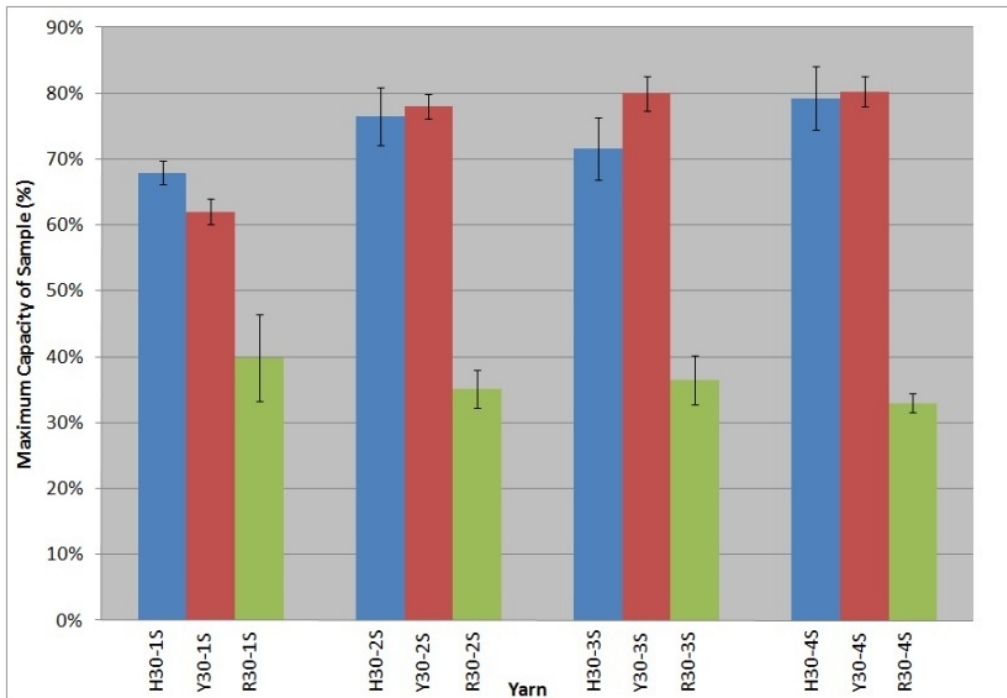

Figure 6.16: The measured maximum capacity of fluid retention for fiber samples with 1600 filaments

the Y and round fiber samples had less fiber in each sample compared to the samples with a D of 75 microns. The samples with 1600 filaments therefore had a higher void volume than the previous samples, but they were not able to fill the entire void space with water as completely as the more densely packed samples.

The H and Y fiber samples consistently had a higher maximum fluid retention capacity than the round shaped fibers as measured by the weight of water adsorbed by the fibers. This was expected due to the channels and inter-fiber structures of the H and Y fibers. The Y fiber samples also appeared to experience a slight increase in the maximum fluid retention capacity when 400 MFI PP was present in the fiber blend. Since this was not an expected result, the procedure was repeated multiple times for the Y30-1S fiber, but every resulting average sorption for the Y30-1S fiber bundle samples matched the previously reported average almost exactly. It is unclear why a capacity decrease occurred in the absence of 400 MFI PP. Possibly, the presence of 400 MFI PP in the fiber could result in a lower modulus and thus an increased likelihood of bending of the fiber legs. If the force of pulling the fiber samples with 400 MFI PP in the blend through the testing tubes resulted in an slight deformation of the Y shape, one of the resulting channels would be smaller than normal causing a larger capillary effect on the water than is possible with the large Y channels. This may have resulted in an increased retention capacity.

The average amount of water retained by the fiber bundle samples is shown in Figures 6.17 and 6.18 in terms of the adsorbed water in grams per gram of fiber for samples prepared with a D of 75 microns and from 1600 filaments, respectively. This calculation showed the capacity of each fiber sample when normalized by the weight of fiber present in the samples. The fiber samples prepared with a D of 75 microns varied in weight, while the samples with 1600 filaments were all of the same weight. When the samples were prepared based on a set D, and the samples were not the same weight, the H fiber samples retained more water in g/g of fiber than the Y fiber samples or the round fiber samples. When the number of filaments and the weight of the fiber samples were equal, the H and Y fiber samples retained approximately the same amount of water while the round fiber samples

Table 6.3: Comparison of calculated Void Volume (VV) and measured Maximum Fluid Capacity (MFC) for Fiber Samples with a D of 75 microns

Fiber	VV (%)	MFC (%)	Difference
H30-1S	81	71	10
H30-2S	79	75	4
H30-3S	81	78	3
H30-4S	77	73	4
Y30-1S	72	54	18
Y30-2S	74	70	4
Y30-3S	74	73	1
Y30-4S	70	69	1
R30-1S	47	43	4
R30-2S	52	49	3
R30-3S	53	48	5
R30-4S	49	46	3

Table 6.4: Comparison of calculated Void Volume (VV) and measured Maximum Fluid Capacity (MFC) for Fiber Samples with 1600 filaments

Fiber	VV (%)	MFC (%)	Difference
H30-1S	81	68	13
H30-2S	81	76	5
H30-3S	82	72	10
H30-4S	82	79	3
Y30-1S	81	62	19
Y30-2S	82	78	4
Y30-3S	82	80	2
Y30-4S	82	80	2
R30-1S	81	40	41
R30-2S	81	35	46
R30-3S	81	36	45
R30-4S	81	33	48

adsorbed only half the amount. This again reiterated the improved retention capabilities of the shaped fibers. Since the Y fiber samples matched the retention of the H fibers when using the same mass of fiber, the two fiber shapes appear to have very similar water retention properties and very little distinction could be made between the two shapes. The packing of the Y fibers does strongly affect the retention properties of the fibers; however, the Y fiber samples with 1600 filaments had fewer filaments than the samples with a D of 75 microns and retained more fluid, indicating that there is a minimum distance between the Y fibers that will result in improved fluid retention and distances smaller than this result in reduced fluid retention.
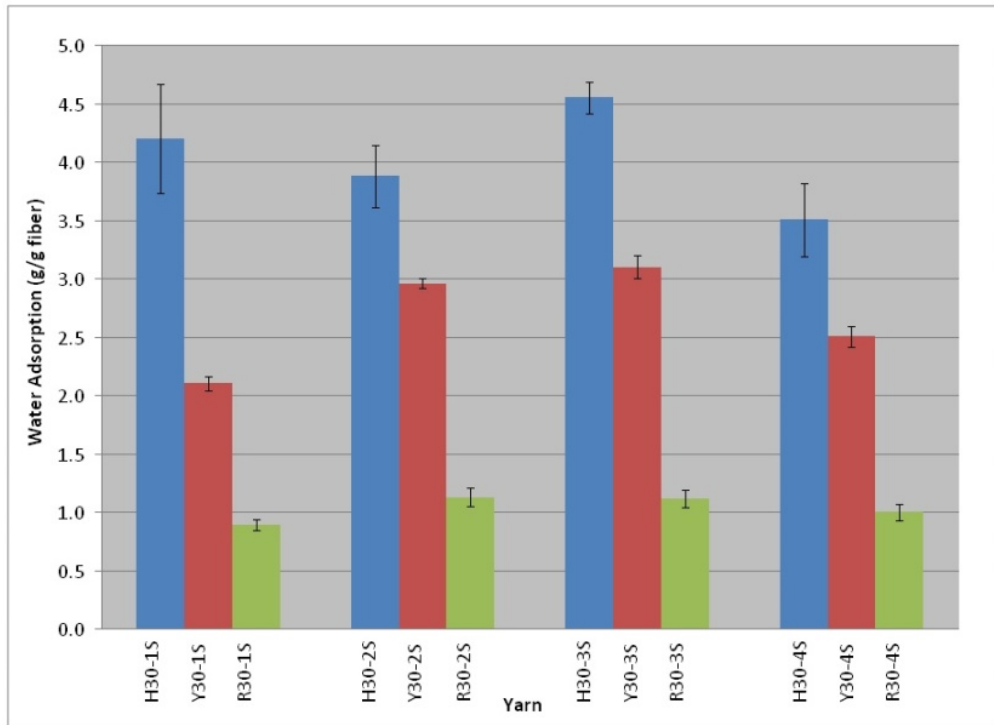
Figure 6.17: Water sorption of samples with a D of 75 microns in grams per gram of fiber
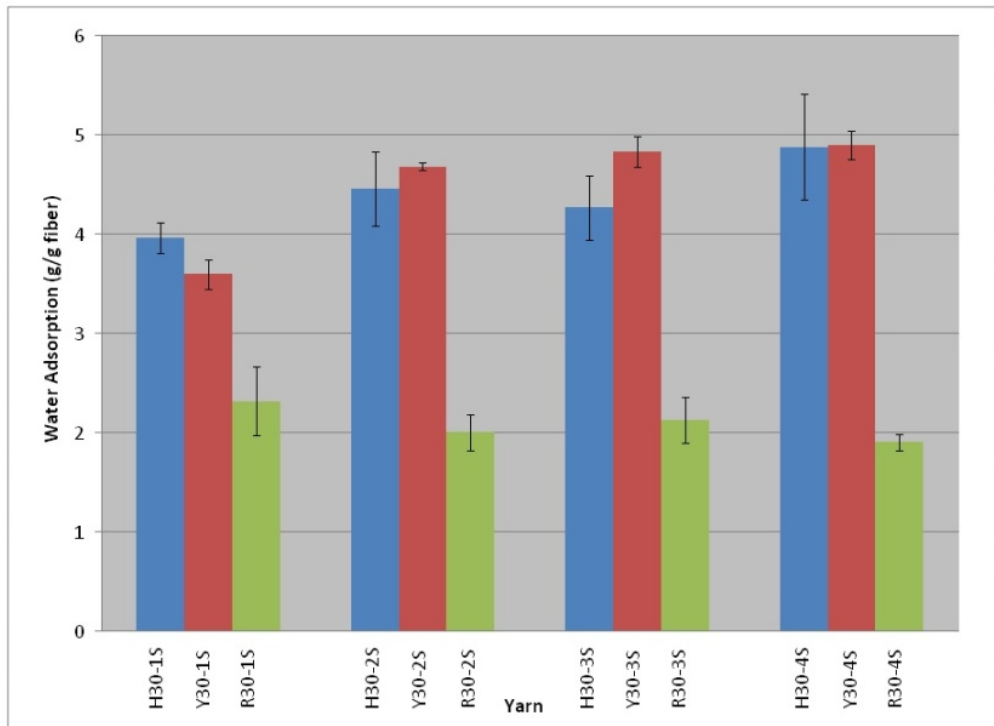

Figure 6.18: Water sorption of samples with 1600 filaments in grams per gram of fiber

Chapter 7

Conclusions and Future Work

7.1 Conclusions

The work investigated the shaped fiber technology donated to Clemson University by Eastman Chemical Company and Procter & Gamble. The investigation of the shaped fiber technology involved the extrusion of PP H, Y, and Octolobal shaped fibers and the improvement of the shape retention of the extruded fibers. The shaped fibers were utilized in the sorption and transport of high and low surface energy fluids and were compared in these areas with conventional round shaped fibers. Y shaped fibers of varying linear densities were evaluated to determine the effect of fiber size on fluid retention and a hydrophilic polyester additive was used to extrude a hydrophilic blended PP fiber.

The fibers extruded from 18 MFI PP using spinnerets with conventional round holes and a spinneret with Y shaped holes showed that the cross-sectional shape of the fibers did not experience any distinct shape distortion during extrusion. When the spinneret with H shaped holes was used to extrude 18 MFI PP fibers, the cross-sectional shape of the fibers was highly distorted from the original spinneret hole shape. The addition of increasing levels of 400 MFI PP to the fiber blend improved the shape retention of the H fiber with respect to the original spinneret hole in increasing amounts. The highest level of shape retention was seen with the H30-4 fibers, the H fibers extruded from 50% 18 MFI PP and 50% 400

MFI PP. The addition of 400 MFI PP to the polymer blend used to extrude round and Y shaped fibers did not affect the shape of the fiber, although the extrusion temperature had to be lowered by a few degrees.

The Y, H, and Octolobal shaped fibers were evaluated according to the standard test method ASTM F-726 to determine their capabilities as an oil sorbent. The conventional round fibers were also evaluated using this standard and the results were compared to the results from the shaped fiber testing. In an oil bath alone, the shaped fibers adsorbed twice the amount of oil the round fibers adsorbed. The Y shaped fibers adsorbed the highest amount of oil, likely due to the structure formed by the interaction of the legs of a single Y fiber with adjacent Y fibers. Although the H and Octolobal fibers had a higher surface area per filament than the Y fibers, they could not create the same inter-fiber structure and thus were unable to adsorb and retain the same amount of oil per surface area as the Y fibers. In the degradation testing, where the fibers were used to adsorb oil from water, the shaped fibers were again shown to adsorb and retain twice the amount of oil that the round fibers could adsorb.

The same test method was used to compare the round and Y fibers of increasing linear density. The comparison of the oil sorption and retention properties of these fibers showed that the amount of oil retained by the Y fibers was not solely due to the increased surface area of the fibers. Round fiber samples with the same surface area as a Y fiber sample retained less oil, supporting the conclusion that the Y fibers formed a structure that increased the oil sorption and retention properties beyond that expected due to the increased surface area. The sorption and transport properties of the round, Y and H shaped fibers coated with Bozetto SF2 spin finish were also evaluated using water. Although the Y and H fibers were shown to have higher wicking capabilities than the round fibers, no true distinction could be made between the transport properties of the two shaped fibers. Further investigation of the fibers showed that although there was no correlation in the wicking properties of the round and Y fibers and the inclusion of the 400 MFI PP. However, the improved shape of the H fibers caused by the addition of the shorter chain polymer

resulted in a decreased wicking capacity but in a faster rate of wicking. When hydrophilic polyester additives were included in the polymer blend for the H fibers, the addition of the short chain PP to the same blend had a positive effect on the transport properties. The blooming of the short chain polymer to the surface of the fiber drew the polyester additive towards the surface of the fiber, increasing the fiber's hydrophilicity. The improved hydrophilicity of the fibers overcame the negative influence of the improved fiber shape and increased the water transport of the fibers.

The shaped fiber technology has many possible applications in fluid sorption and retention of fluids of both high and low surface tension. The shaped fiber samples displayed twice the capacity for fluid that the round fibers showed during these procedures. The technology developed by Eastman Chemical Company and Procter & Gamble shows great promise for utilization in future work.

7.2 Recommendations for Future Work

7.2.1 Shaped Fiber Extrusion

Future work on the extrusion of shaped fibers should focus on using blends of PP and additives to achieve the most effective shape for each spinneret design. The Octolobal and Y fibers had excellent shape retention regardless of the polymer blend, but the H fibers showed a drastic alteration of shape based on the blends. Using the 400 MFI PP improved the shape retention of the H fiber, but this in turn decreased the sorption and transport properties of the fiber. Including the hydrophilic additive in the same blend of 18 and 400 MFI PP caused an increase in the sorption and transport properties. A study that determined the most effective balance of 18 MFI PP, 400 MFI PP and hydrophilic additive in a shaped fiber for water transport would determine the necessary amount of 400 MFI PP to make the hydrophilic additive bloom to the surface of the fiber, thus resulting in the most hydrophilic PP fiber possible with that additive. Determining this mix of polymers would then allow a more effective exploration of the effects of other hydrophilic additives on

the PP surface chemistry. In addition, future work in extruding shaped fibers could focus on extruding them from thermoplastic polymers. Although the issue of shape retention has been addressed for PP, it will need to be explored for other polymers to determine if using the same approach (blending the main polymer with a shorter chain version of the same polymer) would be effective in all cases.

The final focus in continuing shaped fiber extrusion would be to decrease the dpf of the extruded fibers even lower than the size used in this work (30 dpf). The Y fibers investigated in the oil sorption study revealed that fibers with a higher surface area to volume ratio were more effective at adsorbing oil. To further increase this ratio, the next extruded Y fibers should be extruded to a linear density of 15 dpf or smaller. Unfortunately, the thickness of the legs on the 30 dpf Y fibers was already approaching the lower limit of what could be achieved via direct melt spinning. Using a conjugate spinning system would allow Y fibers of the same shape and leg length to thickness ratio as the original Y fibers to be extruded at smaller dpfs. These smaller dpf fibers could then be evaluated for fluid sorption and transport and will likely prove more effective than any of the fibers previously investigated.

7.2.2   Fluid Sorption, Retention and Transport Properties

Although the shaped fibers have been shown to have superior sorption, retention and transport properties as compared to conventional round fibers, much work is still required to truly comprehend the cooperative structure that forms between fibers to increase their fluid capacity. In order to more clearly evaluate the mechanism of this work, studies could be conducted on individual fibers to determine the way fluids adhere to the fibers and how the fluid spreads across the fiber after initial contact. For this exploration and further work, comparing the Y fiber (with its large open channels) to a fiber shaped like a plus sign (i.e. a four-legged cross) would further elucidate the relationship between the number of channels and the sorption of the fibers. Although the H fiber has 2 channels and the Y fiber has 3 channels, the shapes of the channels are extremely different. Using a plus shaped fiber with

173

a similar length-to-leg thickness ratio as the Y fiber would allow a true comparison of the effect of the channel number. Also, such a fiber would likely display the same interaction of adjacent fibers to form a cooperative structure. This would allow evaluation of bulk properties that could also be compared to the Y fiber.

Further exploration of the sorption properties of the fibers should include a study on non-woven fabrics prepared from these fibers. The mechanical forces exerted during a knitting or weaving process would possibly crush the channels within the fibers. Using non-woven fabrics would hopefully allow the channels within the fibers to remain open during processing. The various methods of making a non-woven fiber could be explored to determine the least destructive method, which could then be utilized to produce non-woven fabrics of varying loft, porosity and basis weight. The structure provided by the non-woven fabric may cause an increase in fluid sorption and would definitely improve the mechanical strength of the fiber sample as compared to loose fibers. If these fibers are utilized to recover oil from oil spills, further research could involve determining an effective method for removing the oil from the fibers. It might be possible to press excess oil from the fibers and then remove the residue by using another fluid to wash the fibers. The capillary nature of the fibers might be effective in aiding this washing if the correct solution or chemical wash was chosen that had an even higher affinity for the fibers than the oil.

Another possible avenue for future research is the modeling of the fiber/oil systems. The size and shape of the fibers have been measured using SEM images and the sorption capacities of the fibers have been determined for various sizes of fibers. A mathematical model representing the oil sorption structure of the H and Y fibers could be initiated from this data. This information could be used to further study the interactions of the fibers and could be used to more effectively calculate the distance between the fibers in a sample. This model could then be furthered by studying the extrusion of fibers from the nearly 400 spinnerets included in the Eastman Chemical Company and Procter and Gamble gift. Simplistic fiber shapes should be used to evaluate the model initially so that the geometric shape retention issue of the fibers will not be at issue.

Appendix A

Thermal Evaluation of Fiber Samples

A.1   Heating Curves

The round fibers were extruded as a basis of comparison for the H and Y fibers. If the shape of the fiber had a large affect on the percent crystallinity of the fibers or on the crystal structure and thus melting temperature, it would be apparent when comparing the thermograms for the H and Y fibers to the thermograms for the round fibers.

Figure A.1 presents the thermogram of fiber R30-1, spun from 100% 18 MFI PP. The as spun fiber had a peak melting temperature of 164.2°C and an enthalpy of 83.8 J/g which resulted in a calculated percent crystallinity of 42%. The post quench fiber had a peak melting temperature of 161.4°C and an enthalpy of melting of 81.6 J/g. This resulted in a calculated crystallinity of 42%.

The thermal analysis for R30-2, spun from 90% 18 MFI PP and 10% 400 MFI PP, is shown in Figure A.2. The as spun sample experienced a melting peak at 163.3°C and the post quench sample at 161.5°C. These peaks resulted in enthalpies of melting of 90.0 J/g for the as spun sample and 81.6 J/g for the post quench sample. The percent crystallinity of the R30-2 sample was 45% as spun and 41% post quench.
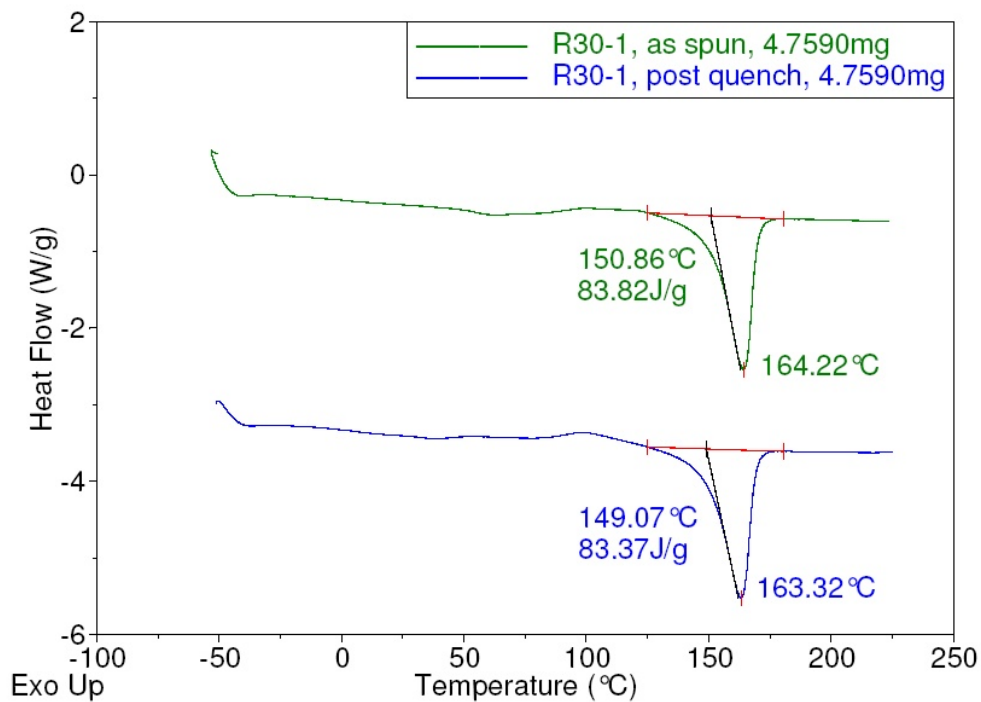
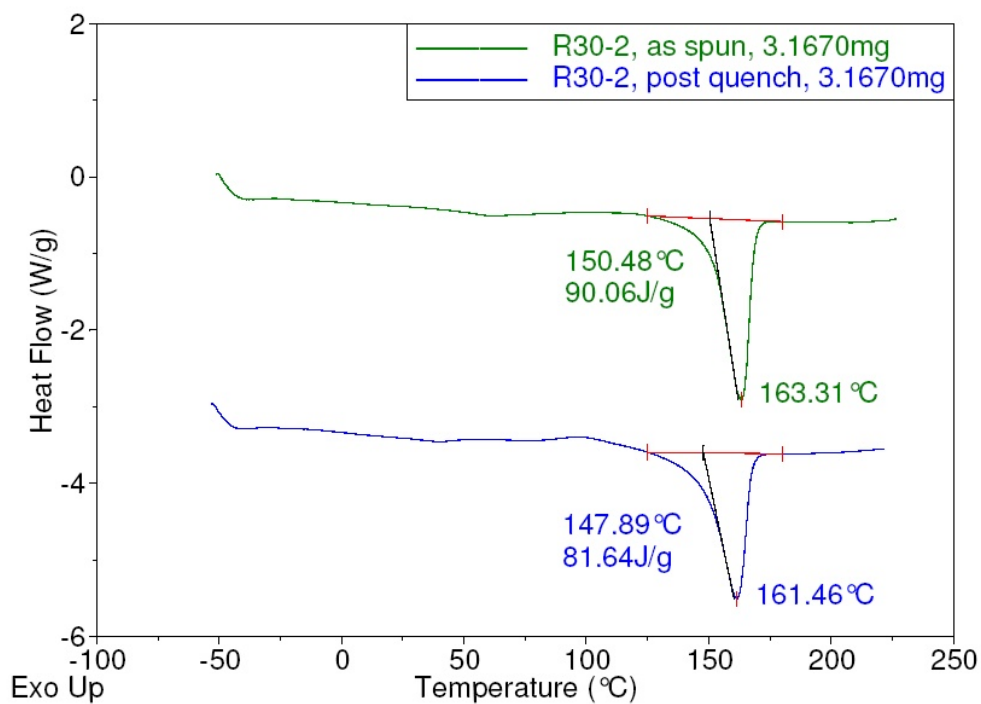Figure A.1: Thermal analysis of fiber R30-1 before and after quenching

Figure A.2: Thermal analysis of fiber R30-2 before and after quenching

176

The thermogram for the DSC analysis of fiber R30-3 is shown in Figure A.3. This fiber was extruded from a 75/25 blend of the 18 MFI PP and the 400 MFI PP. The peak temperature of melting for the as spun sample was 162.8°C and the enthalpy of melting was 93.0 J/g, resulting in a calculated percent crystallinity of 46%. The post quench sample had a peak melting temperature of 161.8°C. The enthalpy of melting was 83.9 J/g and the percent crystallinity was 42%.

Figure A.4 represents the thermogram of fiber R30-4, spun from 50% 18 MFI PP and 50% 400 MFI PP. The as spun fiber had a peak melting temperature of 162.6°C and an enthalpy of 87.5 J/g which resulted in a calculated percent crystallinity of 44%. The post quench fiber had a peak melting temperature of 162.3°C and an enthalpy of melting of 84.7 J/g. This resulted in a calculated crystallinity of 42%.

Thermal analysis by DSC of the Y fibers spun from 18 MFI PP and 400 MFI PP showed that the Y fibers were very similar in thermal characteristics to the round fibers and the original polymers. Again, only a melting peak was observed during these experiments. The Y fibers and round fibers did not have any major difference in percent crystallization or melting temperature for either the as spun or post quench runs.

Figure A.5 represents the thermogram of fiber Y30-1, spun from 100% 18 MFI PP. The as spun fiber had a peak melting temperature of 163.2°C and an enthalpy of 87.2 J/g which resulted in a calculated percent crystallinity of 43%. The post quench fiber had a peak melting temperature of 161.9°C and an enthalpy of melting of 84.2 J/g. This resulted in a calculated crystallinity of 42%.

The thermogram for the DSC analysis of fiber Y30-2 is shown in Figure A.6. This fiber was extruded from a 90/10 blend of the 18 MFI PP and the 400 MFI PP. The peak temperature of melting for the as spun sample was 163.1°C and the enthalpy of melting was 88.9 J/g, resulting in a calculated percent crystallinity of 43%. The post quench sample had a peak melting temperature of 161.8°C. The enthalpy of melting was 83.9 J/g and the percent crystallinity was 42%.

Figure A.7 shows the thermal analysis of fiber Y30-3. This fiber was extruded from
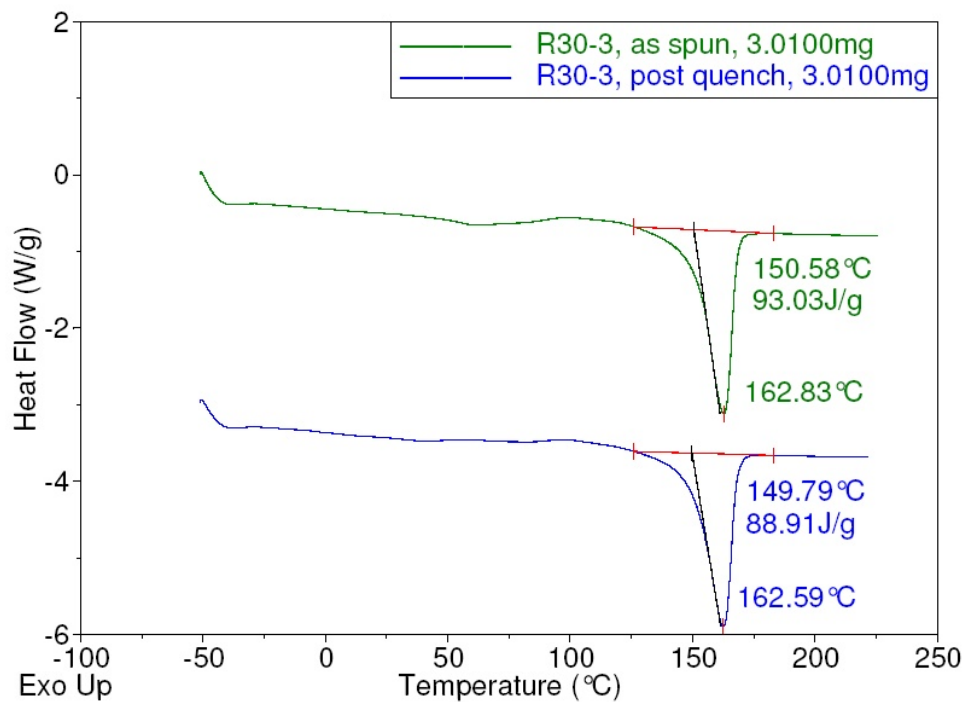
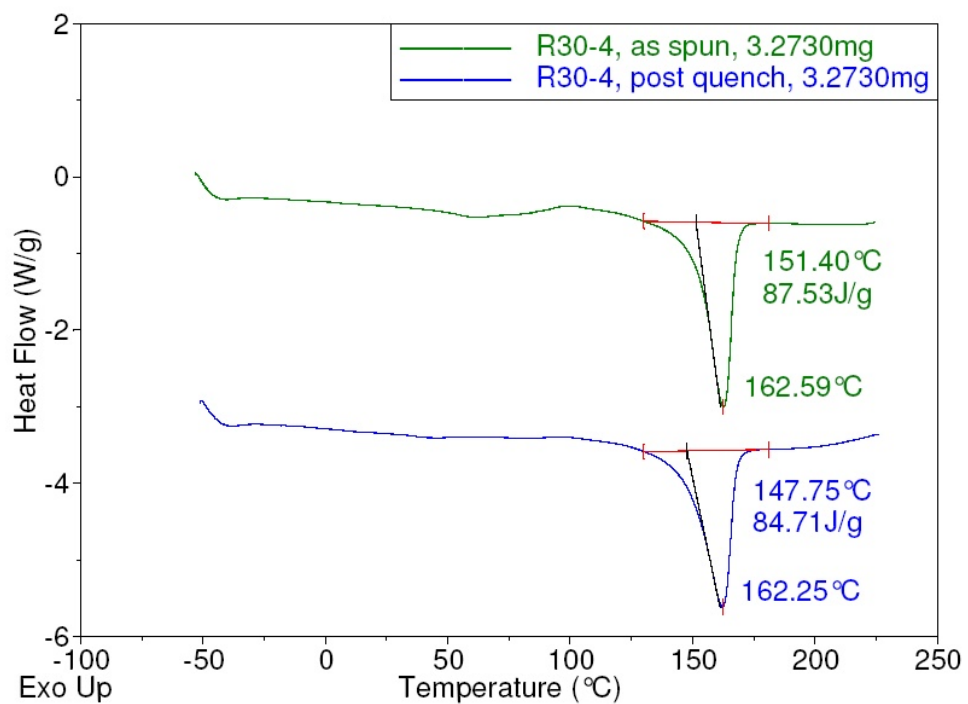Figure A.3: Thermal analysis of fiber R30-3 before and after quenching

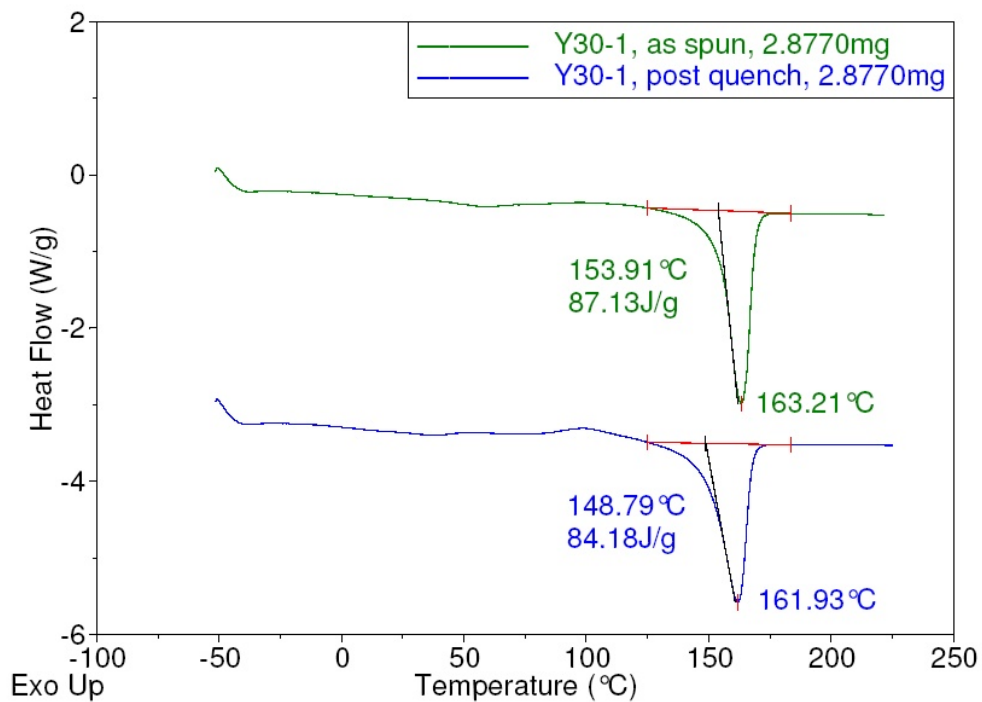Figure A.4: Thermal analysis of fiber R30-4 before and after quenching

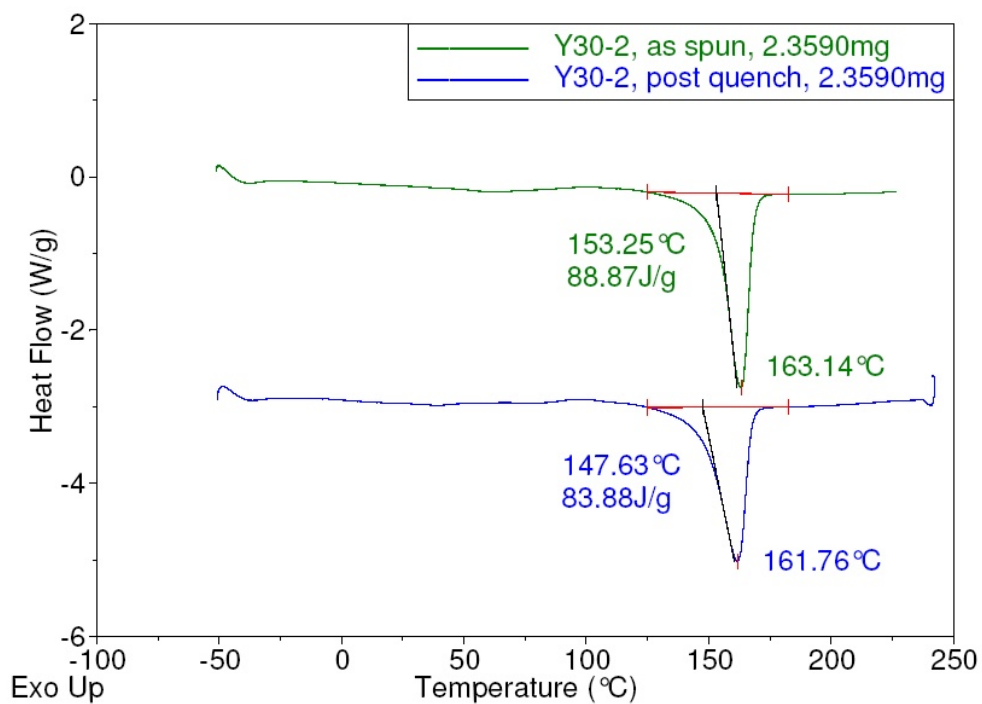Figure A.5: Thermal analysis of fiber Y30-1 before and after quenching

Figure A.6: Thermal analysis of fiber Y30-2 before and after quenching

179

75% 18 MFI PP and 25% 400 MFI PP. Fiber Y30-3 experienced only a melting peak during thermal examination. For the as spun sample, this peak occurred at 163.3°C and had an enthalpy of 90.3 J/g. Quenching the sample resulted in a peak melting temperature of 161.5°C and an enthalpy of 88.5 J/g. The calculated percent crystallinity of the as spun sample was 45% and that of the post quench sample was 44%.

The thermal analysis for Y30-4, spun from 50% 18 MFI PP and 50% 400 MFI PP, is shown in Figure A.8. The as spun sample experienced a melting peak at 163.3°C and the post quench sample at 161.5°C. These peaks resulted in enthalpies of melting of 90.3 J/g for the as spun sample and 88.5 J/g for the post quench sample. The percent crystallinity of the Y30-4 sample was 45% as spun and 44% post quench.

Thermal analysis of the H fibers spun from 18 MFI and 400 MFI PP showed that the fibers had essentially the same thermal properties as the original polymers. The thermograms for these fibers experienced a melting peak but did not display any T_g or crystallization peak during the as spun testing or after the quench.

The thermal analysis of fiber H30-1 is shown in Figure A.9. This fiber was extruded from 18 MFI PP only. The thermal analysis of the as received 18 MFI PP polymer chip did not show the T_g of the polymer and neither did the evaluation of the spun fiber. Both the as spun and post quench runs of the sample resulted in a large endothermic melting peak. For the as spun sample, the peak melting temperature was 162.4°C. Quenching the sample resulted in a similar melting peak temperature of 161.3°C. The enthalpy of melting was similar for both runs of the sample as well. The as spun sample had an enthalpy of 84.2 J/g and the post quench sample had an enthalpy of 83.2 J/g. This resulted in a percent crystallinity of 42% for both samples. This crystallinity was the same as the crystallinity of the as received 18 MFI PP sample.

Figure A.10 shows the thermal analysis of fiber H30-2. This fiber was extruded from 90% 18 MFI PP and 10% 400 MFI PP. As was shown in 3.2.2, the 18 MFI PP and 400 MFI PP exhibited similar thermal characteristics and could not be expected to show up seperately on any future thermal characterization of blends. Fiber H30-2 experienced only
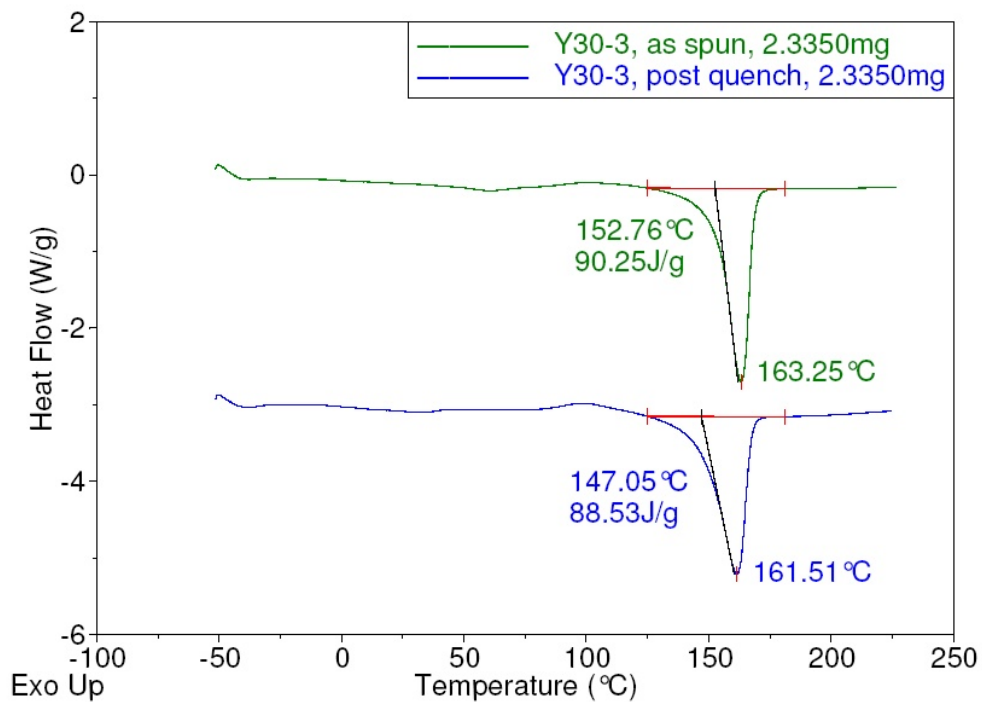
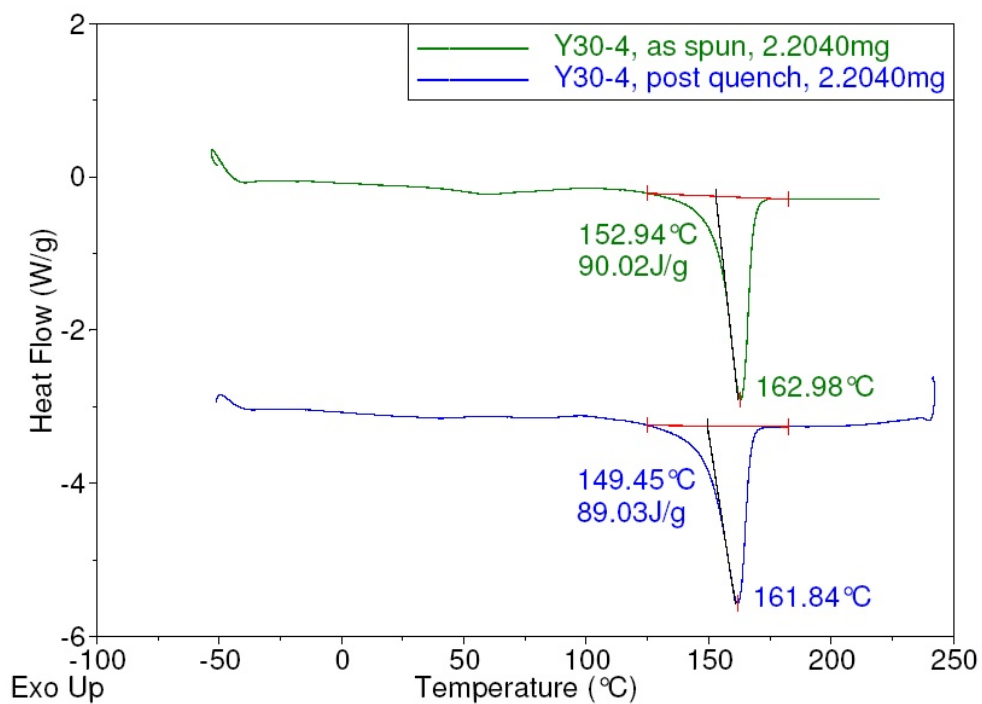Figure A.7: Thermal analysis of fiber Y30-3 before and after quenching

Figure A.8: Thermal analysis of fiber Y30-4 before and after quenching

181

a melting peak during thermal examination. For the as spun sample, this peak occurred at 162.2°C and had an enthalpy of 89.1 J/g. Quenching the sample resulted in a peak melting temperature of 163.5°C and an enthalpy of 84.7 J/g. The calculated percent crystallinity of the as spun sample was slightly higher at 45% than that of the 41% post quench sample.

Figure A.11 represents the thermogram of fiber H30-3, spun from 75% 18 MFI PP and 25% 400 MFI PP. The as spun fiber had a peak melting temperature of 162.2°C and an enthalpy of 88.0 J/g which resulted in a calculated percent crystallinity of 44%. The post quench fiber had a peak melting temperature of 161.1°C and an enthalpy of melting of 85.3 J/g. This resulted in a calculated crystallinity of 43%.

The thermogram for the DSC analysis of fiber H30-4 is shown in Figure A.12. This fiber was extruded from a 50/50 blend of the 18 MFI PP and the 400 MFI PP. The peak temperature of melting for the as spun sample was 162.2°C and the enthalpy of melting was 92.9 J/g, resulting in a calculated percent crystallinity of 46%. The post quench sample had a peak melting temperature of 163.0°C. The enthalpy of melting was 88.4 J/g and the percent crystallinity was 44%.

The results of the DSC for fiber H30-1A are shown in Figure A.13. This thermogram was representative of PP in general and the addition of the polyester additive LB-100 did not alter the thermogram in any discernible way. The peak melting temperature of the as spun fiber was 162.1°C and the enthalpy of melting was 83.3 J/g. This resulted in a calculated percent crystallinity of 42%. The post quench sample experienced a peak melting temperature of 162.5°C, an enthalpy of melting of 80.0 J/g and a percent crystallinity of 40%.

Figure A.14 represents the thermogram of fiber H30-2A, spun from 90% 18 MFI PP and 10% 400 MFI PP with an additional 5% of additive LB-100. The as spun fiber had a peak melting temperature of 162.6°C and an enthalpy of 79.4 J/g. The post quench fiber had a peak melting temperature of 162.8°C and an enthalpy of melting of 79.4 J/g. Both samples had a calculated crystallinity of 40%.

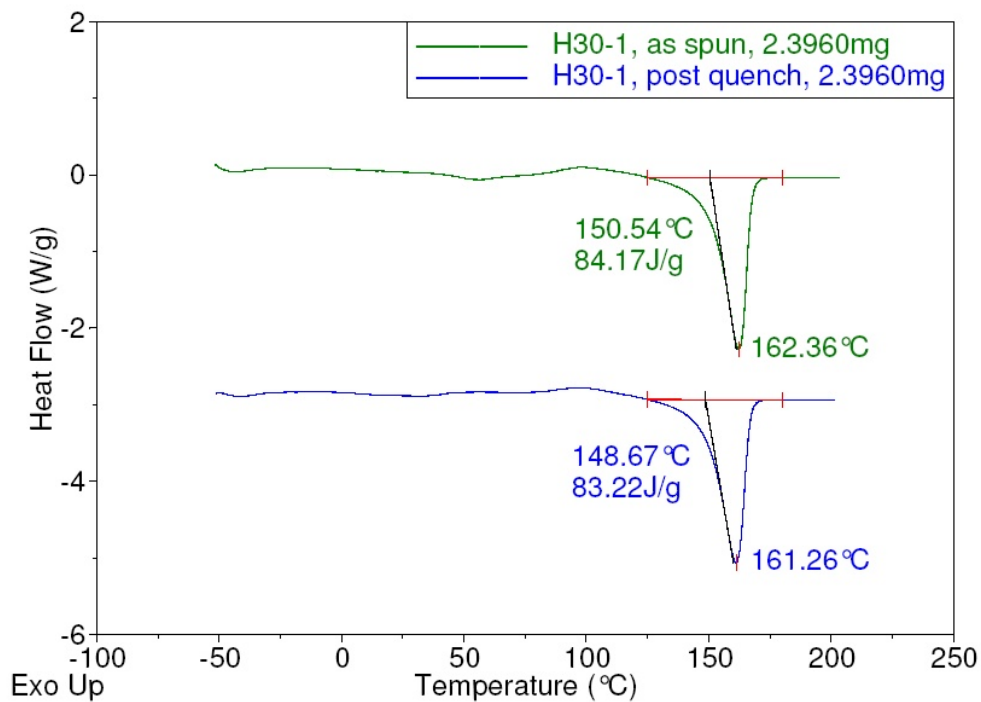The thermogram for the DSC analysis of fiber H30-3A is shown in Figure A.3. This

Figure A.9: Thermal analysis of fiber H30-1 before and after quenching
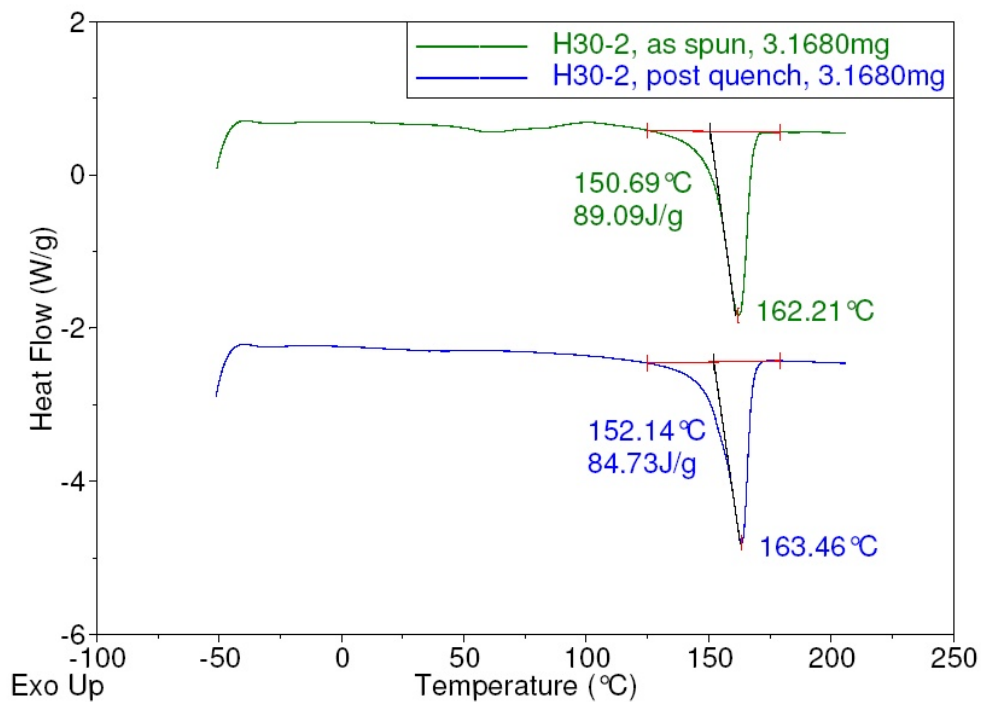

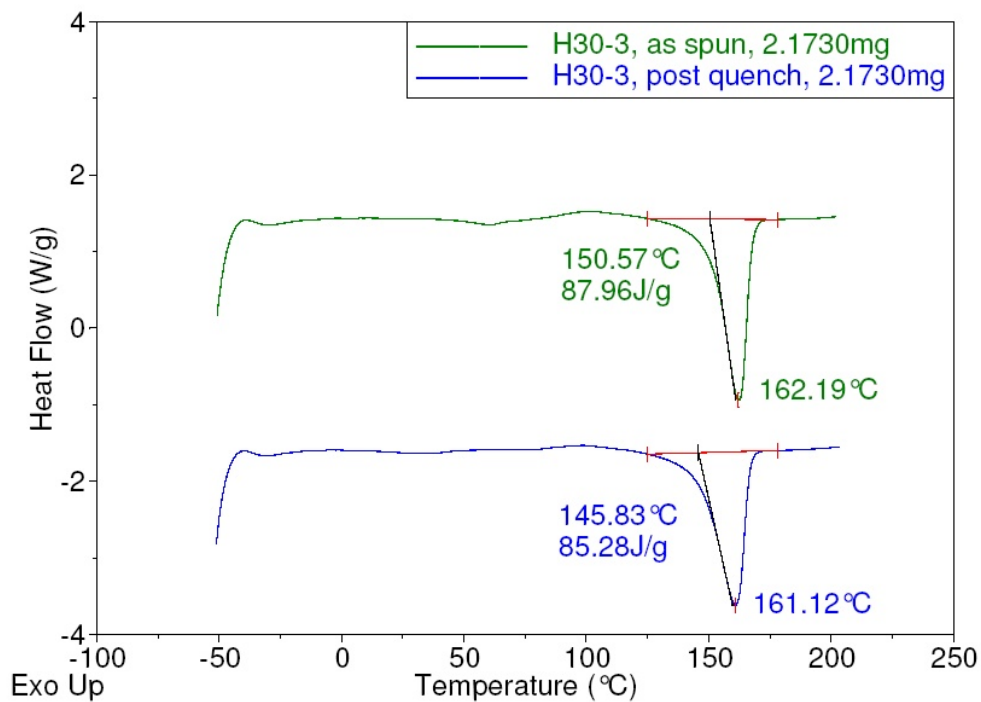Figure A.10: Thermal analysis of fiber H30-2 before and after quenching

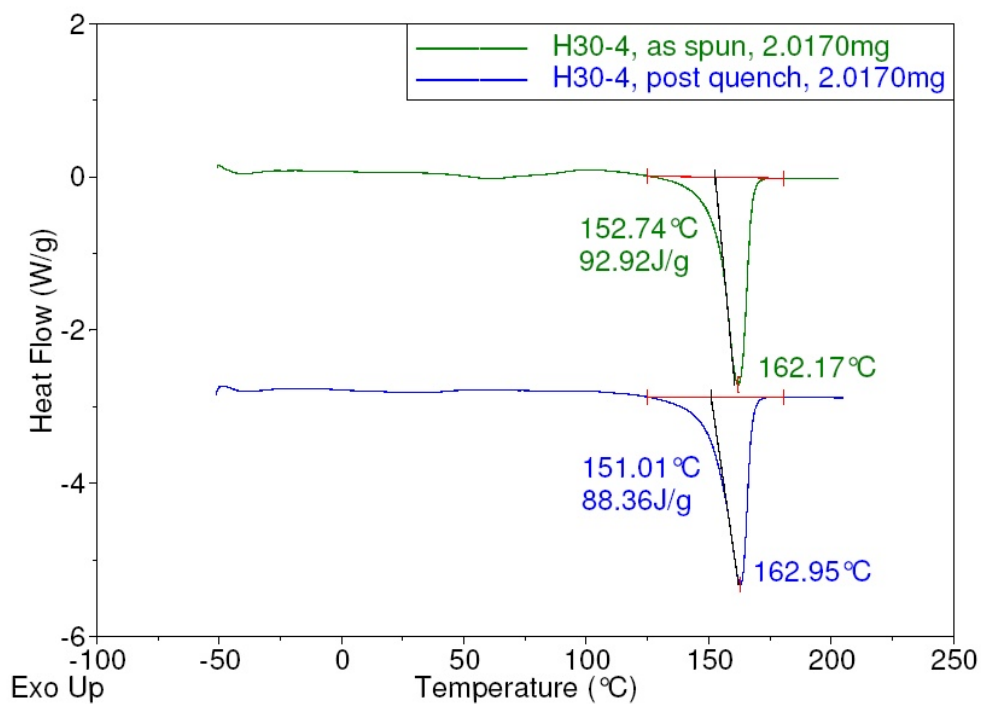Figure A.11: Thermal analysis of fiber H30-3 before and after quenching

Figure A.12: Thermal analysis of fiber H30-4 before and after quenching
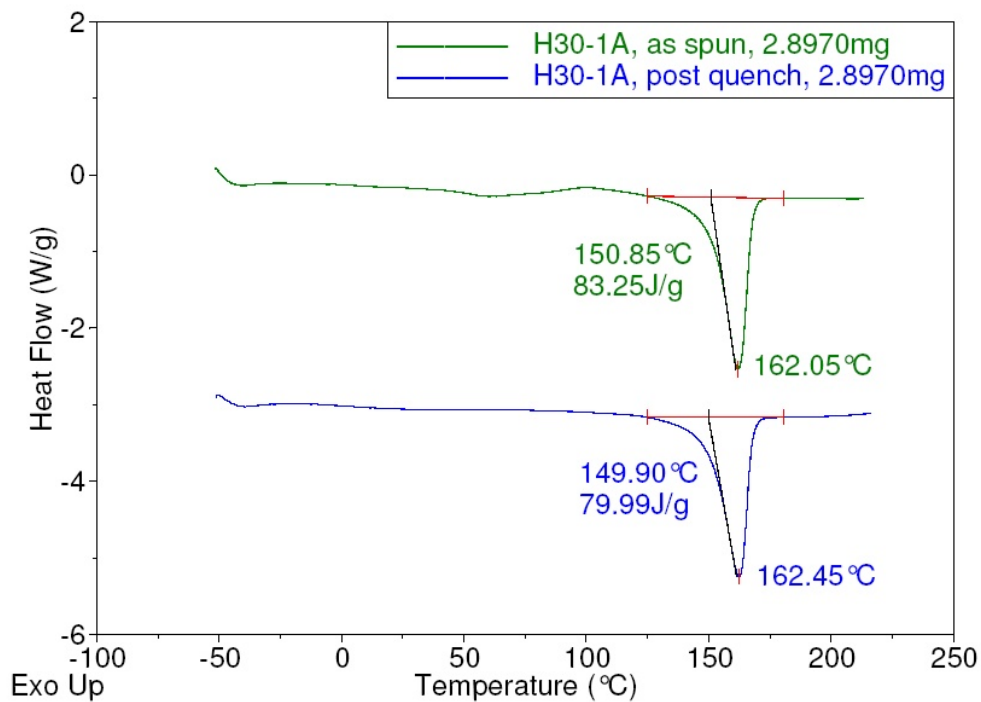
184

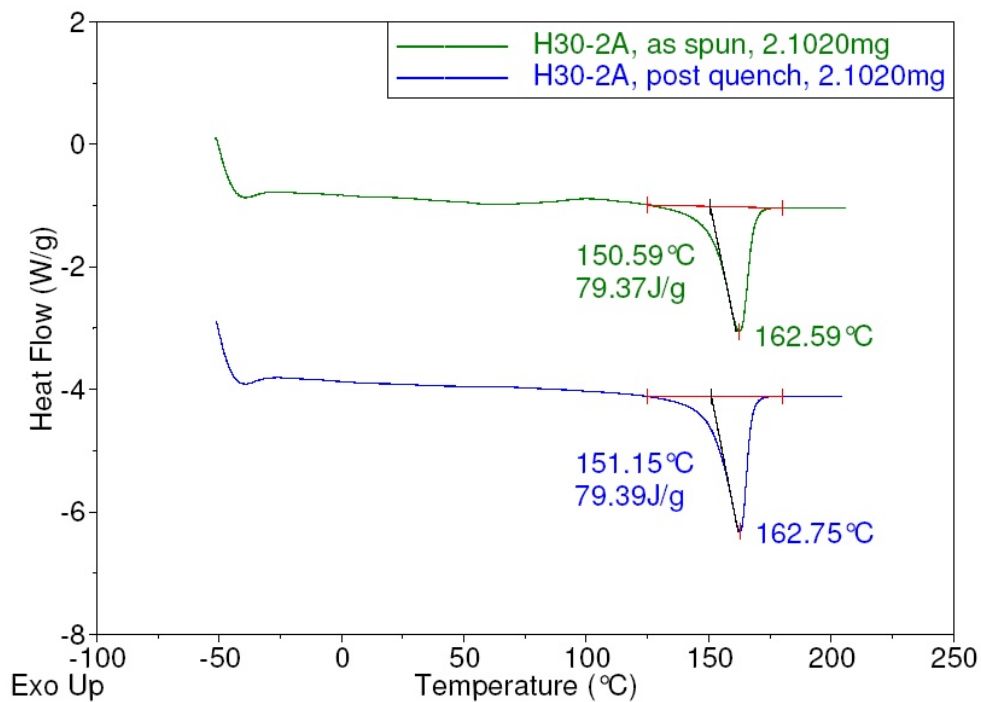Figure A.13: Thermal analysis of fiber H30-1A before and after quenching

Figure A.14: Thermal analysis of fiber H30-2A before and after quenching

185

fiber was extruded from a 75/25 blend of the 18 MFI PP and the 400 MFI PP. 5% of the polyester additive LB-100 was added to the blend. The peak temperature of melting for the as spun sample was 162.2°C and the enthalpy of melting was 85.2 J/g, resulting in a calculated percent crystallinity of 43%. The post quench sample had a peak melting temperature of 162.1°C. The enthalpy of melting was 83.2 J/g and the percent crystallinity was 42%.

Figure A.16 represents the thermogram of fiber H30-4A, spun from 50% 18 MFI PP and 50% 400 MFI PP with an additional 5% of the additive LB-100. The as spun fiber had a peak melting temperature of 162.1°C and an enthalpy of 85.3 J/g which resulted in a calculated percent crystallinity of 43%. The post quench fiber had a peak melting temperature of 162.7°C and an enthalpy of melting of 81.0 J/g which gave a crystallinity of 40%.
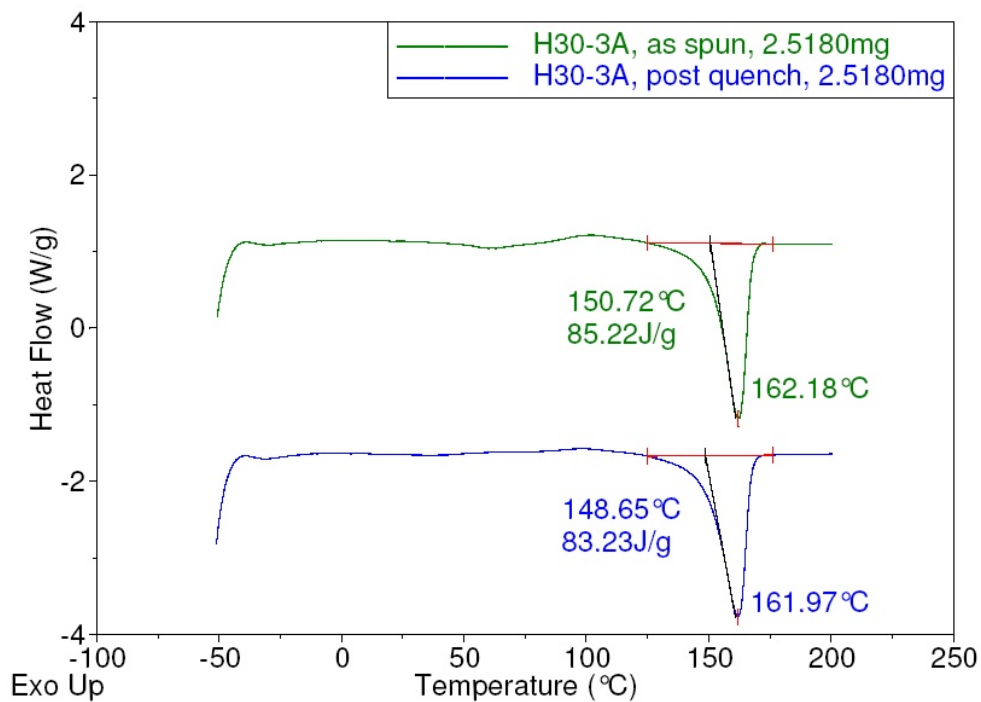
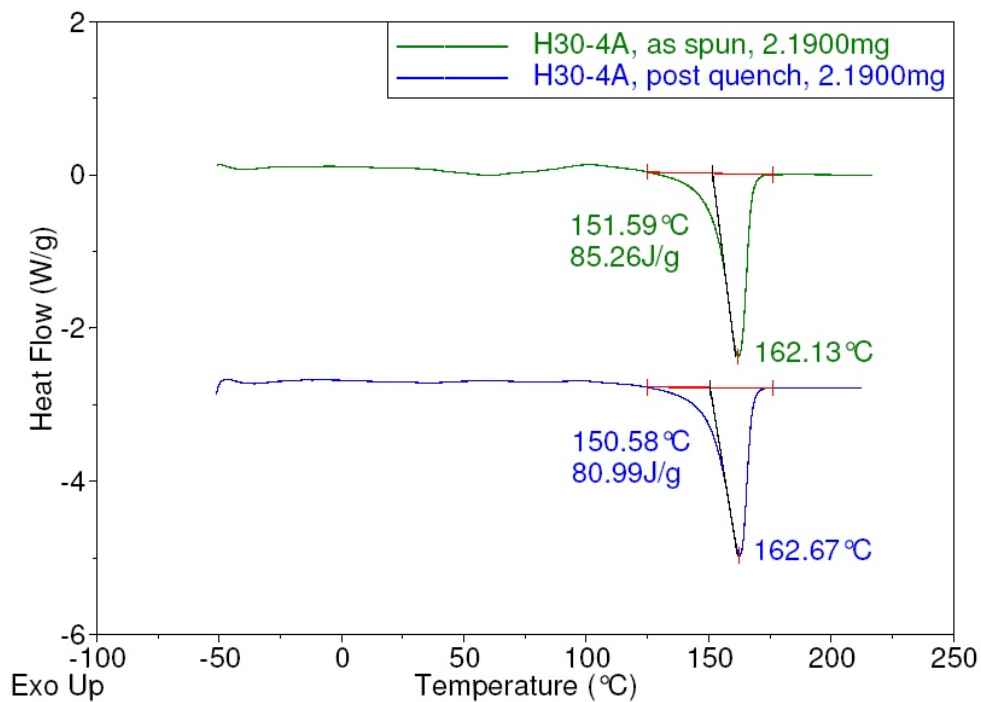Figure A.15: Thermal analysis of fiber H30-3A before and after quenching

Figure A.16: Thermal analysis of fiber H30-4A before and after quenching

187

A.2   Cooling Curves

The results from the heating, cooling and reheating of the 18 MFI PP sample are shown in Figure A.17. The curves for the cooling cycle and the post cooling cycle have been offset manually to improve visibility. During the first run of the sample, the 18 MFI PP had a peak melting temperature of 166.2°C and an enthalpy of melting of 81.2 J/g. This resulted in a calculated crystallinity of the as received sample of 41%, which agrees with the previously run sample of 18 MFI PP. During the cooling cycle, the sample experienced an exothermic peak due to the the crystallization of the polymer. The enthalpy of crystallization for the 18 MFI PP was 96.7 J/g and the peak temperature was 111.1°C. After the sample was run through the cooling cycle, the peak melting point had shifted down three degrees to 163.7°C and the enthalpy of melting was 83.0 J/g. The 18 MFI PP had a crystallinity of 42% after the cooling cycle, which was essentially the same crystallinity as the as received polymer.

Figure A.18 shows the heating, cooling and reheating cycle experienced by the 400 MFI PP sample. The curves for the cooling cycle and the post cooling cycle have been offset manually. The as received 400 MFI PP had a peak melting temperature of 165.3°C and an enthalpy of melting of 65.9 J/g, which resulted in a crystallinity of 33%. This crystallinity was slightly lower than the previously tested 400 MFI PP sample, which was at 37%. After the cooling cycle, the 400 MFI PP had a peak melting temperature of 161.1°C and an enthalpy of melting of 88.5 J/g. This resulted in a calculated crystallinity of 44% for the post cooling cycle sample. This was a large increase in crystallinity for the sample, showing that the as received sample was not as crystalline as the material could be. The cooling cycle for the 400 MFI PP showed a crystallization peak temperature of 110.6°C and an enthalpy of crystallization of 100 J/g. This was comparable to the enthalpy of crystallization for the 18 MFI PP, which was 96.7 J/g. Since the two crystallization energies were similar for the 18 and the 400 MFI PP, it would be difficult to identify the amounts of each individual polymer in a blend based on the crystallization energies. However, the four fiber blends
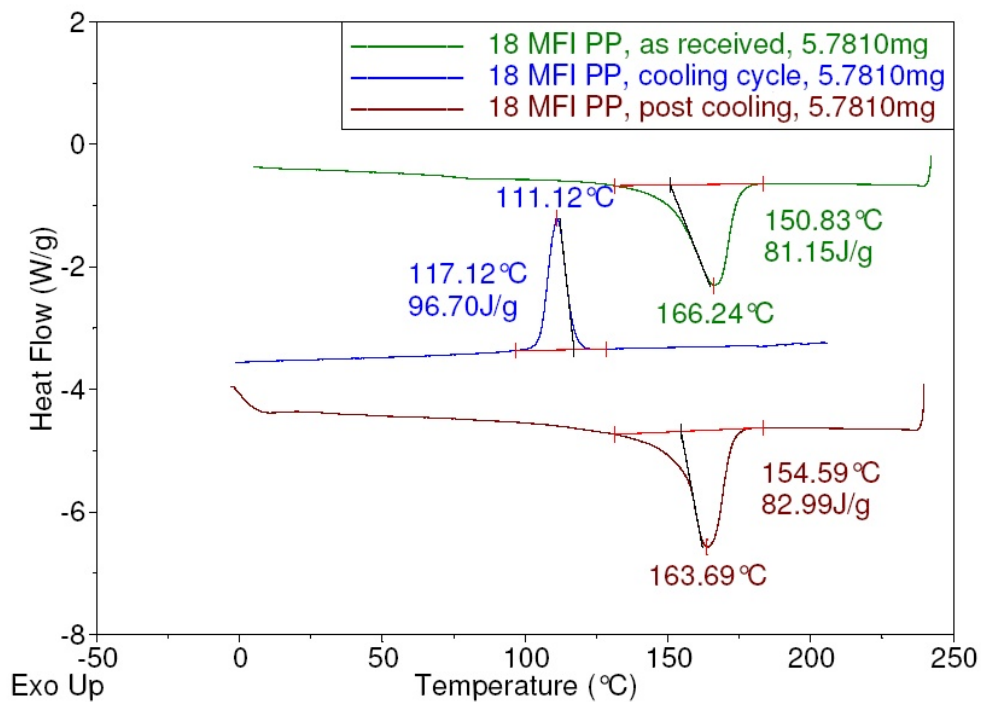
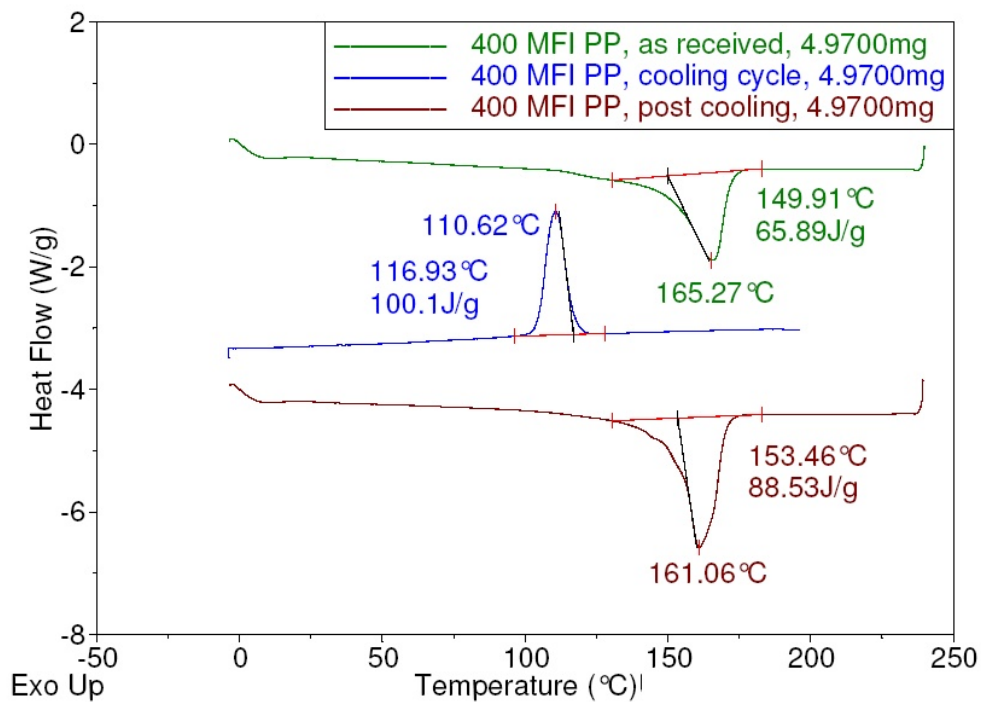Figure A.17: Thermal analysis of 18 MFI PP before and after a cooling run

Figure A.18: Thermal analysis of 400 MFI PP before and after a cooling run

were tested in the same manner in order to determine if blending the polymers changed the crystallization energy of the sample.

Figure A.19 shows the data obtained from heating the R30-1 as spun sample, cooling the sample and then heating it again. The as spun sample showed a peak melting temperature of 164.2°C and an enthalpy of melting of 84.1 J/g. After the cooling cycle, the peak melting temperature of the sample was 162.8°C and the enthalpy of melting was 84.4 J/g. The percent crystallinity of both the as spun and post cooling samples was 42%. The peak crystallization temperature was 116.0°C for this sample and the latent heat of crystallization was 95.3 J/g.

The thermogram for the R30-2 sample is shown in Figure A.20. The peak melting temperatures for the as spun and post cooling sample were very close: 163.3°C and 161.4°C respectively. The enthalpy of melting for the as spun sample was 89.9 J/g, which resulted in a crystallinity of 45%. This was higher than the 41% crystallinity recorded post cooling, which was calculated from the enthalpy of melting of 82.7 J/g. The peak crystallization temperature for the R30-2 sample was 117.2°C and the latent heat of crystallization was 94.5 J/g.

Figure A.21 shows the data obtained for the R30-3 sample. The as spun sample showed a peak melting temperature of 162.8°C and an enthalpy of melting of 93.0 J/g. After the cooling cycle, the peak melting temperature of the sample was 161.7°C and the enthalpy of melting was 88.3 J/g. The percent crystallinity of the as spun sample was 46% and the percent crystallinity of the post cooling sample was 44%. The peak crystallization temperature was 117.0°C for this sample and the latent heat of crystallization was 102 J/g.

The thermogram for the R30-4 sample is shown in Figure A.22. The peak melting temperatures for the as spun and post cooling sample were very close: 162.6°C and 161.0°C respectively. The enthalpy of melting for the as spun sample was 90.4 J/g, which resulted in a crystallinity of 44%. This was higher than the 42% crystallinity recorded post cooling calculated from the enthalpy of melting of 83.6 J/g. The peak crystallization temperature for the R30-4 sample was 116.4°C and the latent heat of crystallization was 94.8 J/g.

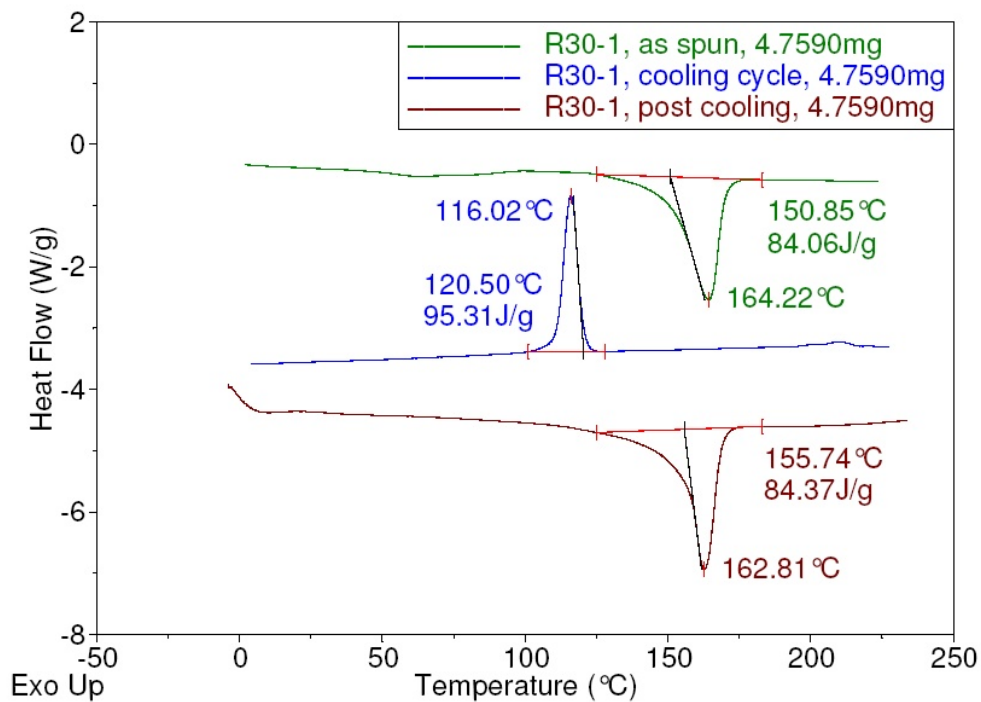Figure A.19: Thermal analysis of R30-1 as spun, during and after cooling
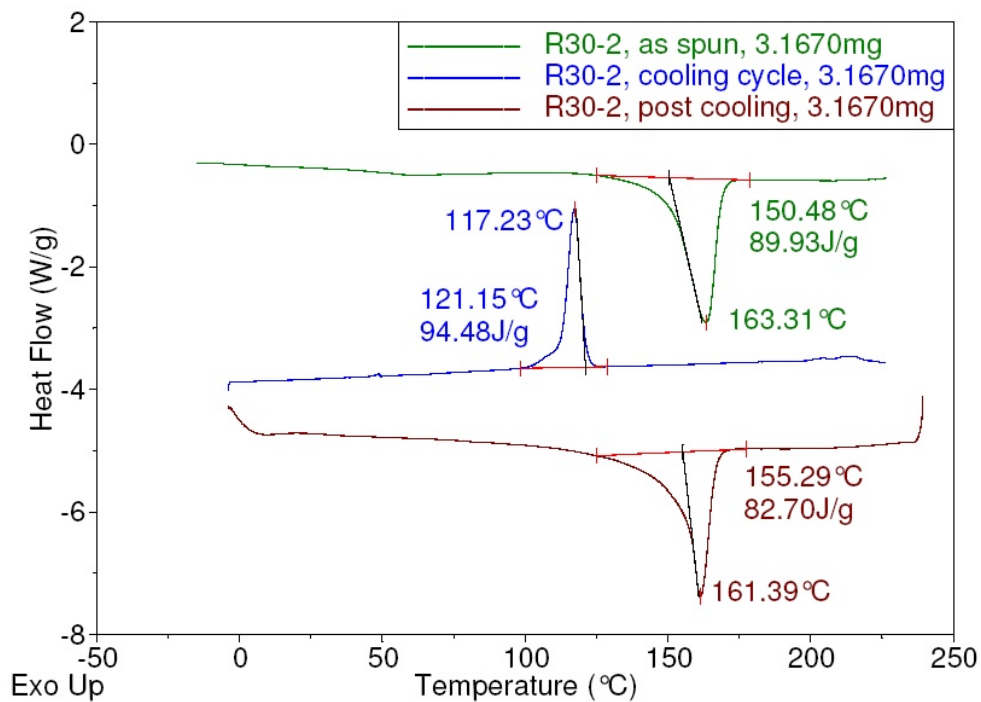

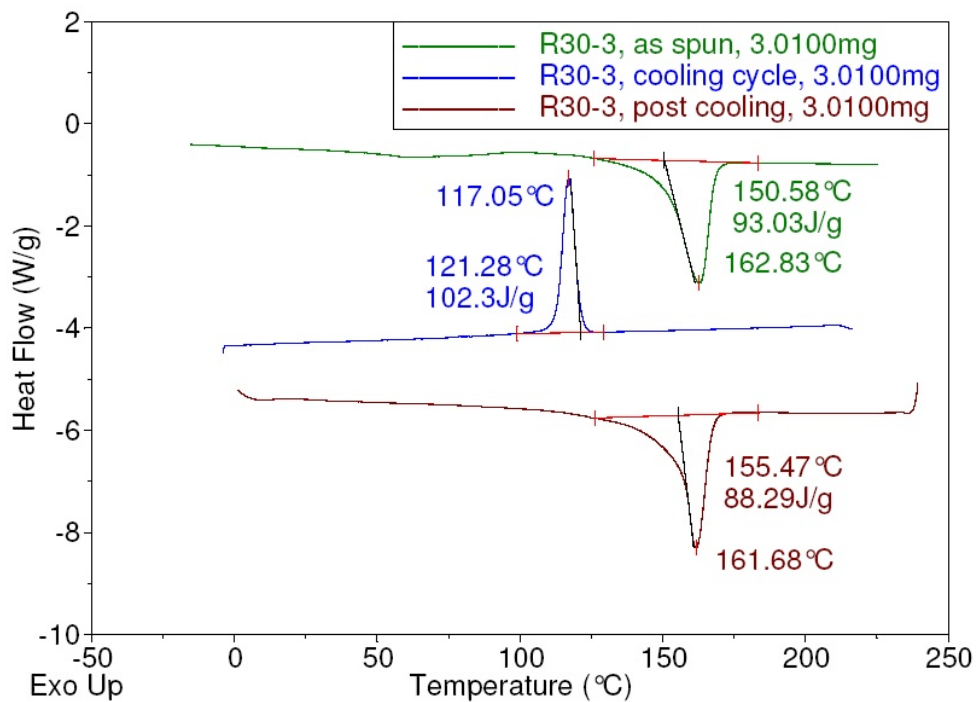Figure A.20: Thermal analysis of R30-2 as spun, during and after cooling

191

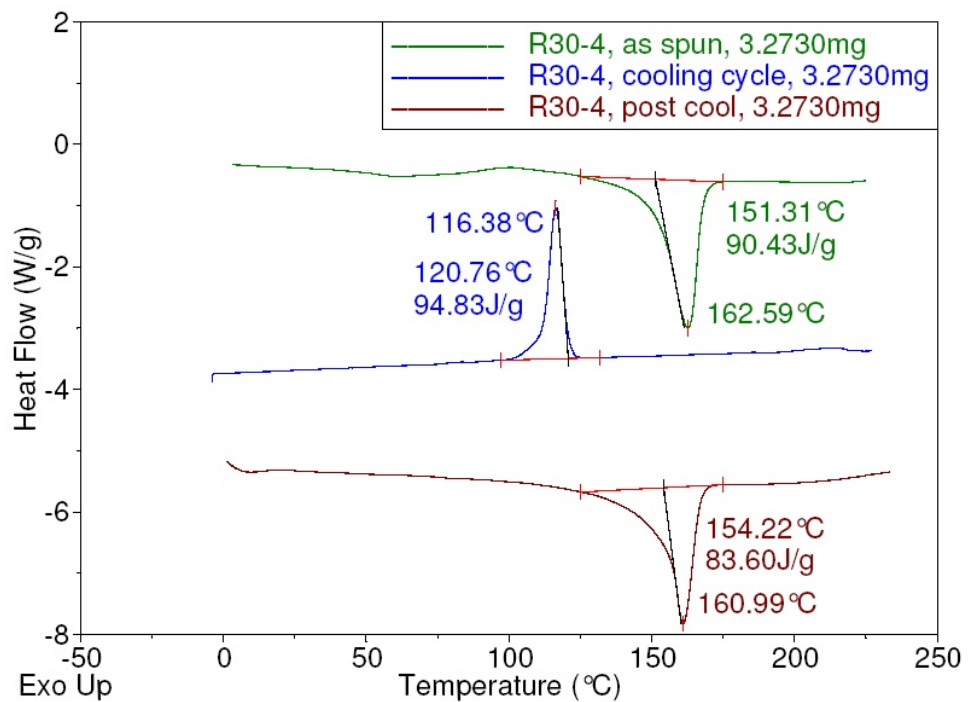Figure A.21: Thermal analysis of R30-3 as spun, during and after cooling

Figure A.22: Thermal analysis of R30-4 as spun, during and after cooling

192

Bibliography

[1] K. Bitz, "Clemson takes on commercialization," *Nonwovens Industry*, vol. 34, pp. 76–78, May 2003.

[2] K. K. Chawla, *Fibrous materials*. New York: Cambridge University Press, 1998.

[3] M. Ahmed, *Textile Science and Technology: Polypropylene Fibers – Science and Technology*, vol. 5. New York: Elsevier Scientific Publishing Company, 1982.

[4] P. T. Nakajima, K. Kajiwara, and J. McIntyre, eds., *Advanced fiber spinning technology*, ch. The spinning of highly aesthetic fibers.

[5] A. de Rovere, B. P. Grady, and R. L. Shambaugh, "The influence of processing parameters on the properties of melt-spun polypropylene hollow fibers," *Journal of Applied Polymer Science*, vol. 83, pp. 1759–1772, 2002.

[6] E. Karaca and F. Ozcelik, "Influence of the cross-sectional shape on the structure and properties of polyester fibers," *Journal of Applied Polymer Science*, vol. 103, pp. 2615–2621, 2007.

[7] W. Nijdam, J. de Jong, C. van Rijn, T. Visser, L. Versteeg, G. Kapantaidakis, G.-H. Koops, and M. Wessling, "High performance micro-engineered hollow fiber membranes by smart spinneret design," *Journal of Membrane Science*, vol. 256, pp. 209–215, 2005.

[8] Q. Huang, B. Seibig, and D. Paul, "Polycarbonate hollow fiber membranes by melt extrusion," *Journal of Membrane Science*, vol. 161, pp. 287–291, 1999.

[9] I. Jung, S. Y. Kim, and T. H. Oh, "Effects of spinning conditions on shape changes of trilobal-shaped fibers," *Textile Research Journal OnlineFirst*, vol. online, pp. 1–7, 2009.

[10] M. S. Lee, T. H. Oh, S. Y. Kim, and H. J. Shim, "Deformation kinetics of polypropylene hollow fibers in a continuous drawing process," *Journal of Applied Polymer Science*, vol. 74, pp. 1836–1845, 1999.

[11] D. Petrulis, "Fundamental study of the effect of the fiber wall thickness and inner diameter on the structure of polyamide and polypropylene hollow fibers," *Journal of Applied Polymer Science*, vol. 92, pp. 2017–2022, 2004.

[12] C. D. Han and J. Y. Park, "A study of shaped fiber formation," *Journal of Applied Polymer Science*, vol. 17, pp. 187–200, 1973.

[13] M. A. Bueno, A. P. Aneja, and M. Renner, "Influence of the shape of fiber cross section on fabric surface characteristics," *Journal of Materials Science*, vol. 39, pp. 557–564, 2004.

[14] R. P. Rohrbach, P. Unger, A. Lobovsky, L. Xue, D. Bause, R. Dondero, and G. Jones, "Properties and applications of externally impregnated shaped fibers," *Polymer Engineering and Science*, vol. 41, pp. 1206–1219, July 2001.

[15] S.-P. Rwei, "Formation of hollow fibers in the melt-spinning process," *Journal of Applied Polymer Science*, vol. 82, pp. 2896–2902, 2001.

[16] T. Oh, "Studies on melt spinning process of hollow polyethylene terephthalate fibers," *Polymer Engineering and Science*, vol. 46, pp. 609–616, May 2006.

[17] W. Takarada, H. Ito, T. Kikutani, and N. Okui, "Studies on high-speed melt spinning of noncircular cross-section fibers. i. structural analysis of as-spun fibers," *Journal of Applied Polymer Science*, vol. 80, pp. 1575–1581, 2001.

[18] A. de Rovere and R. L. Shambaugh, "Melt-spun hollow fibers: Modeling and experiments," *Composites: Part A*, vol. 30, pp. 117–121, 1999.

[19] B. Phillips and S. Bagrodia, *United States Patent 5611981: Process of Making Fibers*. Eastman Chemical Company, 1997.

[20] J. N. Dalton and B. M. Phillips, *United States Patent 5753166: Process of Making a Non-circular Cross-sectional Fiber*. Eastman Chemical Company, 1998.

[21] B. Phillips, J. Nelson, and S. Bagrodia, *United States Patent 6352664: Process of Making a Bundle of Fibers*. Clemson University Research Foundation, 2002.

[22] B. Phillips and S. Bagrodia, *United States Patent 5972505: Fibers Capable of Spontaneously Transporting Fluids*. Eastman Chemical Company, 1999.

[23] H. Thompson and G. Young, *United States Patent 5281208: Fluid Handling Structure for use in Absorbent Articles*. The Procter and Gamble Company, 1994.

[24] S. Bagrodia, B. Phillips, E. P. Smith, K. Parker, and P. Rundquist, *United States Patent 5356405: Absorbent Particles, Especially Catamenials, Having improved Fluid Directionality, Comfort and Fit*. The Procter and Gamble Company, 1994.

[25] H. Thompson, T. Martin, and T. Inglin, *United States Patent 5368926: Fluid Accepting, Transporting, and Retaining Structure*. The Procter and Gamble Company, 1994.

[26] H. Thompson, G. Young, T. Osborn, T. Johnston, J. Hammons, B. Lavash, J. Horney, and L. Hines, *United States Patent 5382245: Absorbent Articles, Especially Catamenials, Having improved Fluid Directionality*. The Procter and Gamble Company, 1995.

[27] B. Phillips and S. Bagrodia, *United States Patent 5977429: Temporary and permanent acquisition/distribution absorbent structures*. Eastman Chemical Company, 1999.

[28] B. Phillips, J. Nelson, and S. Bagrodia, *United States Patent 6103376: Bundles of Fibers Useful for Moving liquids at High Fluxes and Acquisition/Distribution Structures that Use the Bundles.* Eastman Chemical Company, 2000.

[29] B. Phillips and S. Bagrodia, *United States Patent 6251322: Synthetic Polyester Absorbent Materials.* Clemson University Research Foundation, 2001.

[30] B. M. Phillips and J. L. Nelson, *United States Patent 6342299: Bundles of Fibers Useful for Moving liquids at High Fluxes and Acquisition/Distribution Structures that Use the Bundles.* Eastman Chemical Company, 2002.

[31] B. Phillips, J. Nelson, and S. Bagrodia, *United States Patent 6352664: Process of Making a Bundle of Fibers.* Clemson University Research Foundation, 2002.

[32] B. Phillips, J. Nelson, and S. Bagrodia, *United States Patent 6352774: Bundles of Fibers Useful for Moving liquids at High Fluxes and Acquisition/Distribution Structures that Use the Bundles.* Clemson University Research Foundation, 2002.

[33] S. Bagrodia, B. Phillips, E. P. Smith, K. Parker, and P. Rundquist, *United States Patent 5346422: Toy Articles of Manufacture Comprising Spontaneously Wettable Fibers.* Eastman Chemical Company, 1994.

[34] L. Dean, R. Bobalik, and F. H. Dillow, *United States Patent 6100207: Absorbent Head Band.* Eastman Chemical Company, 2000.

[35] B. Phillips, *United States Patent 5414248: Grease and Moisture Absorbing Inserts for Microwave Cooking.* Eastman Chemical Company, 1995.

[36] B. Phillips and J. Nelson, *United States Patent 5837625: Insulation Material.* Eastman Chemical Company, 1998.

[37] H. L. Paul and K. R. Diller, "Comparison of thermal insulation performance of fibrous materials for the advanced space suit," *Journal of Biomechanical Engineering*, vol. 125, pp. 639–647, October 2003.

[38] F. Fortin, S. Yoon, Y. Korai, and I. Mochida, "Structure of round-shaped methylnaphthalene-derived mesophase pitch-based carbon fibres prepared by spinning through a y-shaped die hole," *Journal of Materials Science*, vol. 30, pp. 4567–4583, 1995.

[39] A. Ziabicki, *Fundamentals of Fibre Formation.* London: Wiley Interscience, 1976.

[40] C. D. Han, "Rheology of shaped fiber formation," *Journal of Applied Polymer Science*, vol. 15, pp. 1091–1097, 1971.

[41] R. Forney, L. McCune, N. Pierce, and R. Tompson, "Synthetic fibers: where the chemical engineer fits in," *Chemical Engineering Progress*, vol. 62, no. 3, p. 89, 1966.

[42] A. V. Galanti and C. C. Mantell, *Polypropylene Fibers and Films.* New York: Plenum Press, 1965.

[43] H. P. Frank, *Polypropylene.* New York: Gordon and Breach Science Publishers, 1968.

[44] N. Pasquini, ed., *Polypropylene Handbook.* Cincinnati: Hanser Gardner Publications, 2nd ed., 2005.

[45] G. Odian, *Principles of Polymerization.* Wiley-Interscience, 4th ed., 2004.

[46] A. V. Shenoy and D. R. Saini, "Melt flow index: More than just a quality control rheological parameter. part i," *Advances in Polymer Technology*, vol. 6, pp. 1–58, Spring 1986.

[47] B. P. Federation, "Plastipedia.co.uk: Polypropylene pp." http://www.bpf.co.uk/plastipedia/polymers/pp.aspx, October 2009.

[48] Z. Xu, J. Wang, L. Shen, D. Men, and Y. Xu, "Microporous polypropylene hollow fiber membrane part i. surface modification by the graft polymerization of acrylic acid," *Journal of Membrane Science*, vol. 196, pp. 221–229, 2002.

[49] T. Liu, K. fai Choi, and Y. Li, "Wicking in twisted yarns," *Journal of Colloid and Interface Science*, vol. 318, pp. 134–139, 2008.

[50] J. Zhang, Y. Yao, X.-L. Wang, and J.-H. Xu, "Polypropylene/polypropylene-grafted acrylic acid copolymer/ethylene-acrylic acid copolymer ternary blends for hydrophilic polypropylene," *Journal of Applied Polymer Science*, vol. 101, pp. 436–442, 2006.

[51] I. Novak, I. Krupa, and A. S. Luyt, "Modification of the polarity of isotactic polypropylene through blending with oxidized paraffin wax," *Journal of Applied Polymer Science*, vol. 94, pp. 529–533, 2004.

[52] Y.-F. Yang, L.-S. Wan, and Z.-K. Xu, "Surface hydrophilization for polypropylene microporous membranes: A facile interfacial crosslinking approach," *Journal of Membrane Science*, vol. 326, pp. 372–381, 2009.

[53] T. C. Chung and S. H. Lee, "New hydrophilic polypropylene membranes; fabrication and evaluation," *Journal of Applied Polymer Science*, vol. 64, pp. 567–575, April 1997.

[54] Y.-F. Yang, L.-S. Wan, and Z.-K. Xu, "Surface hydrophilization of microporous polypropylene membrane by the interfacial crosslinking of polyethylenimine," *Journal of Membrane Science*, vol. 326, pp. 70–80, 2009.

[55] A. P. Korikov, P. B. Kosaraju, and K. K. Sirkar, "Interfacially polymerized hydrophilic microporous thin film composite membranes on porous polypropylene hollow fibers and flat films," *Journal of Membrane Science*, vol. 279, pp. 588–600, 2006.

[56] D. Garcia, O. Fenollar, R. Lopez, R. Sanchis, and R. Balart, "Durability of the wettability properties of a polypropylene film with a low-pressure $CH_4 - O_2$ plasma treatment," *Journal of Applied Science*, vol. 110, pp. 1201–1207, 2008.

[57] S. Mosleh, S. M. Gawish, and Y. Sun, "Characteristic properties of polypropylene cationic fabrics and their derivatives," *Journal of Applied Polymer Science*, vol. 89, pp. 2917–2922, 2003.

[58] M.-X. Hu, Q. Yang, and Z.-K. Xu, "Enhancing the hydrophilicity of polypropylene microporous membranes by the grafting of 2-hydroxyethyl methacrylate via a synergistic effect of photoinitiators," *Journal of Membrane Science*, vol. 285, pp. 196–205, 2006.

[59] R. Lopez, R. Sanchis, D. Garcia, O. Fenollar, and R. Balart, "Surface characterization of hydrophilic coating obtained by low-pressure $CH_4 - O_2$ plasma treatment on a polypropylene film," *Journal of Applied Polymer Science*, vol. 111, pp. 2992–2997, 2009.

[60] E. Mathiowitz, J. S. Jacob, Y. S. Jong, T. M. Hekal, W. Spano, R. Guemonprez, A. M. Klibanov, and R. Langer, "Novel desiccants based on designed polymeric blends," *Journal of Applied Polymer Science*, vol. 80, pp. 317–327, 2001.

[61] T. W. Son, S. K. Lim, D. W. Lee, and E. W. Lee, "Physical modification of polypropylene. iii. novel morphology of polypropylene and poly(ethylene-co-vinyl alcohol) with epoxy blend fibers," *Journal of Applied Polymer Science*, vol. 73, pp. 1049–1057, 1999.

[62] T. W. Son, J. H. Park, D. W. Lee, K. H. Park, K. Koo, and S. K. Lim, "Preparation and properties of polar polypropylene blends containing phenolic resin," *Journal of Applied Polymer Science*, vol. 71, pp. 1029–1038, 1999.

[63] Unlisted, "Ciba additive makes polypropylene fibre hydrophilic," *Additives for Polymers*, no. 11, p. 4, 2002.

[64] D. J. Shaw, *Introduction to Colloid and Surface Chemistry.* London: Butterworths, 3rd ed., 1989.

[65] A. W. Adamson and A. P. Gast, *Physical Chemistry of Surfaces.* New York: John Wiley & Sons, Inc., 6th ed., 1997.

[66] T. L. Staples and D. G. Shaffer, "Wicking flow in irregular capillaries," *Colloids and Surfaces A: Physicochemical and Engineering Aspects*, vol. 204, pp. 239–250, 2002.

[67] S. Skinner and W. Reilly, "The exxon valdez oil spill: A report to the president." http://www.akrrt.org/Archives/Response_Reports/ExxonValdez_NRT_1989.pdf, April 2008.

[68] T.-T. Lim and X. Huang, "Evaluation of kapok (*Ceiba pentandra* (l.) Gaertn.) as a natural hollow hydrophobic-oleophilic fibrous sorbent for oil spill cleanup," *Chemosphere*, vol. 66, pp. 955–963, 2007.

[69] C. Teas, S. Kalligeros, F. Zanikos, S. Stournas, E. Lois, and G. Anastopoulos, "Investigation of the effectiveness of absorbent materials in oil spills clean up," *Desalination*, vol. 140, pp. 259–264, November 2001.

[70] D. Bastani, A. A. Safekordi, A. Alihosseini, and V. Taghikhani, "Study of oil sorption by expanded perlite at 298.15 K," *Separation and Purification Technology*, vol. 52, pp. 295–300, 2006.

[71] S. S. Banerjee, M. V. Joshi, and R. V. Jayaram, "Treatment of oil spill by sorption technique using fatty acid grafted sawdust," *Chemosphere*, vol. 64, pp. 1026–1031, 2006.

[72] S. Suni, A.-L. Kosunen, M. Hautala, A. Pasila, and M. Romantschuk, "Use of a by-product of peat excavation, cotton grass fibre, as a sorbent for oil-spills," *Marine Pollution Bulletin*, vol. 49, pp. 916–921, 2004.

[73] Q. F. Wei, R. R. Mather, A. F. Fotheringham, and R. D. Yang, "Evaluation of nonwoven polypropylene oil sorbents in marine oil-spill recovery," *Marine Pollution Bulletin*, vol. 46, pp. 780–783, 2003.

[74] G. Kondo, "Use of sorbents for oil spills," *Marine Pollution Bulletin*, vol. 6, pp. 73–76, 1975.

[75] S. S. Banerjee, M. V. Joshi, and R. V. Jayaram, "Treatment of oil spills using organo-fly ash," *Desalination*, vol. 195, pp. 32–39, 2006.

[76] H.-M. Choi and R. M. Cloud, "Natural sorbents in oil spill cleanup," *Environmental Science Technology*, vol. 26, pp. 772–776, 1992.

[77] O. Carmody, R. Frost, Y. Xi, and S. Kokot, "Surface characterisation of selected sorbent materials for common hydrocarbon fuels," *Surface Science*, vol. 601, pp. 2066–2076, 2007.

[78] M. Saito, N. Ishii, S. Ogura, S. Maemura, and H. Suzuki, "Development and water tank tests of sugi bark sorbent (sbs)," *Spill Science & Technology Bulletin*, vol. 8, no. 5–6, pp. 475–482, 2003.

[79] T. R. Annunciado, T. H. D. Sydenstricker, and S. C. Amico, "Experimental investigation of various vegetable fibers as sorbent materials for oil spills," *Marine Pollution Bulletin*, vol. 50, pp. 1340—, 2005.

[80] Zafustore.com, "Kapok fibers." http://www.zafustore.com/kapok.html, October 2009.

[81] E. Britannica, "kapok (fiber)." http://www.britannica.com/EBchecked/topic/311770/kapok, October 2009.

[82] Q. F. Wei, R. R. Mather, and A. F. Fotheringham, "Oil removal from used sorbents using a biosurfactant," *Bioresource Technology*, vol. 96, pp. 331–334, 2005.

[83] B. M. Phillips, S. Bagrodia, W. A. Haile, H. P. Hall, D. A. Casey, J. N. Dalton, R. J. Jones, R. S. Scalf, R. D. Neal, L. C. Trent, and J. L. Nelson, *United States Patent 5855798: Process for Spontaneously Transporting a Fluid.* Eastman Chemical Company, 1999.

[84] D. A. Skoog, F. J. Hollar, and S. R. Crouch, *Principles of Instrumental Analysis.* Thomas Brooks/Cole, 6th ed., 2007.

[85] G. Barnes and I. Gentle, *Interfacial Science An Introduction*. Oxford: Oxford University Press, 2005.

[86] Sigma-Aldrich, "Material safety data sheet crude oil internal standard," January 2004.

[87] L. Fuller, "CHYX fibers," 2005.

[88] T. J. Swihart and P. E. Campbell, "How silicones affect fabric flammability," *AATCC*, vol. 6, pp. 109–112, May 1974.

[89] P. Brown and K. Stevens, "Private communication regarding the extrusion of C fibers," 2006.

[90] A. L. Cimecioglu, S. H. Zeronian, K. W. Alger, M. J. Colins, and G. C. East, "Properties of oligomers present in poly(ethylene terephthalate)," *Journal of Applied Polymer Science*, vol. 32, pp. 4719–4733, September 1986.

[91] A. S. Nielsen, D. N. Batchelder, and R. Pyrz, "Estimation of crystallinity of isotactic polypropylene using raman spectroscopy," *Polymer*, vol. 43, pp. 2671–2676, April 2002.

[92] C. D'Aniello, L. Guadagno, G. Gorrasi, and V. Vittoria, "Influence of the crystallinity on the transport properties of isotactic polypropylene," *Polymer*, vol. 47, pp. 2515–2519, March 2000.

[93] J. Brandrup and E. H. Immergut, eds., *Polymer Handbook*, ch. Physical Constants of Poly(propylene), pp. V/27–V/31. New York: Wiley Interscience, 3rd ed., 1989.

[94] L. Struik, *Physical Aging in Amorphous Polymers and Other Materials*. The Netherlands: Elsevier Scientific Publishing Company, 1978.

[95] R. M. Silverstein, F. X. Webster, and D. J. Kiemle, *Spectrometric Identification of Organic Compounds*. John Wiley & Sons, 7th ed., 2005.

[96] E. C. Company, "Product data sheet: *Eastman* lb-100 water–dispersible polymer (100% solids)," August 2009.

[97] S. Aldrich, "Poly(ethylene glycol) and poly(ethylene oxide)," August 2009.

[98] R. J. Koopmans, "Die swell-molecular structure model for linear polyethylene," *Journal of Polymer Science: Part A: Polymer Chemistry*, vol. 26, pp. 1157–1164, 1988.

[99] J. I. Corp., "Material safety data sheet canola oil," December 2004.

[100] C. E. T. Company, "Material safety data sheet havoline motor oil (deposit shield)," October 2006.

[101] ASTM International, *Annual Book of Standards: F 726-06 Standard Test Method for Sorbent Performance of Adsorbents*, vol. 11.05, pp. 1188–1193. West Conshohocken, PA: ASTM International, 2002.

[102] D. Enterprises, "Critical surface tension and contact angle with water for various polymers," September 2009.

[103] G. Ercilla and F. Vilas, "Geological characterization of the galicia bank region (atlantic ocean, nw iberia): The marine geology community's response to the *Prestige* disaster," *Marine Geology*, vol. 240, pp. 1–6, March 2008.

[104] B. Phillips, "Private communication regarding the testing of fiber bundles by Eastman Chemical Company," 2007.